Annual Report on
Nuclear Physics Activities

July 1, 1988 – June 30, 1989

Editors:
G. Drexlin, H. J. Gils
Institut für Kernphysik

Kernforschungszentrum Karlsruhe

KERNFORSCHUNGSZENTRUM KARLSRUHE

Institut für Kernphysik

KfK 4660

ANNUAL REPORT

on

NUCLEAR PHYSICS ACTIVITIES

July 1, 1988 - June 30, 1989

Editors:

G. Drexlin and H.J. Gils

Kernforschungszentrum Karlsruhe GmbH, Karlsruhe

ABSTRACT

This report surveys the research activities from July 1, 1988 to June 30, 1989 at the Institute for Nuclear Physics (IK) of the Kernforschungszentrum Karlsruhe. The research program of the institute comprises fast neutron physics, neutrino physics, nuclear astrophysics, nuclear reactions with light ions, laser spectroscopy and applied gamma-ray spectroscopy as well as detector technology. As a new field of basic research an experiment in cosmic ray physics has been started.

ZUSAMMENFASSUNG

Der vorliegende Bericht gibt einen Überblick über die Arbeiten am Institut für Kernphysik (IK) des Kernforschungszentrums Karlsruhe im Zeitraum vom 1. Juli 1988 bis zum 30. Juni 1989. Das Forschungsprogramm umfaßt die Gebiete Neutronenphysik, Neutrinophysik, nukleare Astrophysik, Kernreaktionen mit leichten Ionen, Laserspektroskopie und angewandte Gammaspektroskopie sowie Detektortechnologie. Als neues Arbeitsfeld wurde im Berichtszeitraum mit Vorstudien zu einem Höhenstrahlexperiment begonnen.

PREFACE

This annual report on nuclear physics activities at the Kernforschungs-zentrum Karlsruhe describes experiments carried out in the Institut für Kernphysik (IK). The institute is divided into two sections labelled, for historical reasons, sections IK I and IK III.

A new joint project of both sections is the development and construction of a large detector system for studying cosmic rays. It is called KASCADE which stands for KArlsruhe Shower Core and Array DEtector. The main aim of the experiment is to obtain information on the elemental composition of the primary cosmic ray particles. In addition the measurements will help to clarify the question of cosmic ray point sources which have been discovered several years ago and show some enigmatic features.

Prototype detectors have been built and studied and extensive simulation calculations of the passage of cosmic rays through the atmosphere have been performed. A detailed proposal of the experiment has been written and reviewed by an external committee. The experiment which has been approved in the meantime will become by far the largest project of our institute in the years to come.

Additional activities of Section IK I lie in the fields of experimental nuclear and particle physics :

- Fast Neutron Physics : The polarized neutron beam of the facility POLKA at the Karlsruhe Cyclotron was used for capture reaction studies on light nuclear systems in the energy range up to 50 MeV. A scintillating liquid Ne sample was employed successfully as an active capture target in these experiments.

The development of cryogenic detectors was continued. Superconducting tunnel junctions have been applied for the detection of X-rays with improved resolution. The investigation of bolometric detection methods has been started.

- Neutrino Physics : The KArlsruhe Rutherford interMediate Energy Neutrino experiment KARMEN makes use of the pulsed 'beam dump' neutrinos ν_μ, ν_e and $\bar\nu_\mu$ produced at the spallation neutron source ISIS of the Rutherford Appleton Laboratory (England). The program involves experimental studies of fundamental questions in the fields of particle physics (v - oscillations, v - e scattering) and nuclear physics (v - nucleus interactions). In summer 1988 the scintillation calorimeter with half of its detector modules installed was moved into the measuring position in a massive 6000 t steel blockhouse. In a first three month data taking run detector and electronics performance were studied with electrons from muon decay and the first neutrino interactions were identified due to their

specific delayed coincidence signatures. Following the end of the 1988 ISIS beam period assembly and installation of the detector was completed.

- Detector Development : The work concentrates on liquid ionization chambers using room temperature liquids like TMS and HMDS. The investigations have been done in order to use this type of chambers for the large scale calorimeter of the KASCADE central detector. With a set of chambers first calorimeters with Fe, Pb and U as absorber slabs have been tested in a 6 GeV particle beam of pions, muons and electrons. Preparations for mass production of chambers have been performed.

Section IK III is mainly working in the following fields :

- Nuclear Astrophysics : Capture cross sections of fast neutrons in the keV to MeV range are measured in order to understand in detail the synthesis of heavy elements in stars. In this work, a considerable increase in accuracy has been achieved by use of a novel 4π scintillation counter made of BaF_2. First results are reported here and demonstrate a level of accuracy not attained before. Further experiments deal with the measurement of very small neutron capture cross sections by activation and with nuclear spectroscopy to obtain nuclear structure information required for the astrophysical interpretation of the data.

- Nuclear Reactions : Work in this field makes use of the 26 MeV / nucleon ^6Li beam from the Karlsruhe Isochronous Cyclotron and of the magnetic spectrometer for investigating continuous spectra in break-up reactions. Theoretical studies had shown that Coulomb break-up should allow the determination of radiative capture cross sections between light nuclei at very low relative velocities. Such cross sections are of great importance in astrophysics. Experiments on the Coulomb break-up of ^6Li have demonstrated the feasibility of the method.

- Laser spectroscopy : This technique is applied to sub-ng amounts of radioactive atoms in order to determine hyperfine structure and isotopic shifts of atomic transitions. The results yield information on nuclear moments and on the change of nuclear charge radii due to varying neutron number. Work at present concentrates on elements beyond lead using different experimental techniques such as spectroscopy on collimated atomic beams and on ions stored in an rf trap.
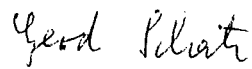
- Applied Gamma-Ray Spectroscopy : Here instruments are developed to determine concentration and isotopic composition of fissile materials. The instruments make use either of the intrinsic radioactivity or of X-ray absorption and fluorescence. Their main applications are in the safeguards of nuclear fuel and in process control during fabrication and reprocessing.
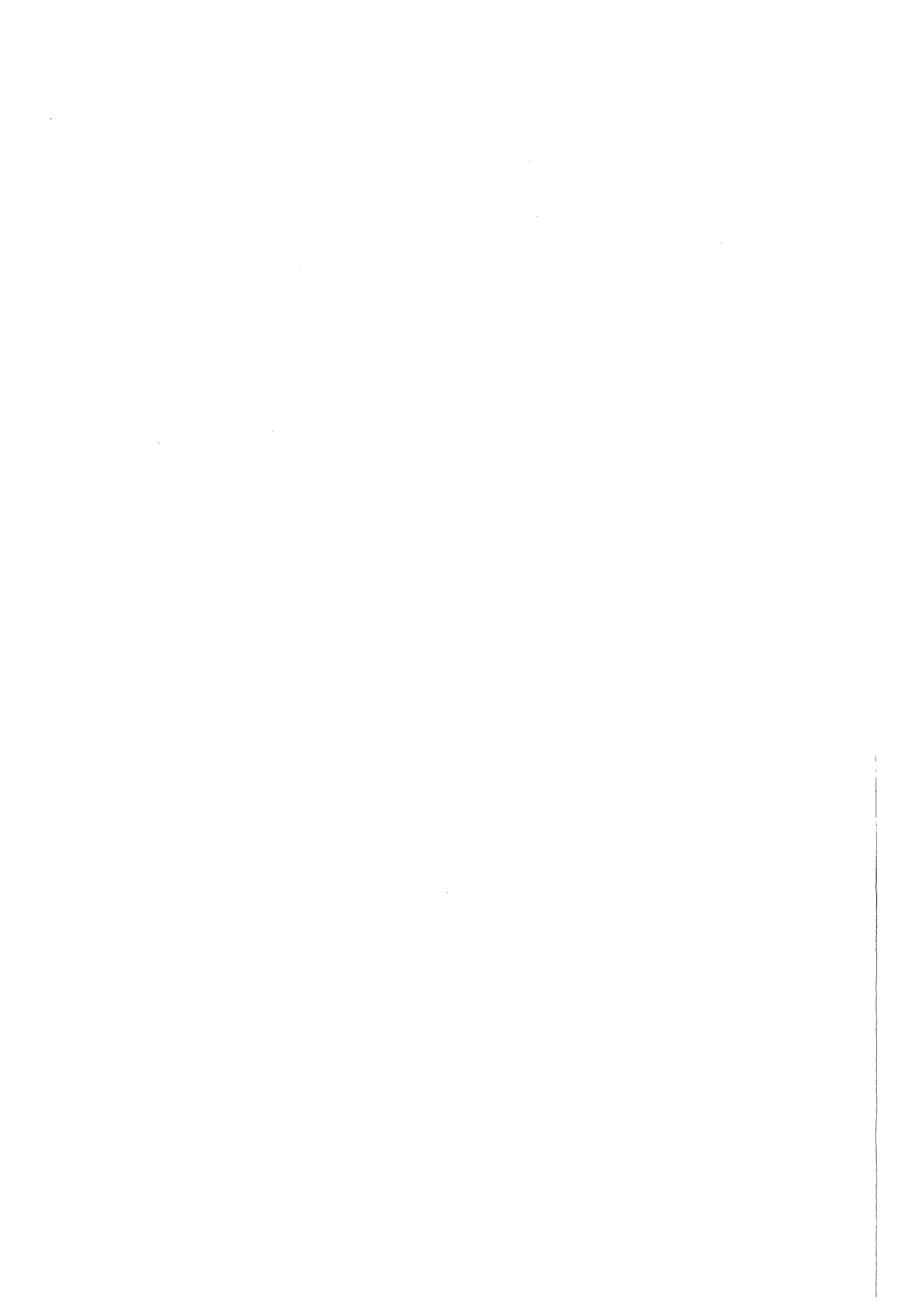
- Section IK III is also responsible for operating the three accelerators of our institute. The Karlsruhe Isochronous Cyclotron which is mainly used for fast neutron physics and nuclear reaction experiments; the 3.75 MeV Van de Graaff accelerator which serves mainly as a source of keV neutrons for the nuclear astrophysics studies; and a compact cyclotron which is basically a commercial installation to produce radioactive isotopes for nuclear medicine and mechanical engineering.

(B. Zeitnitz)   (G. Schatz)

CONTENTS   Page

1. NUCLEAR PHYSICS

1.1 NUCLEAR ASTROPHYSICS

1.1.1 ^{7}Li $(n,\gamma)^8$Li – TRIGGER REACTION TO A PRIMORDIAL r-PROCESS ?

M. Wiescher*, R. Steininger, F. Käppeler (1)

The cross section of the ^{7}Li$(n,\gamma)^8$Li reaction was studied in the neutron energy range 25-420 keV, to investigate the role of this reaction in a primordial r-process. The experimental results are compared with theoretical model calculations. The obtained reaction rate is significantly smaller than previously suggested. This results in a reduced feeding of a proposed primordial r-process.

(1)   Ap. J. 344 (1989) 464
*   University of Notre Dame, Dept. of Physics, Notre Dame, Indiana, U.S.A.

1.1.2 MEASUREMENT OF THE ^{22}Ne(n, γ) CROSS SECTION AT kT = 25 keV

H. Beer, G. Rupp, F. Voß, F. Käppeler

The ^{22}Ne(α, n) reaction is considered as one of the primary neutron sources for the nucleosynthesis of the heavy elements. At the same time ^{22}Ne is effective as a neutron poison via the ^{22}Ne(n, γ) reaction. Therefore, its neutron capture cross section is of essential importance for the assessment of the neutron balance (1,2).

A ^{22}Ne(n,γ) measurement was performed using the activation technique. The ^{22}Ne(n,γ)^{23}Ne(38s) reaction is characterized by a clear signature. The radioactive nucleus ^{23}Ne decays in 32% of the cases via a 439 keV γ-ray line. With a high resolution germanium detector for activity counting this signature allowed us to accumulate the activation events into a sharp line distinct from the background countrate.

The activations were carried out at the Karlsruhe 3.75 MV van de Graaff accelerator. Using the ^{7}Li(p,n)^{7}Be reaction near the reaction threshold, a Maxwellian neutron spectrum with a thermal energy kT = 25 keV can be obtained for the irradiations (3,4). The short half-life of ^{23}Ne required the build-up of an experimental arrangement for fast cyclic activation in order to carry out irradiation and activity counting efficiently.

The ^{22}Ne capture cross section was determined relative to the well-known ^{197}Au cross section in two steps. This is necessary because of the special properties of neon as a noble gas. In the first step the ^{22}Ne(n, γ)^{23}Ne(38s) reaction was measured relative to five different Kr reactions :

^{78}Kr(n, γ) ^{79}Kr^m(50s), ^{78}Kr(n, γ) ^{79}Kr(34.9h), ^{80}Kr(n, γ) ^{81}Kr^m(13.3s),

^{84}Kr(n, γ) ^{85}Kr^m(4.48h), ^{86}Kr(n, γ) ^{87}Kr(76.3m). For these activations stainless steel spheres (20 mm diameter, 0.5 mm wall thickness) were filled with a mixture of enriched (99.9%) ^{22}Ne and natural Kr gas. In the second step, the same Kr reactions were measured relative to the ^{197}Au(n, γ)^{198}Au(2.69d) reaction. For this purpose Kr loaded zeolite was pressed to self-supporting tablets of 6 mm diameter and irradiated together with Au disks of the same diameter.
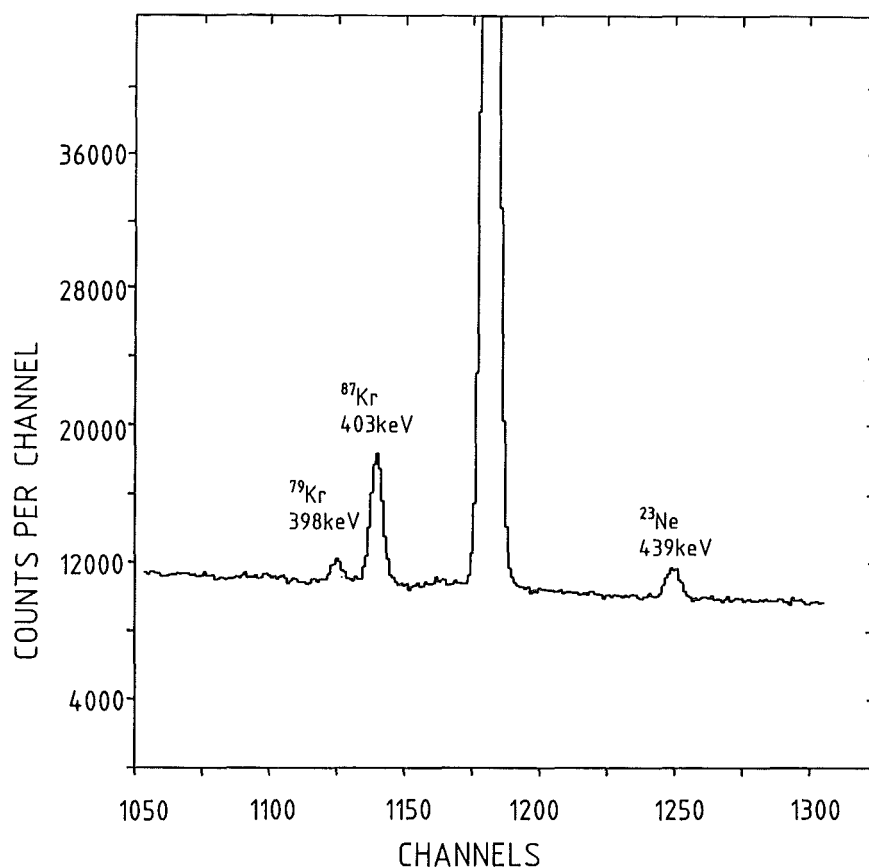
Fig. 1   A section of the accumulated data of one of the activations. The pressurized gas sample contained 250.36 mg ^{22}Ne and 210.88 mg natural Kr. Results on ^{22}Ne, ^{86}Kr and ^{78}Kr are shown. The capture events are determined from the intensities of the corresponding γ-ray lines of ^{23}Ne, ^{79}Kr and ^{78}Kr. The ^{23}Ne line contains 10,785, the ^{87}Kr line 41,096 and the ^{79}Kr line 5,245 counts. The strong line in the center is the 417 keV background line from the activation of ^{115}In by scattered neutrons.

The final analysis resulted in a Maxwellian averaged [22]Ne capture cross section of σ [[22]Ne, kT = 25 keV] = (0.066 ± 0.005) mb; extrapolated to kT = 30 keV one obtains σ [[22]Ne, kT = 30 keV] = (0.060 ± 0.005) mb. The quoted uncertainty was determined by quadratic error propagation from the following individual uncertainties : Statistics ([22]Ne/Kr) 3.6%, Statistics (Kr/Au) 0.5%, Ge-detector efficiency 2%, Au cross section 1.5%, gas sample weight 5%, Kr weight in zeolite 2.5%, intensity per decay of [23]Ne line 3.04%, intensity per decay of [198]Au line 0.105%, γ-ray attenuation 1.5%, neutron multiple scattering <1%.

(1)   M. Busso, G. Picchio, R. Gallino, A. Chieffi, Ap. J. **326** (1988) 196
(2)   N. Prantzos, M. Arnould, J.-P. Arcoragi, Ap. J. **315** (1987) 209
(3)   H. Beer, F. Käppeler, Phys. Rev. **C21** (1980) 534
(4)   W. Ratynski, F. Käppeler, Phys. Rev. **C37** (1988) 595

1.1.3 CAPTURE CROSS SECTION MEASUREMENTS OF Xe AND Kr ISOTOPES BY FAST CYCLIC ACTIVATION

H. Beer

The measurement of particular isotopic capture cross sections of Kr and Xe is made difficult because of the high costs for separate isotopes. In this situation the selectivity of the activation technique was used to determine these capture cross sections with samples of natural composition.

The measurements were carried out by fast cyclic activation [see also the contribution 1.1.2 on [22]Ne(n,γ)]. This technique is an extension of the conventional activation method (1) which can be applied conveniently <u>only</u> to nuclei with half lives ≥ 0.5 h. The present setup, however, allows for the simultaneous measurement of activities with half lives ≥ 10 s. The samples consisted of a mixture of natural Kr and Xe gas contained in stainless steel spheres [20 mm dia, 0.5mm wall thickness]. The half lives of the activities to be counted ranged from 13 s to 36.4 d. In the runs it was posible to measure 5 isotopic Kr cross sections and 11 isotopic Xe cross sections. The following reactions are especially interesting:

(1) The reactions [128]Xe(n,γ) [129]Xe^m (8.89d) and [130]Xe(n,γ) [131]Xe (11.9d) will be used for a better assessment of the corresponding total capture cross sections of these two s-only isotopes.

(2) The very small [136]Xe(n,γ) [137]Xe (3.83 m) cross section is an important input quantity for the analysis of the isotopic Xe anomalies (2).

The figures 1 and 2 show two parts of an accumulated spectrum with the characteristic γ ray lines of the activated nuclei. The 456 keV line to determine
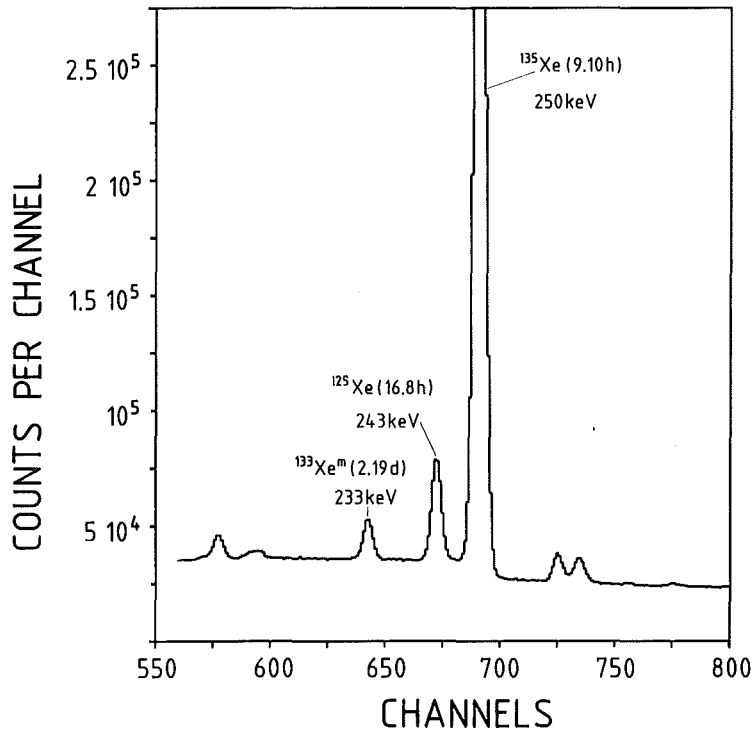
Fig. 1   A section of the accumulated data with activity lines from the reactions
132Xe(n,γ) 133Xe^m, 124Xe(n,γ) 125Xe (16.8 h), 134Xe(n, γ) 135Xe (9.10 h).
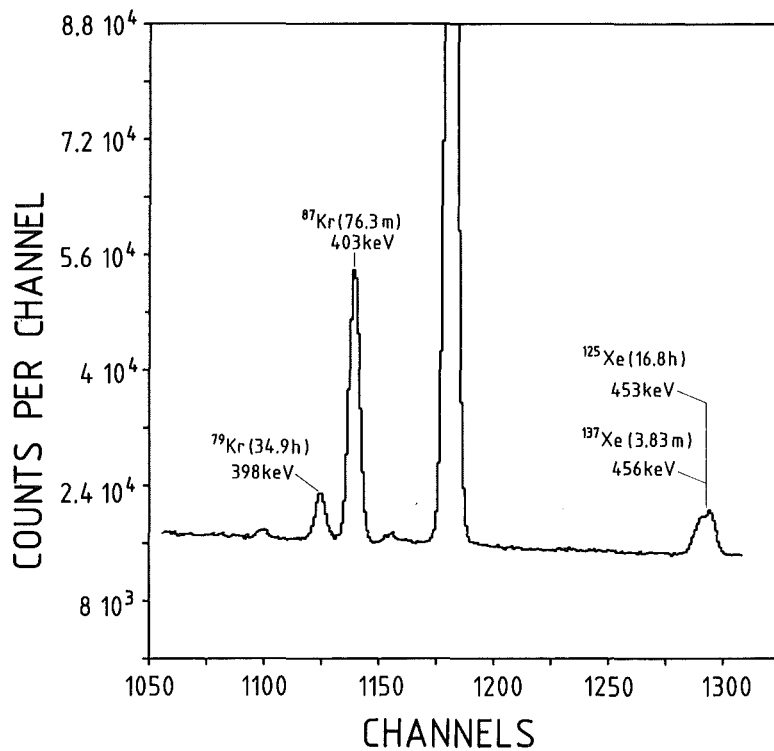
Fig. 2 A section of the accumulated data with lines corresponding to the reactions
78Kr(n,γ) 79Kr (34.9 h), 86Kr(n,γ) 87Kr (76.3 m) 124Xe (n,γ) 125Xe (16.8 h),
136Xe (n,γ) 137Xe (3.83 m).

the ^{136}Xe capture cross section overlaps with a line at 453 keV from the ^{125}Xe (16.8 h) decay (Fig. 2). But a separation of the intensities is obtained using another ^{125}Xe line at 243 keV (Fig. 1) and the well known intensity ratio of the 453 and 243 keV lines.

(1)   H. Beer, F. Käppeler, Phys. Rev. C21 (1980) 534
(2)   D.D. Clayton, Ap. J. 340 (1989) 613

1.1.4   MEASUREMENT OF THE ^{85}Rb AND ^{87}Rb CAPTURE CROSS SECTIONS FOR s–PROCESS STUDIES

H. Beer, R.L. Macklin* (1)

The excitation functions for the reactions ^{85}Rb(n,γ) and ^{87}Rb(n,γ) have been measured over the neutron energy range of 175 eV to 700 keV. Maxwellian-averaged capture cross sections for thermal energies kT = 5–100 keV have been calculated. The data were used to carry out s-process calculations. Solar s-process abundances were reproduced with a two-component phenomenological model below mass number 90, a single-flux weak s-process, and a pulsed s-process characterized by exponentially distributed neutron exposures. The solar s-process abundances, as well as s-process abundances from Ba stars and the Murchison meteorite, were studied in the framework of the asymptotic giant branch models. Constraints were derived concerning the properties of the neutron pulses for a description of the empirical s-process data.

(1)   Ap. J. 339 (1989) 962
*   Oak Ridge National Laboratory, Oak Ridge, Tennessee, U. S. A.

1.1.5 ^{88}Sr AND ^{89}Y: THE s-PROCESS AT MAGIC NEUTRON NUMBER N = 50

F. Käppeler, W. Zhao*, H. Beer, U. Ratzel (1)

The neutron capture cross sections of ^{88}Sr and ^{89}Y were measured in a quasi-stellar neutron spectrum for kT = 25 keV via the activation method. Relevant systematic uncertainties were determined experimentally by repeated activations under different conditions and with different samples. Gold was used as a cross section standard. The resulting stellar cross sections for kT = 30 keV are 6.13 ± 0.18 mb for ^{88}Sr and 19.0 ± 0.6 mb for ^{89}Y. The partial cross section

$86Sr(n,\gamma)87mSr$ was measured to 48.1 $\pm$ 1.2 mb. Compared to previous data, the associated uncertainties are reduced by factors of 3 and 5, respectively. The implications for s-process nucleosynthesis around magic neutron number N = 50 are discussed in the light of new information on neutron density and temperature.

(1)   Ap. J. (submitted)

*   On leave from Institute of Atomic Energy, Academica Sinica, Beijing, People's Republic of China

1.1.6 THE STELLAR NEUTRON CAPTURE CROSS SECTIONS OF 94Zr AND 96Zr

K.A. Toukan*, F. Käppeler (1)

The neutron capture cross sections of 94,96Zr have been determined relative to that of gold by means of the activation method. The samples were irradiated in a quasi-stellar neutron spectrum for kT = 25 keV using the $7Li(p,n)7Be$ reaction near threshold. Variation of the experimental conditions in different activations and the use of different samples allowed to reliably determine corrections and to evaluate systematic uncertainties. The resulting stellar cross sections can be given with uncertainties around 4%, considerably lower than previous data. The new data allowed for the first time to deduce the s-process neutron density from the branching at 95Zr.

(1)   Ap. J. (in press)

*   On leave from University of Jordan, Amman, Jordan

1.1.7 s–PROCESS STUDIES ON TIN

H. Beer, G. Walter*, F. Käppeler (1)

We have measured the excitation function of the reaction $116Sn(n,\gamma)$ in the energy range from 3 keV to 200 keV neutron energy. Maxwellian average capture cross sections for thermal energies kT = 10 to 100 keV have been calculated. The empirical product of cross section and abundance for the s-only isotope 116Sn indicates an inconsistency between the solar tin abundance obtained from meteorites and from s-process calculations. From our s-process analysis we find $N_O(Sn)$ = 2.95 $\pm$ 0.23 (Si = 10^6), which is 23% lower than the respective meteoritic value. This result is discussed with regard to the origin of 115Sn.

(1)   Astron. Astrophys. 211 (1989) 245

*   Fa. Bosch, D-7410 Reutlingen, Germany

1.1.8 THE LEVEL SCHEME OF 176Lu – A KEY FOR THERMAL EFFECTS DURING s-PROCESS NUCLEOSYNTHESIS

N. Klay, H. Börner*, F. Käppeler, H. Beer, G. Schatz, B. Krusche*,
S. Robinson*, F. Hoyler*, K. Schreckenbach*, U. Mayerhofer**,
T. v. Egidy**, G. Hlawatsch**

The extension of the level scheme of 176Lu (1) has been completed. By combination of our results obtained at the ILL Grenoble with that of a 175Lu(d,p) study at the TU Munich (2) it was possible to determine now the excitation energy of the isomeric state in 176Lu to E = 122.861 ± 0.017 keV. This energy window is small enough that additional γ-transitions between the level systems based on isomer and ground state can be assigned unambiguously.

The whole level scheme of the present study consists of 80 levels, which are connected by more than 250 γ-transitions. The assignments are mainly based on the energy combination principle, which appeared to be a useful tool since the γ-ray energies were measured with a precision of typically 1-10 eV. Additional confidence was provided by the known multipolarities and a measurement of (n,γ-γ') coincidences with two Ge(Li)-detectors.

Comparison of all experimentally deduced rotational bandheads with those predicted in a semiempirical model (3) shows a good overall agreement; below $\simeq$ 900 keV all predicted bandheads with $1 \le K \le 6$ could be verified. The energies and proposed Nilsson configurations derived in this study are given in Fig. 1. The rotational states which are built on these bandheads as well as the huge number of corresponding γ-transitions are omitted in this picture.

One important assignment is the decay of a level at 838.65 keV, which can be identified as the $I^\pi = 5^-$ member of a $K^\pi = 4^-$ bandhead at 722.93 keV. For the astrophysical aspect of a thermal enhancement of the 176Lu decay, this is the first level for which γ-transitions both to isomer and ground state have been established. Its assignment as a member of a rotational band rather than as a bandhead implies a short half-life. This could be confirmed by a life-time measurement of Andrejtscheff and Petkov (4) who found "zero" life-time with the technique of delayed coincidences. From the sensitivity of their method a life-time shorter than 0.5ns must be assumed.

With the improved knowledge on the level scheme we can investigate the s-process branching at 176Lu in detail. Similarly to the previous investigations of Beer et al. (5) an effective branching factor f_n can be introduced by the following equations:

$$(\sigma N)_{176Lu} = f_n \cdot (\sigma N)_{175Lu}$$
$$(\sigma N)_{176Hf} = (1-f_n) \cdot (\sigma N)_{175Lu} \cdot$$
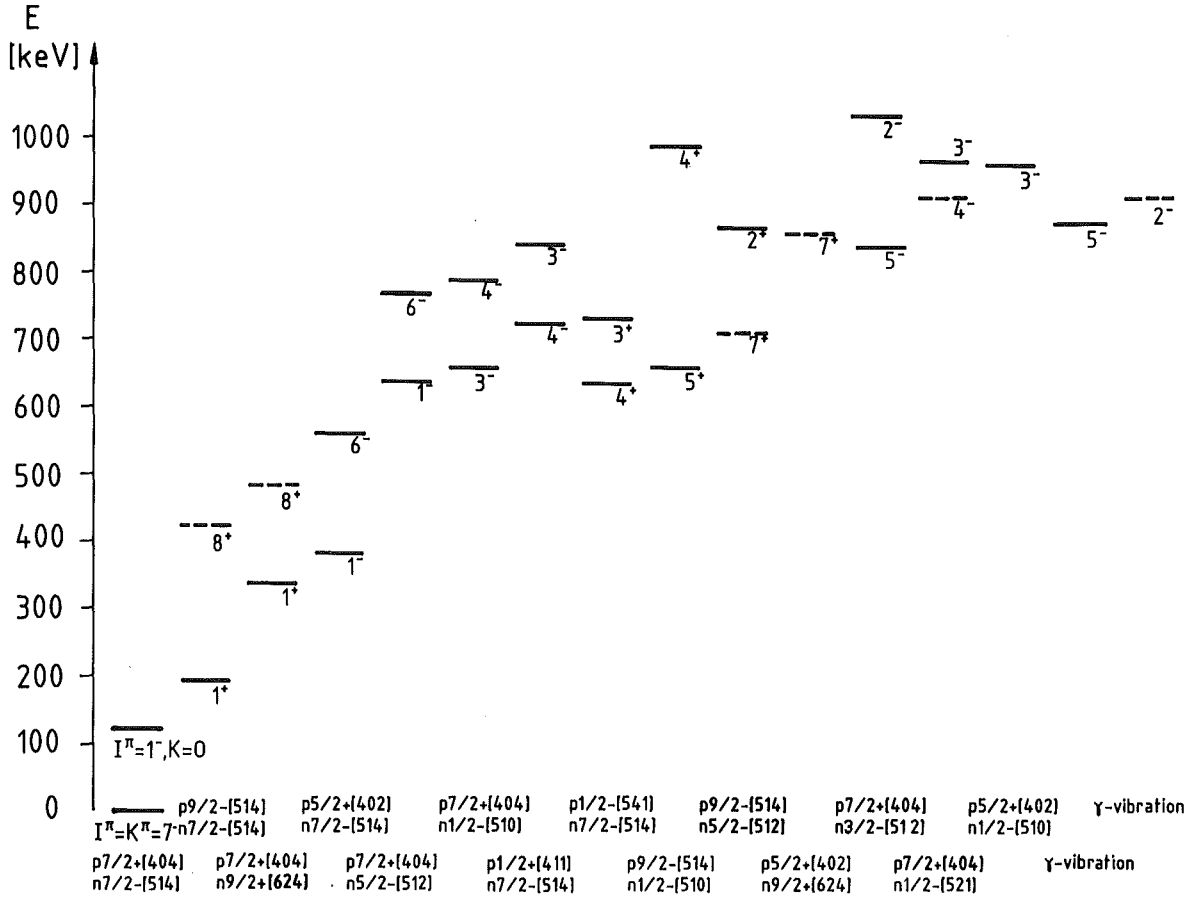
Fig. 1 Rotational bandheads in 176Lu with the respective parities and K-quantum numbers. For the $K^\pi = 0^-$ band the $I^\pi = 1^-$ isomeric state is drawn instead of the $I^\pi = 0^-$ bandhead. Less well established levels are given by dashed lines.

where σ denotes the neutron capture cross cross section and N the s-process abundance of the respective nuclide. The branching factor f_n accounts for the s-process flow through 176Lu, and $(1-f_n)$ for the corresponding flow through 176Hf. The above equations allow for a calculation of the initially produced 176Lu/176Hf abundance ratio provided that f_n is precisely known.

At low stellar temperature thermal effects can be neglected and the branching factor f_n is only determined by the partial neutron capture cross section of 175Lu to the ground state of 176Lu. In the other extreme, at temperatures high enough to achieve thermal equilibration between 176Lu and 176mLu, the same branching factor f_n is only determined by the competition between the effective stellar β-decay and neutron capture rate on 176Lu. The numerical values of f_n differ considerably for these extreme assumptions; the transition between these regimes is determined by the level scheme.

Since the onset of thermal effects is determined by induced upward γ-transitions, both the excitation energies as well as the γ half-lives of the involved mediating levels must be taken into account. The upward γ-transition rate, which has to compete with external destruction rates (i.e. β-decay and neutron capture), is given by the product of the spontaneous γ-emission rate and the Boltzmann factor. The onset of thermal effects is therefore provided by the mediating level with the lowest excitation energy and shortest γ half-life which is, in our case, the 838.65 keV level.
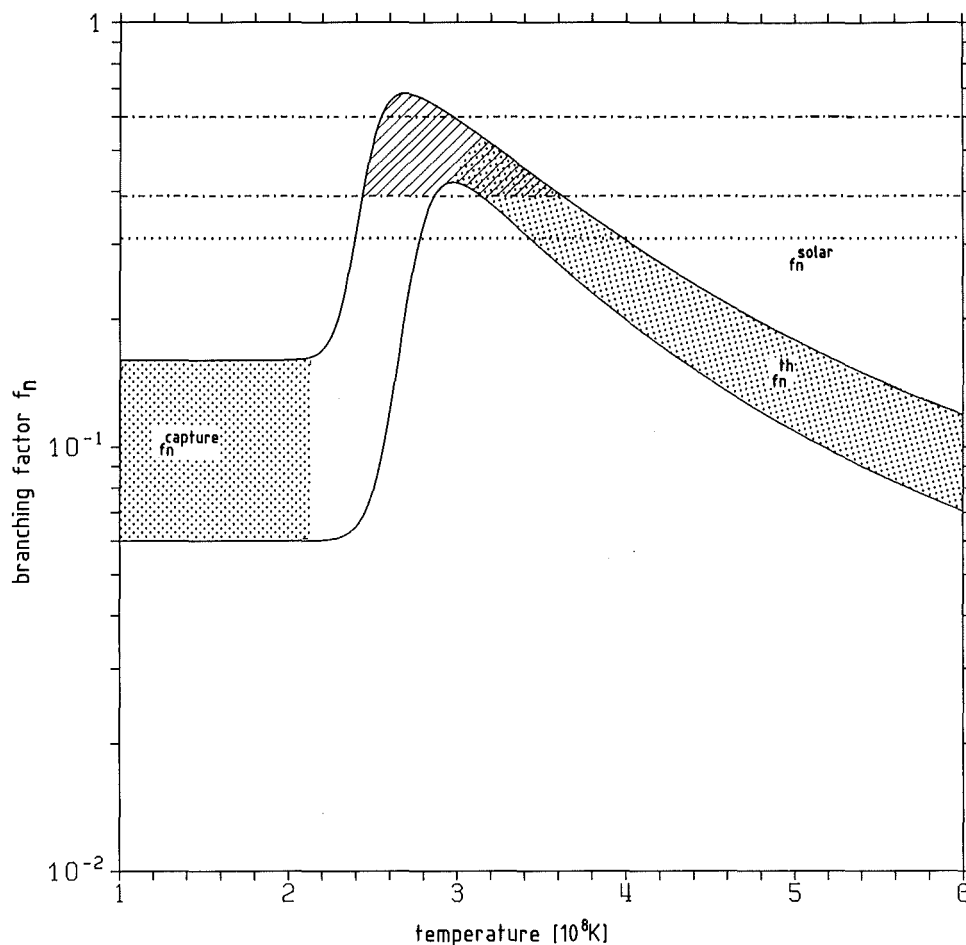
Fig. 2   The s-process branching factor f_n as a function of stellar temperature (error band between solid lines). For comparison the dotted line marks the lower limit from the solar abundances. The range between the dashed-dotted lines is adopted from the s-process analysis of Beer et al. (5). The hatched region is compatible with all studies and determines the s-process temperature limits.

For a steady state s-process the branching factor can be calculated as a function of stellar temperature by due consideration of the 838.65 keV level. Such calculations have been performed for a γ half-life of 0.5 ns which corresponds to

the experimental upper limit (4) and for an assumed lower limit of 10 ps. The results of this calculation, which was carried out with a formalism described by Ward and Fowler (6), are given in Fig. 2.

The upper and lower limit of f_n in this graph are determined by completely different input parameters : The low temperature boundaries denoted f_n capture are adopted from a recent measurement of the partial neutron capture cross section for the reaction ^{175}Lu (n,γ) ^{176m}Lu (7). For intermediate temperatures the branching factor is limited by the assumed life-time of the 838.65 keV level. Finally, at high temperatures, where the neutron density n_n becomes important, the limits $1.8 \leq n_n/10^8$ cm$^{-3} \leq 3.2$ of a recent investigation of Lesko et al. (8) have been used. The resulting error band for the region of complete thermal equilibration has been denoted f_nth in Fig. 2.

The temperature dependence of the branching factor can be compared with the constraints on this quantity derived by an analysis following the s-process path both above and below ^{176}Lu (5) arriving at a range $0.38 \leq f_n \leq 0.60$. A comparison of this error band with the temperature dependence of f_n yields a possible temperature range for the main component of the s-process of

$$2.4 \cdot 10^8 \text{ K} \leq T \leq 3.6 \cdot 10^8 \text{ K}.$$

This result is in perfect agreement with the analysis of other branchings (9). It should be noted that the high temperature limit is determined as a function of neutron density. The lower limit, however, is only dependent on the level scheme of ^{176}Lu; it corresponds to an estimated lower limit for the half-life of the 838.65 keV level.

(1)   N. Klay, H. Börner, F. Käppeler, H. Beer, G. Schatz, B. Krusche, S. Robinson, F. Hoyler, K. Schreckenbach, U. Mayerhofer, T. v. Egidy, G. Hlawatsch, Report KfK 4508, Kernforschungszentrum Karlsruhe (1989) p. 7
(2)   U. Mayerhofer, G. Hlawatsch, T. v. Egidy (1987) private communication
(3)   R.W. Hoff, R.F. Casten, M. Bergoffen, D.D. Warner, Nucl. Phys. **A437** (1985) 285
(4)   W. Andrejtscheff, P. Petkov (1988) private communication
(5)   H. Beer, G. Walter, R.L. Macklin, P.J. Patchett, Phys. Rev. **C30** (1984) 464
(6)   R.A. Ward and W.A. Fowler, Ap. J. **238** (1980) 266
(7)   W.R. Zhao, F. Käppeler, in 'Astrophysical Ages and Dating Methods', 5th IAP Astrophysics Meeting (1989), Paris, France
(8)   K.T. Lesko, E.B. Norman, R.M. Larimer, J.C. Bacelar, and E.M. Beck, Phys. Rev. **C39** (1989) 619
(9)   F. Käppeler, R. Gallino, M. Busso, G. Picchio, C.M. Raiteri, Ap.J. (1990) (in press)

*   Institut Laue - Langevin, Grenoble, France
**   Physik Department, Technische Universität München, Germany

1.1.9 AN IMPROVED $^{175}Lu(n,\gamma)^{176m}Lu$ CROSS SECTION AND ITS IMPLICATIONS FOR THE s-PROCESS CHRONOMETER

W.R. Zhao*, F. Käppeler

Among the long-lived nuclei observed in nature, ^{176}Lu seems to be particularly promising with respect to galactic history: it has a suited half-life of $36 \cdot 10^9 y$ and it is the only potential chronometer that can be attributed unambiguously to the slow neutron capture process (s-process (1, 2)). The only complication in interpreting ^{176}Lu as an s-processs chronometer seemed to be the existence of an isomeric state, which causes part of the s-process flow to bypass the long-lived ground state. Neutron capture on ^{175}Lu leading more frequently to the isomer than to the long-lived ground state implies that the partial cross section to the isomer needs to be known with good accuracy, because its difference to the total capture cross section

$^{175}Lu + n$

$123\ keV,\ 1^- \qquad 3.68h$

1^-

^{176}Lu

$Q_\beta = 1186\ keV$

$36\ Gy$

6^+

4^+

60% 2^+

40% 0^+
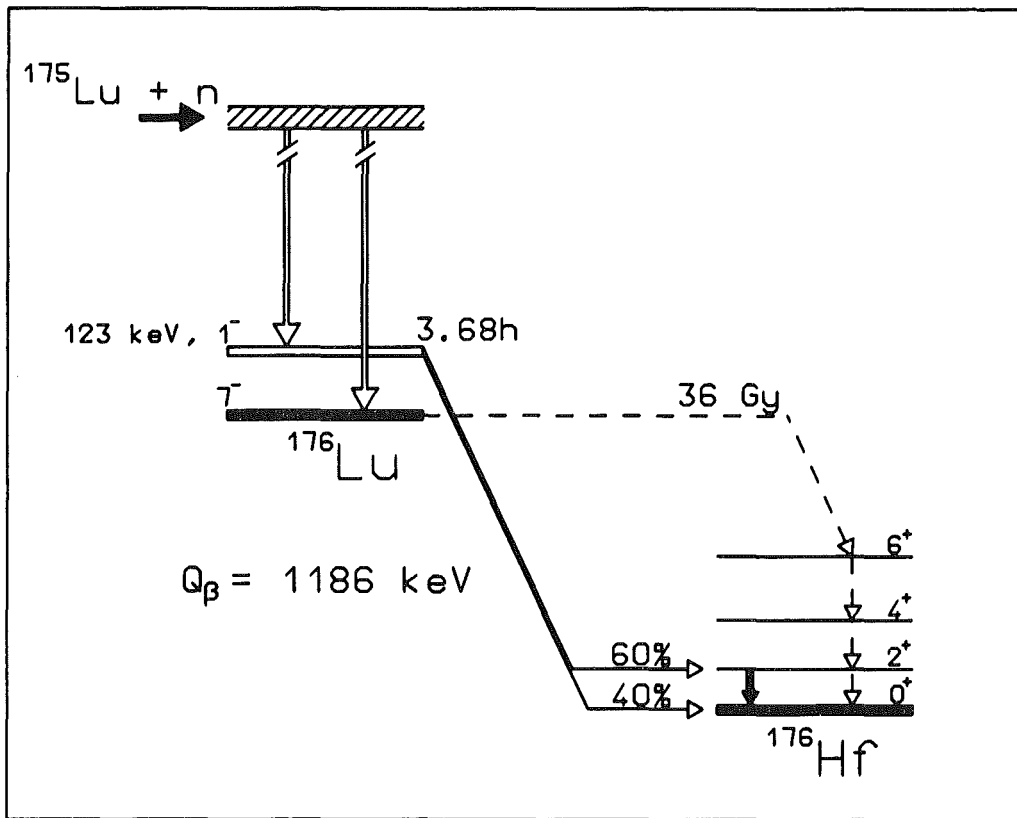
^{176}Hf

Fig. 1   Production and decay of ^{176}Lu illustrated by the schematic level schemes of ^{176}Lu and ^{176}Hf.

of ^{175}Lu determines the production cross section for the ground state. The total cross section has been determined to $\sigma_{tot}(^{175}Lu) = 1281 \pm 44$ mb at kT = 25 keV by renormalization of the value given by Bao and Käppeler (3) to the new gold cross section of Ratynski and Käppeler (4).

Previous results for the partial capture cross section $^{175}Lu(n,\gamma)^{176m}Lu$ have been renormalized to the new gold cross section (4) and are listed in Table 1. Obviously,

Table 1: Previous results for the partial neutron capture cross section of ^{175}Lu leading to the isomeric state in ^{176}Lu; the data refer to 25 keV neutron energy and are renormalized to the gold cross section of Ratynski and Käppeler (5).

Reference	Year	Stellar Cross Section (mb) (kT = 25 keV)	Probability for Feeding of Ground State (%)
(5)	1980	874 ± 49	32
(6)	1981	1244 ± 55	3
(7)	1981	1072 ± 52	16
(8)	1988	1199 ± 43	6

the various data yield very different probabilities for feeding the long-lived ground state (column 4); keeping in mind that the observed ^{175}Lu abundance at the formation of the solar system requires at least a 25% feeding probability, this means that there is no straightforward way of interpreting ^{176}Lu as an s-process chronometer, if the large partial cross sections of Refs. (6) to (8) are correct. In that case, the only explanation for the large observed abundance of ^{176}Lu were thermally induced transitions through higher lying mediating states, which could be excited at the high temperatures of the stellar plasma. Direct transitions between the isomer and the ground state are highly forbidden by selection rules due to the large difference in spin and K quantum numbers, and can be completely neglected.

In view of the above discrepancies, we have remeasured the partial ^{175}Lu cross section to the isomer in ^{176}Lu, using the activation technique in a quasi-stellar neutron spectrum at kT = 25 keV (4, 5). In order to avoid the uncertainty associated with the intensity of the 88 keV gamma transition, the activity measurement after neutron irradiation was performed via direct detection of the electrons emitted in beta decay of the isomer.

After irradiation, the induced activities of the gold samples were counted by means of a well calibrated HPGe detector (5), whereas those of the Lu foils were determined in a 4π beta spectrometer consisting of two Si(Li) detectors of 16 mm diameter in close geometry (9). An example for the measured electron spectrum is given in Figure 2. Superimposed on the smooth electron spectrum one observes a sharp line due to conversion electrons associated with the 88 keV transition from the first excited state in ^{176}Hf (Figure 1). These conversion electrons yield a characteristic signal only if the accompanying beta decay electron, that feeds the first excited state in ^{176}Hf, escapes detection in the 4π spectrometer. Hence, the
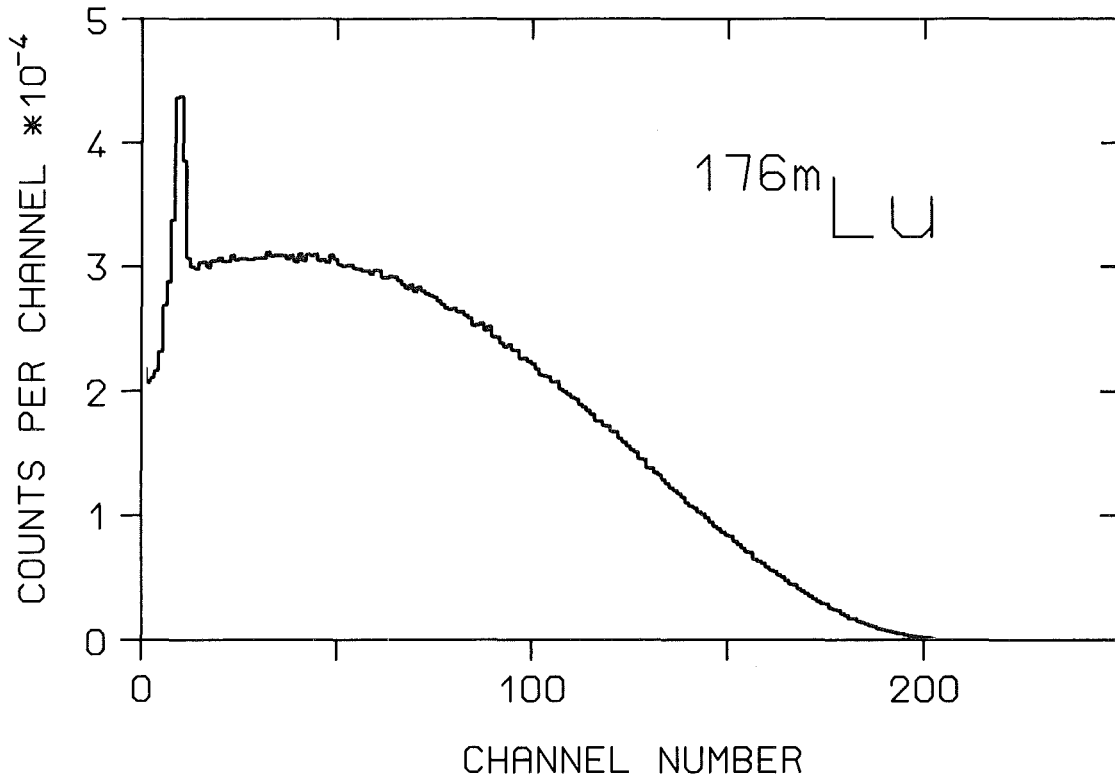
Fig. 2   Typical beta spectrum of [176mLu] measured with the 4π electron
spectrometer (6.4 keV per channel).

intensity ratio of the conversion electron line relative to the total electron
spectrum represents directly the escape probability $P_{esc} = (1-E_\beta)$.

The measured sample activities were corrected for decay during the
irradiations, absorption effects, the influence of electronic thresholds, and for
conversion electrons. The related uncertainties were carefully evaluated, yielding
cumulated total uncertainties between 2.6 and 3.1% for the five activations with
thin Lu samples. In all cases, counting statistics contribute very little to the total
uncertainties. Therefore, it was conservatively assumed that the average cross
section of 1153 ± 30 mb is also characterized by a 2.6% uncertainty, though the
mean deviation of the individual results is only 1.6%. Comparison with Table 1
shows that the uncertainty could be reduced by 40 to 80 % relative to the previous
data, and that the present result is incompatible only with the value of Ref. 6.

In order to investigate this discrepancy further, a sixth activation was
carried out using the 88 keV gamma transition for counting the induced [176mLu]
activity. In this measurement, the identical sample sandwich of gold and lutetium
foils of Ref. 5 could still be used, and the same technique was applied as described
there. The resulting cross section of 1106 ± 48 mb is in good agreement with the
activations on thin samples presented above! The only plausible explanation for

the smaller cross section of Ref. 5 could be that the previously used gamma-ray source for calibration of the detector efficiency was defect.

Combination of all activations yields finally a weighted mean stellar cross section of

$$\sigma_p\,(^{175}\text{Lu}\,) = \frac{<\sigma v>}{v_T} = 1135 \pm 30\,\text{mb} \qquad \text{for}\,kT = 25\,\text{keV}$$

corresponding to a feeding probability for the long-lived ground state of 11.4 ± 4.3% in s-process neutron captures. This confirms the result of Refs. 6, 7, 8 that the observed ^{176}Lu abundance in the solar system requires additional feeding of the long-lived ground state, for example by thermal equilibration between ground state and isomer via excitation of a mediating state in the hot stellar photon bath (see proceeding contribution 1.1.8)

(1)   J. Audouze, W.A. Fowler, C.N. Schramm, Nature **238** (1972) 8
(2)   M. Arnould, Astron. Astrophys. **22** (1973) 311
(3)   Z.Y. Bao, F. Käppeler, Atomic Data and Nuclear Data Tables **36** (1987) 411
(4)   W. Ratynski, F. Käppeler, Phys. Rev. C37 (1988) 595
(5)   H. Beer, F. Käppeler, Phys. Rev. C21 (1980) 534
(6)   B.J. Allen, G.C. Lowenthal, J.R. de Laeter, J. Phys. G7 (1981) 1271
(7)   B.J. Allen, G.C. Lowenthal, J.W. Boldeman, J.R. de Laeter, in 'Neutron Capture Gamma-Ray Spectroscopy and Related Topics', eds. T von Egidy, F. Gönnenwein, and B. Maier, IOP Conf. Series No. 62, London: The Institute of Physics (1982) p. 573
(8)   F. Stecher-Rasmussen, K. Abrahams, J. Kopecky, J. Lindner, P. Polak, P., in 'Capture Gamma-Ray Spectroscopy 1987', eds. K. Abrahams and P. van Assche, IOP Conf. Series No. 88, Bristol: The Institute of Physics (1988) p. 574
(9)   U. Ratzel, Diploma thesis, Universität Karlsruhe (1988)
*   On leave from Institute of Atomic Energy, Academica Sinica, Beijing, People's Republic of China

1.1.10   THE s-PROCESS BRANCHING AT ^{185}W AND ^{186}Re.

F. Käppeler, Z.Y. Bao*, G. Reffo, S.N. Wang*

Nucleosynthesis in the mass region between tungsten and osmium has received considerable attention, mostly due to the possible use of ^{187}Re as a chronometer for the r-process. Figure 1 illustrates the s-process flow through the W-Re-Os isotopes and the corresponding contributions from the r-process beta decay chains. Obviously, ^{186}Os and ^{187}Os are shielded against the r-process by their isobars, and hence are produced as pure s-process isotopes. However, ^{187}Os has received an additional abundance contribution from the decay of ^{187}Re, which is predominantly produced in the r-process. The s-process part of the ^{187}Os

abundance can be reliably determined as the σN values of ^{186}Os and ^{187}Os are known to be equal according to the 'local approximation'. The excess in the ^{187}Os abundance can then be ascribed to the decay of ^{187}Re, which therefore was long considered as a chronometer for the r-process (1, 2, 3).

The quantitative interpretation of the chronometer pair ^{187}Re-^{187}Os is, however, complicated by the influence of stellar temperature and pressure on the decay of ^{187}Re (4), but also by problems concerning the stellar neutron capture rate of ^{187}Os (5), and the chemical evolution of galactic material (6, 7). Apart from their importance for cosmochronometry, the isotopes ^{186,187}Os are of interest as normalization points for the s-process branchings at ^{185}W and ^{186}Re, which are indicated in figure 1. These branchings define the small s-process contribution to
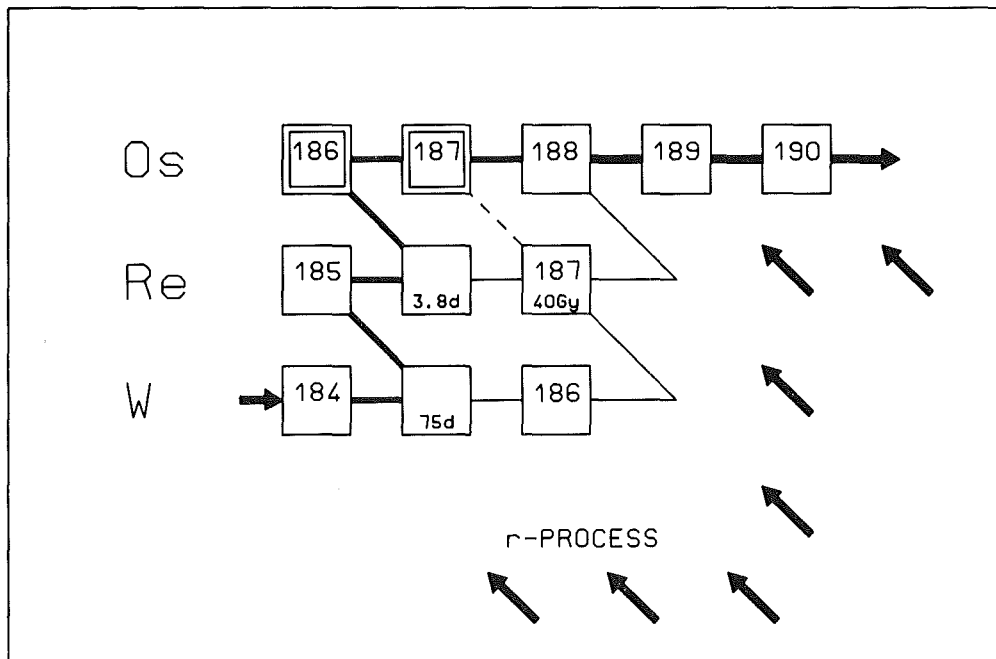
Fig. 1   The s-process flow through the W-Re-Os isotopes.

the ^{187}Re abundance, but are mainly useful for estimating the mean neutron density during the s-process. It is important in this respect that the beta decay rates of the branch point isotopes ^{185}W and ^{186}Re are almost unaffected at typical s-process temperatures (4). The main uncertainty in previous analyses of these branchings (7, 8, 9) resulted from the cross sections of the branch point isotopes. These data were obtained by statistical model calculations with a parametrization for a wide mass range (10, 11), and are estimated to be uncertain by a factor of two. Moreover, the available experimental data for the stable Re isotopes showed uncertainties of typically 10 to 20%, but differed by up to 100%. A new and accurate measurement of the stellar cross sections for ^{185}Re and ^{187}Re has

therefore been initiated in order to complete a reliable set of cross section data for the stable isotopes in the mass range of interest. In turn, these data could be used to establish and to check a consistent local parameter systematics for improved statistical model calculations for the relevant branch point nuclei [185]W and [186]Re.

The measurements were carried out at the Karlsruhe Van de Graaff accelerator via the activation technique, using the quasi stellar neutron spectrum at kT = 25 keV (12, 13). After irradiation of a sample sandwich consisting of metallic rhenium and gold foils, the induced activities were counted with a HPGe detector in a low background environment. Figure 2 shows the gamma-ray spectrum measured after irradiation of a 14.7 mg Re sample for 5.4 h. The background is mostly due to beta decay electrons and appears rather high, because the relative intensities of both gamma-ray transitions are relatively weak. Nevertheless, the signal to background ratios are high enough to allow for counting statistics well below 1%. This holds the more for the gold activity, which was determined via the 411.8 keV transition. The various uncertainties were carefully evaluated by repeated activations with systematically modified experiment parameters. The resulting cross sections are $<\sigma v>$ / v_T = 1689 ± 65 mb and 1269 ± 62 mb for [185]Re and [187]Re, respectively. The basic idea for refining statistical model calculations of neutron capture cross sections is to evaluate a local systematics of the relevant model parameters for the neighboring stable
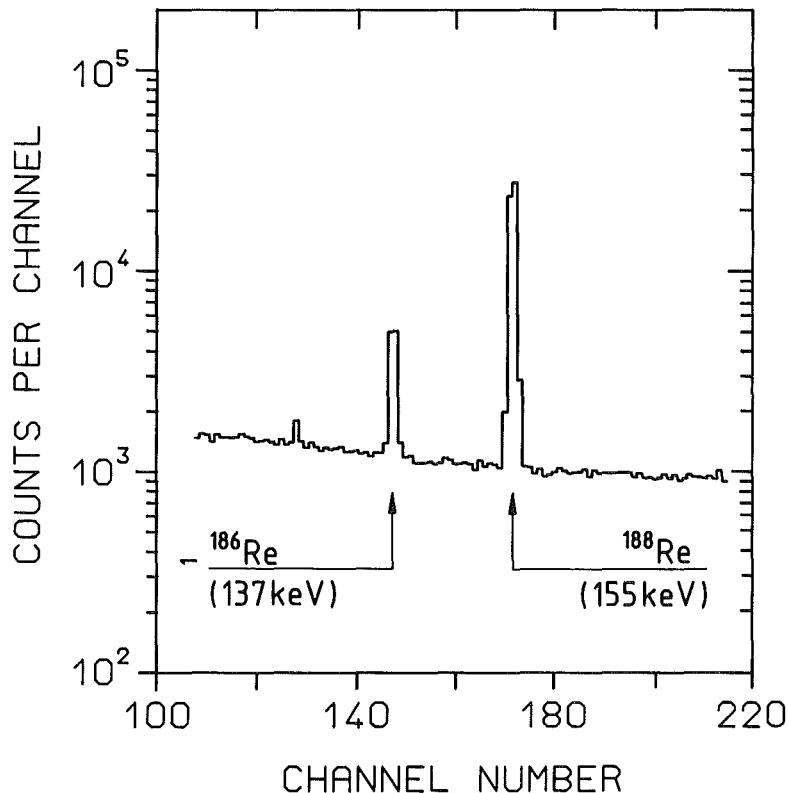
Fig. 2   Gamma-ray spectrum of a 14.7 mg Re sample measured after activation.

isotopes, including as much experimental information as possible. The concept of the adopted technique has been described previously. For the present cases the level density parameter a for the compound systems [186,188]Re was deduced from the spacing of s-wave neutron resonances, and at low excitation energies from the respective level schemes. Spin and parity distributions were also carefully considered, and the so obtained parametrization has been tested by comparison of the calculated average radiative widths at the neutron binding energy with experimental values. An uncertainty of 20% was estimated for the calculated cross sections by considering the uncertainties in the involved parameters.

With the new information on the relevant cross sections, the s-process branchings at [185]W and [188]Re have been reanalyzed in terms of the classical approach. The deduced s-process neutron density of

$$n_n = (3.5^{+1.7}_{-1.1}) \cdot 10^8 \, cm^{-3}$$

is in good agreement with other branchings in the mass range A < 100 (14).

(1)   E.M.D. Symbalisty, D.N. Schramm, Rep. Prog. Phys. 44 (1981) 293
(2)   J.C. Browne, B.L. Berman, Phys. Rev. C23 (1981) 1434
(3)   R.R. Winters, R.L. Macklin, Phys. Rev. C25 (1982) 208
(4)   K. Takahashi, K. Yokoi, Atomic Data and Nuclear Data Tables 36 (1987) 375
(5)   R.R. Winters, R.F. Carlton, J.A. Harvey, N.W. Hill, Phys. Rev. C34 (1986) 840
(6)   K. Yokoi, K. Takahashi, M. Arnould, Astron. Astrophys. 117 (1983) 65
(7)   M. Arnould, K. Takahashi, K. Yokoi, Astron. Astrophys. 137 (1984) 51
(8)   H. Beer, G. Walter, R.L. Macklin, P.J. Patchett, Phys. Rev. C30 (1984) 464
(9)   H. Beer, R.L. Macklin, Ap. J. 331 (1988) 1047
(10)   J.A. Holmes, S.E. Woosley, W.A. Fowler, B.A. Zimmerman, Atomic Data and Nuclear Data Tables 18 (1976) 305
(11)   M .J. Harris, Astrophys. Space Sci. 77 (1981) 357
(12)   H. Beer, F. Käppeler, Phys. Rev. C21 (1980) 534
(13)   W. Ratynski, F. Käppeler, Phys. Rev. C37 (1988) 595
(14)   F. Käppeler, R. Gallino, M. Busso, G. Picchio, C.M. Raiteri, Ap. J. (1990) (in press)
*   On leave from the Institute of Atomic Energy, Academica Sinica, Beijing, People's Republic of China

1.1.11   RADIOGENIC [207]Pb FOR THE [235]U CLOCK
H. Beer

Since the first thorough analysis of radiogenic [207]Pb by Beer and Macklin (1) many new informations are available which make a reanalysis necessary:

1. A new compilation of solar abundances has been published (2) and a measurement of the solar Pb-abundance via the spectrum of the sum has been carried out (3).

2. The values for the s-process neutron density and temperature had to be increased (4) due to new estimates for important cross sections and effective half lives (5) of branch point isotopes. As a consequence additional branchings may become significant so that the useful number of normalization points for the adjustment of the σN-curve has to be reduced and the solar Pb-abundance determined via s-only ^{204}Pb becomes slightly dependent on the neutron density and temperature.

3. The cross sections of fundamental nuclides ^{122,123,124}Te (6) and ^{208}Pb (7) have been measured with improved accuracy.

4. New investigations of the properties of the total energy detector (8) show that the Maxwellian averaged ^{207}Pb capture cross section reported by Allen et al. (9) must be reduced. We have calculated a new value [$\sigma(^{207}$Pb) = (8.91 $\pm$ 0.44) mb] using the measured resonance parameters of Köhler et al. (10). This reduction leads to a larger s-process abundance for ^{207}Pb and makes a reasonable ^{235}U age calculation feasible.

The analysis required an improved new s-process calculation of the main and strong (11) s-process components including all branchings of unstable isotopes of half lives $\geq$ 10d. From these calculations the part of the σN(A) curve at Pb and Bi is plotted in Fig. 1.

In addition to the composite curve also the main component alone is shown to demonstrate that especially for the reproduction of ^{208}Pb the high exposure component is needed. For ^{207}Pb not only the current empirical data point is plotted in Fig. 1 (left) but also the value one obtains with the old ^{207}Pb (9) capture cross section (open symbol). Both data points are significantly above the s-process curve, but only with the current empirical value a meaningful ^{235}U age is obtained. The s-process calculation displayed in Fig. 1 (right) shows that in contrast to ^{206}Pb, ^{207}Pb is only negligibly affected by the branchings at ^{210}Bi and ^{210}Po.

In order to obtain the radiogenic component, ^{207}Pb$_c$, we have to subtract from the solar abundance ^{207}Pb$_O$,the main and strong s-process components, ^{207}Pb^M_s and ^{207}Pb^S_s, and the total r-process component, ^{207}Pb^t_r

$$^{207}\text{Pb}_c = {}^{207}\text{Pb}_O - {}^{207}\text{Pb}^M_s - {}^{207}\text{Pb}^S_s - {}^{207}\text{Pb}^T_r = (0.95 \pm 0.45)/10^6\text{Si}.$$

This result corresponds to

$$^{207}\text{Pb}_c / {}^{235}\text{U} = 16.6 \pm 8.0$$

^{207}Pb^t_r is determined via

$$209\text{Bi}^t_r = 209\text{Bi}_O - 209\text{Bi}^M_S - 209\text{Bi}^S_S$$

and the assumption that $207\text{Pb}^t_r = 209\text{Bi}^t_r$. Cowan (12) found in his calculations that this quantity is very insensitive to a variation of the input parameters. Without quantitative results of r-process calculations one would deduce simply $207\text{Pb}^t_r = (7/12)^{209}\text{Bi}^t_r$ taking into account the number of different transbismuth
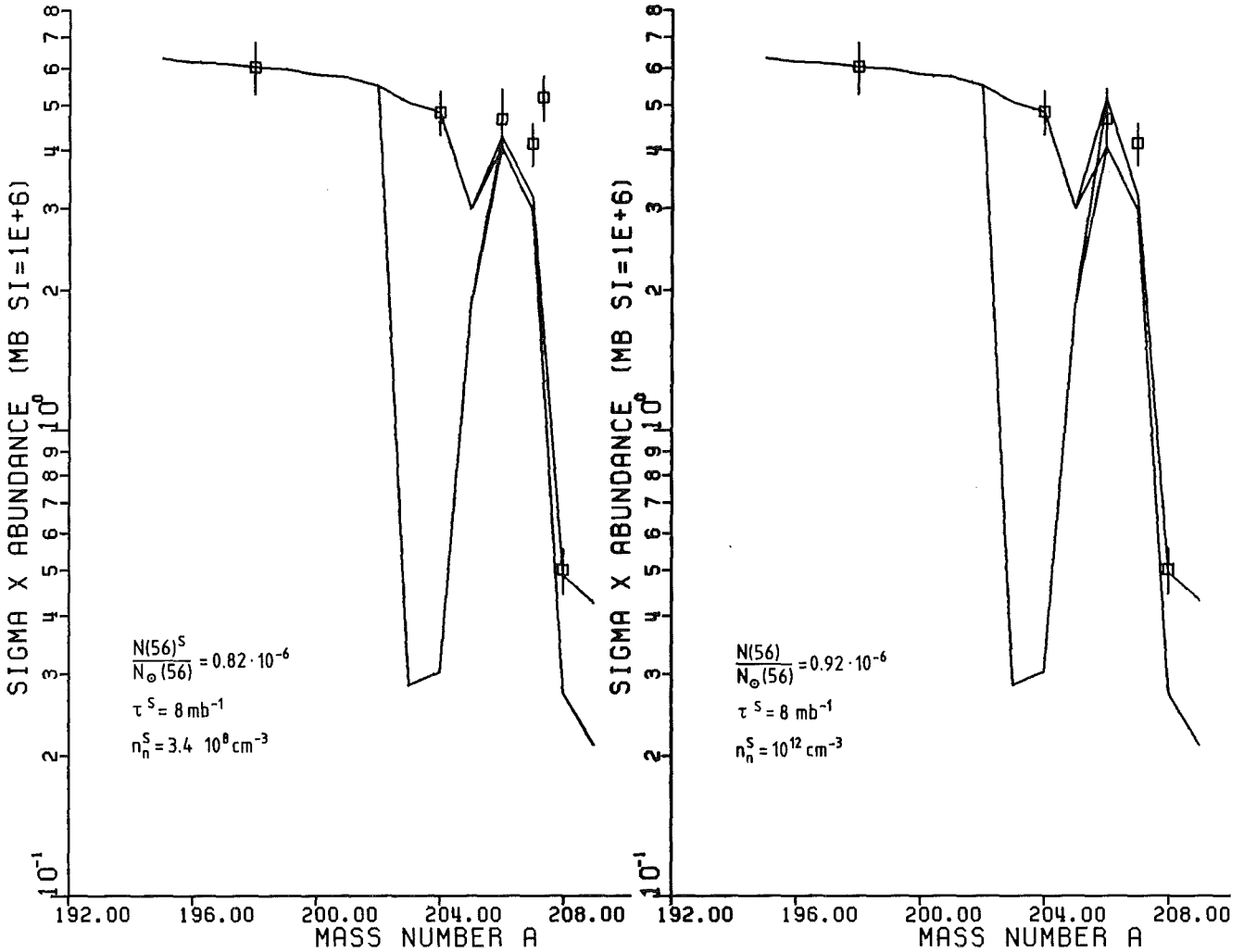
Fig. 1   A section of the σN(A) curve at s-process termination: The left and right plot differ with regard to the neutron density of the high exposure component. For the assumed neutron density of the right plot the ^{210}Bi and ^{210}Po branchings become significant. The net effect is that the abundance of ^{206}Pb contains a sizeable abundance fraction from ^{210}Bi and ^{210}Po.

progenitors. This would result in a larger radiogenic 207Pb_c component. It is important to note that the present method of determining 207Pb^t_r is very insensitive to the neutron density of the strong component. For our assumed extreme assumption, Fig. 1 (right), we obtain for $207\text{Pb}_c = (0.101 \pm 0.044)/10^6\text{Si}$. As 207Pb^S_S is relatively small and of the same size as 209Bi^S_S our result is, in fact,

also relatively independent of the real existence of a strong s-process component. Without strong component we calculate $^{207}Pb_c$ = (0.099 ± 0.044)/10^6Si.

The ^{235}U age is strongly dependent on the chemical evolution of our Galaxy. In Clayton's (13) linear models our result would predict a lower bound for the galactic age T_G > 12 Gyr. But there is also evidence that it may be inadequate to use linear models of star formation (14).

It should be stressed that meteoritic Pb_0 = 3.15 ± 0.24)/10^6Si (2) would lead to an unrealistic high ^{235}U age additionally to the discrepancy with the $\sigma N(A)$ curve at A = 204, whereas Pb_0 =(2.62 ± 0.19)/10^6Si determined in this work is in agreement with the photospheric value (3).

(1)   H. Beer, R.L. Macklin, Phys. Rev. **C32** (1985) 738
(2)   E. Anders, N. Grevesse, Geochim. Acta **53** (1989) 197
(3)   N.H, Youssef, N.M. Khalil, Astron. Astrophys. **208** (1989) 271
(4)   F. Käppeler, R. Gallino, M. Busso, G. Picchio, C.M. Raiteri, Ap. J. (1990) (in press)
(5)   K.T. Lesko, E.B. Norman, R.M. Larimer, J.C. Bacelar, E.M. Beck, Phys.Rev. **C39** (1989) 619
(6)   R.L. Macklin, private communication
(7)   U. Ratzel, Diploma thesis, Universität Karlsruhe (1988)
(8)   F. Corvi, A. Prevignano, H. Liskien, Nucl. Instr. and Meth. **A265** (1988) 475
(9)   B.J. Allen, R.L. Macklin, R.R. Winters, C.Y. Fu, Phys. Rev.**C8** (1973) 1504
(10)   R. Köhler, J.A. Wartena, H. Weigmann, L. Mewissen, F. Poortmans, J.P. Theobald, Phys. Rev. **C35** (1987) 1646
(11)   D.D. Clayton, M.E. Rassbach, Ap. J. **148** (1967) 69
(12)   J.J. Cowan, private communication
(13)   D.D. Clayton, Mon. Not. R. Astr. Soc. **234** (1988) 1
(14)   B.E.J. Pagel, in 'Evolutionary Phenomena in Galaxies', Puerto de la Cruz, Tenerife, eds. J. Beckmann, B.E.J. Pagel, Cambridge University Press (1988)

1.1.12   THE KARLSRUHE 4π BARIUM FLUORIDE DETECTOR

K. Wisshak, K. Guber, F. Käppeler, J. Krisch, H. Müller, G. Rupp, F. Voß
(1)

A new experimental method has been implemented for accurate measurements of neutron capture cross sections in the energy range from 3 to 200 keV. The Karlsruhe 4π Barium Fluoride Detector is used for the determination of the neutron capture cascade. It consists of 42 crystals shaped as hexagonal and pentagonal truncated pyramids forming a spherical shell with 10 cm inner radius and 15 cm thickness. All crystals are supplied with reflector and photomultiplier

thus representing independent gamma ray detectors. Each detector module covers the same solid angle with respect to a gamma ray source located in the centre.

The energy resolution for the sum energy signal of the 4π detector is 14% at 662 keV and 7% at 2.5 MeV gamma ray energy, the time resolution is 500 ps and the peak efficiency 90% at 1 MeV. This unique combination for a gamma ray detector became possible with the availability of large barium fluoride crystals with volumes up to 2.5 l. The detector allows to register capture cascades with 95% probability above a threshold energy of 2.5 MeV in the sum energy spectrum.

Neutrons are produced via the ^{7}Li(p,n)^{7}Be reaction using the pulsed proton beam of a Van de Graaff accelerator. The neutron spectrum can be taylored according to the experimental requirements in an energy range from 3 to 200 keV by appropriate settings of the proton energy. A collimated neutron beam is guided through the detector hitting the sample in the centre. The energy of captured neutrons is determined via time of flight at a flightpath of 77 cm.

The combination of short flightpath, a 10 cm inner radius of the BaF$_2$ detector, good energy resolution, and the low capture cross section of barium allows to discriminate background due to capture of sample scattered neutrons in the scintillator by time of flight, leaving part of the neutron energy range completely undisturbed. This feature together with the high efficiency and good energy resolution for capture gamma rays allows to reliably separate the capture events from various sources of background. In this way it is possible to determine the capture cross section ratio of two isotopes with an uncertainty of the order of 1%.

The detector will be used for astrophysical applications to investigate the nucleosynthesis of the heavy elements in the so called s-process.

(1)   Report KfK 4652, Kernforschungszentrum Karlsruhe (1989)
        (submitted for publication in Nucl. Instr. and Meth.)

1.1.13   A NEW APPROACH FOR HIGH PRECISION MEASUREMENTS
         OF NEUTRON CAPTURE CROSS SECTIONS IN THE keV
         NEUTRON ENERGY RANGE : NEUTRON CAPTURE OF
         NIOBIUM, RHODIUM AND TANTALUM RELATIVE TO A
         GOLD STANDARD

K. Wisshak, F. Voß, F. Käppeler, G. Reffo*

A new experimental method has been implemented for high precision measurements of neutron capture cross sections in the energy range from 5 to 200 keV.

Neutrons are produced via the 7Li(p,n)7Be reaction using a pulsed 3 MV Van de Graaff accelerator. The neutron energy is determined by the time of flight technique using a flightpath of less than 1 m. Capture events are detected with the Karlsruhe 4π Barium Fluoride Detector. This detector combines a gamma ray energy resolution of 14% at 662 keV and 7% at 2.5 MeV and a time resolution of 500 ps with a peak efficiency of 90% at 1 MeV. Capture events are registered with ~95% probability above a gamma ray threshold of 2.5 MeV.

The combination of short flight path, 10 cm inner radius of the detector and low capture cross sections of BaF_2 allows to discriminate background due to capture of sample scattered neutrons in the scintillator material by time of flight leaving part of the neutron energy range completely undisturbed. The high efficiency and good energy resolution for capture gamma rays allows to reduce this background further by selecting appropriate energy channels for data evaluation.
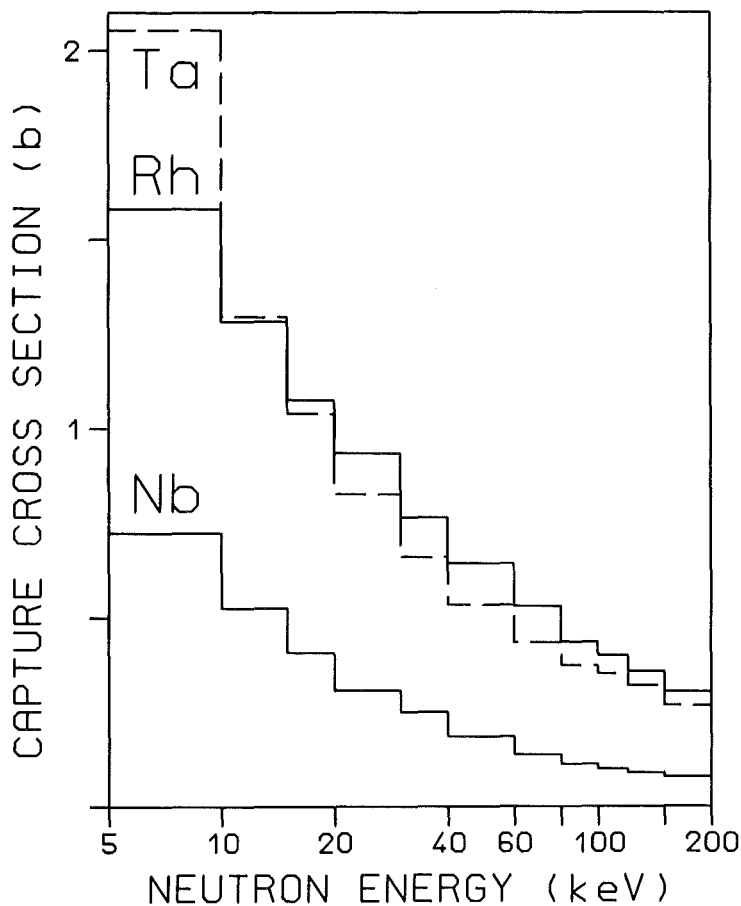
Fig. 1   The neutron capture cross sections of 93Nb, 103Rh and 181Ta in the energy range fom 5 to 200 keV.

The first test measurements were made on ^{93}Nb, ^{103}Rh and ^{181}Ta; neutron capture cross sections were determined in the energy range from 5 to 200 keV relative to a gold standard. The cross section ratio could be determined with an overall systematic uncertainty of 0.7 - 0.8% and a statistical uncertainty of less than 1% in the energy range from 20 to 100 keV if the data are combined in 20 keV wide bins. The necessary sample masses were of the order of one gram. The accuracy of the experimental method will be further increased and simultaneously the required sample mass will be reduced by several improvements already implemented or under development.

In Fig. 1 values for the absolute cross sections are plotted that are obtained by multiplying the experimental ratio with the gold cross section known from literature. The uncertainty of these values is dominated by the 1.5% uncertainty in the absolute normalization by the gold cross section.

*   ENEA, Bologna, Italy

1.1.14   s-PROCESS NUCLEOSYNTHESIS : CLASSICAL APPROACH AND AGB-MODELS FOR LOW MASS STARS

F. Käppeler, R. Gallino*, M. Busso**, G. Picchio**, C.M. Raiteri***

A critical comparison is made between the results on s-process nucleosynthesis obtained with the phenomenological classical approach and a stellar model for helium shell burning in low mass stars.

In the classical model, the stellar environment is simplified to the point that, in the first instance, any time dependence for temperature and neutron density is neglected. By this simplification, the classical approach offers an empirical tool that not only can describe the observed s-process abundances, but can also provide estimates for mean physical conditions during the s-process. Being completely independent of stellar models., the classical approach can be used to constrain the results obtained with those models. This is an important fact, because stellar models are plagued by many parameters due to the complexity of stellar structure during the late stages of evolution. Further constraints to stellar models come from the prescriptions of galactic chemical evolution and from spectroscopic observations of evolved red giants.

In stellar models, s-process studies follow evolutionary calculations in detail, analyzing the nucleosynthesis induced by the time-dependent physical conditions through a complete network of nuclear reactions. From this point of view, numerous investigations over the past year dealt with the contributions
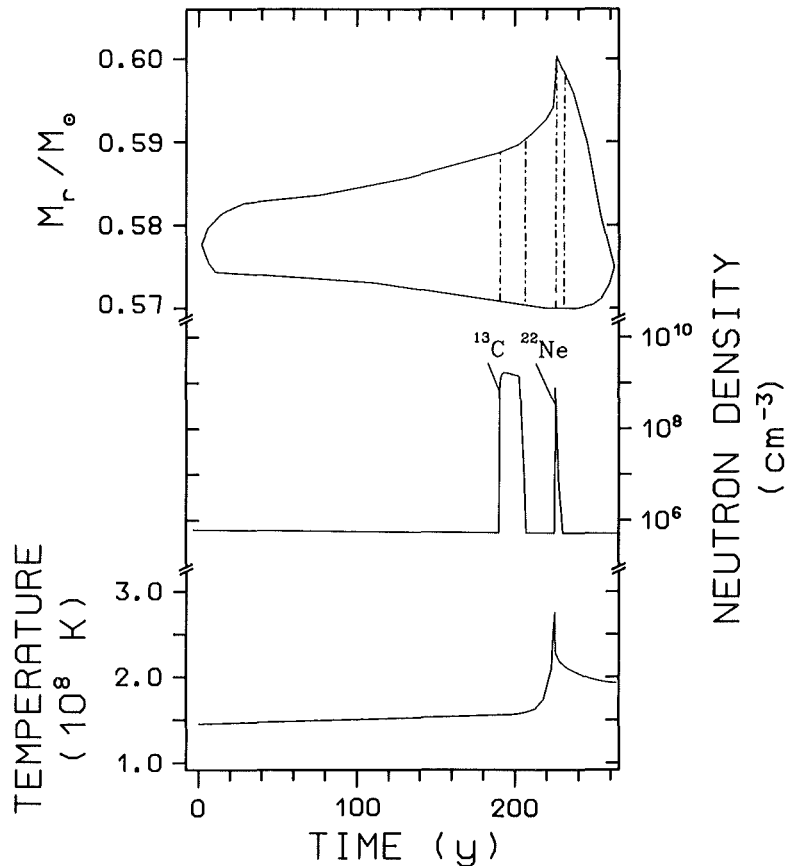
Fig. 1   Top: Typical development of the convective region during a thermal instability of the helium shell. Mid: The two neutron bursts of the LMS model originating from the ^{13}C and ^{22}Ne sources. Bottom: Time dependence of the maximum temperature in the shell.

from various neutron capture episodes occurring during helium burning stages in stars of different mass.

For the production of the bulk of the s-process nuclei with mass numbers $A > 90$ (the so-called main component), operation of the $^{13}C(\alpha,n)^{16}O$ neutron source in thermal pulses of low mass stars (LMS) of rather low metallicity seems to be at present the most promising scenario (1,2,3). In fact, it appears to reproduce the observed abundances in the solar system and in evolved stars as well as to satisfy the main constraints imposed by the chemical evolution of the Galaxy (4). However, this is accomplished through a complex mechanism, in which both, temperature and neutron density, exhibit strong variations during thermal pulses as illustrated in Figure 1. At first sight, these physical conditions appear to be very different from those of the classical approach.
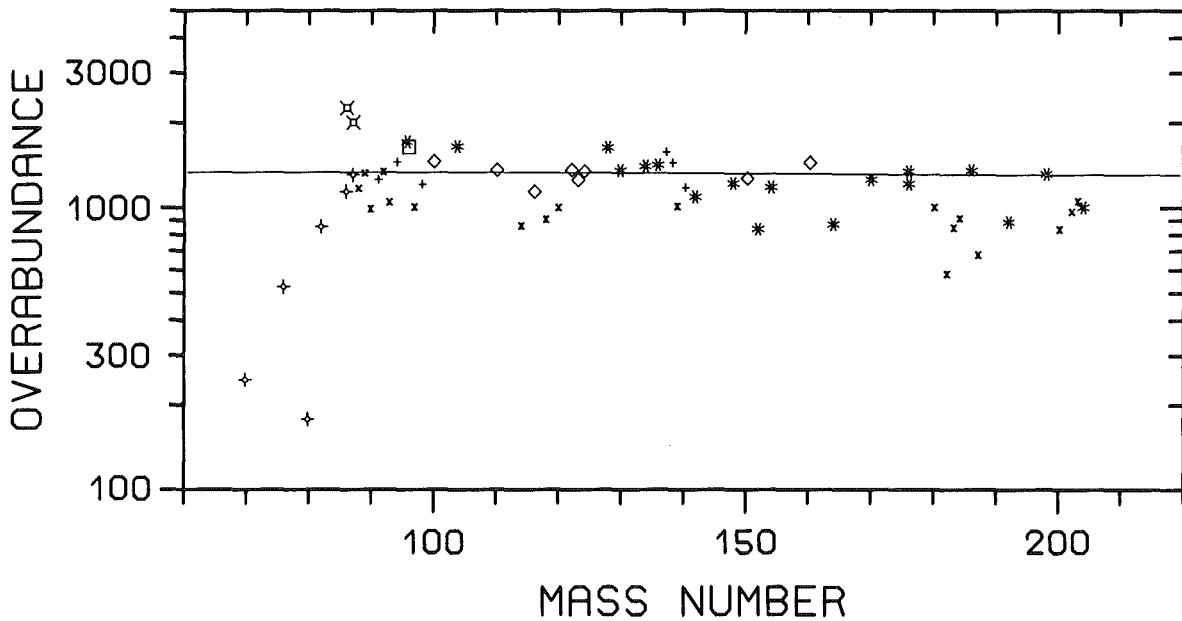
Fig. 2 The overabundances calculated with the LMS model. The s-only isotopes are indicated by stars and diamonds; the latter are not affected by branchings and can therefore be used to define the mean overabundance (solid line). Other symbols denote relative s-process contributions of $\geq 80\%$ ($+$), and 60 to 80% (x), according to Ref. (5). The largest overabundances are observed for ^{96}Zr (square) and $^{88}Kr/^{87}Rb$ ( ); the underabundant s-isotopes with A <90 and ^{187}Os receive additional contributions from other nucleosynthesis processes.

The abundances calculated with the LMS model are found in good agreement with the s-process yields observed in solar material as can be seen from the constancy of the overproduction factors plotted in Figure 2.For the first time, close agreement is found between the abundances determined by the classical analysis and the results of a stellar model. Despite the conceptual differences between the steady approximation of the classical approach and the dynamical environment of thermal pulses in low mass stars the results of both models are quite similar, but still obscured by the present uncertainties of the nuclear input data; further improvements are required to quantify the trends of the true physical conditions during the s-process which start to emerge from the above studies.

(1)   I. Iben Jr., A. Renzini, Ap. J. Lett., **259** (1982) L79
(2)   I. Iben Jr., A. Renzini, Ap. J. Lett., **263** (1982) L23
(3)   D.E. Hollowell, I. Iben Jr., Ap. J. Lett. **333** (1988) L25
(4)   R. Gallino, M. Busso, G. Picchio, C.M. Raiteri, Ap. J. Lett. **334** (1988) L45
(5)   F. Käppeler, H. Beer, K. Wisshak, Rep. Prog. Phys. **52** (1989) 945

*   Istituto di Fisica Generale dell' Università di Torino, Italy
**   Osservatorio Astronomico di Torino, Italy
***   International School for Advanced Studies, Trieste, Italy

1.1.15   s–PROCESS NUCLEOSYNTHESIS – NUCLEAR PHYSICS AND THE CLASSICAL MODEL

F. Käppeler, H. Beer, K. Wisshak (1)

Among the various processes responsible for the formation of the heavy elements in stars, the slow neutron capture process (s-process) is distinguished by the fact that it involves mostly stable isotopes. Therefore, the relevant nuclear physics data can be determined by experiments. With this rather reliable data basis, s-process nucleosynthesis offers an important testground of models for the late stages of stellar evolution, which are supposed to be the s-process site. The empirical counterpart for such models is the so-called classical s-process, a purely phenomenological picture, that is successfully used to derive the resulting abundances as well as information on the physical conditions during the s-process. The status of this classical approach is reviewed with emphasis on the implications for various stellar models of the s-process and in the light of results obtained by stellar spectroscopy. A brief account of the potential s-process chronometers is also presented.

(1)   Rep. Prog. Phys. 52 (1989) 945

1.1.16   NEUTRON CAPTURE RATES FOR STELLAR NUCLEOSYNTHESIS

F. Käppeler (1)

The quantitative description of neutron capture nucleosynthesis requires the neutron capture cross sections of all involved isotopes. Only with this data base the observed abundances can be interpreted in terms of the physical conditions prevailing at the respective stellar sites. In this contribution, importance and status of stellar capture rates for the s- and r-process are outlined. The role of model calculations is emphasized as an essential complement to laboratory measurements, e.g. for determining the cross sections of short-lived isotopes that are not accessible to present experimental techniques as well as for describing the influence of temperature. The latter may cause the stellar rate to deviate

significantly from laboratory values. Possible experimental improvements are discussed in connection with new developments in detector techniques and neutron sources.

(1)   Nuclear Data for Science and Technology
        ed. S. Igarasi, Tokyo : Saikon Publ. (1988) p. 1107

1.1.17   NUCLEAR EXCITATION AND STELLAR TEMPERATURE

F. Käppeler (1)

The chemical elements in nature are the products of stellar burning processes. If the underlying nuclear physics is sufficiently known, it may be possible to decipher the respective nucleosynthesis mechanisms, e.g. the production of the heavy elements by slow neutron capture (s-process).

The observed abundance patterns can be strongly affected by temperature because beta decay rates and capture cross sections may become temperature dependent via significant population of excited nuclear states in the hot stellar photon bath; in turn, this allows to derive estimates for the temperature. The status of such analyses is presented with particular emphasis on the example of [79]Se. The results of the (empirical) classical model constitute important constraints for stellar models of helium burning zones in Red Giant stars.

The long-lived radioisotope [176]Lu represents a potential cosmic clock for the age of the s-process elements. For some time it is suspected that the decay of [176]Lu was temporarily enhanced and that this clock is therefore misadjusted. In spite of several attempts, this enhancement is not yet understood quantitatively.

(1)   Capture Gamma-Ray Spectroscopy 1987
        eds. K. Abrahams and P. Van Assche, Bristol: Inst. of Phys., Conf. Ser.
        No. 88 / J. Phys. G 14 Suppl. (1988) p. S297

1.1.18   COMPRESSION MODULUS

P. Doll

The compression modulus K presented in the previous annual report (1) and indicated as quasi nucleon has been derived from the spreading and strength of single-particle states in light nuclei. Since these states are mainly single-particle plus vibrational in character, a dynamical coupling between the surface and bulk vibrations is expected. We find that k varies with the spreading width Γ of the

single-particle strength ($K \sim \Gamma^{-2}$), see fig. 1, which can extend to high excitation energy. Therefore, our number may represent an upper limit for light nuclei
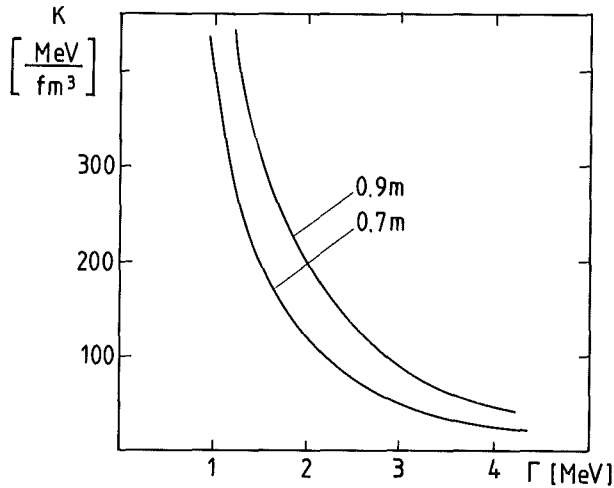
Fig. 1
Compression modulus
K versus spreading
width Γ.

which have a comparatively large surface contribution. The importance of K as the stiffness of the nuclear matter equation of state (EOS) is of current interest. There are basically two different suggestions, one advocates a "stiff" EOS with a $K \sim 300$ MeV, while the other a soft one with $K \sim 120$ MeV (2). The soft EOS is also predicted by Dickhoff et al. (3) using the Bonn potential. Very recent studies (4) of several EOS for rapidly rotation neutron stars sharpened the constraints on the EOS. The frequency observed for a neutron star in SN 1987 A seems to favour smaller K values. However the frequency is near to the termination point (4) where the star is unstable against radical oscillations, favouring than a stiff EOS above nuclear density. The Reynold number for extended nuclear matter like neutron stars can be very large.

(1)   P. Doll, Report KfK 4508, Kernforschungszentrum Karlsruhe (1989)
        p. 29
(2)   G.E. Brown, E. Osnes, Phys. Lett. **159B** (1985) 225
(3)   W.H.Dickhoff, A.Faessler, H.Müther, S.S.Wu, Nucl.Phys. **A405**
        (1983) 534
(4)   J.L. Friedmann, J.R. Ipser, L. Parker, Phys. Rev. Lett. **62** (1989) 3015

1.2   NEUTRON SCATTERING

1.2.1   RESULTS ON THE H($\vec{n}$,γ)^{2}H CAPTURE EXPERIMENT

P. Doll, G. Fink, S. Hauber, M. Haupenthal, H.O. Klages, H. Schieler,
F. Smend*, G.D. Wicke*

Recent studies of the ^{2}H(γ,n)H reaction (1, 2) and the inverse process have indicated that besides meson exchange current (MEC) corrections even the basic reaction mechanism is not fully understood already at low photon energies. Therefore, we performed a neutron-proton capture experiment (3) using polarized neutrons between 18 and 50 MeV. Our set-up is described in a previous annual report and in a forthcoming report (3). We used a scintillating target (NE213) allowing simultaneous measurement of neutron - proton and neutron - carbon capture (see 1.2.3). Fig. 1 shows the pulse height resolution in the target for recoiling deuterons arising from neutron-proton capture. The pulse height resolution turned out to be sufficient (~ 16 %) to separate recoil events from multiple scattering events in the target. The evaluation of the photon yields is performed in the NaI spectra, supported by pulse-shape discrimination technique in the NaI crystal (4) and the flight-time measurement between the capture target and the NaI-detector. The relative efficiency of the NaI detectors at 55°, 90° and 125° in the laboratory system was determined through the angular distribution of the decay of the 15.1 MeV state in ^{12}C. Fig. 2 shows the angular distributions of the differential cross sections for various incident
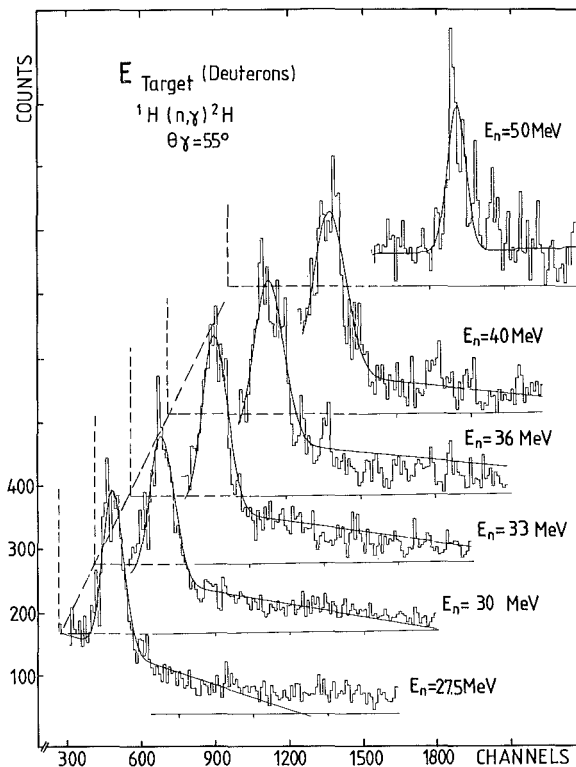
Fig. 1 Pulse height spectra of recoil deuterons for various incident neutron energies.

neutron energies. The absolute cross sections are based on total capture and disintegration cross sections related through the detailed balance. Fig. 2 shows Legendre fits to the data and as dashed curves extensive theoretical calculations, by P. Wilhelm et al (5). The cross sections for $0°$ and $180°$ were taken for the Legendre fit in the range as known in the literature. The angular distributions exhibit only a smooth variation of the forward - backward asymmetry as function of neutron energy revealing a small admixture of higher multipole transitions. Analyzing powers at the three scattering angles were measured simultaneously. Very preliminary results have been given in the previous annual report. Our results compared to data from ref. 1, 2 for $\Theta = 90°$ seem to indicate slightly larger analyzing powers in the present experiment, after considering multiple scattering effects in the target.
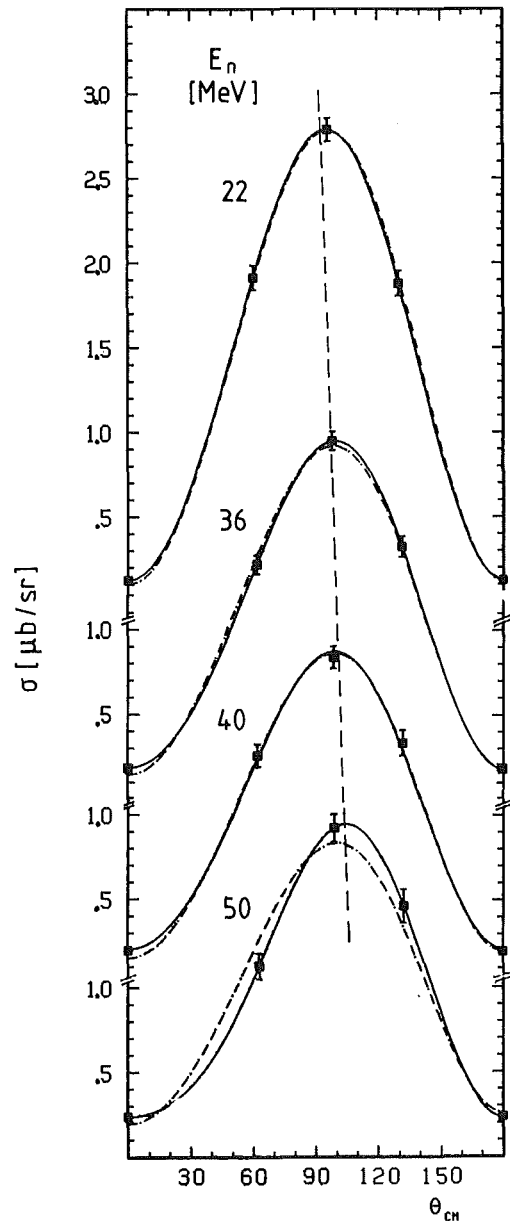
Fig. 2 Angular distributions of differential cross sections for $^1H(n,\gamma)^2H$ at $E_n = 50$, 40, 36 and 22 MeV.

(1)   J.P. Soderstrum, L.D. Knutson, Phys. Rev. C35 (1987) 1246
(2)   R.J. Holt, K. Stephenson, J.R. Specht, Phys. Rev. Lett. 50 (1983) 5
(3)   G. Fink, P. Doll, S. Hauber, M. Haupenthal, H.O. Klages, H. Schieler, F. Smend, G.D. Wicke, Report KfK 4405, Kernforschungszentrum Karlsruhe (1987) p. 29 and to be published
(4)   P. Doll, G. Fink, R.W. Finlay, S. Hauber, M. Haupenthal, H.O. Klages, H. Schieler, F. Smend, G.D. Wicke, Nucl. Instr. and Meth.285(1989)464
(5)   P. Wilhelm, W. Leidemann, H. Arenhövel, private communication (1989)
*   II. Physikalisches Institut, Universität Göttingen, Germany

1.2.2 ñ + ^{3}He - RADIATIVE CAPTURE TO ^{4}He

P. Doll, G. Fink, S. Hauber, W. Heeringa, H.O. Klages, H. Schieler,
F. Smend*, G.D. Wicke*

The photodisintegration of ^{4}He and the inverse reactions have been of great interest for some time. However, no information so far has been obtained for the analyzing power of the photodisintegration at high excitation energies in ^{4}He. With our set-up of 3 large NaI-detectors at 55°, 90° and 125° in the laboratory system at the Karlsruhe cyclotron (1) we measured polarized neutron capture on ^{3}He from 19 to 50 MeV using a scintillating liquid ^{3}He-target. At these high energies we are not able to clarify the long standing discrepancy between photo-proton and photo-neutron cross sections on ^{4}He, related to the existence of charge symmetry violation of nuclear forces in the A = 4 system (2).
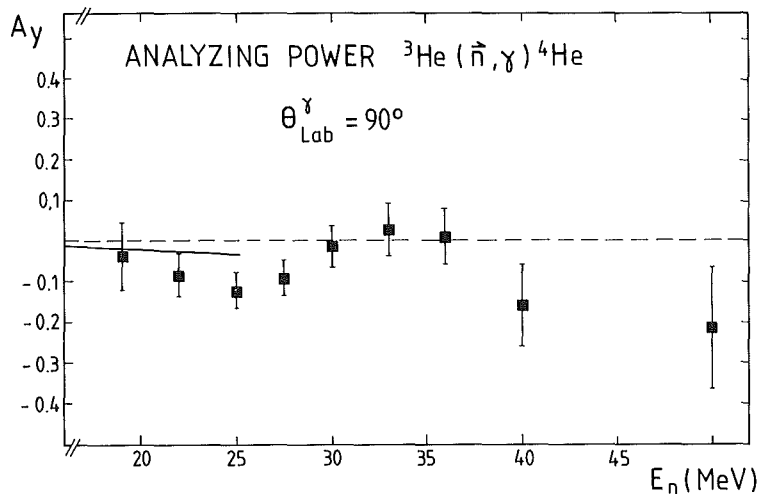
Fig. 1
Analyzing power of
the reaction
^{3}He(ñ,γ)^{4}He for
neutron energies
from 19 to 50 MeV.

However, the experiment should provide valuable information on high multipoles in ^{4}He at high excitation energies ranging from 35 to 58 MeV. These are characterized by interfering amplitudes exhibiting structures in the excitation function of the (ñ,γ) analyzing powers and forward-backward asymmetries (3). Our preliminary results for the 90° analyzing power are given in fig. 1 exhibiting a pronounced variation as a function of the neutron energy. Also included is as solid line the variation of the $B_1 = 3/2 \cdot A_y(\Theta^{cm} = 90°)$ coefficient, which is mostly responsible for the 90° analyzing power, from unpublished clustermodel calculations of the Erlangen group (4). It would be interesting to have other independent theoretical predictions extending to larger excitation energies in ^{4}He.

(1)   S. Hauber, P. Doll, G. Fink, M. Haupenthal, W. Heeringa, H.O. Klages, H. Schieler, F. Smend, G.D. Wicke, Report KfK 4508, Kernforschungs-zentrum Karlsruhe (1988) p. 34
(2)   B. Wachter, T. Mertelmeier, H.F. Hofmann, Phys. Rev. C38 (1988) 1139
(3)   H.R. Weller, N.R. Roberson, G. Mitev, L. Ward, D.R. Tilley, Phys. Rev. C25 (1982) 2111
(4)   H.M. Hofmann, private communication (1989)
*   II. Physikalisches Institut, Universität Göttingen, Germany

1.2.3 CAPTURE OF POLARIZED NEUTRONS BY ^{12}C BETWEEN 20 AND 50 MeV

G.D. Wicke*, F. Smend*, P. Doll, G. Fink, S. Hauber, M. Haupenthal, H.O. Klages, H. Schieler

With the experimental set-up described in (1), the experiments on the ^{12}C(n,γ) capture reaction were continued. Fig. 1 shows a gamma spectrum from neutron capture in the NE 213 scintillator at a neutron energy of (35 ± 1) MeV.
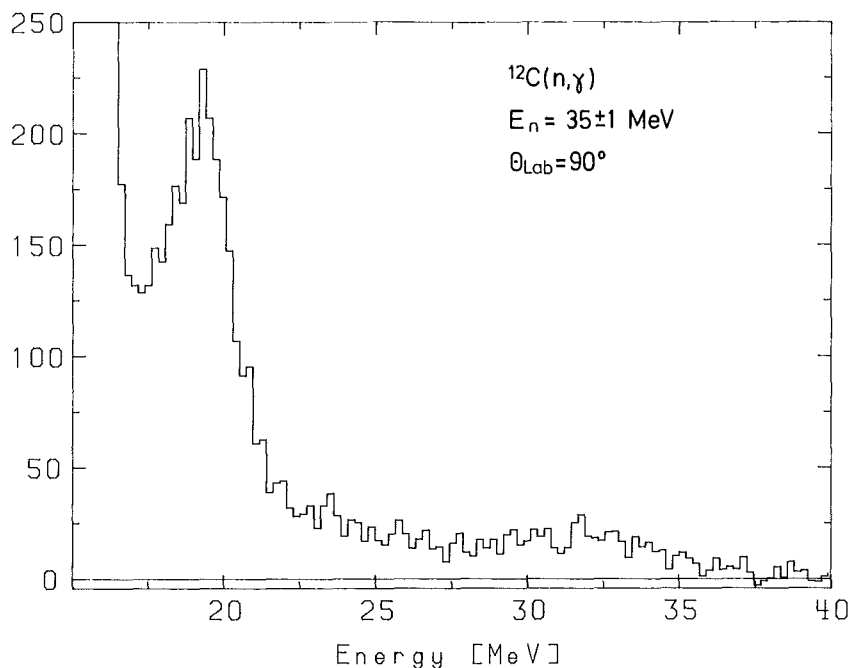
Fig. 1 Energy spectrum of capture γ rays at 90° lab.

The strong peak near 20 MeV is due to neutron capture by hydrogen. This reaction is analyzed elsewhere (2). The gamma rays having energies up to 38 MeV are produced in neutron capture reactions by ^{12}C. Apparently, there is capture not only into the ground state but also into excited states of ^{13}C. Furthermore, the spectrum is influenced by the scattering and the energy degradation of the neutron beam during its passage through the capture target. Monte Carlo simulations of these latter effects are in progress.

(1)   F. Smend, G.D. Wicke, P. Doll, G. Fink, S. Hauber, M. Haupenthal, H.O. Klages, H. Schieler, Report KfK 4508, Kernforschungszentrum Karlsruhe (1989) p. 36
(2)   G. Fink, P. Doll, S. Hauber, M. Haupenthal, H.O. Klages, H. Schieler, F. Smend, G.D. Wicke, this report, contr. 1.2.1.

*   II. Physikalisches Institut, Universität Göttingen, Germany

1.2.4 RADIATIVE CAPTURE OF POLARIZED NEUTRONS BY NEON

G. Mondry*, F. Smend*, P. Doll, G. Fink, H.O. Klages

The capture reaction Ne(n,γ) was investigated using the arrangement of three large NaI gamma detectors set up at the polarized, continuous neutron beam POLKA (1). The capturing target consisted of liquid neon at a temperature of T = 25.5K and a pressure of p = 900 Torr. To our knowledge, this is the first use of liquid neon as a scintillation detector. The target is described elesewhere in this Annual Report (2).

Gamma spectra from neutron capture by neon were measured and will be analyzed in complete analogy to the experiments with H and C using a scintillating NE 213 target (3). The analysis of the new data is still in a preliminary stage.

(1)   G. Fink, P. Doll, S. Hauber, M. Haupenthal, H.O. Klages, H. Schieler, F. Smend, G.D. Wicke, Report KfK 4405, Kernforschungszentrum Karlsruhe (1988) p. 29
(2)   G. Mondry, F. Smend, P. Doll, H.O. Klages, H. Skacel, this report, contr. 5.1.3
(3)   G.D. Wicke, P. Doll, G. Fink, S. Hauber, M. Haupenthal, H.O. Klages, H. Schieler, F. Smend, this report, contr. 1.2.1
*   II. Physikalisches Institut, Universität Göttingen, Germany

1.2.5 CROSS SECTIONS AND ANALYZING POWERS OF THE CHARGE EXCHANGE REACTION $^{12}C(\tilde{n},p)^{12}B$

P. Doll, S. Scheib, G. Fink, H.O. Klages

As reported in the 1988 annual report (1) an improved large solid angle detector system ($\Theta_{lab} = 7° - 29°$) had been set up at the polarized neutron facility POLKA (2) to investigate neutron induced reactions (E_n = 20 - 50 MeV) on light nuclei leading to charged particles in the exit channel. We started to investigate the neutron interaction with ^{12}C, an element abundantly contained in organic scintillators.

So far we have only analyzed the proton energy spectra for scattering angles between 15° and 29° and for neutron energies from 30 MeV to 50 MeV. Through the flux-normalized deuteron yields from a pure carbon target and a polyethylene target the $^{12}C(n,p)$ cross sections were normalized to the well known neutron-proton elastic scattering cross-sections (3) in the same energy range. In fig. 1 we have normalized the cross sections to DWBA calculations using the optical model parameters as given in ref. (4) and β^2 values for $\Delta l = 0$ and $\Delta l = 2$ from a 56.3 MeV experiment (5) ($\beta_0{}^2$ = 0.11, $\beta_2{}^2$ = 0.25). In spite of the fact, that the

$$^{12}C\,(\vec{n},p)\ ^{12}B_x \quad E_x \simeq 0,0\,MeV$$
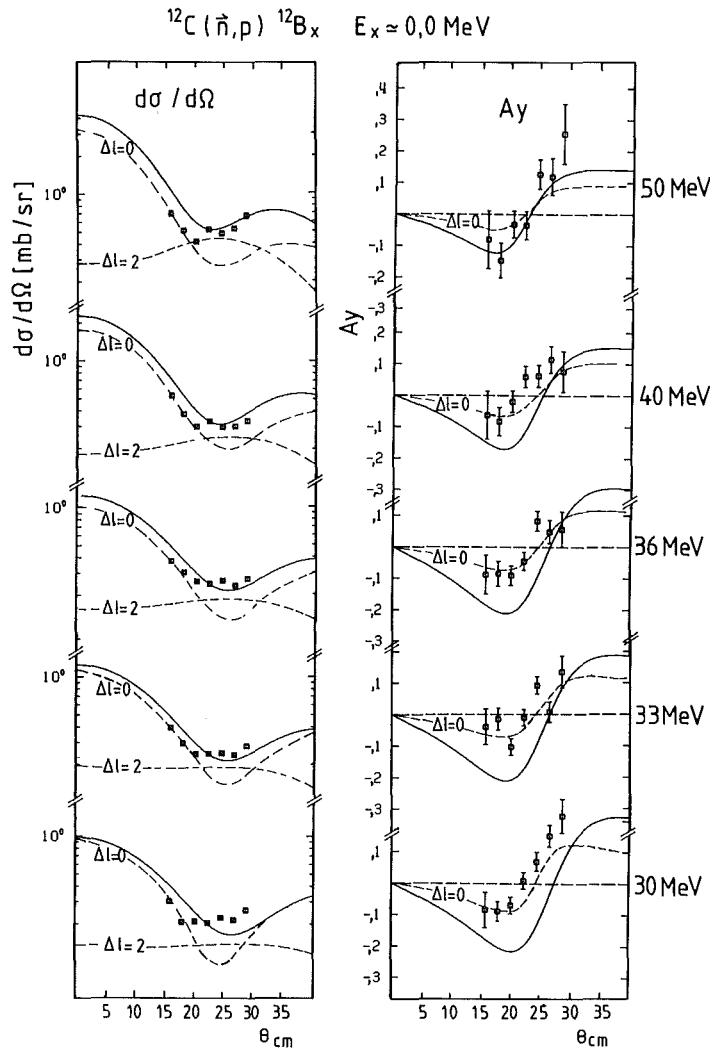
Fig. 1 Differential cross sections and analyzing powers of the
$^{12}C(\vec{n},p)^{12}B$ reaction to the ground state Gamov Teller state in
^{12}B for $E_n = 30, 33, 35, 40$ and 50 MeV.

experimental energy resolution is rather limited, the DWBA analysis indicates the importance of the $\Delta l = 0$ component for states around $E_x \approx 0$ MeV in the ^{12}B nucleus. The analyzing power for the dominant $\Delta s = 1$ transition seems to indicate an increasing importance of the $\Delta l = 2$ transition with increasing incident neutron energy. The dashed curves in fig. 1 represent the separate Δl transitions. Therefore, fig. 1 indicates that the analyzing power is an additional means combined with the differential cross section for selecting the angular momentum transfer in the charge exchange reaction (n,p). It is interesting to note

that the analyzing power found for the giant dipole excitation at around $E_x = 7.7$ MeV in ^{12}B exhibits little analyzing power and is, therefore, in agreement with a non spin-flip $\Delta s = 0$ excitation mechanism. After improving the energy resolution of the detector system, the polarized (ñ,p) reaction would present a powerful tool in investigating spin and non spin-flip excitations in nuclei.

(1)   S. Scheib, P. Doll, G. Fink, H.O. Klages, Report KfK 4508, Kern-forschungszentrum Karslruhe (1988) p. 41
(2)   H.O. Klages, H. Dobiasch, P. Doll, H. Krupp, M. Oexner, P. Plischke, B. Zeitnitz, F.P. Brady, J.C. Hiebert, Nucl.Instr.and Meth. 219 (1984) 269
(3)   G. Fink, P. Doll, T.D. Ford, R. Garrett, W. Heeringa, K. Hofmann, H.O. Klages, H. Krupp, to be published
(4)   A.S. Meigooni, J.S. Petler, R.W. Finlay, Phys. Med. Biol. 29 (1984) 643
(5)   F.P. Brady, J.L. Romero, University of California Davis Report (1981)111

1.2.6   COLD NUCLEAR FUSION: NEUTRON LIMITS FROM GAS-LOADED TI-D SYSTEMS

V.Eberhard, W.Heeringa, H.O.Klages, R.Maschuw, G.Völker, B.Zeitnitz

Several reports of the past few months suggest evidence for cold nuclear fusion of deuterium nuclei inside metal lattices. The methods to incorporate the deuterium into the metal were electrolysis of heavy water (1,2,3) and bringing the metal into contact with deuterium gas at different pressures and temperatures (3,4). The d-d fusion reactions with a positive Q-value are :

$$d + d \rightarrow {}^3He \,(0.817\ MeV) + n\,(\ 2.452\ MeV)$$

$$d + d \rightarrow {}^3H \ \,(1.008\ MeV) + p\,(\ 3.025\ MeV)$$

$$d + d \rightarrow {}^4He \,(0.076\ MeV) + \gamma\,(23.025\ MeV)$$

The first two have quite similar low-energy cross sections (5), the capture reaction is several orders of magnitude less probable.

Intense neutron emission has been reported by a group from Frascati (4). They loaded about 100 g of titanium shavings with 50 bar deuterium gas at room temperature. The pressure cell was subjected to several cooling cycles by immersing it in liquid nitrogen. During this the authors observed neutron count rates corresponding to a neutron source strength of about 400 n/s during several periods of many hours. After pumping the deuterium from the cell an even higher count rate was observed, cumulating during one hour in a neutron source strength of about 10.000 n/s. The neutron detector in the Frascati experiment was a BF_3 counter.

We have carried out similar experiments as in Frascati using titanium in the form of sponge and shavings. Liquid NE 213 scintillators were used for

neutron detection in detector cells of 10 cm diameter and 10 cm length. The final set up is shown in Fig.1. It comprised 4 detectors viewing the sample from angles differing by 90°. Below the detectors a plastic paddle detector was situated with dimensions 70x40x2 cm^3. It was used for off-line subtraction of background from cosmic rays. The lead shielding reduced the gamma background from the ground, which was mainly due to ^{40}K. The paraffin was necessary to moderate the neutrons, created by spallation reactions from cosmic rays in the lead, to energies below the threshold of the neutron detectors.

Each measured event was characterized by the energy signal and the pulse-shape signal from the neutron detectors, a signal for detector identification and the energy signal from the paddle detector. The events were processed by an LSI 11/73 microcomputer via a CAMAC system and were stored in list mode on magnetic tape.

The neutron efficiency of the set up was verified with a calibrated ^{252}Cf source. It amounted to about 6%, the exact value depending on the actual position of the windows in the energy and in the pulse-shape spectra. The energy window was set between 1 and 3 MeV.
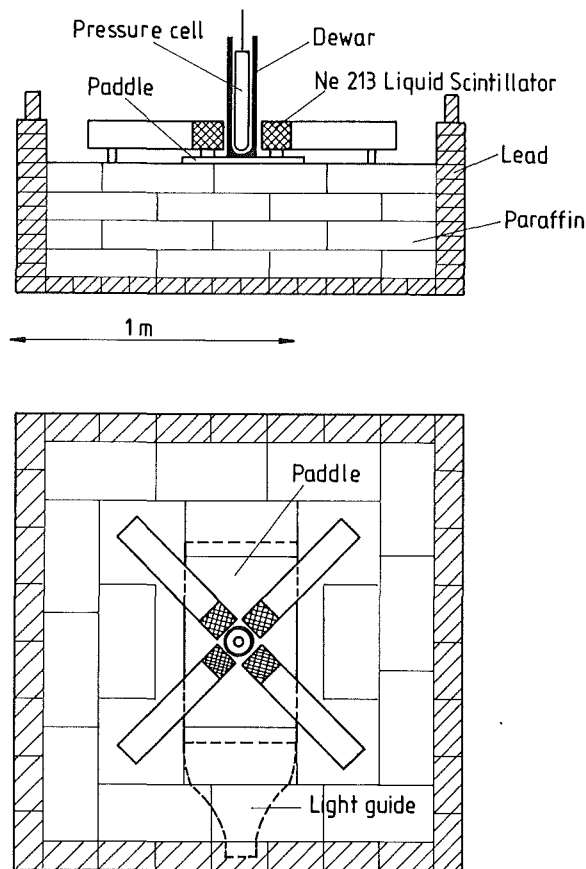
Fig. 1 Side view and top view of the final experimental set-up.

Four different experiments were carried out to load deuterium gas into titanium. The first two were carried out in a UHV hydrogenation apparatus, equipped with a quartz tube inside an oven. It has a calibrated volume to allow for volumetric determination of the amount of absorbed deuterium. The second two were carried out in high-pressure stainless steel cylinders (200 mm high, 30 mm internal diameter, 5 mm wall thickness). The experimental procedure is described in detail elsewhere (6).

The measured countrates for various cooling and pressure cycles of a D-loaded Ti sample are shown in fig. 2. For details, see ref. 6. Our results can be summarized in an upper level for the excess neutron flux of Φ_n (3σ) $\leq$ 0.6 s^{-1}. This value is normalized to a Ti sample mass of 100 g.
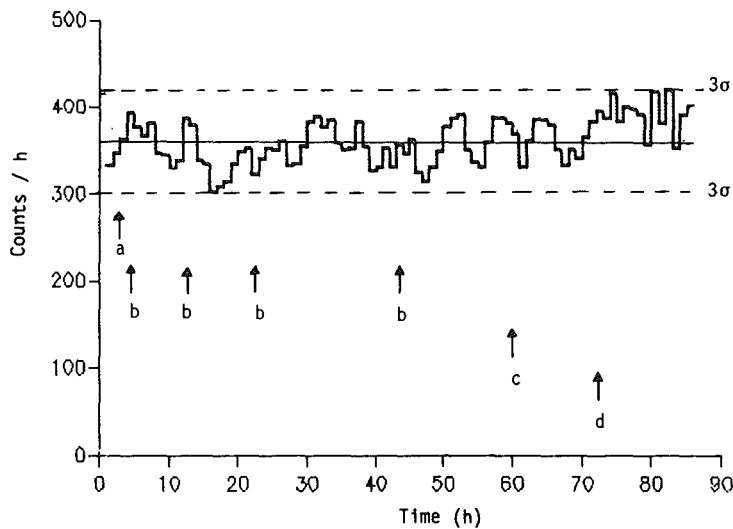
Fig.2 Results of experiment 4: a) start of deuterium loading
b) liquid nitrogen refill
c) warm up to 120°C
d) removal of deuterium.

We conclude, that our results show no indication for neutron emission down to a level of a few tenths of neutrons/s. Hence we do not confirm the large neutron intensities reported in Ref.4, which were up to 10^4 n/s. A letter by the authors of Ref.4 has appeared recently (7), describing the same experiment as in Ref.4. In this letter the largest neutron intensities have been withdrawn, maximum neutron source strengths reported here are up to 10^3 n/s. Also this lower neutron intensity has not been confirmed by us. On the contrary, there seems to be a tendency to lower and lower neutron intensities, also in reports that confirm the existence of cold nuclear fusion. In the paper by Menlove et al. from Los Alamos and Jones from Provo (3) bursts of the order of 100 neutrons and

random neutron emissions of 0.05 - 0.2 n/s are reported. Such intensities are below the sensitivity of our experiment. The detector in Ref.3 was a set up of ^{3}He proportional counters embedded in polyethylene. Due to their insensitivity to γ-rays BF$_3$ and ^{3}He gas counters have low background count rates. Therefore, they are useful for the monitoring of weak neutron sources of well known origin. We feel, however, that they are inadequate to identify d-d fusion neutrons, because of the lacking energy information and of insufficient discrimination against spurious signals due to disturbances in detectors or electronics.

(1)   M.Fleischmann, S.Pons, Electroanal. Chem. **261** (1989) 301

(2)   S.E.Jones, E.P. Palmer, J.B. Czirr, D.L. Decker, G.L. Jensen, J.M. Thorne, S.F. Taylor, J. Rafelski, Nature **338** (1989) 737

(3)   H.O.Menlove, M.M. Fowler, E. Garcia, A. Mayer, M.C. Miller, R.R. Ryan, S.E. Jones, submitted to Nature

(4)   A. De Ninno et al.,submitted to Europhysics Letters

(5)   A.Kraus, H.W. Becker, H.P. Trautvetter, C. Rolfs, Nucl. Phys. **A465** (1987) 150

(6)   V.Eberhard, W. Heeringa, H.O. Klages, R. Maschuw, G. Völker, B. Zeitnitz, Z. Phys. **A334** (1989) 357

(7)   A.De Ninno, A. Frattolillo, G. Lollobattista, L. Martinis, M. Martone, L. Mori, S. Podda, F. Scaramuzzi, Il Nuovo Cim. **101A** (1989) 841

1.3 NUCLEAR REACTIONS BY CHARGED PARTICLES

1.3.1 INCLUSIVE MEASUREMENTS OF THE BREAK-UP OF 156 MeV ^{6}Li-IONS AT EXTREME FORWARD ANGLES

H. Jelitto, J. Buschmann, V. Corcalciuc*, H.J. Gils, N. Heide, J. Kiener, H. Rebel, C. Samanta**, and S. Zagromski (1)

Inclusive alpha particle and deuteron spectra from collisions of 156 MeV ^{6}Li-ions with ^{12}C and ^{208}Pb were measured at extreme forward emission angles including zero degree. The measurements were performed with the Karlsruhe magnetic spectrograph "Little John" and required an efficient reduction of the background from small-angle scattering. The observed double differential cross sections and angular distributions have been analysed on the basis of Serber's spectator break-up model. When going to angles smaller than grazing, where Coulomb effects are expected to be dominating, transitional features may appear. Corresponding effects probably associated with Coulomb break-up are observed with the ^{208}Pb-target and require a slight extension of the Serber approach. In the case of the ^{12}C-target the break-up cross sections in forward direction seem to reflect the shape of the internal momentum distribution of the alpha particle and deuteron cluster in the ^{6}Li-projectile and are in agreement with a 2S-type wave function. However, at larger angles the shape appears to be distorted, possibly by final state interactions.

(1)   Z. Phys. A332 (1989) 317; Report KfK 4480, Kernforschungszentrum Karlsruhe (1989)

*   Central Institute of Physics, IFIN, Bucharest, Romania
**   SAHA Institute of Nuclear Physics, Calcutta, India

1.3.2 OBSERVATION OF NONRESONANT COULOMB BREAK-UP OF 156 MeV ^{6}Li PROJECTILES

J. Kiener, H.J. Gils, H. Rebel, and G. Baur* (1)

We communicate a particular aspect of our current experiments investigating nonresonant Coulomb break-up of 156 MeV ^{6}Li projectiles in the field of ^{208}Pb. The triple differential cross sections measured at very forward emission angles and low relative energies of the α and d fragments show neither any conspicuous "forward-backward" asymmetry in the system of the decaying ^{6}Li nor do they

indicate any significant E1 contribution. This is an apparent contrast to the findings recently reported for a different experiment at 60 MeV, the results of which can hardly be understood in the frame of the Coulomb excitation approach.

(1)   Z. Phys. **A332** (1989) 359

*   Institut für Kernphysik, Kernforschungsanlage Jülich, Jülich, Germany

1.3.3   ANALYSIS OF THE SEQUENTIAL BREAK-UP OF 156 MeV ^{6}Li PROJECTILES SCATTERED FROM ^{208}Pb

H. Rebel, G. Baur*, S.K. Basu**, V. Corcalciuc***, H.J. Gils, J. Kiener and J. Raynal****

The sequential break-up of ^{6}Li projectiles : ^{6}Li $\rightarrow$ ^{6}Li* $(3_1{}^+) \rightarrow \alpha + d$ proceeding via the first excited state provides the possibility to study the extent to which break-up observed for extreme forward angles can be ascribed to Coulomb dissociation. In order to approach this question double differential cross sections for the elastic sequential break-up of 156 MeV ^{6}Li : ^{208}Pb (^{6}Li, ^{6}Li* ($E_x = 2.18$ MeV)) ^{208}Pb$_{g.s.}$ have been measured by observing the break-up α-particles and deuterons in nearly parallel emission at reaction angles far below the grazing angle. The experiments used a special set-up with a split focal plane detector of the magnetic spectrograph "Little John" at the Karlsruhe Isochronous Cyclotron. The observed double differential cross sections $d^2\sigma$ / $d\Omega_\alpha$ $d\Omega_d$ have been transformed into the differential cross section $d\sigma/d\Omega_{Li*}$ assuming E2-decay of the excited projectile.

Fig. 1 compares the experimental results with the theoretical predictions and demonstrates the dominance of the Coulomb dissociation mechanism in the considered angular range. The prediction for Coulomb break-up, based on the experimentally known B (E2; 1^+-3^+_1) value, reproduces the absolute magnitude and the overall shape of the observed angular distribution while nuclear contributions seem to be at least one order of magnitude smaller. Looking more closely to the data some oscillations of the experimental data are observed, which may indicate effects from nuclear - Coulomb interaction interferences. In order to explore such effects in more detail we started coupled channel analyses of projectile excitation, coupling the ground state (for which elastic scattering data are available for very forward angles) and the first excited state of ^{6}Li. Though most likely due to some constraints in the shape of the form factors (provided by the coupled channel code ECIS (2)) the calculations do not reproduce the elastic ^{208}Pb (^{6}Li, ^{6}Li) ^{208}Pb and inelastic ^{208}Pb (^{6}Li, ^{6}Li*) ^{208}Pb scattering data simultaneously with the same quality, following conclusions can be drawn:
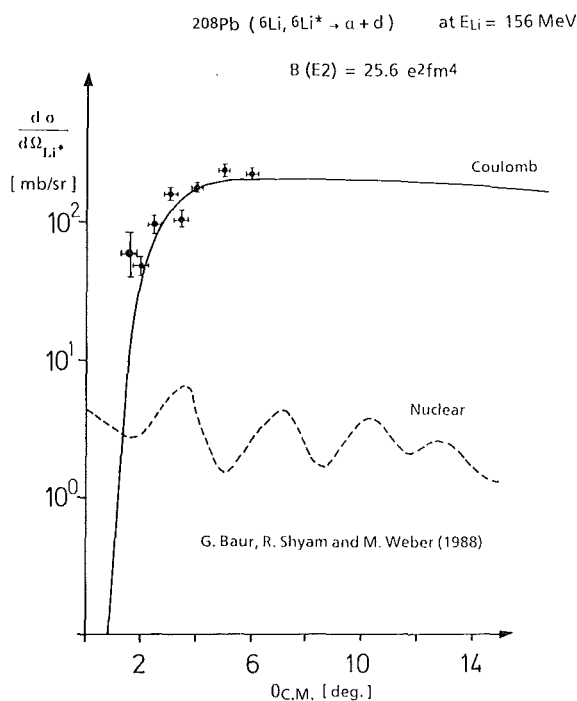
Fig. 1   Differential cross section for the reaction ^{208}Pb (^{6}Li, ^{6}Li* (2.18 MeV))
^{208}Pb$_{g.s.}$. The solid line results from the semiclassical Coulomb excitation
theory, the dashed line is an estimate of the nuclear break-up by the post-
form DWBA theory (1).

(i)   The optical potential which is able to describe the observed differential cross
section of elastic scattering in the angular region near the grazing angle, in
particular the region of the "Fresnel wiggles" around $\sigma / \sigma_R \approx 1$ proves to be
considerably different from the Woods-Saxon potential obtained from the
analysis of larger scattering angles (3).

(ii)   The calculated cross sections for angles smaller than ca. 4° are negligibly
influenced by the nuclear potential. Modulations of the inelastic cross sec-
tion seen in the experimental data are qualitatively reproduced, even with
"switched - off" nuclear potentials in case of realistic charge distributions
taken into account. The latter findings may be affected by an approximation
of the radial shape of the Coulomb excitation form factors for large distances.
More refined coupled channel calculations are in progress.

(1)   G. Baur, F. Rösel, D. Trautmann and R. Shyam, Phys. Rep. 111 (1984)333
(2)   J. Raynal, Computer program ECIS 79 (unpublished)
(3)   J. Cook, H.J. Gils, H. Rebel, Z. Majka and H. Klewe-Nebenius,
Nucl. Phys. A388 (1982) 173

*   Institut für Kernphysik, Kernforschungsanlage Jülich, Jülich, Germany
**   Bhabha Atomic Research Centre, V.E.C.C., Calcutta, India
***   Central Institute of Physics, IFIN, Bucharest, Romania
****   CEA, Service de Physique Théorique, Saclay, France

1.3.4 THE COULOMB DISSOCIATION OF ^{6}Li AND THE DETERMINATION OF THE ASTROPHYSICAL S-FACTOR FOR THE ^{4}He(d,γ) ^{6}Li RADIATIVE CAPTURE PROCESS AT ASTROPHYSICAL ENERGIES

G. Baur*, H.J. Gils, J. Kiener, H. Rebel, M. Weber*

Following the proposal (1) to use the Coulomb dissociation

$$a + Z \to b + c + Z \tag{1}$$

for a determination of astrophysically relevant radiative capture cross sections, we have studied the process in 1th order Coulomb excitation theory, taking special care of the angular correlation of the emitted fragments (2). For sufficiently high energies and forward angles, the electromagnetic interaction is dominant. Small nuclear contributions, persisting down to zero degrees, have a characteristic angular dependence and can be unambiguously identified . The triple differential cross section can be written as

$$\frac{d^3\sigma}{d\Omega_{bc}\, d\Omega_a\, dE_{bc}} = \frac{d\sigma^{ruth}}{d\Omega_a} \sum_{LM} A_{LM}\, Y_{LM}(\hbar) \tag{2}$$

The Rutherford cross section is denoted by

$$\frac{d\sigma^{ruth}}{d\Omega_a} \quad ,$$

the angular correlation coefficients A_{LM} can be expressed in terms of the familiar orbital integrals of Coulomb excitation and by the electromagnetic matrix-elements governing the b (c,γ) a radiative capture process. The result of the calculations (2) are compared with recent experimental data (3) in Fig. 1.

The absolute value of the cross section is directly proportional to the astrophysical S-factor. The S-factor chosen is consistent with the radiative capture data of Robertson et al., (4) measured at much higher c.m. energies. We note that the present experimental results cover a range of relative energies of the $\alpha + d$ system down to about 30 keV.
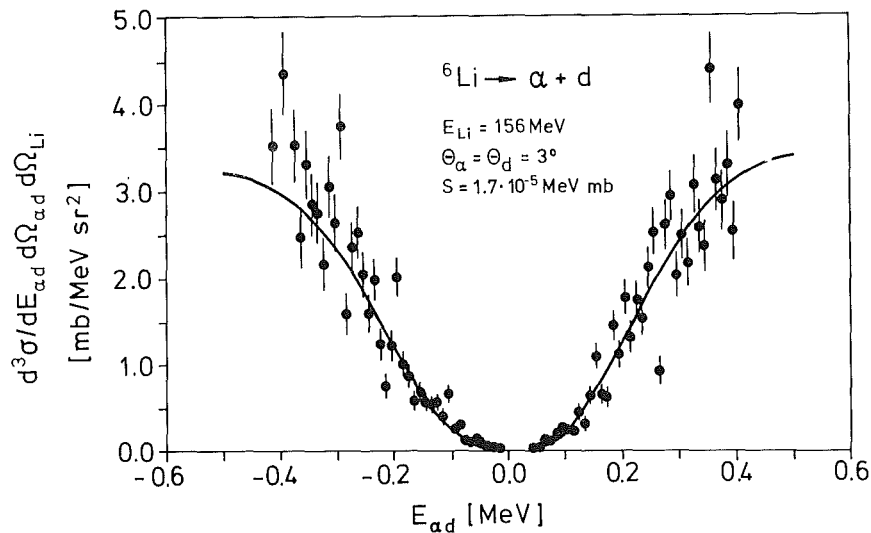
Fig. 1   Coulomb break-up cross section vs relative energy of the emitted frag-
ments in the ^{208}Pb (^{6}Li,α d)^{208}Pb g.s. reaction: Experimental data
compared to theoretical predictions.

The present investigations show the feasibility of the Coulomb
dissociation approach for nuclear astrophysic studies. Equivalent photon spectra
can be reliably calculated from the kinematics of the process. The error bars which
have to be attached to the S-factor, as extracted from the data, reflect essentially
the error bars of the experiment (absolute values and determination of relative
c.m. energies). Nevertheless, more detailed investigations of the influence of
nuclear break up and "postacceleration" are called for, and they are in progress.
With the experience and confidence gained in the ^{6}Li-test case we can proceed to
other, equally or even more interesting cases, like ^{12}C(α,γ)^{16}O or ^{13}N(p,γ)^{14}O (for
astrophysical implications see e.g. Ref. 5).

(1)   H. Rebel, Workshop "Nuclear Reaction Cross Sections of Astrophysical
         Interest" unpubl. report, Kernforschungszentrum Karlsruhe (1985)
         G. Baur, C.A. Bertulani, H. Rebel, Nucl. Phys. A459 (1986) 188
(2)   G. Baur and M. Weber, submitted to Nucl. Phys. A
(3)   J. Kiener, H.J. Gils, H. Rebel and G. Baur, Z. Phys. A 332 (1989) 359
(4)   R.G.H. Robertson et al., Phys. Rev. Lett. 47 (1981) 1867
(5)   W.A. Fowler, Rev. Mod. Phys. 56 (1984) 145,
         C.E. Rolfs and W.S.Rodney, Cauldrons in the Cosmos, University of
         Chicago Press (1988)

*   Institut für Kernphysik, Kernforschungsanlage Jülich, Jülich, Germany

1.3.5 OBSERVATION OF INELASTIC SEQUENTIAL BREAK-UP
OF 156 MeV 6Li-PROJECTILES

J. Kiener, H.J. Gils, G. Gsottschneider, N. Heide, H. Jelitto, H. Rebel,

J. Wentz, S. Zagromski, S.K. Basu* and I.M. Brâncuş**

In kinematically complete measurements of the break-up of 6Li- projectiles at the magnetic spectrograph "Little John" (1), elastic as well as inelastic break-up have been observed. The different processes can be identified by the sum of the kinetic energies of the α-particle and deuteron fragments. It is given by

$$E_\alpha + E_d = E_{Li} - Q_{\alpha d} - E_{exc}.$$

where

E_{Li} = 156 MeV is the beam energy,

$Q_{\alpha d}$ = 1.47 MeV the break-up threshold of 6Li and

$E_{exc.}$ = the excitation energy of 208Pb.

In a two dimensional plot of the deuteron energy versus the alpha-particle energy (Fig.1) the inelastic break-up can be recognized as an accumulation of events below the line corresponding to elastic break-up. These events can be attributed to projectile break-up with additional excitation of the 208Pb target nucleus to its first excited state at 2.61 MeV.
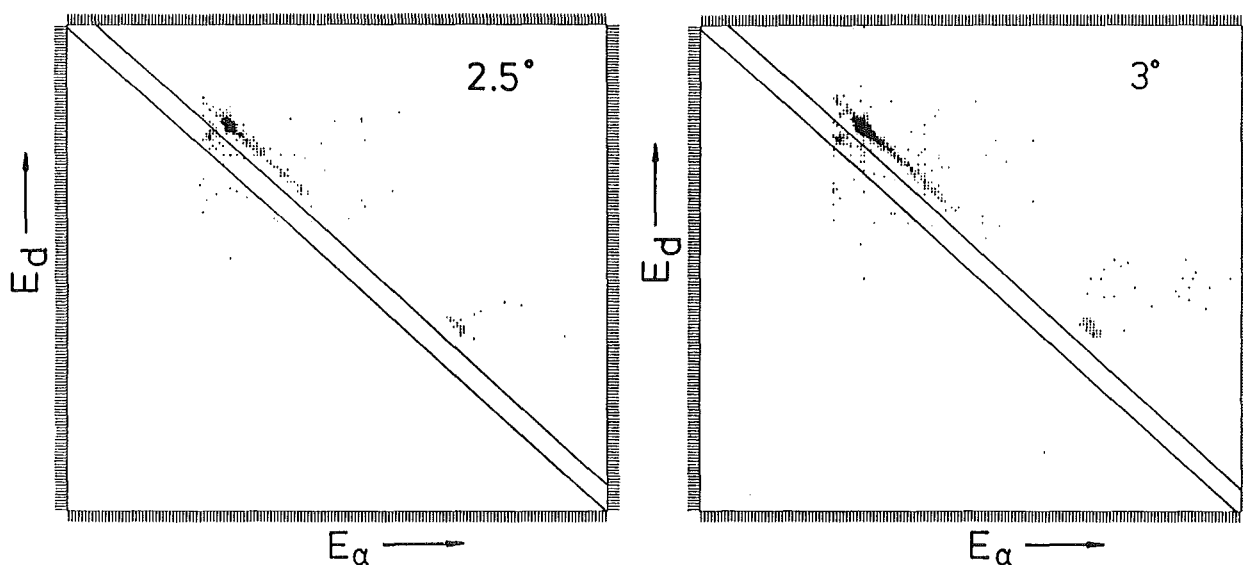
Fig.1   Deuteron energy versus α-particle energy for the reaction 208Pb (6Li,αd) 208Pb at two different reaction angles.

Considering only events in a sum energy window of 151.85 ± 1.15 MeV (see Fig.1), the relative energy spectra have a pronounced peak at 710 keV (Fig.2). This is due to the sequential break-up of 6Li via its first excited state at 2.18 MeV, 710 keV above the break-up threshold.
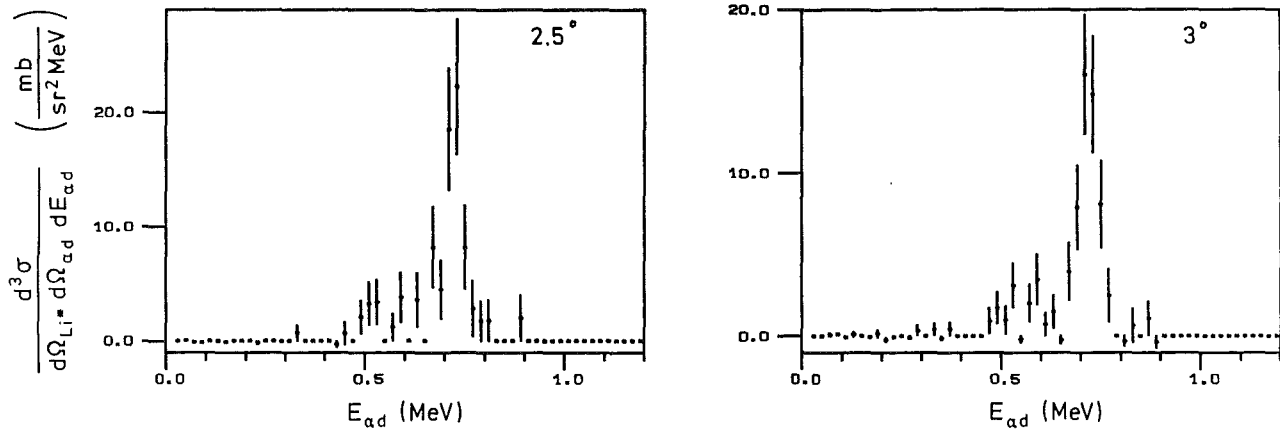
Fig.2   Relative energy spectra for the reaction $^{208}Pb(^6Li,\alpha d)^{208}Pb^*_{2.6\ MeV}$.

Double differential cross sections for this inelastic sequential break-up were obtained by integration over the resonant peak. The angular distribution for this process is shown in Fig.3 together with the angular distribution for elastic sequential break-up. A relatively large cross section for the inelastic reaction is seen at angles below 4°, while it drops drastically for larger angles.
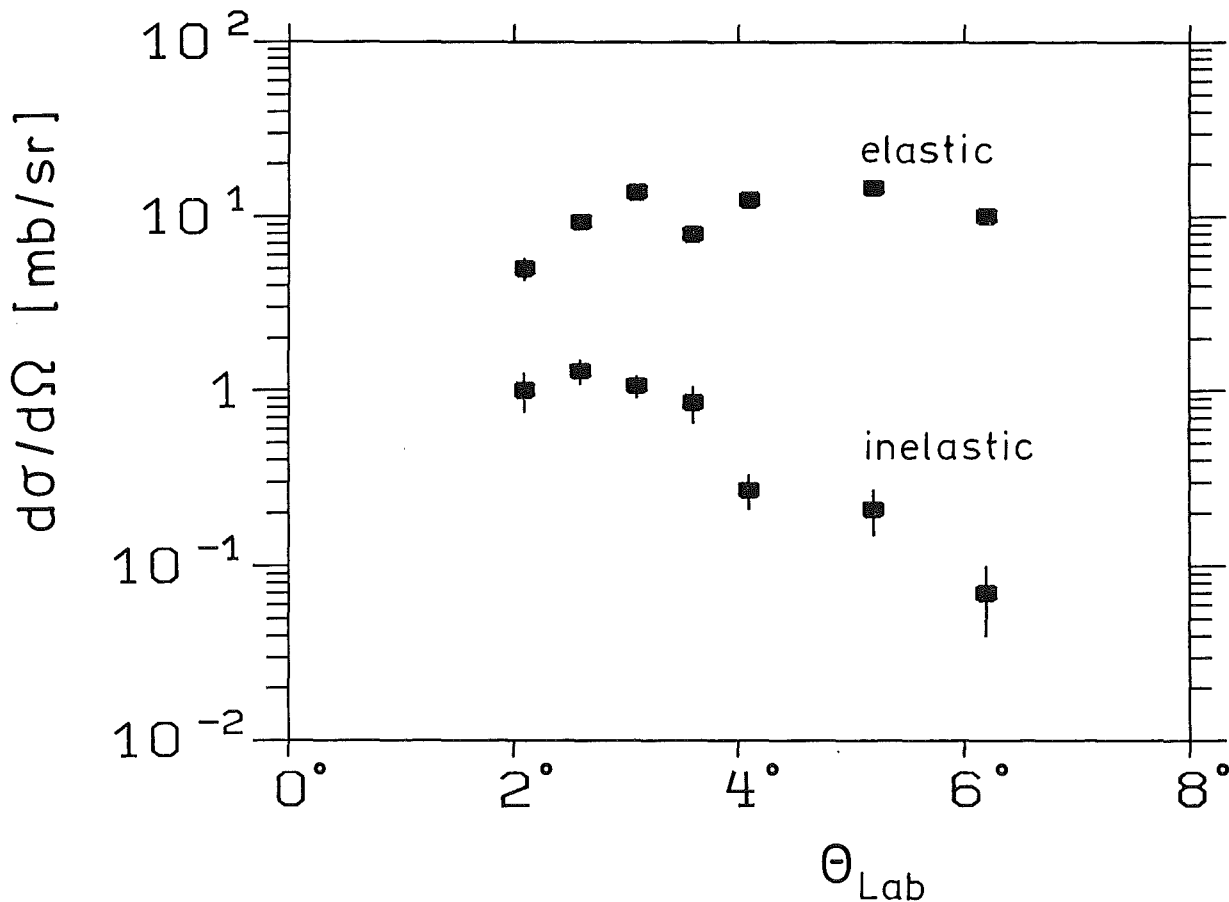
Fig.3   Angular distribution for elastic and inelastic sequential break-up of ^6Li.
Ω_α, Ω_d = 9 mrad x 40 mrad.

In view of the recently started coupled-channel analysis of the elastic sequential break-up (2), the inelastic data might provide a further insight in the break-up mechanism in the measured angular region. For a better comparison with theoretical predictions a compilation of cross sections for the inelastic and elastic sequential break-up is given in table 1. The differential cross sections have been obtained assuming an E2-decay of the excited projectile. The quoted errors include the statistical uncertainty and an estimated error due to the peak integration.

Table 1: : Double differential and differential cross sections for the inelastic and elastic sequential break-up

$\theta_{c.m.}$ (deg.)	$\dfrac{d^2\sigma}{d\Omega_{Li^*}\, d\Omega_{\alpha d}}$ $[\,mb/sr^2\,]$		$\dfrac{d\sigma}{d\Omega_{Li^*}}$ $[\,mb/sr\,]$	
	elastic	inelastic	elastic	inelastic
2.1	5.02 ± 0.71	1.00 ± 0.25	45.3 ± 6.4	8.3 ± 2.0
2.6	9.32 ± 0.61	1.29 ± 0.21	96.4 ± 6.3	12.6 ± 2.1
3.1	13.80 ± 0.55	1.06 ± 0.15	159.7 ± 6.4	11.9 ± 1.7
3.6	7.90 ± 0.65	0.85 ± 0.20	101.6 ± 8.4	10.5 ± 2.5
4.1	12.46 ± 0.40	0.27 ± 0.06	177.4 ± 5.7	3.7 ± 0.8
5.2	14.60 ± 0.59	0.21 ± 0.06	254.7 ± 10.3	3.6 ± 1.0
6.2	10.08 ± 0.40	0.07 ± 0.03	215.3 ± 5.0	1.5 ± 0.6

(1)   J. Kiener, H.J. Gils, H. Rebel, G. Gantenbein, N. Heide, H. Jelitto,
       J. Wentz, S. Zagromski, S.K. Basu, I.M. Brâncuş, Report KfK 4508,
       Kernforschungszentrum Karlsruhe (1989) p. 46
(2)   H. Rebel, G. Baur, H.J. Gils, J.Kiener, S.K. Basu, V. Corcalciuc, this
       report, contr. 1.3.4

*   Bhabha Atomic Research Centre, V.E.C.C., Calcutta, India
.**   Central Institute of Physics, IFIN, Bucharest, Romania

1.3.6 FEATURES OF DIRECT AND SEQUENTIAL COULOMB BREAK-UP OF 6Li IONS

D.K. Srivastava*, D.N. Basu*, H. Rebel (1)

Coulomb dissociation of 6Li in the field of 208Pb at different energies via resonance and continuum levels is discussed in detail. Relations are given which can be used to directly relate the Coulomb break-up cross section to the astrophysical S-factor. Predictions for energy dependence and angular-distributions are given. The direct Coulomb-break-up of 6Li is found to be of the same order of magnitude as the sequential break-up at higher projectile energies. The effect to elastic scattering can be accounted for by introducing a dynamic polarization potential.

(1)   Phys. Rev. C38 (1988) 2148
*   Bhabha Atomic Research Centre, V.E.C.C., Calcutta, India

1.3.7 PARTICLE CORRELATION MEASUREMENTS USING AN INTERMEDIATE DETECTOR AT THE SPECTROGRAPH "LITTLE JOHN"

G. Gsottschneider, H. J. Gils, J. Kiener, H. Rebel, S. Zagromski

In the measurements of the Coulomb break-up of 156 Mev 6Li on 208Pb performed at the Karlsruhe Isochronous Cyclotron the two fragments are detected using the magnetic spectrograph 'Little John' with a divided focal plane detector (1). In order to obtain an angular resolution $\leq$ 9 mrad between the fragments the horizontal acceptance angle was previously limited to 7 mrad.

Because of the small cross section of this coincidence experiment it was desirable to measure with a larger acceptance maintaining, however, the emission angular resolution. This can be achieved by subdividing the horizontal acceptance range by means of an additional detector system (2). Ion optically the angle of incidence into the focal plane θ_{fp} depends on the emission angle θ_0 at the target:

$$\theta_{fp} = R_{22}\,\theta_0 + R_{26}\,\delta_0 + \text{second order terms} \quad [1]$$

where R_{22}, R_{26} are characteristic of the magnetic system and the imaging property. δ_0 is the relative deviation from the nominal momentum of the central trajectory.

For the measurement of θ_{fp} we used an additional position sensitive proportional counter insert in front of the focal plane detector at a distance of 0.48 m (Fig. 1).

In first calibration measurements the position and angular resolution of the detector system was tested with elastically scattered 6Li particles. By setting the
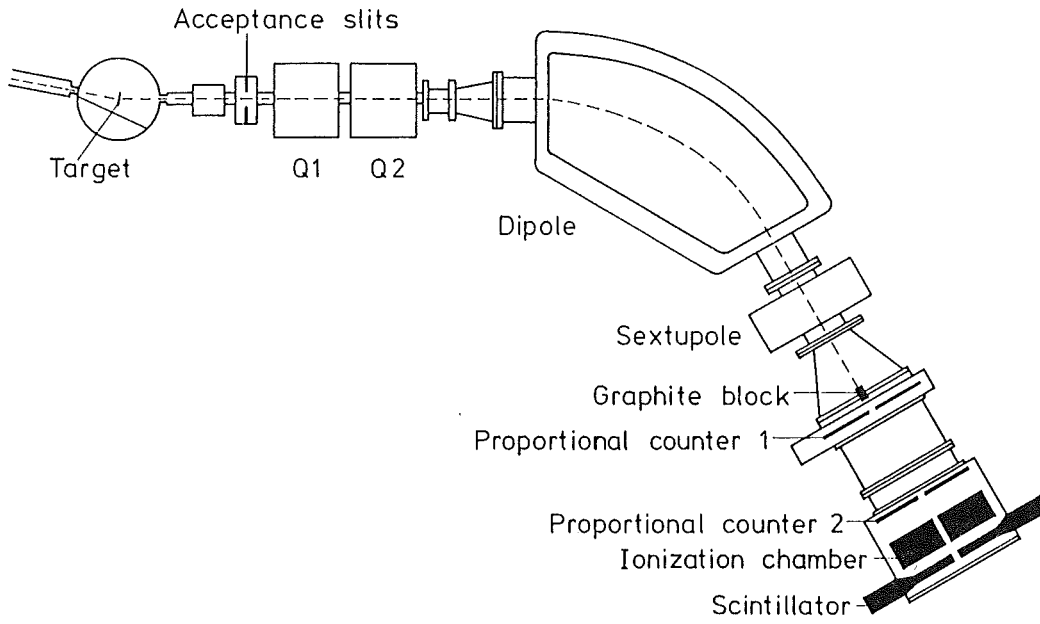
Fig. 1   Magnetic spectrograph 'Little John' with inserted detector system for improved correlation measurements.
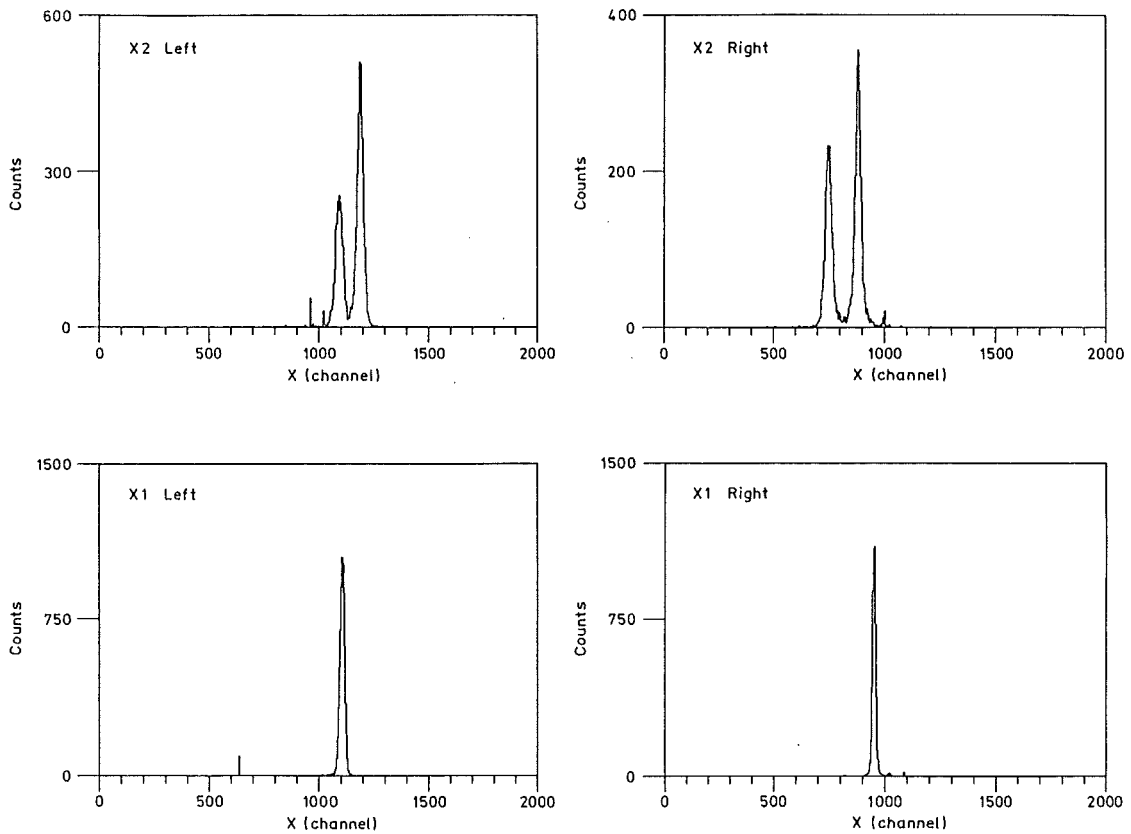
Fig. 2   Position spectra of the first (x1) and second (x2) proportional counter plane.

acceptance slits (horizontal width 1 mrad) on different horizontal positions the angular resolution was determined to be 5 mrad.

Fig. 2 shows the position spectra of the left and right parts of both detectors with the acceptance slit of the spectrograph subsequently set at two horizontal positions (-8 mrad, 8 mrad).Using a special diaphragm mounted in front of the inserted detector a position resolution of $\pm$ 1 mm has been measured.

With the calibration of the angle imaging function [1] obtained as characterized in fig. 2 the horizontal emission angle θ_0 of the fragments can be determined.

A resolution of the relative emission angle of the fragments of 7 mrad could be obtained using the full acceptance of 20 mrad of the magnetic spectrograph. Thereby the coincidence efficiency was increased by a factor of 9.

(1)   J. Kiener, H. J. Gils, H. Rebel, G. Gantenbein, G. Gsottschneider, N. Heide, H. Jelitto, J. Wentz, S. Zagromski, S. K. Basu, G. Baur, D. K. Srivastava, Report KfK 4508, Kernforschungszentrum Karlsruhe (1989) p. 45

(2)   R. Rudeloff, S. Zagromski, W. Eyrich, H. J. Gils, H. Jelitto, A. Lehmann, H. Schlösser, H. Wirth, Report KfK 4508, Kernforschungszentrum Karlsruhe (1989) p. 124

1.3.8   ELASTIC BREAK–UP OF 156 MeV ^{6}Li PROJECTILES WITH LARGE ASYMPTOTIC RELATIVE MOMENTA OF THE FRAGMENTS

N. Heide, H. Rebel, V. Corcalciuc*, H.J. Gils, H. Jelitto, J. Kiener, J. Wentz, S. Zagromski and D.K. Srivastava** (1)

The triple differential cross sections for elastic break-up of 156 MeV ^{6}Li projectiles by the reactions ^{208}Pb (^{6}Li, αd) ^{208}Pb$_{g.s.}$ and ^{12}C (^{6}Li, αd) ^{12}C$_{g.s.}$ have been measured with large asymptotic relative momenta of the outgoing fragments. The data exhibit rather unfamiliar shapes of the energy spectra, often replacing the usual bell-shape distributions by double-peaked structures and varying rapidly with the relative emission angles. The origin of these features has been explored and the cross sections have been analysed on the basis of a diffractive disintegration approach.

(1)   Report KfK 4564, Kernforschungszentrum Karlsruhe (1989)

*   Central Institute of Physics, IFIN, Bucharest, Romania
**   Bhabha Atomic Research Centre, V.E.C.C., Calcutta, India

1.3.9 INTERFERENCE AND OFF - SHELL EFFECTS OF FRAGMENT SCATTERING IN ELASTIC BREAK - UP OF LIGHT IONS

N. Heide, D.K. Srivastava*, H. Rebel

The elastic break-up of 156 MeV ^{6}Li projectiles has been studied by measuring the triple-differential cross sections $d^3\sigma / d\Omega_d \, dE_\alpha$ for the direct elastic break-up reactions ^{208}Pb (^{6}Li, αd)^{208}Pb g.s. and ^{12}C (^{6}Li, αd)^{12}C$_{g.s.}$, using a detector set-up of two position-sensitive semiconductor ΔE (Si(Li)) - E (intrinsic Ge) telescopes in an in-plane geometry arrangement (1). As long as the relative angles of emitted α-particle and deuterons fragments are not too large the data exhibit the familiar bell-shaped energy distributions around the beam-velocity energy. Proceeding to larger relative angles, thus selecting the larger relative momenta, unfamiliar shapes evolve: *double - peaked structures of the energy distributions of the correlated fragments, rapidly changing with the emission angles.*

We discuss these features within the prevailing formulation of the prior-form DWBA amplitude (2)

$$T_{prior}^{DWBA} = \langle X_{a*}^{(-)} \phi_k^{(-)} | U_{bA} + U_{cA} | X_a^{(+)} \phi_a \rangle$$

for the break-up reaction

$$a + A \rightarrow (b+c)^* + A \rightarrow b+c+A,$$
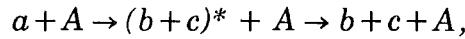
virtually proceeding (in a quasisequential way) through the excited complex projectile. Here $X_a^{(+)}$ (R,k_i) and $X_{a*}^{(-)}$ (R,$k_f = k_b + k_c$) denote the distorted waves, ϕ_a (r) and $\phi_k^{(-)}$ (r) the ground and continuum states, respectively, with the relative momentum

$$k = \frac{m_b}{m_a} k_c - \frac{m_c}{m_a} k_b$$

in the exit channel, and U_{bA} (R - $m_c/m_a \cdot$r) and U_{cA} (R + $m_b/m_a \cdot$r) are the fragment-target interactions. The final state interactions of the fragments are exactly included when choosing a proper relative motion wave function $\phi_k^{(-)}$. Using the plane wave approximation the DWBA amplitude can be simplified to the quasi free amplitude

$$T^{PW} \approx U_{bA} (Q) \phi_a \left[k_c - \frac{m_c}{m_a} k_a \right] + U_{cA} (Q) \phi_a \left[\frac{m_b}{m_a} k_a - k_b \right] \quad ,$$

where ϕ_a is the Fourier transform of the wave function ϕ_a. Thus, in the case where the half-off-shell scattering amplitudes U_{bA} or U_{cA} (the Fourier transforms of the scattering potentials) would significantly vary, crossing a minimum, e.g. when changing $Q = | k_a - k_b - k_c |$ along the kinematic correlation of k_b and k_c, the transition amplitudes T_b and T_c may exhibit considerable structures of their dependence on E_c and E_b, respectively, not arising from the presumably

monotonic shape of the momentum distribution $\mid \phi_a \mid^2$. For a typical experimentally studied situation of elastic break-up of 156 MeV ^{6}Li $\to \alpha + d$ (see Fig. 1), Q varies from approximately 0.25 to 0.50 fm^{-1} with E_a = 80 to 120 MeV, and the minima in the triple differential cross sections are found located at Q_{min}^{expt} = 0.36 fm^{-1}.

The DWBA calculations are principally able to reproduce the observed structure of the break-up cross section. However,when adopting for U_{aA} and U_{dA} potentials resulting from elastic scattering analyses, the conspicuous minima are located at a total momentum transfer Q_{min}^{DWBA} = 0.50 fm^{-1} whereas it appears experimentally at Q_{min}^{exp} = 0.36fm^{-1}. We tentatively associate this discrepancy to the inadequacy of elastic- (on-shell) scattering optical potentials to represent the transition potentials of the quasielastic interaction of a bound cluster with the target, inducing break-up with larger energy transfer. As an example, Fig. 1 compares the measured cross sections with the results of DWBA calculations, first
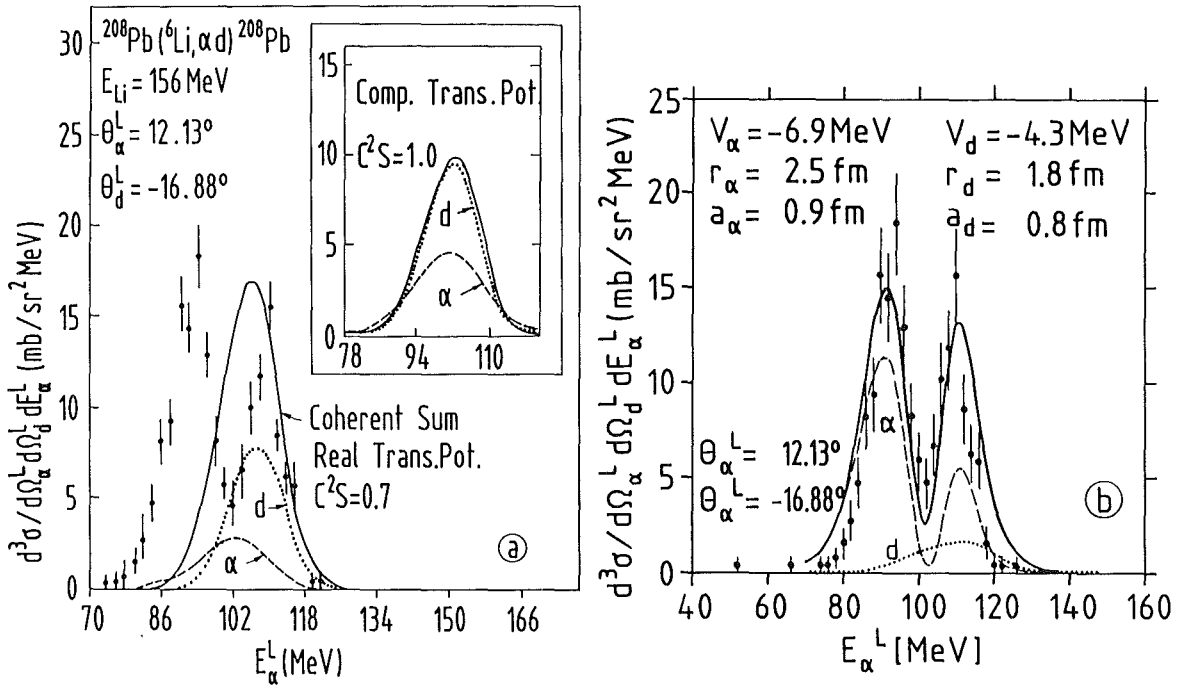
Fig. 1   Triple-differential cross section for the elastic break-up of 156 MeV ^{6}Li projectiles on ^{208}Pb as compared to prior-form DWBA calculations (a) adopting the (on-shell) elastic-scattering potentials for the α-target and d-target interactions (dashed and dotted curves) and (b) using modified interaction potentials adjusted to the data.

using potentials deduced from elastic-scattering experiments and subsequently modified potentials resulting from a fit to the break-up data. Obviously the half-off-shell potentials empirically required for describing the data appear to be more extended. The radii of the potentials (Saxon-Woods form) appear rather sensitively determined by the position of the cross section minimum. The strengths, however, depend additionally on the specific choice of the (2S) wave function ϕ_a.

The requirement of unusual transition potentials for the break-up studies can be understood by realizing that the exact T matrix for the break-up can be written as

$$T = <X_a^{(-)} \phi_k^{(-)} \mid (U_{bA} + U_{cA} - U_{aA}) \, \Omega \mid X_a^{(+)} \phi_a >$$

where U_{aA} is the exit-channel distortion potential generating X_a, and Ω is similar to the Moeller's operator defined by $\psi^{(+)} = \Omega X_a^{(+)} \phi_a$. Insofar as the effect of the coupling of break-up channels is large, Ω will be different from unity and one can visualize the requirement of unusual transition potentials in a manner not unlike the requirement of unusual optical potentials U_{aA} alternatively advocated by Austern (2, 3). This, of course is in addition to the inadequacy of the used break-up model itself, and to the fact that the scattering potential is, in general, nonlocal which is different from the local on-shell scattering potential.

(1)   N. Heide, H. Rebel, V. Corcalciuc, H.J. Gils, H. Jelitto, J. Kiener,
        J. Wentz, S. Zagromski, D.K. Srivastava, Nucl. Phys. A (in press)
(2)   F. Rybicki and N. Austern, Phys. Rev. C6 (1970) 1525
(3)   N. Austern, Phys. Rev. C30 (1984) 1130

*   Bhabha Atomic Research Centre, V.E.C.C., Calcutta, India

1.3.10   A PRIOR–FORM DISTORTED WAVE BORN APPROXIMATION ANALYSIS OF THE ELASTIC BREAK–UP OF 156 MEV 6Li PROJECTILES

D.K. Srivastava*, H. Rebel, and N. Heide (1)

Features of the prior-form distorted wave Born approximation theory of elastic break-up of 156 MeV 6Li ions scattered off 208Pb are investigated. Nuclear break-up for large relative energies of the outgoing α-particle and deuteron fragments ($E_{\alpha d} > 5$ MeV) studied here is found to proceed dominantly via the quadrupole scattering state of the $\alpha + d$ system when transition potentials from elastic fragment-target scattering are used for the calculations. The coherent contributions of different multipole components to the triple differential cross-sections appear to be very sensitive to the potentials generating the distorted waves and

representing the cluster fragment-target interactions. The results of the analysis of the experimental data require transition potentials rather different from the on-the-mass shell optical potentials deduced from elastic α-particle and deuteron scattering.

(1)   Report KfK 4565, Kernforschungszentrum Karlsruhe (1988)

*   Bhabha Atomic Research Centre, V.E.C.C., Calcutta, India

1.3.11   COINCIDENCE CROSS SECTIONS WITHIN THE BREAK-UP MODEL OF SERBER

V. Corcalciuc*, H. Jelitto

The geometrical break-up model introduced by Serber (1) for the description of nuclear break-up had provided a basis for several further investigations of break-up processes. Originally, the model allows to calculate single differential cross sections like energy and angular distributions of the break-up fragments. Studying the energy spectra of the ejectiles an expression for the double differential cross section $d^2\sigma/(d\Omega dE)$ was deduced by Utsunomyia (2). Scrutinizing the break-up model in more detail it appears to be possible to derive therefrom also an analytical expression for the triple differential cross sections, as measured in particle-particle coincidence experiments.

In the original article of Serber an expression for the quantity $\psi(p_y, p_z, p_{x1}, p_{x2})$ is given which represents the wave function for the relative motion of the two clusters in the projectile within a coordinate system fixed to the target edge. The arguments are the components of the relative momentum between the two clusters and the subcripts 1 and 2 refer to the first and second fragment, respectively. The basic idea is to associate the absolute square of this wave function to the quintuple differential cross section $d^5\sigma_{op}/(dp_y dp_z dp_{x1} dp_{x2} dl)$. Hereby, the variable l defines the break-up position by an adequately defined length around the edge of the target nucleus. In order to reach an expression for the observable triple differential cross sections $d^3\sigma/(d\Omega_1 d\Omega_2 dE_1)$ the Jacobian

$$J = \frac{\partial(p_{x1}, p_{x2}, p_z, p_y, l)}{\partial(\theta_1, \theta_2, E_1, \phi_1, \phi_2)}$$

was evaluated.

The model suggests to assign this cross section to the elastic nonresonant projectile break-up due to the nuclear interaction. Distortions by the Coulomb field of the target could be included (2). The model should be reasonable in the
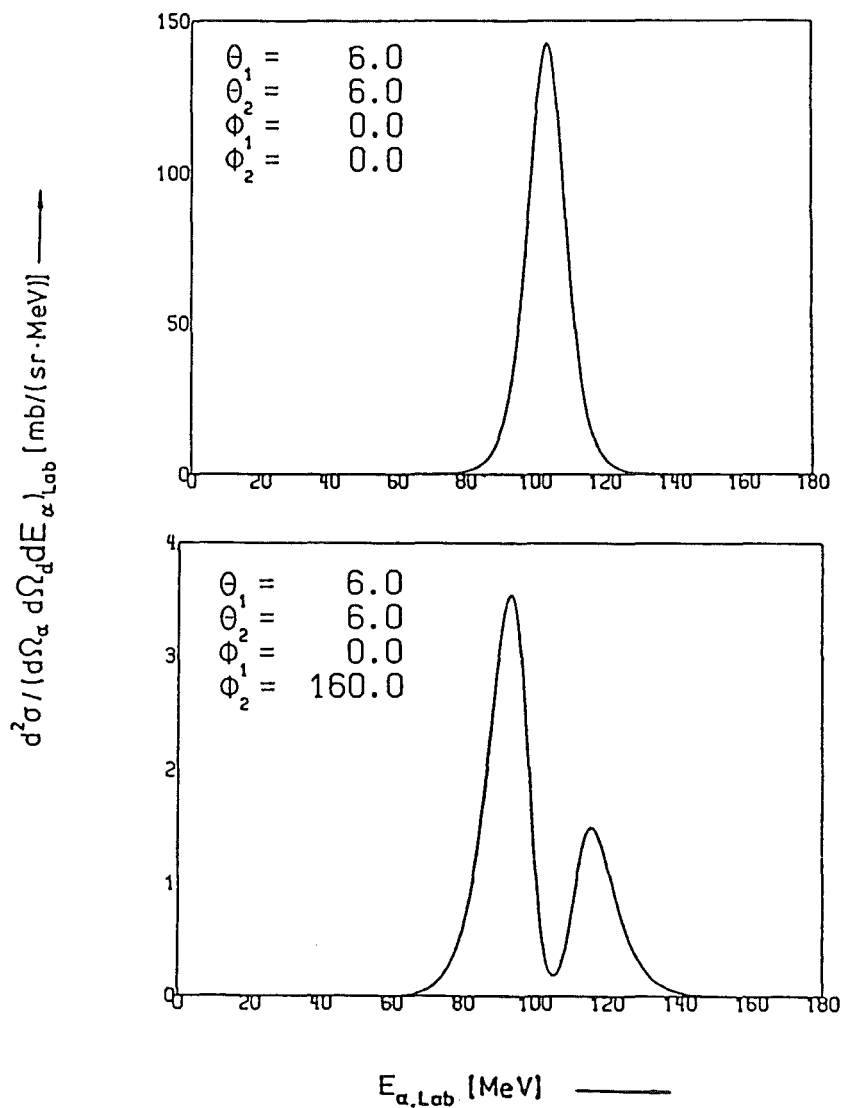
Fig. 1   Theoretical coincidence energy spectra of alpha particles for the elastic
nuclear break-up (opaque-model), with neglection of Coulomb effects.
The detection angles with respect to the beam direction are $\theta_1 = \theta_2 = 6°$
and the azimuth angle for the fixed detector is $\phi_1 = 0°$. The input
parameters are taken for the reaction 156 MeV $^6Li \to \alpha + d$.

region of forward emission angles, especially in the angular range of the classical
Coulomb deflection. Besides the well known single maximum in the break-up
spectra double and triple peak structures appear at particular combinations of the
observation angles. Similar multiple peak structures have been already observed
by Heide et al. (3) at larger relative angles between the two fragments, whereby in
this case the structure probably originates from interference effects.

Based on the present extension of the Serber model approach some theoretical predictions for the triple differential cross sections of alpha particles from the reaction 156 MeV ^{6}Li→ a + d are shown in Figure 1.

(1)   R. Serber, Phys. Rev. **72** (1947) 1008
(2)   H. Utsunomiya, Phys. Rev. **C30** (1984) 1748
(3)   N. Heide, D.K. Srivastava, H. Rebel, Phys. Rev. Lett. **63** (1989) 60

*   Central Institute of Physics, IFIN, Bucharest, Romania

1.3.12   SLOWLY CONVERGING INTEGRALS IN THE DWBA THEORY OF STRIPPING TO UNBOUND STATES AND BREAK-UP

D.K. Srivastava*, H. Rebel (1)

Analytical expressions are given for slowly converging integrals involving three distorted waves encountered in the study of stripping to unbound states and zero-range post-form distorted waves Born approximation for break-up of light ions.

(1)   J. Phys. G **15** (1989) L35

*   Bhabha Atomic Research Centre, V.E.C.C., Calcutta, India

1.3.13   A MULTISTEP EVAPORATION MODEL FOR INTERMEDIATE MASS FRAGMENT EMISSION

A.J. Cole*, K. Grotowski**, T. Kozik** and H. Rebel (1)

A multistep evaporation model for intermediate mass fragment emission in heavy ion reactions is described. It applies the canonical transition-state method for the determination of the probability for disintegration of a fused system. The energy and angular momentum relations at the saddle and scission points are calculated on the basis of the finite range liquid drop model. The derivation of the total kinetic energy release uses the concept of amplifying modes which is equivalent to that of shape fluctuations at the ridge point. The model reproduces fairly well the mass and angular distributions and the energy spectra of intermediate mass fragments yields from inclusive and coincidence experiments.

(1)   Report KfK 4484, Kernforschungszentrum Karlsruhe (1988)

*   Institut des Sciences Nucléaires, Grenoble, France
**   Institute of Physics, Jagellonian University, Cracow, Poland

1.3.14 COMPOUND NUCLEUS EMISSION OF INTERMEDIATE MASS FRAGMENTS IN THE 6Li + Ag REACTION AT 156 MeV

K. Grotowski*, J. Ilnicki,* T. Kozik*, J. Lukasik*, S. Micek*, Z. Sosin*, A. Wieloch*, N. Heide, H. Jelitto, J. Kiener, H. Rebel, S. Zagromski, A.J. Cole** (1)

It is shown that emission of intermediate mass fragments in a wide range of masses and angles can be well described by sequential binary decay of the equilibrated compound system produced in the 26 MeV/A 6Li + Ag reaction.

(1)   Phys. Lett. 223B (1989) 287

*   Institute of Physics, Jagellonian University, Cracow, Poland
**   Institut des Sciences Nucléaires, Grenoble, France

1.3.15 INTERMEDIATE MASS FRAGMENT EMISSION IN 6Li INDUCED NUCLEAR REACTIONS AT E/A = 26 MEV

H. Rebel, I.M. Brâncuş*, A.J. Cole**, K. Grotowski** and T. Kozik*** (1)

The emission of intermediate mass fragments (IMF) from complex nuclei in nuclear reactions well above the interaction barrier is believed to be a signature of highly excited nuclear matter. At low bombarding energies (E/A < 10 MeV) the complex fragment emission has been characterized as a statistical-binary decay of a classical compound nucleus formed in complete fusion reactions. However, at larger energies the origin of the fragments has not been understood in detail at present time since more complicated reaction paths do show up.

We discuss results of inclusive type experimental studies with 156 MeV 6Li projectiles and study the extent to which IMF (Z > 3) emission is present in nuclear reactions of a relatively fragile projectile like 6Li in the transitional energy regime of 26 MeV / amu. The data are analyzed in terms of a multistep-evaporation model. In addition, the experimental Z-distributions are considered in the frame of an extended sum-rule model. The results give evidence that the dynamical behaviour of the dinuclear system on its way to fusion is essential in reproducing the observed element distributions of the fragments.

(1)   Symp. Nucl. Physics (India) 31A (1988) 209

*   Central Institute of Physics, IFIN, Bucharest, Romania
**   Institut des Sciences Nucléaires, Grenoble, France
***   Institute of Physics, Jagellonian University, Cracow, Poland

1.3.16 EXTENDED SUM–RULE MODEL ANALYSES OF COMPLEX – FRAGMENT EMISSION IN LIGHT AND HEAVY ION COLLISIONS

I.M. Brâncuş*, H. Rebel and J. Wentz

Light and intermediate mass fragment (IMF) emission is a quite general phenomenon in nuclear reactions. Though the details may depend in a rather complicated way on the specific properties of the particular system under consideration, the general features and overall tendencies, evident in results of inclusive experiments, are conspicuously similar and point to a common basic process and origin which should be accessible to a simple phenomenological description of the most prominent global observations. Generalizing the original sum-rule model (1) for complete and incomplete fusion processes, the *extended* sum-rule model (ESM) (2), adopts the view that IMF emission preferentially originates from cluster emission during the dissipative evolution of the dinuclear system *before* complete equilibration. The ESM writes the integrated cross section for a particular channel i

$$\sigma^{tot}(i) = \pi\lambda^2 \sum_{\ell=0}^{\infty} K_\ell (2\ell+1) \frac{(T_\ell(i) + T_\ell') \cdot P(i)}{\sum_{j=1}^{n} T_\ell(j)P(j) + \sum_{j=2}^{n} T_\ell' P(j)} \quad (1)$$

in terms of two different entrance channel transmission coefficients $T_\ell(i)$ and T_ℓ', respectively and (following the Q_{gg} systematics) by the probability for the channel i

$$P(i) \propto exp\{ [Q_{gg}(i) - Q_c(i)]/T \} \quad . \quad (2)$$

T is the apparent temperature of the partial equilibrium, Q_c a Coulomb correction and K_ℓ is an overall entrance transmission factor limiting the contribution around grazing angular momentum. The ESM includes the nearly equilibrated component of IMF emission with

$$T_\ell' = \left\{ 1 + exp \left[(\ell - \ell_{cr}^{dyn})/\Delta\ell \right] \right\}^{-1} \quad , \quad (3)$$

limited through a smooth cut-off parametrization at the dynamical value of the critical angular momentum which takes into account the orbital angular momentum dissipation due to frictional forces.

Various cases of complex fragment emission reported in literature, in particular the case of ^{6}Li induced reactions at E_{Li} = 156 MeV, have been analysed. Fig. 1 displays two examples. In all cases the values of the apparent temperature T required by the fit to the data are consistent with the estimate based on the excitation energy. The successful description of the element distribu-
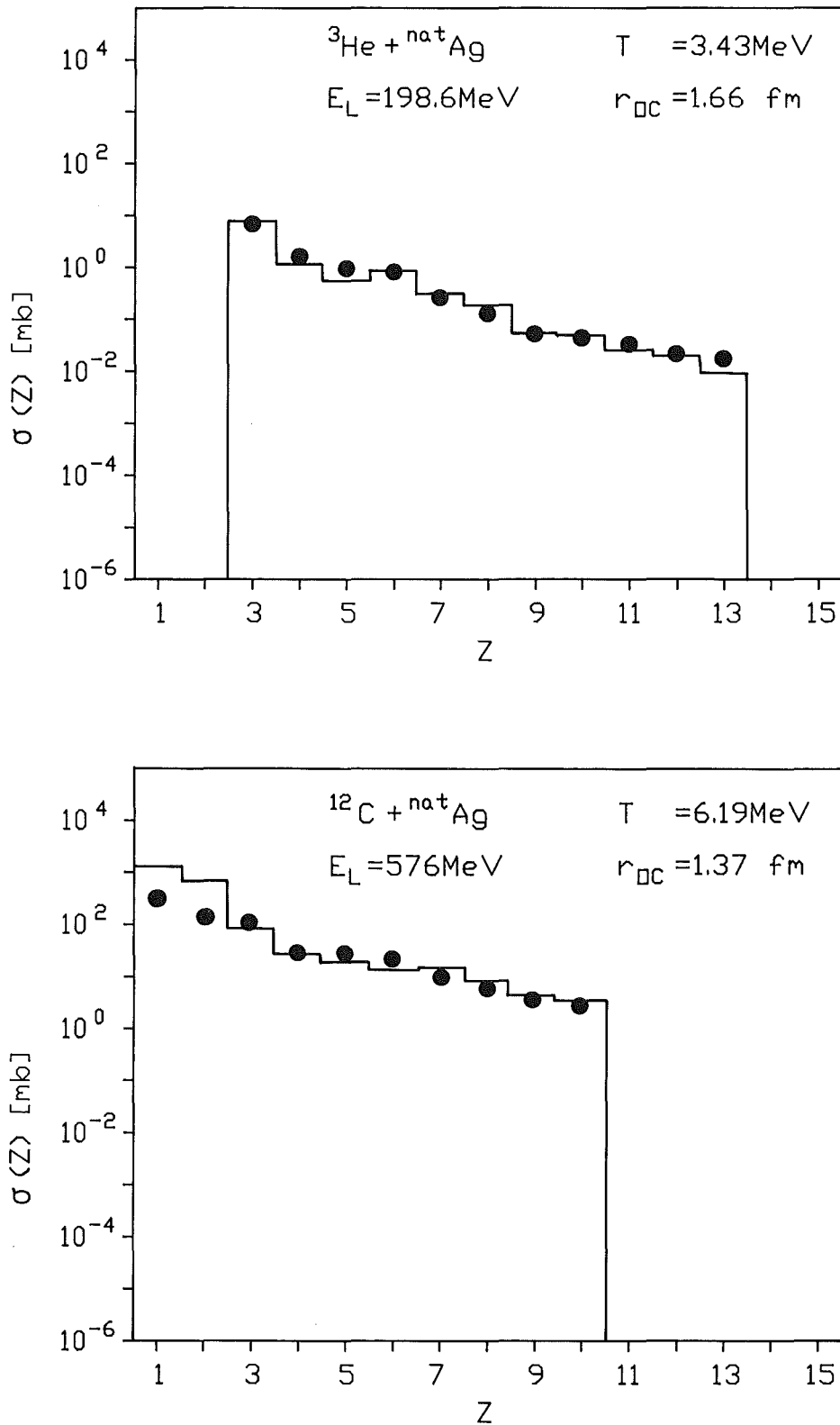
Fig. 1   Extended sum-rule description of the element cross section σ (Z) of complex-fragment emission in collissions of 198.6 MeV 3He (3) and 576 MeV 12C (4) with natAg.

tions, correctly reproducing the observed absolute values $\sigma^{tot}(i)$ and providing reasonable predictions of the angular momentum localization support the view of the ESM. Although the ESM cannot specify the underlying dynamics in detail and is based only on very general assumptions, one may envisage a variant of one of the various dissipative processes, say some type of rather asymmetric fast fission or deep inelastic processes.

(1)   J. Wilczyński, K. Siwek-Wilczyńska, J. van Driel, S. Gonggrijp, D.C.J.M. Hageman, R.V.F. Janssens, J. Lukasiak, R.H. Siemssen and S.Y. van der Werf, Phys. Rev. Lett. 45 (1980) 606; Nucl. Phys. A373 (1982) 109

(2)   I.M. Brâncuş and H. Rebel, Rev. Roum. Physique 34 (1989) No 10
        I.M. Brâncuş, Report KfK 4453, Kernforschungszentrum Karlsruhe (1988)

(3)   K. Kwiatowski, J. Bashkin, H. Karworski, M. Fatyga and P.E. Viola, Phys. Lett. 171B (1986) 41; K. Kwiatowski, Nucl. Phys. A471 (1987) 271c

(4)   R. Trockel, Report GSI-87-17, Gesellschaft für Schwerionenforschung, Darmstadt (1987)

*   Central Institute of Physics, IFIN, Bucharest, Romania

1.3.17 DISSIPATIVE FRAGMENTATION IN 336 MeV ^{40}Ar + ^{nat}Ag REACTIONS VIEWED BY THE EXTENDED SUM-RULE MODEL

I.M. Brâncuş*, J. Wentz and H. Rebel

Both equilibrium and nonequilibrium reaction mechanisms appear to coexist for complex-fragment emission in heavy ion reactions at intermediate energies. Their relative importance depends as much on the mass asymmetry of the entrance channel as on the bombarding energy. In addition to quasifree and deep-inelastic processes, which are responsible for the fragment production, in particular, in the vicinity of the target and projectile masses, near-equilibrium emission from fusion-like processes has been found to be a most important source. This latter component must not be necessarily attributed to the decay of a fully equilibrated compound nucleus. The extended sum-rule (ESM) model (1) adopts the view that this component may arise with the dynamical evolution of the system via partially equilibrated states on the way to fusion and to some type of a rather *asymmetric fast* or *quasi - fission process* (1) : *"dissipative fragmentation"*.

We apply the ESM to the analysis of the intermediate-mass fragment emission (IMF : $3 \leq Z \leq 9$) as measured (2) for the backward angular region in 336 MeV ^{40}Ar + ^{nat}Ag reactions. Recent coincidence studies (3) of this system at the same incident energy determine the angular-momentum windows for various components of the IMF cross sections and may provide a test of the predictions based on the ESM.

With a value $T = 3.97$ MeV for the effective temperature and $r_{oc} = 1.75$ fm for the radius parameter characterising the relative distance where charge transfer takes place the calculated angle-integrated (inclusive) cross sections are found to be in good agreement with the experimental results. The somewhat enlarged value of r_{oc} may indicate an increased deformation of the dinuclear system (2) while the value of T is consistent with the estimate based on the excitation energy.
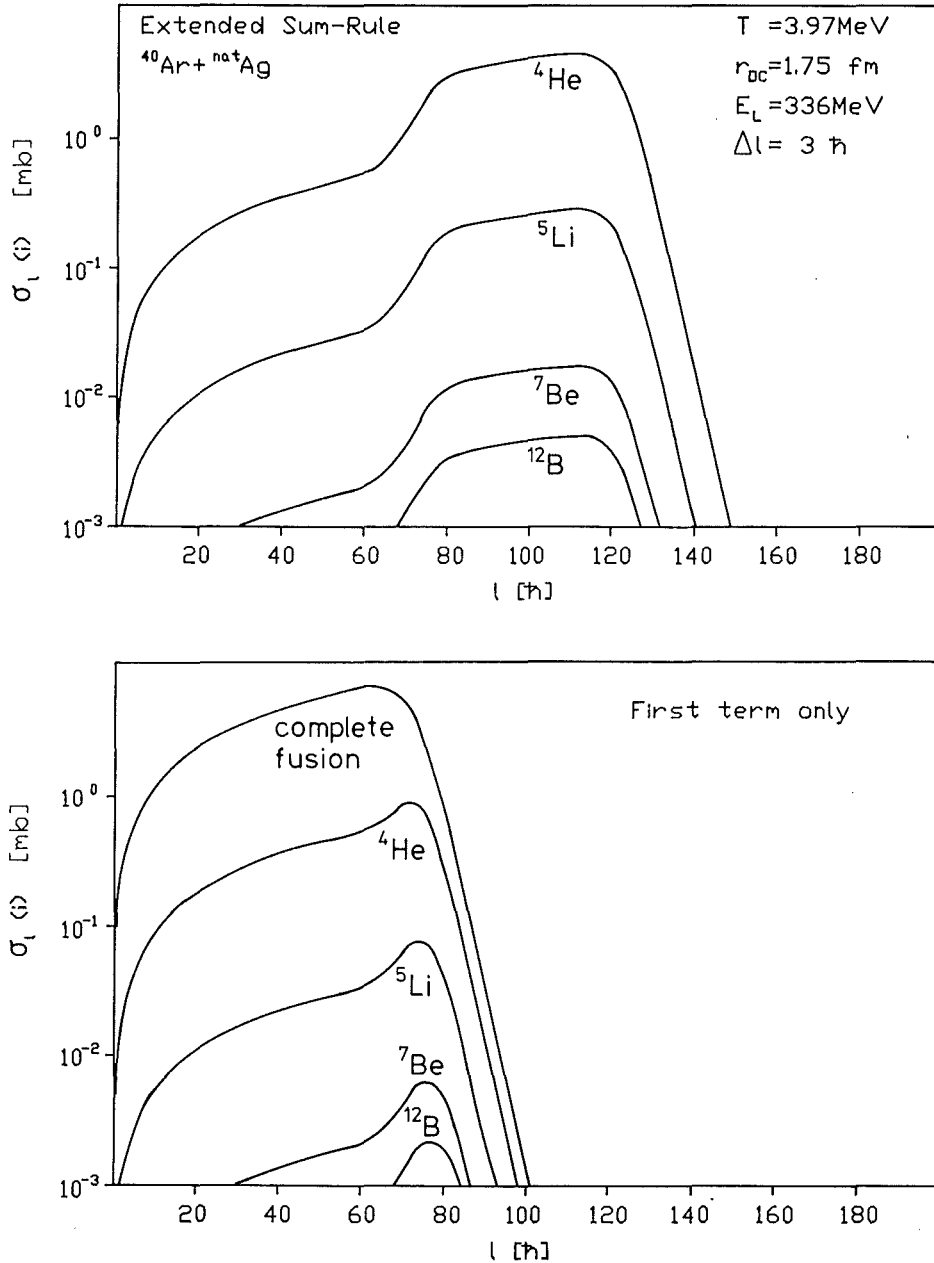
Fig. 1 Partial cross sections σ_ℓ for the emission of various complex fragments in 336 MeV ^{40}Ar + ^{nat}Ag collisions: Prediction of the extended sum-rule model.

While the first term of the expression of the ESM represents the contribution of complete and incomplete fusion (like in the original sum rule), the second term (depending on the critical angular momentum for fusion in dissipative collisions) accounts for the dissipative fragmentation. Fig. 1 shows that the major part of IMF emission (in the backward angular region) has to be attributed to the second term. Obviously fragments ($3 \leq Z \leq 9$) originating from incomplete fusion are concentrated in angular momentum range of 60 - 100 $\hbar$. This is in remarkable agreement with the results of ref. 3, associating the quasi fission channel to 103 - 135 $\hbar$, e.g..

Though ESM does not specify the underlying reaction mechanism in detail, it is able to give a global description of the observed (inclusive) cross sections and to predict the angular momentum windows of various contributions.

(1)   I.M. Brâncuş and H. Rebel, Rev. Roum. Phys. (in press)
        H. Rebel, I.M. Brâncuş, K. Grotowski, T. Kozik, A. Cole
        Symp. Nucl. Physics (India) **31A** (1988) 209
(2)   R. Vaz, D. Logan, B.M. Alexander, E. Duek, G. Guerreau, L. Kowalski,
        M.F. Rivet, M.S. Zisman, Z. Phys. **A 311** (1983) 89
(3)   R. Lacey et al., Phys. Rev. **C37** (1988) 2540
*   Central Institute of Physics, IFIN, Bucharest, Romania

1.3.18 NUCLEAR STRUCTURE EFFECTS IN ELASTIC ^{12}C + ^{12}C SCATTERING

S. Galachmatova*, E. Romanovsky*, A. Shirokova*, K.V. Shitikova*, H.J. Gils and H. Rebel (1)

Elastic ^{12}C + ^{12}C scattering cross sections measured at incident energies of 13.8 MeV/amu and of 9.8 MeV/amu are analysed within the semimicroscopic approach of the standard double-folding model. The influence of different forms of the ^{12}C-nucleon density distribution is studied. It turns out that the experimental cross sections give some preference for a density distribution resulting from an α-cluster model description of ^{12}C.

(1)   Report KfK 4589, Kernforschungszentrum Karlsruhe (1989)
*   Institute of Nuclear Physics, Moscow State University, Moscow, USSR

1.3.19 EXPERIMENTAL METHODS FOR STUDYING NUCLEAR DENSITY DISTRIBUTIONS

C. J. Batty*, E. Friedman**, H. J. Gils and H. Rebel (1)

The review addresses a fundamental problem that has been of long-standing interest: exploring experimentally the density distributions of constituents within the nucleus. As the energy and specificity of probes have increased over the years, the degree of spatial resolution and ability to select specific charge, current, spin, and isospin densities have correspondingly increased. The article provides a critical discussion of what has been learned about nuclear density distribution using electrons, muons, nucleons, antinucleons, pions, alpha particles and kaons as probes. This current understanding, and the limitation thereof, are crucial in framing the questions that motivate the next generation of experimental facilities to study atomic nuclei with electromagnetic and hadronic probes.

(1)   Adv. Nucl. Phys. 19 (1989) 1, Plenum Press, New York - London
*   Rutherford Appleton Laboratory, Chilton, Didcot, United Kingdom
**   Hebrew University, Racah Institute of Physics, Jerusalem, Israel

1.3.20 EVIDENCE FOR A NEUTRON HALO IN ^{11}Li

H. J. Gils and H. Rebel (1)

Various recent experimental results pointing to the existence of a neutron-halo in the shortliving nucleus ^{11}Li are critically commented.

(1)   Phys. Bl. 45 (1989) 58 (in German)

1.3.21 DECAY OF ISOSCALAR GIANT RESONANCES IN ^{124}Sn AND ^{116}Sn

A. Lehmann*, E. Aschenauer*, W. Eyrich*, H.J. Gils, A. Hofmann*,
M. Moosburger*, H. Rebel, R. Rudeloff*, H. Schlösser*, H. Wirth*,
S. Zagromski

The investigation of giant resonance decay is a very sensitive method to get detailed insight in nuclear structure effects. From a systematic extraction of the components of direct and statistical decay we can learn about the transport of energy within the nucleus after excitation. A further aspect of such decay experiments is the search for giant resonance modes with higher multipolarities

(L ≥ 4) using the information from the population of states with higher spins in the residual nucleus.

To clarify those questions we perform (^{6}Li, ^{6}Li'n)-coincidence experiments at the 156 MeV ^{6}Li beam of the Karlsruhe Isochronous Cyclotron. The scattered ^{6}Li particles are detected by the magnetic spectrograph "Little John" at forward angles. The coincident decay neutrons are measured with eight large scintillation detectors at backward angles using time-of-flight technique, similar as described in ref. 1. In continuation of our earlier decay experiment at ^{208}Pb (2) and ^{90}Zr (1) we choose the Sn-isotopes for this experiment in order to make statements over a wide mass range of nuclei.
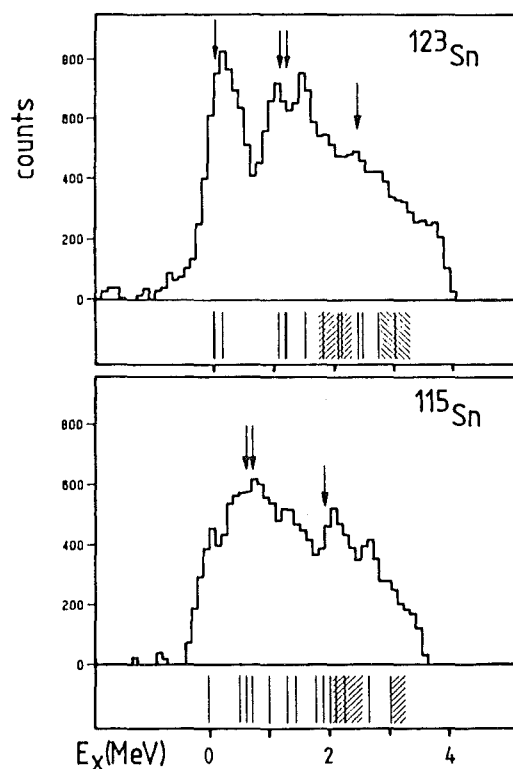
Fig. 1   n-decay spectrum of the giant quadrupole resonance region from (^{6}Li, ^{6}Li'n) measurements at 3.0° in ^{124}Sn (upper part) and ^{116}Sn (lower part).

In Fig. 1 the neutron decay spectra of the giant quadrupole resonance region (E2 GR) in ^{124}Sn and ^{116}Sn are shown. The most dominant feature in the first spectrum is a clearly separated peak around the ground state of the residual nucleus ^{123}Sn (Fig. 1), upper). This peak consists of three unresolved states, 11/2$^-$, 3/2$^+$ and 1/2$^+$. Comparing this strength to the less populated 1/2+ ground state of ^{115}Sn (Fig. 1, lower), we may conclude that the 11/2$^-$state in ^{123}Sn is populated strongly. This is a first hint for strength with higher multipolarity in the giant resonance region of ^{124}Sn. Further indications for multipolarities L≥4 are the

structures at higher excitation energies (marked by arrows) in the decay spectra of Fig. 1, which represent states with spins of 11/2⁻ and 7/2⁺.

The neutron decay spectra of the giant monopole resonance region (E0 GR) in ^{124}Sn and ^{116}Sn are presented in Fig. 2. We recognize an evaporation spectrum (dashed line) with significant deviations at energies $E_{final} \leq 3$ MeV in both nuclei. These deviations correspond to an enhanced population of hole states in the residual nuclei ^{123}Sn and ^{115}Sn, respectively - a clear evidence for a direct decay component. At energies $E_{final} > 1.8$ MeV phonon coupled states /hatched areas) in ^{123}Sn and ^{115}Sn are overlapping the hole states. In Fig. 2 (upper) two structures around 2.0 MeV and 2.5 MeV can be recognized. From this we conclude that also preequilibrium decay components contribute.
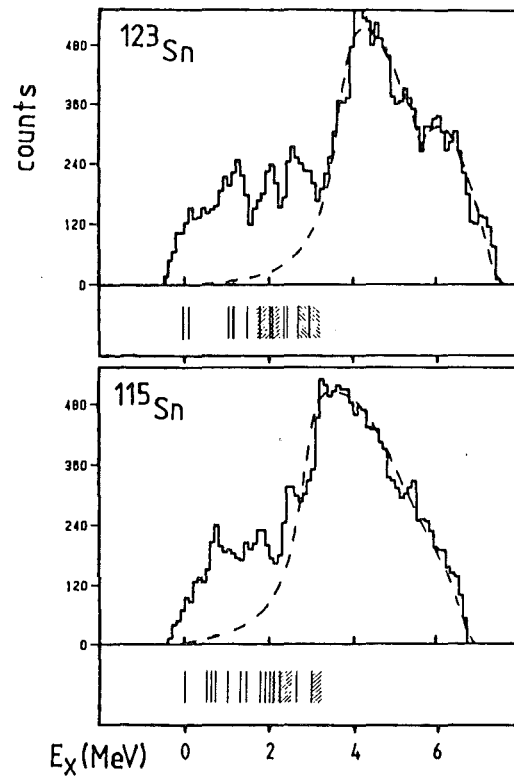
Fig. 2   n-decay spectrum of the giant monopole resonance region from (^{6}Li, ^{6}Li'n) measurements at 3.0° in ^{124}Sn (upper part) and ^{116}Sn (lower part).

From the shape of the monopole decay spectra we estimate a direct decay component of $\approx$ 15% in ^{124}Sn and $\approx$ 20% in ^{116}Sn. The amount of the preequilibrium decay component is about $\approx$ 10% in ^{124}Sn and $\approx$ 5% in ^{116}Sn.

These results are consistent with earlier measurements at ^{208}Pb (2) and ^{90}Ze (1). The direct decay component of around 15% and the contribution of additional strength with multipolarity L $\geq$ 4 in the giant resonance region seems to be a general property of medium heavy nuclei.

(1)   K. Fuchs, W. Eyrich, A. Hofmann, B. Mühldorfer, U. Scheib,
        H. Schlösser, H. Rebel, Phys. Rev. C32 (1985) 418
(2)   W. Eyrich, K. Fuchs, A. Hofmann, U. Scheib, H. Steuer, H. Rebel,
        Phys. Rev. C29 (1984) 418
*   Physikalisches Institut, Universität Erlangen-Nürnberg, Germany

1.3.22 GAMOW-TELLER TRANSITIONS IN LIGHT NUCLEI

M. Moosburger*, E. Aschenauer*, H. Dennert*, W. Eyrich*, H.J. Gils,
A. Hofmann*, A. Lehmann*, H. Rebel, R. Rudeloff*, H. Schlösser*,
H. Wirth*, S. Zagromski

The (^{6}Li, ^{6}He) reaction is of special interest for the investigation of spin- isospin-dependent phenomena in nuclear reactions. The selection rules $\Delta S = \Delta T = 1$ show the good ability for the examination of Gamow-Teller (GT) transitions (1,2).

The experiments were performed at the 156 MeV ^{6}Li^{3+} beam of the Karlsruhe Isochronous Cyclotron KIZ. We used the magnetic spectrograph "Little John" to measure the ^{6}He particles at extreme forward angles. Zero degree measurements were carried out for all targets. The examined targets of ^{12}C, ^{18}O, ^{26}Mg, and ^{42}Ca were selected in the region of light nuclei with respect to the fact, that analog β-decays of the final or mirror nucleus are known. The intention was to look for a correlation between 0° cross sections and B(GT)-values for known GT-transitions.

In Fig. 1 we present the 0° spectra of the (^{6}Li, ^{6}He) reaction on the four target nuclei. The 1$^+$ states representing GT strength are marked. It should be noted,, that each spectrum is free of any experimental background. At the right the level schemes with the important GT transitions are shown.

Each spectrum is dominated by the peak of a strong GT transition, which is known from β-decay. In the case of ^{12}N and ^{18}F these are the ground states, in ^{26}Al and ^{42}Sc the states at 1.06 MeV and 0.61 MeV, respectively. The cross sections of these transitions can be compared with B(GT) values calculated from known ft-values. In table 1 the data of β-decay and measured 0°-cross sections are listed. Due to the different Q-values of the (^{6}Li, ^{6}He) reaction it is necessary to correct σ(0°) to a momentum transfer of q=0. We got the modified values σ(0°)$_{corr.}$/B(GT) on the mass number A (plotted in Fig. 2) in agreement with (p,n) measurements (3).
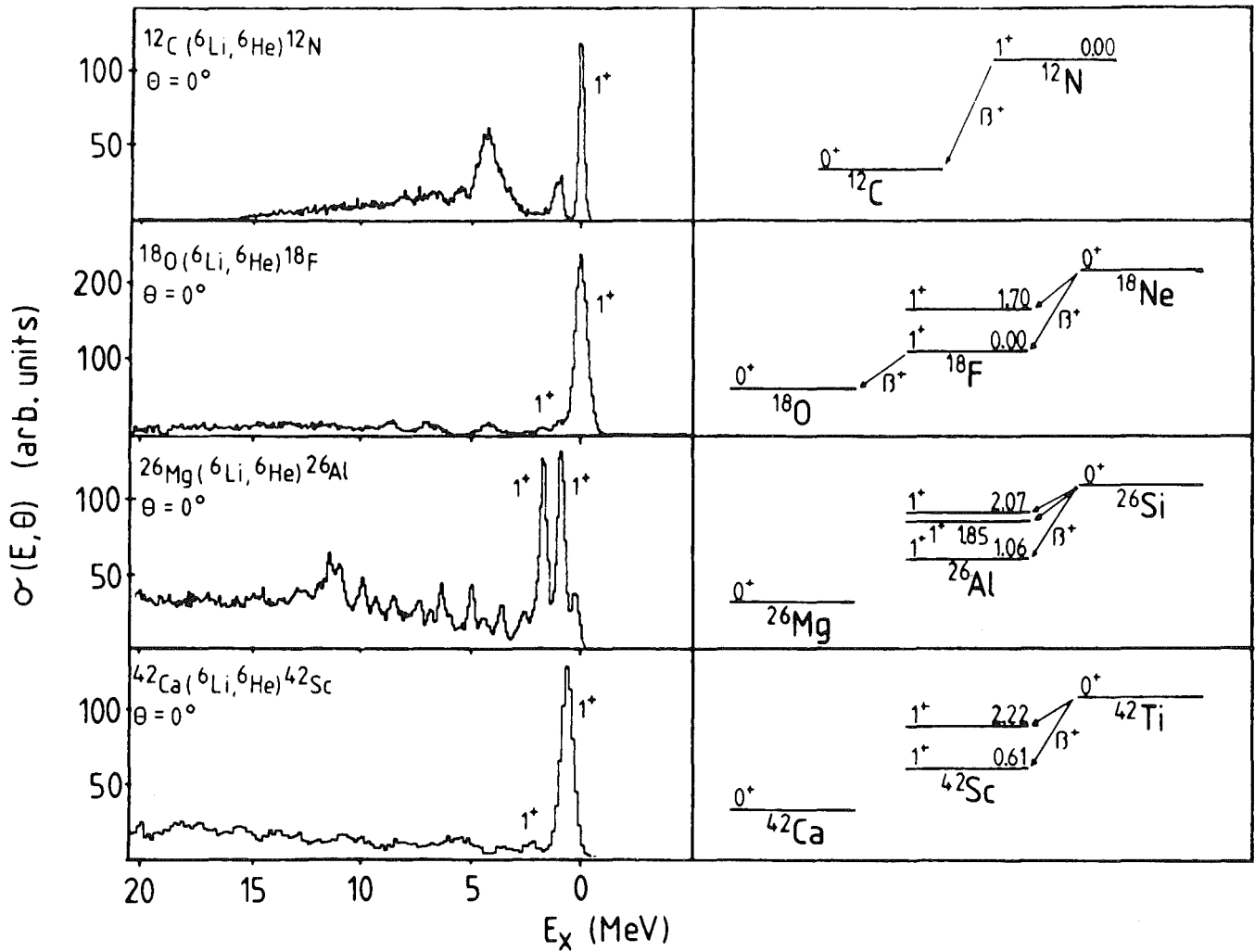
Fig. 1   Left: Zero degree spectra of the reactions $^{12}C(^6Li,^6He)^{12}N$, $^{18}O(^6Li,\ ^6He)^{18}F$, $^{26}Mg(^6Li,\ ^6He)^{26}Al$, and $^{42}Ca(^6Li,\ ^6He)^{42}Sc$ 1^+ states are indicated.

Right: Level diagrams showing the analog β-decays of the corresponding (^6Li, ^6He) reactions.
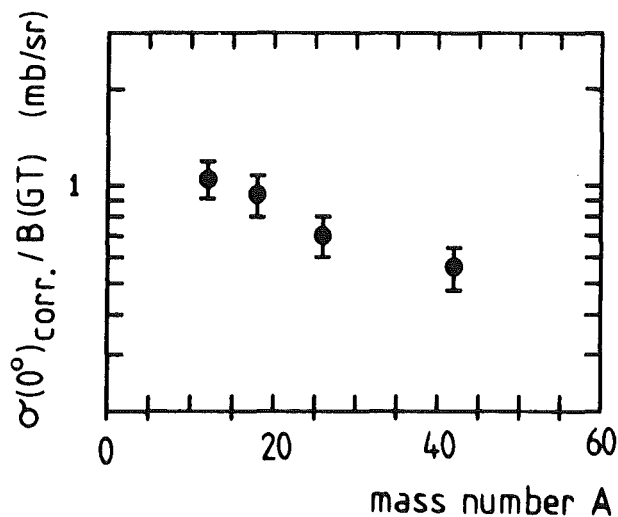
Fig. 2
Plot of the ratio between corrected 0°-(^6Li, ^6He) cross sections and B(GT) values of known strong β-transitions vs. mass number A.

Table 1: Comparison of 0°-(^{6}Li, ^{6}He) cross sections with analog β-decay.

Reaction	E_x (MeV)	σ(0°) (mb/sr)	σ(0°)$_{corr.}$ (mb/sr)	B(GT)	β-decay
^{12}C(^{6}Li, ^{6}He)^{12}N	0.00	0.3	0.93	0.885	^{12}N(β$^+$)^{12}C
^{18}O(^{6}Li, ^{6}He)^{18}F	0.00	2.8	2.97	3.16	^{18}Ne(β$^+$)^{18}F
^{26}Mg(^{6}Li, ^{6}He)^{26}Al	1.06	0.64	0.77	1.10	^{26}Si(β$^+$)^{26}Al
^{42}Ca(^{6}Li, ^{6}He)^{42}Sc	0.61	1.1	1.5	2.63	^{42}Ti(β$^+$)^{42}Sc

(1)   J.S. Winfried, N. Anantaraman, S.M. Austin, Z. Chen, A. Galonsky, J. van der Plicht, H.L. Wu, Phys. Rev. **C35** (1987) 1734

(2)   M. Moosburger, E. Aschenauer, H. Dennert, W. Eyrich, A. Lehmann, R. Rudeloff, H. Schlösser, H. Wirth, H.J. Gils, H. Rebel, S. Zagromski, submitted to Phys. Rev. C

(3)   T.N. Taddeucci, C.A. Goulding, T.A. Carey, C. Byrd, C.D. Goodman, C. Gaarde, J. Larsen, D. Horen, J. Rapaport, E. Sugarbaker, Nucl. Phys. **A469** (1987) 125

*   Physikalisches Institut, Universität Erlangen-Nürnberg, Germany

1.3.23   THE (^{6}Li, ^{6}He) REACTION ON ^{37}Cl AND ^{71}Ga

E. Aschenauer*, H. Dennert*, W. Eyrich*, H.J. Gils, A. Hofmann*,

A. Lehmann*, M. Moosburger*, H. Rebel, H. Wirth*, H. Schlösser*,

S. Zagromski

The solar neutrino problem has turned out to be an important unsolved question of relevance for the nature of the neutrino and for astrophysics. It originates from a discrepancy between the measured and predicted neutrino flux. There are two types of sources of uncertainties affecting the predictions for counting rates of solar neutrino experiments: the production and the detection. In order to reveal new information carried by the neutrinos uncertainties due to the neutrino source have to be separated from unknown features of the detector sensitivity.

Though there are great problems with background subtraction (p,n) measurements are the most used method to calibrate radiochemical solar neutrino detectors. The (^{6}Li, ^{6}He) reaction should be an useful alternative method, providing a sensitive tool to study Gamow-Teller transitions involved in the detection reactions (1).

With respect of the great importance of the Davis experiment and the future Gallex experiment we measured the cross sections of the reactions ^{37}Cl(^{6}Li,
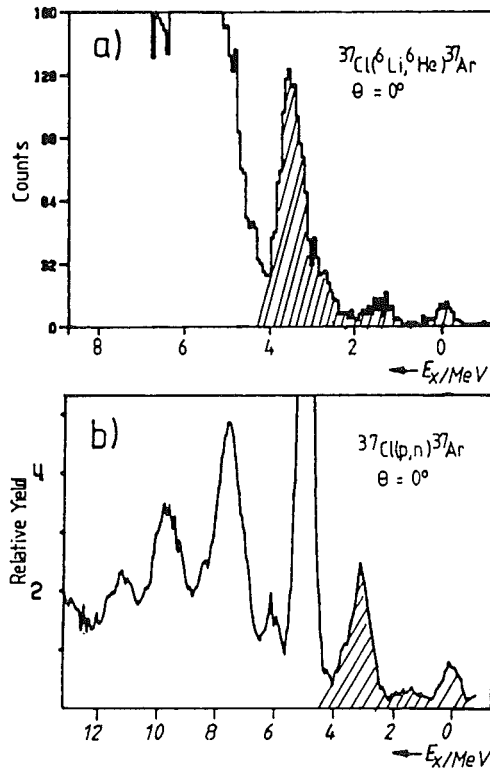
Fig. 1   a: Spectrum of the reaction ^{37}Cl (^6Li, ^6He)^{37}Ar taken at zero degree.
           b: Spectrum of the reaction ^{37}Cl (p,n)^{37}Ar taken at zero degree.
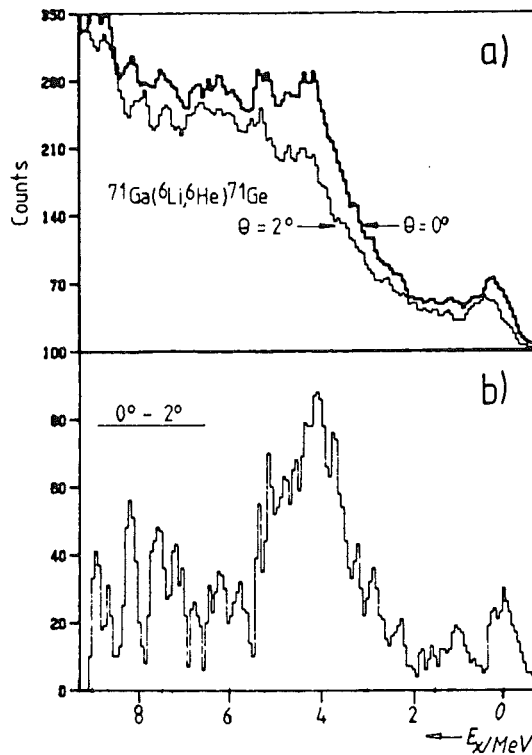
Fig. 2   a: Spectra of the reaction ^{71}Ga (^6Li, ^6He)^{71}Ge taken at zero and two
              degree, respectively.
           b: Difference spectrum.

^{6}He)^{37}Ar and ^{71}Ga(^{6}Li, ^{6}He)^{71}Ge with the intention to determine experimentally the Gamow-Teller strengths.

Fig. 1 shows a spectrum of the ^{37}Cl(^{6}Li, ^{6}He)^{37}Ar reaction taken at zero degree with the 156 MeV ^{6}Li beam of the Karlsruhe Isochronous Cyclotron. The hatched area corresponds to Gamow-Teller states, which are important for solar neutrino interaction with ^{37}Cl. For comparison Fig. 1b presents a spectrum of the reaction ^{37}Cl(p,n)^{37}Ar (2) and is in good agreement with our spectrum in the region of interest. Fig. 2a shows two (^{6}Li, ^{6}He) spectra from ^{71}Ga taken at zero degree and two degree, respectively. In Fig. 2b the difference spectrum is displayed resulting from the maximum-minimum method (3). This represents, in particular, the Gamow-Teller strength of the most important energy range (0 to 2 MeV) for the neutrino interaction.

(1)	M. Moosburger, E. Aschenauer, H. Dennert, W. Eyrich, A. Lehmann, R. Rudeloff, H. Schlösser, H. Wirth, H.J. Gils, H. Rebel, S. Zagromski, submitted to Phys. Rev. C
(2)	J. Rapaport, T. Taddeucci, P. Welch, C. Gaarde, J. Larsen, C.D. Goodman, C.C. Foster, C.A. Goulding, D. Horen, E. Sugarbaker, T. Mastersen, Phys. Rev. Lett. 47 (1981) 1518
(3)	H. Wirth, E. Aschenauer, W. Eyrich, A. Lehmann, M. Moosburger, H. Schlösser, H.J. Gils, H. Rebel, S. Zagromski, submitted to Phys Rev. Lett.

*	Physikalisches Institut, Universität Erlangen-Nürnberg, Germany

2. ASTROPHYSICS WITH EXTENDED AIR SHOWERS

2.1 THE KASCADE PROJECT

P. Doll, J. Engler, H. J. Gils, D. Heck, N. Heide, H. Keim, H. O. Klages, J. Knapp, H.J. Mayer, H. Müller, J. Oehlschläger, H. Rebel, G. Schatz, G. Schmalz, T. Thouw, S. Zagromski, and B. Zeitnitz

KASCADE (KArlsruhe Shower Core and Array DEtector) is an extensive air shower experiment whose main aim is to obtain information on the primary chemical composition at energies above 3×10^{14} eV. In addition the arrangement will be able to identify point sources in the quoted energy range. The basic approach is to measure a large number of parameters for each individual shower. The main components of the arrangement are an array of detectors which register both electrons and muons and a central detector for hadrons and muons. The experiment is to be set up at the site of the Research Centre (49° north, 8° east, 110 m a.s.l.). The detector array (1), the central detector (2) and the simulations performed during the design of the experiment (3) are described in more detail in other contributions to this report.

General Considerations It is well known that a number of observable quantities depend on the nature of the primary particle. Among these are the ratio of electron and muon numbers (cf. ref. (4), e.g.), the energy spectrum of hadrons and their lateral distribution (5). Nevertheless, considerable discrepancies exist in literature on the chemical composition of the primaries in the energy range around 10^{15} eV and above. In our opinion, this is at least partly due to the fact that most experiments so far have only measured one or two characteristic shower properties and have employed insufficient sampling. The latter refers especially to the measurement of the muon number, since this is the component of the shower which is spread out the most and therefore requires the largest detector area for registering a sizable fraction. In most previous experiments the fluctuation of the measured muon number was governed by the statistics of sampling rather than by the intrinsic fluctuation between showers. In addition, only the mean lateral muon distribution averaged over the (unknown) chemical composition was determined.

The KASCADE experiment attempts to measure a larger number of parameters for each individual shower. These include electron and muon numbers, their lateral distribution, as well as number, energy and spatial distribution of hadrons in the shower core. In view of the large intrinsic fluctuations of

all shower properties a simultaneous measurement of several parameters which are sensitive to composition can be expected to yield a more reliable result. Such a multiparameter experiment requires a large detector area in order to obtain statistically significant multiparameter distributions. These requirements (and the inevitable financial restrictions) determine the arrangement to a large extent.

Point sources will be identified by the usual timing method. Due to the large number of detectors in the array and the good time resolution an excellent angular resolution is obtained (1). The location of the experiment near sea level sets an energy threshold near 3×10^{14} eV, though. Above that energy the large area of the array will make it one of the most sensitive arrangements presently under construction.

General Lay-out The general lay-out of the experiment is shown in Fig. 1. It consists of an array of 200x200 m² and a central detector of 18x18 m².

The array consists of 316 detector stations spaced at about 12 m distance. Each station houses 4 scintillation detectors of 0.78 m² each for measuring the electron density and a fifth scintillation detector of 3.2 m² for muon detection. The latter is shielded by 20 radiation lengths of lead and iron to absorb the electromagnetic component. This results in a muon threshold of c. 300 MeV. The electron detectors are covered by 5 mm of lead to convert gamma rays for a better timing of the shower front. Details of the array detectors and their performance, including that of identifying point sources, are given in ref. (1).

The central detector is a hadron calorimeter of 10 interaction lengths thickness. It will be made of iron and concrete with 7 layers of ionisation chambers filled with liquid tetramethylsilane. The electrodes of the ionization chambers are divided into pads of 25x25 cm² which are read out independently, so a spatial resolution of 25 cm is obtained in both horizontal coordinates. The spacing of the layers is chosen in such a way as to obtain an energy resolution of about 35 % independent of energy. An additional layer of scintillators is introduced to provide a fast hadron trigger.

Beneath the central calorimeter muons above 2 GeV will be detected and localized by means of multiwire proportional chambers. Details of the central detector are given in ref. (2)

The total sensitive area for muons is 1300 m² (i.e. 3.2 % of the array area). The corresponding number for electrons is 1000 m² (2.5 %).

There will be two types of registered events, those triggering the array and a subsample of these (0.8 %) in which the shower core hits the central detector. For a maximum zenith angle of 30° the expected rates are c. 5000 and 40 d⁻¹, respectively, for a primary energy above 10^{15} eV.
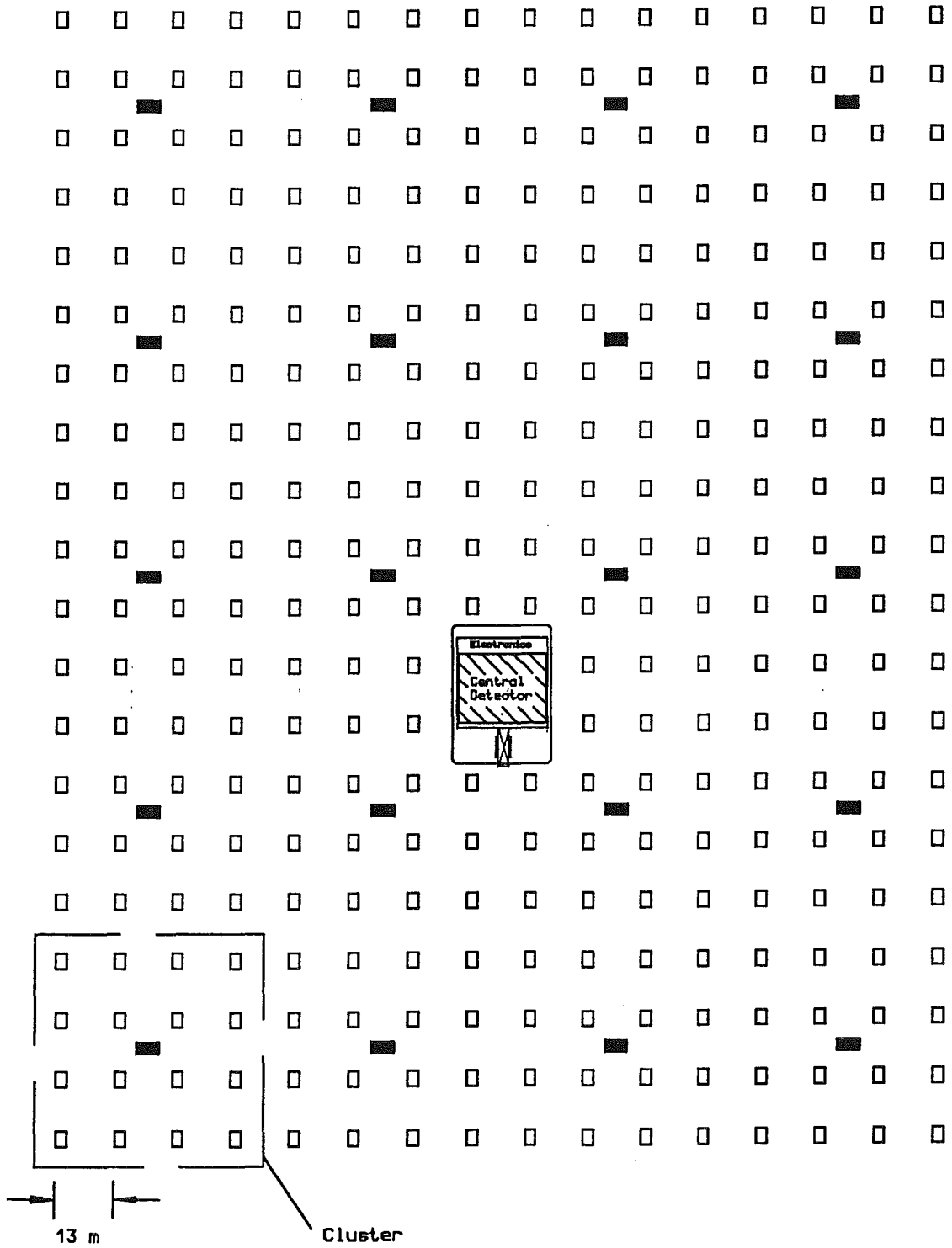
Fig. 1 General lay-out of the KASCADE arrangement. The hatched square represents the central detector, the open squares the detector stations of the array, and the black squares the electronic stations supplying 16 of the detector stations (one cluster). The detailed lay-out will depend on the precise location of the experiment.

Extensive simulations have been performed for the KASCADE project (3) They show that the fluctuations of the measured electron and muon numbers will not be governed by the sampling but rather by the intrinsic shower properties. The additional information on the energy and number of hadrons allows for a much clearer separation of protons from complex nuclei than by electron and muon number alone.

(1)   K. Daumiller, P. Doll, H.J. Gils, D. Heck, H.O. Klages, W. Kriegleder, H.J. Mayer, H. Müller, H. Schieler, G. Schmalz, G. Völker, this report, contr. 2.2
(2)   J. Engler, P. Gabriel, H.J. Gils, N. Heide, H. Keim, J. Knapp, H. Rebel, S. Zagromski, this report, contr. 2.3
(3)   J. N. Capdevielle, P. Gabriel, H.J. Gils, P.K.F. Grieder, D. Heck, N. Heide, J. Knapp, H.J. Mayer, J. Oehlschläger, H. Rebel, G. Schatz, T. Thouw, this report, contr. 2.4
(4)   P.G. Edwards, R.J. Protheroe and E. Rawinski, J. Phys. G 11 (1985) L101
(5)   P. K. F. Grieder 1984, Nuovo Cimento 84A, 285

2.2   THE DETECTOR ARRAY OF THE KASCADE PROJECT

K. Daumiller, P. Doll, H.J. Gils, D. Heck, H.O. Klages, W. Kriegleder, H.J. Mayer, H. Müller, H. Schieler, G. Schmalz, G. Völker

The distributed array of detectors will be used to determine:

- the number and lateral distribution of electrons and photons in the 'soft' component of extensive air showers,
- the muon number outside the shower core and the muon lateral distribution,
- the direction of the primary particle by measurement of the inclination of the shower front using the method of relative arrival times,
- the position of the shower core,

and to trigger the muon counters of the central detector system (2) for those showers whose cores fall outside the calorimeter.

For these purposes 1264 scintillation detectors (total area: 993m^2) for the measurement of the electron / photon component are foreseen. For the muons 316 scintillation detectors (shielded by ~ 20 r.l. lead / iron absorbers) with a total area of 1024 m^2 will be used.

Extensive Monte Carlo calculations have been performed using the programme package GEANT (3) to simulate electromagnetic shower events and the response of the detector system.

Detectors for the e/γ component A cylindrical slab of fast plastic scintillator (100 cm ∅ x 5 cm) is viewed by a single 3" photomultiplier tube at a distance of about 60 cm. The topside of the scintillator is covered with highly

reflective aluminium foil. A lucite light collecting cone above the photomultiplier tube is used to enhance the photon statistics by about a factor of 2. A lead converter foil (d = 5 mm) on top of the scintillator improves the detector efficiency for photons and hence the angular resolution of the array. The system is embedded in a cylindrical black polyethylene barrel. The layout of the detectors is shown in Fig. 1.

Prototype detectors have been developed and tested using penetrating cosmic muons. Using high quality scintillators (e.g. NE 102A) and a PM tube with small transit time spread a reasonable energy resolution of $\sigma(E) \sim 0.30 \cdot E$ at 9 MeV and very good timing properties ($\sigma(t) \sim 0.8$ ns) could be obtained.

Detectors for the muon component An absorber composed of lead (10 cm) and iron (4 cm), corresponding to 20 r.l., is foreseen to shield the muon detectors against the electron/photon component of the showers. Each muon detector is composed of 4 squares of high quality scintillator (90 x 90 x 3 cm^3), read out by wavelength shifter strips at all edges. Four 1.5" photomultiplier tubes are used as can be seen in Fig. 1.
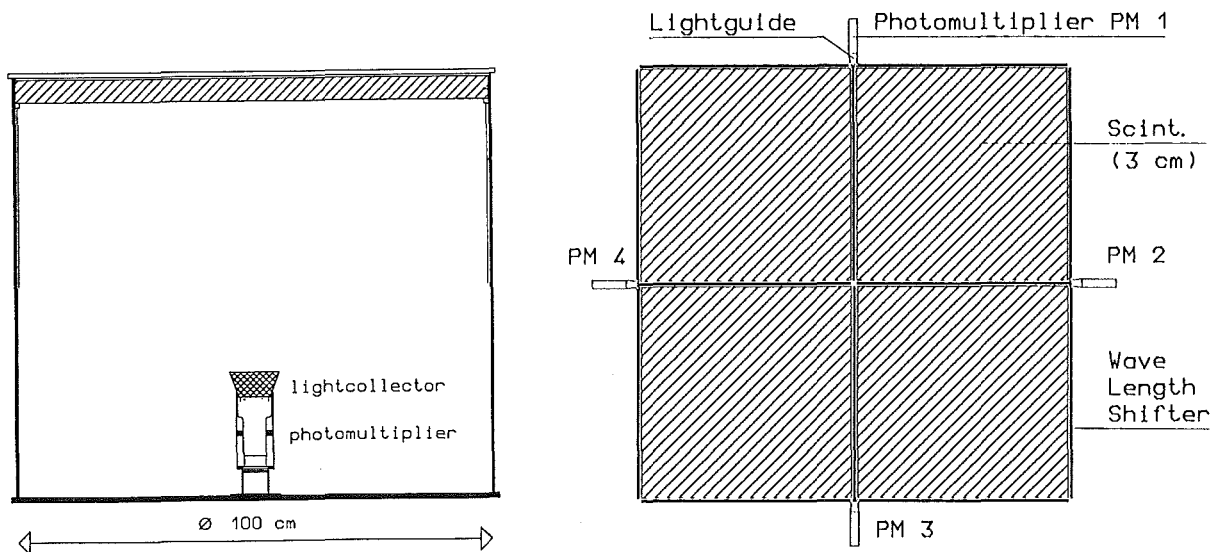
Fig.1   Schematic drawing of the e/γ detector (left) and the muon detector design (right).

Prototype measurements have proven sufficient uniformity of the detector response. The problem of detecting 'faked muons', generated by punch-through of the high energy part of the e / γ component through the lead-iron absorber, was studied carefully using the GEANT code. The result is, briefly, that the proposed method of muon detection is adequate when using an energy

threshold of ~ 2.5 MeV and neglecting detectors with core distances < 15 m. This radius cut also reduces the problems arising from the energetic hadrons in the shower core. At our low energy threshold, for an air shower induced by a proton of $3 \cdot 10^{14}$ eV, a total of 20 muons will be detected in array detectors with core distances > 15 m. This has to be compared to a punch-through probability of about one 'faked muon'. At higher energies an even larger radius cut can be used, reducing the punch-through effect further.

Structure of the array The 1264 e / γ detectors and the 316 muon detectors are combined in 20 independent clusters. Each cluster is composed of 16 detector stations on a rectangular grid and a central electronics station as shown in Fig. 2. In the central part of the KASCADE array 4 clusters contain only 15 detector stations each to leave the space for the hadron calorimeter.
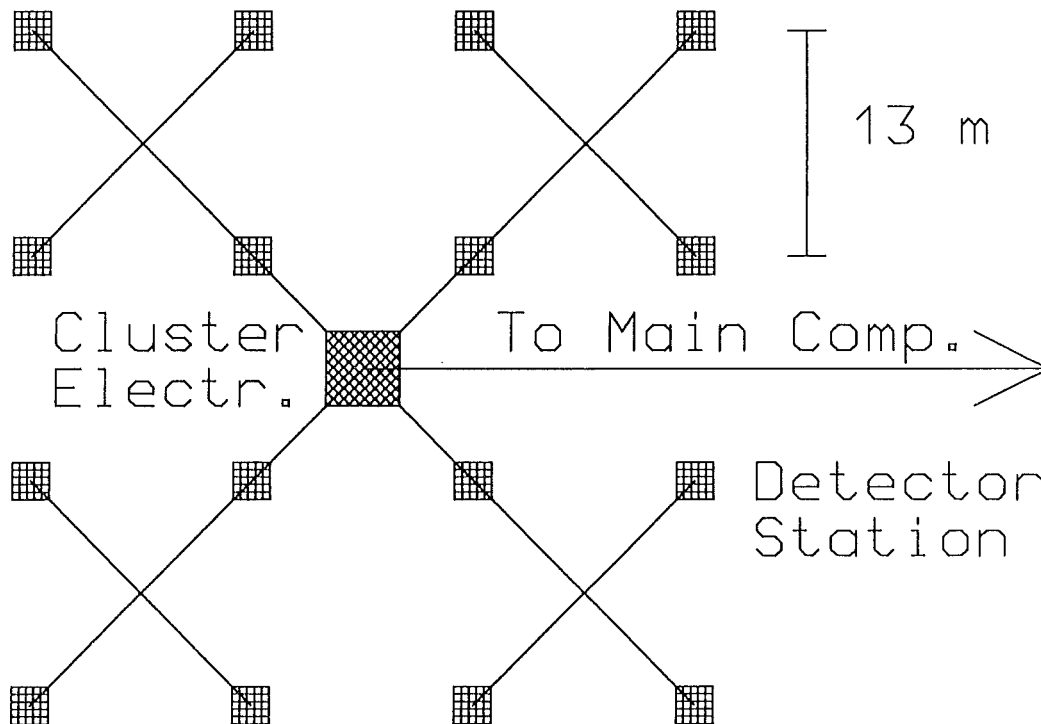
Fig.2   Structure of a cluster of detector stations in the KASCADE array.

Each detector station contains a muon detector below a lead-iron absorber plate and 4 e / γ detectors above the shielding. Power supplies, controls, and the front end electronics are located in the central station of the cluster. A VME crate based transputer system in each cluster central station organizes data acquisition and detector control as well as the data transfer to the main computer of the KASCADE experiment via fast serial links.

A 5 MHz clock running simultaneously in all clusters is used to generate a time label for valid events. Data from different clusters are combined in the main computer according to these labels. Subnanosecond timing is performed in

the clusters relative to the 5 MHz clock for all accepted detector signals. A fast hardware trigger in the cluster is used to reduce the dead time from the conversion of uncorrelated signals. The absolute time (UTC) of a valid event is measured with an accuracy of about 10 μs and added to the data in the main computer.

Array performance For the system described above the response to extensive air showers has been calculated using the code GEANT (3). Simulated air shower events generated by the code CORSIKA (4) are part of the input to these calculations. A sample of the results is shown in Fig. 3. The spatial and angular resolution of the array are improving with growing shower size. In the case of a vertical air shower induced by a $2 \cdot 10^{14}$ eV photon about 120 detectors fire, yielding $\sigma(r) \sim 3.3$ m and $\sigma(\theta) \sim 0.4°$. In an air shower induced by a $5 \cdot 10^{14}$ eV proton with a zenith angle of 20° about 230 detectors are hit, leading to a core position uncertainty of 2.0 m and an angular resolution of 0.25°.

The calculations indicate the necessity of a careful modelling of the shower front for event reconstruction. The accepted event rate for the total KASCADE array will be about 1 sec^{-1}, assuming an angular dependent threshold of 1 - 3 x 10^{14} eV, set by the trigger conditions.
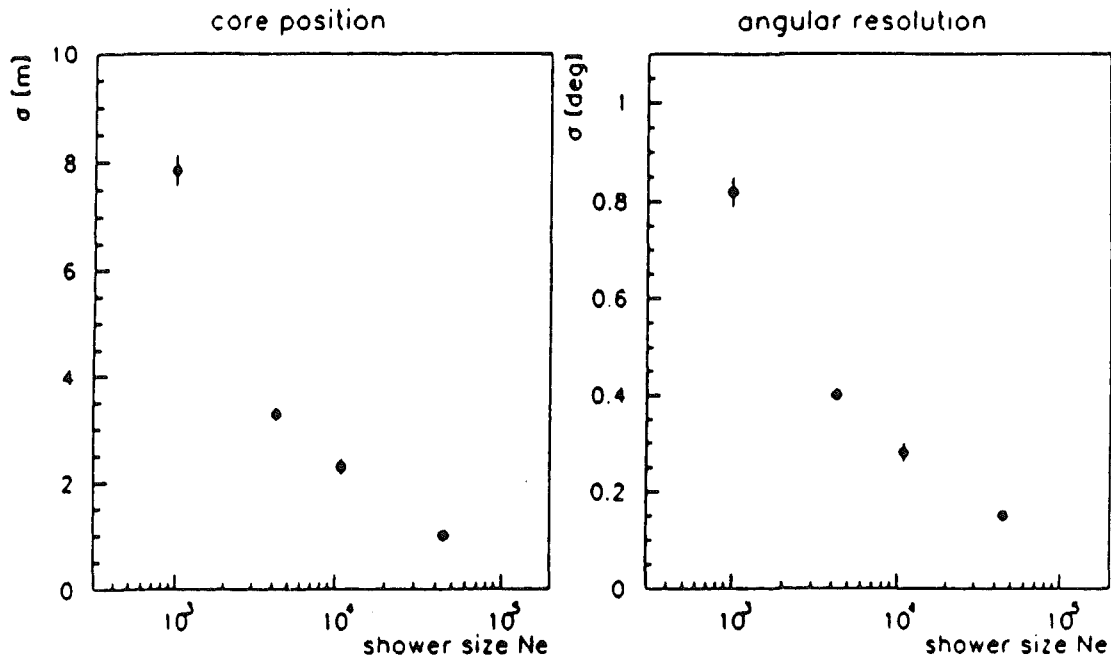
Fig.3 Anticipated performance of the KASCADE detector array. The shower size parameter N_e is used with an energy cut of 10 MeV.

UHE point sources The main goal of the KASCADE experiment (1) is the determination of the primary chemical composition of cosmic rays in the energy range 10^{14} - 10^{17} eV. The high sampling and the good angular resolution of

the array combined with the large muon detection area, however, lead to high efficiency also in the search for UHE point sources, at least for primary energies above 10^{15} eV.

Already without the use of time correlations (e.g. to X-ray ephemerides) or restrictions in muon numbers a photon flux of $8 \cdot 10^{-16}$ cm^{-2}sec^{-1} can be detected at 10^{16} eV with 5 σ accuracy in 3 years of observation. With about this sensitivity a source scan for a large part of the northern sky can be carried out. Both prominent source candidates, Cygnus X-3 and Hercules X-1, which are at the focus of scientific interest at present, are well within the view of the KASCADE array (49°N).

Schedule A prototype cluster will be set up starting at the end of 1989. The begin of construction work for the KASCADE experiment is scheduled for early 1990. First measurements with about 10 clusters working will be possible at the end of 1991.

(1)   P. Doll, J. Engler, H. J. Gils, D. Heck, N. Heide, H. Keim, H. O. Klages, J. Knapp, H.J. Mayer, H. Müller, J. Oehlschläger, H. Rebel, G. Schatz, G. Schmalz, T. Thouw, S. Zagromski, B. Zeitnitz, this report, contr. 2.1
(2)   J. Engler, P. Gabriel, H.J. Gils, N. Heide, H. Keim, J. Knapp, H. Rebel, S. Zagromski, this report, contr. 2.3
(3)   GEANT, CERN data division (1989)
(4)   J.N. Capdevielle, P. Gabriel, H.J. Gils, P.K.F. Grieder, D. Heck, N. Heide, J. Knapp, H.J. Mayer, J. Oehlschläger, H. Rebel, G. Schatz, T. Thouw, this report, contr. 2.4

2.3   THE CENTRAL DETECTOR OF KASCADE

J. Engler, P. Gabriel, H.J. Gils, N. Heide, H. Keim, J. Knapp, H. Rebel, S. Zagromski

The KASCADE experiment (1) is under construction at Karlsruhe with the principal aim to study the mass composition of cosmic rays in the energy range of 3×10^{14} eV to 10^{17} eV. In the centre of an array for electron and muon detection KASCADE contains a detector for hadron detection which will considerably improve the mass separation as obtained from electron and muon measurements alone (2). For this purpose the central detector has to provide particle detection in the shower core with the following properties:

- Identification and energy measurement for hadrons from 10 GeV to 10 TeV with sufficient precision.
- Separation of individual hadron showers by a fine grain spatial segmentation.
- Effective separation of the soft and hard component.
- Measurement of the muon component at the bottom of the calorimeter.
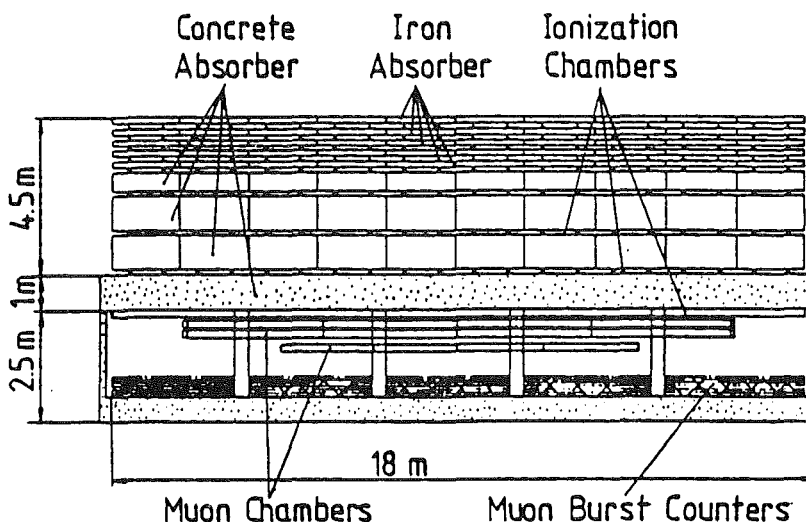
Fig. 1   Principal lay-out of the central detector.

The main component of the detector consists of an iron concrete calorimeter with lateral dimensions of 18 x 18 m^2 and a longitudinal depth of 5 m. The total thickness corresponds to 11 λ_0. A schematic sketch of the lay-out is shown in Fig. 1. Shown are the iron and concrete absorber and also the basement where the chambers for muon detection are to be installed. The basement will be high enough in order to allow for future improvement programs, e. g. installation of muon burst counters or transition radiation detectors.

The absorber block is sliced into 8 layers starting with iron slabs of 10 cm thickness at the top and ending in a tail catcher of concrete absorbers of 100 cm thickness at the bottom. The iron slabs will be slightly radioactive being cast from iron of a dismanteled nuclear plant. In between the absorber blocks will be interspersed 7 layers of liquid ionization chambers and 1 layer of a fast scintillator for trigger purposes. This ensures that low energy hadrons of approximately 10 GeV as well as high energy hadrons of up to more than 10 TeV can be well recognized and measured with a nearly constant energy resolution of $\sigma(E)/E = 35$ %.

At the bottom of the calorimeter all throughgoing muons are detected by multi-wire proportional chambers. The calorimeter thickness corresponds to a muon threshold of 2 GeV.

Active Layers   A particularity of the detector are the ionization chambers which are introduced between the absorber layers to sample the deposited shower energy. They are filled with tetramethylsilane, a room temperature liquid, and are a new development of the Karlsruhe Nuclear Research Centre. They are particularly well suited as active detectors in calorimeters due to the following reasons:

-    Signal proportional to energy deposition, and no saturation in dense cores.

- Absolute calibration by charge injection possible.
- Long term stability due to feed-back amplification.
- Large dynamic range of amplification.
- Signal independent of space location, no edge effects.
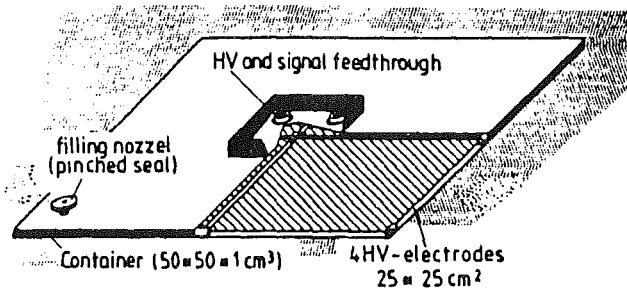
Fig. 2
Sketch of a liquid ionization chamber.
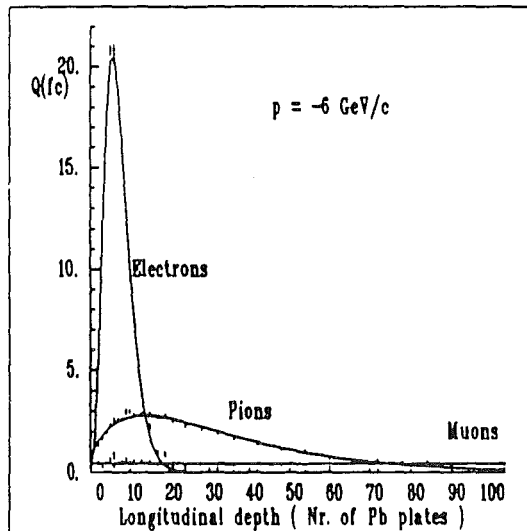
Fig. 3
Transition curves of 6 GeV particles in Pb as measured with TMS ionization chamber (plate thickness 5 mm).

The first four properties are especially important for a calorimeter as considered for a long-term EAS intallation. With showers in the TeV energy range high ionization densities have to be measured which spread up to 3 orders of magnitude. Due to shower fluctuations even 4 orders have to be encountered in practice. The calorimeter cannot be calibrated in a particle beam, hence we rely on the simulated energy deposition by Monte Carlo codes and an absolute calibration of the ionization chamber itself. In an ionization chamber the charge is collected without being amplified. Amplification occurs only feed-back controlled entailing a stable operation even over years.

A scheme of the counter is shown in Fig. 2. In a stainless steel box of $50 \times 50 \times 1 \, cm^3$ four electrodes are positioned in the middle of the gap. Approximately 5 kV will be applied to the electrodes, which ensures enough collected charge from

a minimal ionizing particle to allow throughgoing muons to be seen in coincidences. With prototype chambers, calorimetric measurements have been performed at accelerator beams. As an example the transition curves for lead are shown for 6 GeV particles in Fig. 3. They compare well with M. C. simulations. The first chambers exhibit a signal stability over 8 months at the time of writing without any noticeable signal decrease.

Simulated Performance The response of the calorimeter to incoming hadrons has been simulated using a frame containing several widely used codes. For hadronic particles it uses the codes GHEISHA, HETC and MORSE and for electromagnetic particles the code EGS4. The energy resolution for incoming pions is shown in Fig. 4. In the calculations GHEISHA was used for the high energy part, but when hadrons slowed down to energies lower than 5 GeV, they are followed by HETC and neutrons below 20MeV by MORSE. One observes that in the energy range from 1GeV to 10 TeV the calorimeter yields a fairly constant energy resolution of $\sigma(E)/E = 35\%$.

In order to resolve individual hadrons an important figure is the lateral spread of a cascade which is shown for concrete and iron in Fig. 5. Plotted are the radii of the cylinders around the shower axis within which 90 % of the energy are deposited. We learn from the figure, that in iron the cascades are better confined, hence individual hadrons can be better separated. Together with the fine spatial segmentation of 25 x 25 cm^2, and with each pad read out separately a reliable reconstruction of individual hadrons from 10 GeV to 10 TeV will be possible.
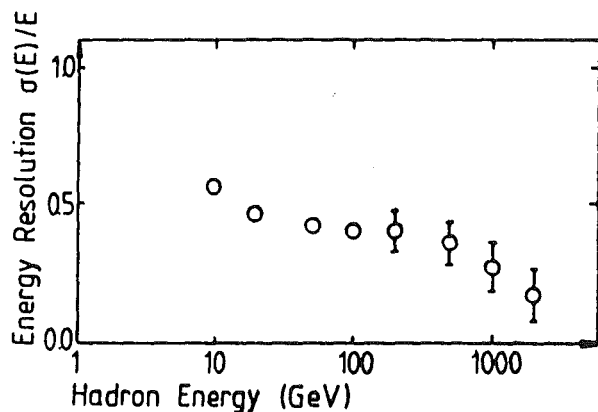
Fig. 4 Energy resolution of the calorimeter versus primary energy (M.C. results).
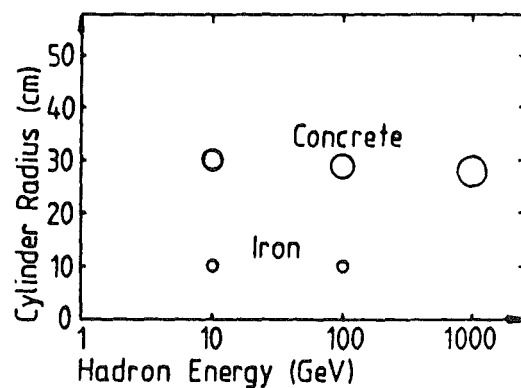
Fig. 5 Shower radii in iron and concrete versus primary energy (M.C. results).

Another interesting parameter is the position of the maximum of the cascade in the calorimeter. The calculations show that this position does not

change drastically with energy. The trigger counters, which are positioned as near to the mean maximum as possible are foreseen at 1.8 λ_0 which coincides with the peak for 100 GeV pions.

Conclusions The central detector is well suited to obtain detailed information of the particle distribution in an EAS core. With this information the mass separation of the primary cosmic rays will be considerably improved. The new technique of liquid ionization chambers promises a continuous calorimeter operation for many years with a maximum of reliability.

(1) P. Doll, J. Engler, H.J. Gils, D. Heck, N. Heide, H. Keim, H.O. Klages, J. Knapp, H.J. Mayer, H. Müller, J. Oehlschläger, H. Rebel, G. Schatz, G. Schmalz, T. Thouw, S. Zagromski, B. Zeitnitz, this report, contr. 2.1

(2) J.N. Capdevielle, P. Gabriel, H.J. Gils, P.K.F. Grieder, D. Heck, N. Heide, J. Knapp, H.J. Mayer, J. Oehlschläger, H. Rebel, G. Schatz, T. Thouw, this report, contr. 2.4

2.4 AIR SHOWER SIMULATIONS FOR KASCADE

J.N. Capdevielle[*], P. Gabriel, H.J. Gils, P.K.F. Grieder[**], D. Heck,

N. Heide, J. Knapp, H.J. Mayer, J. Oehlschläger, H. Rebel, G. Schatz

and T. Thouw

A detailed simulation program for extensive air showers and first results are presented. The mass composition of cosmic rays with $E_0 \geq 10^{15}$ eV can be determined by measuring electrons, muons and hadrons simultaneously with the KASCADE detector.

The KASCADE project is an extensive air shower experiment being under construction at Karlsruhe. It is described in contribution 2.1 to this report. Extensive simulations with the program CORSIKA (COsmic Ray SImulations for KASCADE) have been performed for the design of the experiment. This paper outlines the program and gives the main results.

The Program The basic approach of the Monte Carlo program CORSIKA (written in FORTRAN 77) is to rely on experimental data wherever possible.

Strong interactions above 10 GeV c.m. energy are calculated by a method (1) based on the dual parton model, which describes well all relevant distributions from the ISR, SPS and p$\bar{\text{p}}$ collider experiments. The energy dependent production rates of γ, π, K and p$\bar{\text{p}}$, the dependence of $p_\perp$ on energy, particle type and multiplicity are parametrized according to data from the experiments mentioned above (2).

The treatment of interactions below 10 GeV c.m. energy has been taken from a program based on an isobar model (3), which describes well the experimental data up to ISR energies.

The probability of multiple collisions in a target nucleus is calculated by a simple geometric model based on experimental nucleon densities of atomic nuclei (4). Following an analysis of proton-nucleus data (5), we suppress diffractive interactions in case of multiple collisions. For nucleus-nucleus reactions the number of interacting projectile nucleons is calculated in a similar way, assuming the non interacting nucleons to proceed further as free particles.

For the electromagnetic part two options are available. In the first one, the 3 dimensional development of each individual subshower is calculated with a modified NKG formula (6). In the second version a taylored version of the EGS4 electromagnetic shower program (7) is used.

Most calculations have been performed with a low cost, multi transputer farm, which has been developed for this purpose (8).

Results The results presented refer to 110 m above sea level, the altitude of the KASCADE location. The table gives the mean values and fluctuations (r.m.s.) of three observables, which we can measure simultaneously for each shower. N_e is the number of electrons and N_μ is the number of muons with $E_\mu \geq$ 1GeV falling into the KASCADE array within a core distance $r \leq 100$ m. ΣE_h is the energy sum in GeV of all hadrons with $E_h \geq 10$GeV and $r \leq 5$ m. The total muon number rises like $E_0^{0.9}$, but the lateral distribution steepens with increasing energy in such a way that N_μ is almost proportional to E_0 and not depending on the type of the primary particle.

Table: Means and r.m.s. as calculated with CORSIKA.

		$\log_{10}(N_e)$	$\log_{10}(N_\mu)$	$\log_{10}(\Sigma E_h)$
$E_0 = 5 \cdot 10^{14}$eV	p	4.82 ± 0.21	3.15 ± 0.17	4.04 ± 0.49
	^{16}O	4.49 ± 0.13	3.16 ± 0.06	3.50 ± 0.33
	^{56}Fe	4.24 ± 0.10	3.12 ± 0.04	2.93 ± 0.44
$E_0 = 10^{15}$eV	p	5.21 ± 0.22	3.45 ± 0.15	4.49 ± 0.34
	^{16}O	4.92 ± 0.11	3.48 ± 0.06	4.07 ± 0.20
	^{56}Fe	4.70 ± 0.07	3.45 ± 0.04	3.66 ± 0.27
$E_0 = 2 \cdot 10^{15}$eV	p	5.59 ± 0.19	3.75 ± 0.12	4.87 ± 0.34
	^{16}O	5.29 ± 0.11	3.78 ± 0.05	4.51 ± 0.20
	^{56}Fe	5.12 ± 0.07	3.76 ± 0.04	4.24 ± 0.15

For equal N_e, iron induced showers contain three times more muons than proton induced ones, which is a factor of 2 less than given in ref. (9). The distribution of N_μ / N_e of proton showers has a long tail to small values, i.e. into a
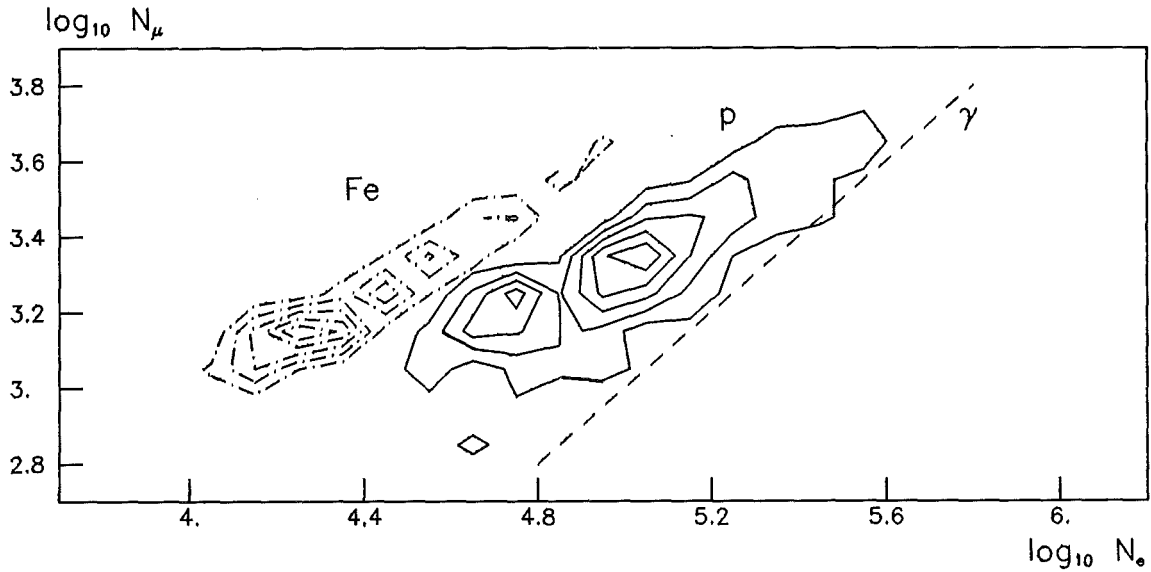
Fig. 1 $\log_{10}(N_\mu)$ vs $\log_{10}(N_e)$ for p and ^{56}Fe.
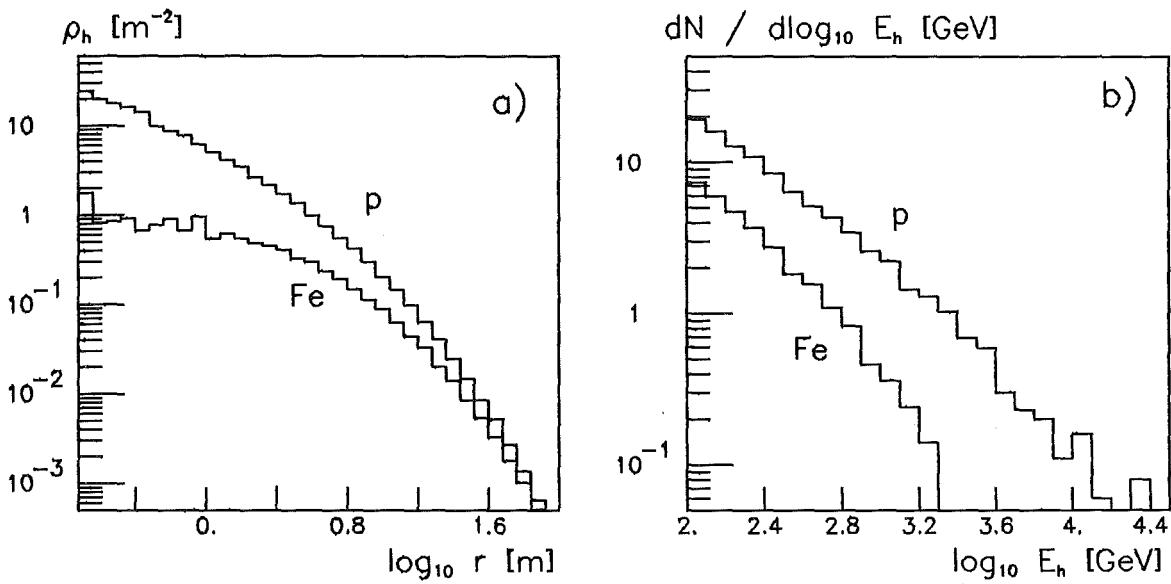
Fig. 2   The lateral and energy distributions of hadrons for $E_0 = 10^{15}$eV.

region where γ induced showers would be expected. Figure 1 shows the plot of $\log_{10}(N_\mu)$ versus $\log_{10}(N_e)$ for p and ^{56}Fe initiated showers in the energy region $2.5 \cdot 10^{14}$eV $\leq E_0 \leq 2 \cdot 10^{15}$eV. The primary energy spectrum $dN/dE \propto E_0^{-2.7}$ has been folded in. The dashed line indicates the ratio $N_\mu / N_e = 0.01$.

In Figs. 2a and 2b the radial dependence of the mean density ρ_h of hadronic particles with $E_h \geq 10$ GeV and the mean hadron energy distribution are plotted for different primaries with $E_0 = 10^{15}$eV. One observes that the hadrons in p showers are more concentrated in the shower core and have on the

average higher energies than those of ^{56}Fe showers. These differences influence the observable ΣE_h and allow therefore to improve the separation of p and ^{56}Fe.

As an example, a logarithmic plot of the detected hadronic energy ΣE_h^{det} versus the number of detected electrons N_e^{det} is shown in figure 3a). The plot contains only showers with a fixed number of detected muons, namely $2.0 \leqq \log_{10}(N_\mu^{det}) \leqq 2.2$. The primary energy spectrum ($\propto E_0^{-2.7}$) and the sampling rate of 2 % for the electron and 3 % for the muon detectors are taken into account.
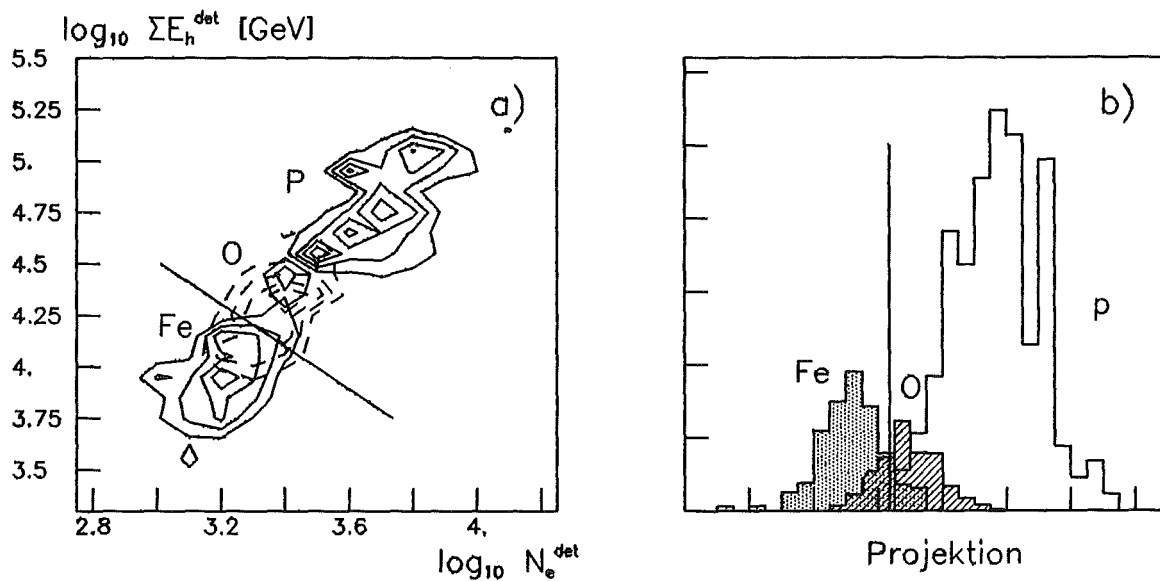
Fig. 3 $\log_{10}(\Sigma E_h^{det})$ vs $\log_{10}(N_e^{det})$ for different primaries.

These showers originate on the average from primaries with $E_0 \approx 1.5 \cdot 10^{15}$eV. The straight line in Fig. 3a indicates how ^{56}Fe can be separated. Fig. 3b gives the projection of figure 3a) along this line assuming a relative rate of 6 : 1 : 1.75 for p, ^{16}O and ^{56}Fe as extrapolated from lower energies (10). The region left of the line contains 90% of the iron showers and a background of oxygen and proton showers of 14%. The separation becomes better for increasing E_0. Using only the numbers of detected electrons and muons for separating iron from oxygen and protons, the corresponding numbers are 85% and 17% respectively.

The results of our simulation let expect that the envisaged experiment can considerably contribute to the open question of mass composition of cosmic rays in the PeV region.

(1)   J.N. Capdevielle, Proc. 5th ISVHECRI, Lodz (1988)
         J.N. Capdevielle, J.Phys.G 15 (1989) 909

(2)   C. Geich-Gimbel, Int.J.Mod.Phys. **A4** No7(1989)
        C. De Marzo et al., Phys. Rev. **D26** (1982) 1019
        W. Thomé et al., Nucl.Phys. **B129** (1977) 365
        J.L. Bailly et al., Z.Phys. **C35** (1987) 309
        G.J. Alner et al., CERN-EP (1986)
(3)   P.K.F. Grieder, Nuovo Cimento **84A** (1984) 285
(4)   H. De Vries, C.W. De Jager, C. De Vries, Atomic Data and Nucl. Data
        Tables **36** (1987) 495
(5)   J. Hüfner, M. Kutschera, B. Liu, K. Werner, Phys.Lett. **166B** (1986) 31
(6)   A. Lagutin, V. Uchaikin, Proc. 16th ICRC, Kyoto, **7** (1979) 18
(7)   W.R. Nelson, H. Hirayama, D.W.O. Rogers, SLAC-**265** (1985)
(8)   H.J. Gils, D. Heck, J. Oehlschläger, G. Schatz, T. Thouw, A. Merkel,
        Comp.Phys.Comm. **56** (1989) 105
(9)   P.G. Edwards, R.J. Protheroe, E. Rawinski, J.Phys.G **11** (1985) L101
(10)   J.M. Grunsfeld, J. L'Heureux, P. Meyer, D. Müller, S.P. Swordy,
        Ap.J. Lett. **327** (1988) L31

*   Laboratoire de Physique Théorique, Université de Bordeaux, Gradignan,
        France
**   Physikalisches Institut, Universität Bern, Bern, Switzerland

3. LASER SPECTROSCOPY

3.1 NUCLEAR RADII OF THORIUM ISOTOPES FROM LASER SPECTROSCOPY OF STORED IONS

W. Kälber, J. Rink, K. Bekk, W. Faubel*, S. Göring, G. Meisel, H. Rebel, and R.C. Thompson** (1)

Isotope shifts and hyperfine splittings in optical transitions for atomic ions of the thorium isotopes ^{227}Th to ^{230}Th and ^{232}Th have been measured by laser spectroscopy on stored ions. From the isotope shift data, changes of the mean square charge radii are determined. A continuous increase of the charge radius with mass number A is observed, in agreement with droplet model calculations. The results indicate that the odd-even staggering for Th is different from that one of the neighbouring isotones of Fr and Ra. There is some empirical evidence from systematics for an inversion of the staggering and the appearance of an octupole deformation at N ≤ 137. The hyperfine splitting for ^{229}Th for 3 electronic levels is given.

3.2 REANALYSIS OF THE Am I LEVEL SPECTRUM AND THE NUCLEAR QUADRUPOLE MOMENTS OF Am–ISOTOPES

J. Dembczynski*, M. Elantkowska*, K. Bekk, H. Rebel, and M. Wilson** (1)

The fine structure (fs) and hyperfine structure (hfs) level scheme of Am I is reanalysed using a semi empirical fitting procedure which incorporates experimental data. Especially new laserspectroscopic measurements of the hfs of some electronic transitions in the Am atom enables us to make a more detailed analysis of $5f^7$ 7s 7p fine structure in Am I. In particular a relation is given between the B-factor values and the value of the nuclear electric quadrupole moment of ^{241}Am independent of a calibration by results of nuclear spectroscopy.

**   Department of Physics, Royal Holloway & Bedford New College, University of London, Egham, United Kingdom

3.3   LASER SPECTROSCOPY OF STORED IONS WITH REDUCED DOPPLER BROADENING

W. Kälber, J. Rink, G. Meisel, and R.C. Thompson*

Laser spectroscopy of stored thorium ions was found to be a highly sensitive method in terms of the minimum required sample size (1). It has been used to determine mean-square charge radii and nuclear moments of several thorium isotopes (1,2). The resolution, however, was found to be rather low because of the wide Doppler broadening of spectral lines that is due to the fast motion of ions in the confining rf quadrupole field (3).

A new method for laser spectroscopy of stored ions has been developed in order to reduce and even to eliminate the Doppler broadening of spectral lines. An experimental setup for this new method is shown in Fig. 1. The basic concept is to excite ions and to detect the fluorescence during selected time intervals only which are chosen with respect to the phase of the confining rf voltage. Excitation of ions during time intervals of typically 100 ns duration is attained by switching on and off the laser power by means of an electro-optical modulator; time resolved detection of fluorescence is done by gating the photomultiplier signal.
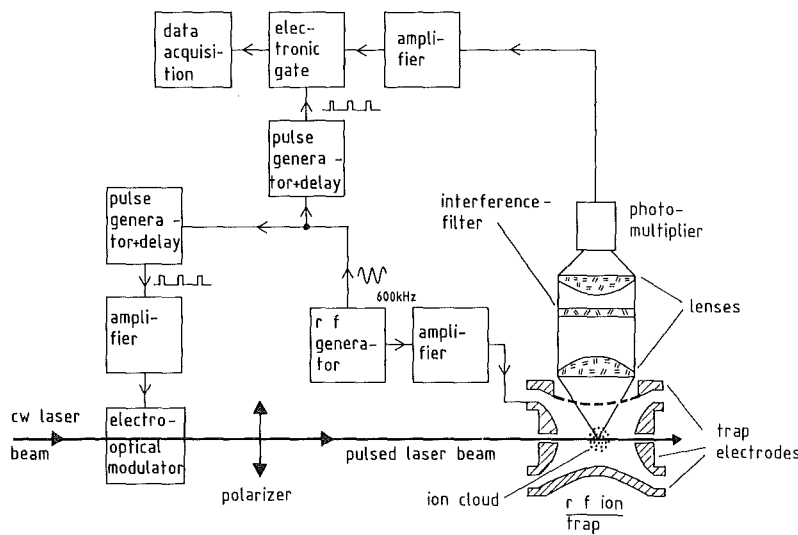
Fig.1   Experimental setup for time resolved spectroscopy of stored ions.

In single step excitation (1,2), the observed spectrum reflects the ions' velocity distribution along the laser beam axis (see Fig. 2a). In a simplified model the motion of a single ion has two main contributions (4), namely the secular (or

macro) motion and the micromotion. For our operating point ($q_r = 0.2$, $a_r = 0.01$, $\beta_r = 0.17$), the secular motion is slow ($\omega_r = 2\pi \cdot 52$ kHz) compared to the rf voltage oscillation ($\Omega_r = 2\pi \cdot 600$ kHz) which is identical to the micromotion frequency. The ratio of their amplitudes r_{macro}/r_{micro} is about Ω/ω_r; the velocities therefore are of the same size. The micromotion acceleration of the ions follows the applied voltage rather strictly, therefore the micromotion speed has a 90 degrees phase lag with respect to the rf voltage. Thus the micromotion velocities are close to zero when the voltage reaches its peak values, leading to a narrow micromotion velocity spread irrespective of their individual amplitudes. The macromotion superimposes almost uncorrelated to the correlated micromotion.

In agreement with the above consideration, we observe a linewidth reduction by a factor of about 4 if we excite the ions only when the rf voltage is reaching its peaks (Fig. 2b). The remaining Doppler width corresponds to an effective ion temperature of about 600 K. In contrast to this, the velocities and thus their spread is largest, when the rf voltage crosses zero (Fig. 2c). Simultaneously, a zero longitudinal velocity is unlikely to occur.

It is to be noted that the signal loss is only 20 to 50 %, i.e. much less than the duty cycle suggests. The reason is that the ions are not left unused by the time selective measurement; they are all used in the right instance instead.
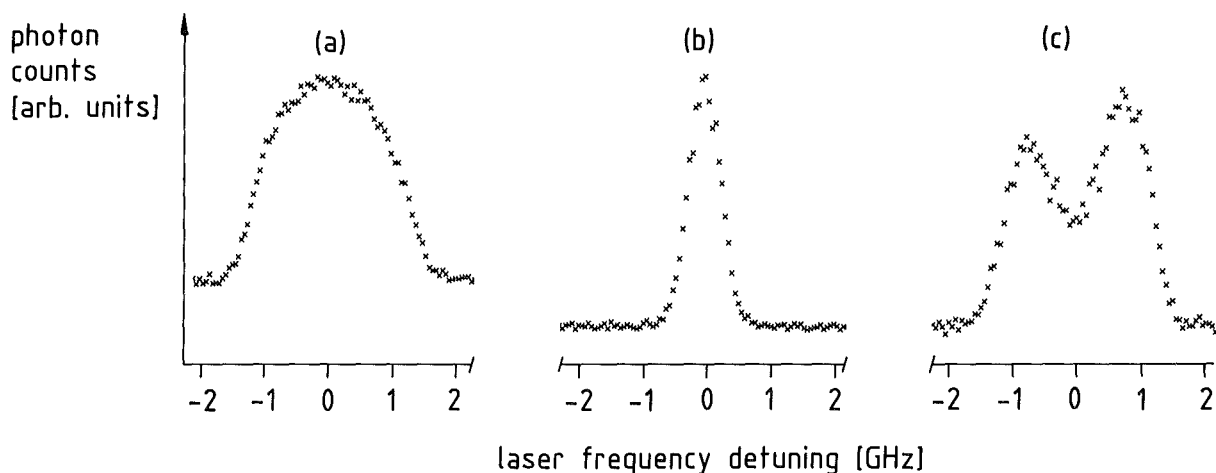
Fig. 2 Single step spectra of stored ^{232}Th$^+$ ions; the transition is Th II $0 \rightarrow 17122$ cm^{-1}.

a. With cw laser excitation.

b. Excitation only at time intervals close to the peak of the rf voltage.

c. Excitation at times around the zero crossing of the rf voltage.

In two step excitation experiments (1,2), ions with a specific velocity component are prepared by a first excitation into an intermediate level. This

velocity distribution is probed by a second exciting step and a lineshape close to the natural one may be expected. In fact a line narrowing is observed, but the line still is considerably broader than the natural one (1,2). The broadening is due to the acceleration of ions by the confining rf field while the ions stay in the intermediate state waiting for the second excitation. The acceleration effect is rather pronounced in our case, since the intermediate level lifetime is about 1 μs (5), i.e. it is not short compared to the rf cycle time of 1.67 μs.

To eliminate the effect of acceleration broadening, ions are only excited and observed when the applied voltage is close to zero since then the acceleration is small, too. This concept of time selective excitation and/or observation was realized in different combinations; the best results are obtained if both lasers are chopped and the photon counter is gated accordingly. There is no remarkable loss in resolution if only the laser for the first step is chopped, and the photon counter is gated; a plot of the line obtained in this way is given in Fig. 3. Its shape is almost Lorentzian with a FWHM of 35 MHz demonstrating a linewidth narrowing by a factor of 40 to 50 as compared to the full Doppler width. As above, the line narrowing is obtained without severe signal loss. The low counting duty cycle in the contrary is advantageous since the background counts are reduced accordingly. For further details on time resolved spectra see Ref. 6.
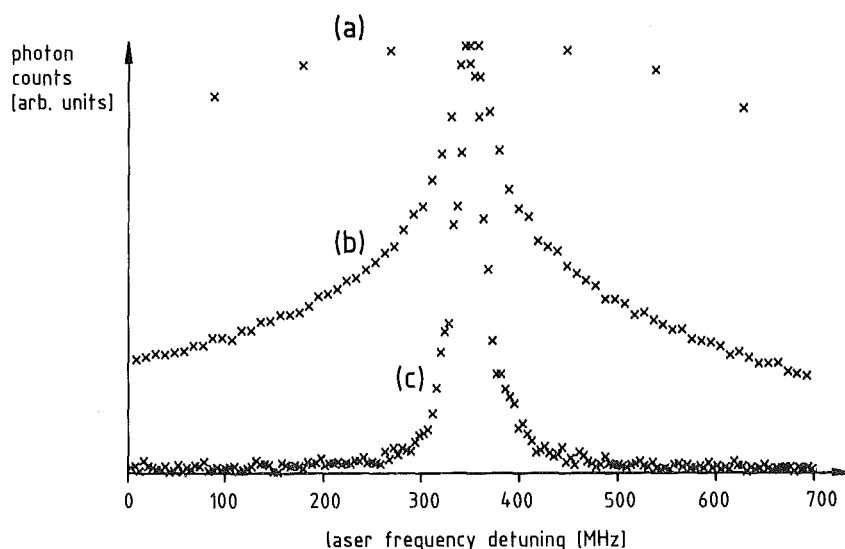
Fig. 3   Spectra of stored ^{232}Th$^+$ ions.

Curve a: Single step excitation $0 \rightarrow 17122$ cm^{-1}.

Curve b: Two step excitation $0 \rightarrow 17122 \rightarrow 34544$ cm^{-1}.

Curve c: As curve b, but with time selective operation.

(1)   W. Kälber, thesis, Universität Heidelberg,
        Report KfK 4513, Kernforschungszentrum Karlsruhe (1989)
(2)   W. Kälber, J. Rink, K. Bekk, W. Faubel, S. Göring, G. Meisel, H. Rebel,
        R.C. Thompson, Report KfK 4508, Kernforschungszentrum Karlsruhe

(1988) p. 71
W. Kälber, J. Rink, K. Bekk, W. Faubel, S. Göring, G. Meisel, H. Rebel, and R.C. Thompson, Z. Phys. A 334 (1989) 103
(3)   E. Fischer, Z. Phys. 156 (1959) 1
(4)   H.G. Dehmelt, Adv. At. Mol. Phys. 3 (1967) 53
(5)   W. Kälber, J. Rink, G. Meisel, R.C. Thompson (to be published)
(6)   W. Kälber, G. Meisel, J. Rink, K. Bekk, Third European Conference on Atomic and Molecular Physics, Book of Abstracts, ed. A. Salin (1989) p.669

*   Blackett Laboratory, Imperial College, London, United Kingdom

3.4 SEPARATION OF POLONIUM FROM IRRADIATED BISMUTH AND LEAD TARGETS IN ORDER TO PREPARE A POLONIUM ATOMIC BEAM

B. Feurer, A. Hanser

Atomic beams of polonium isotopes are needed for the current laserspectroscopic work on these isotopes. The long-lived Po isotopes ^{208,209}Po could be purchased in form of solutions, from which they can readily be deposited on foils of suitable metals and then heated off at moderate temperatures. However, the shorter-lived Po isotopes must be produced in nuclear reactions using the accelerators available in our institute. Table 1 comprises these isotopes with their half-lifes and the corresponding main generation reactions. After the irradiation, the Po isotopes produced are imbedded as tracers in the target material. In order to prepare a sufficiently pure atomic beam of polonium, this element must be separated from the target material.

Table 1:   Short-lived Po isotopes of interest

Po isotope	half-life	main generation reaction
^{207}Po	5,8 h	^{209}Bi(p, 3n)
^{206}Po	8,8 d	^{209}Bi(d, 5n)
^{205}Po	1,8 h	^{206}Pb(α, 5n)
^{204}Po	3,5 h	^{206}Pb(α, 6n)
^{203}Po	0,6 h	^{204}Pb(α, 5n)
^{202}Po	0,7 h	^{204}Pb(α, 6n)

The half-lifes of the Po isotopes produced with bismuth targets are sufficiently large for a chemical separation procedure. Therefore the following

procedure (1) was proved: The bismuth is irradiated in form of oxid ($\sim$ 70 mg Bi_2O_3) and then dissolved in 2.5 ml 3 N HCl. After this, 0.3 ml N_2H_4, 20 mg NaCN and just such a quantity of 3 N HCl redissolving the precipitating BiOCl are added. Silver foil, on which the polonium is deposited spontaneously, is immersed into this solution ($\sim$ 3 ml). About 70% of the polonium in solution is deposited on a foil of 2 cm^2 within 60 minutes at a solution temperature of 60° C. The silver foil surface is completely clean after deposition, which is not the case without adding hydrazine and sodium cyanide.

Traces of instable Bi isotopes are found on the silver foils by γ-ray measurement. These Bi isotopes originate from polonium decay and lable radio-actively the bismuth target material. As it is not clear to what extent Bi atoms originating from polonium already deposited adhere at the foil surface for some time, only the statement $\geq$ 200 can be deduced from the γ-ray measurements for the separation factor of bismuth from polonium. The clean surface of the silver foils indicates that the separation factor presumedly is much higher.

The polonium can be heated off readily from the silver surface. About 75% of the deposited polonium evaporate at a temperature of $\sim$ 550° C within two minutes (in vacuum), which results from experiments using the apparatus described in the following section.

As two of the Po isotopes to be generated by irradiation of lead have half-lifes of only 45 an 30 minutes, respectively, it seemed to be necessary to study the separation of polonium from the less volatile lead by a distillation method directly combined with the generation of an atomic beam. The apparatus shown in Fig. 1 was set up for such studies. The heating arrangement (electron bombardment) is the same as one of the possible arrangements of the atomic beam apparatus for the laserspectroscopic measurements. In order to produce samples, natural lead foils (30 mm^2, 100 μ thick) were cyclotron-irradiated twofold. First, ^{203}Pb was produced via the $^{206}Pb(d,5n)^{203}Bi$ $\xrightarrow{\beta}$ ^{203}Pb-reaction as a tracer for the lead. After a waiting time of two days needed for the ^{203}Bi decay, the foil was irradiated a second time to produce ^{207}Po via a $^{206}Pb(\alpha,3n)$-reaction. The double-irradiated lead foils were heated up in the oven of the trial apparatus (see Fig. 1). By means of the germanium detector it was possible to detect to what extent the polonium and the lead would leave the oven at different heating powers. Ovens of different lengths made of graphite and tantalum were tested out. Results most satisfactory were obtained using a 60 mm long oven as shown in Fig. 1. This oven is made of graphite and is heated only at the bottom where the irradiated lead is located at the beginning. The higher temperature (about 800° - 900° C) in this region favours the diffusion of the polonium out of the lead. Evaporated lead is recondensed at the
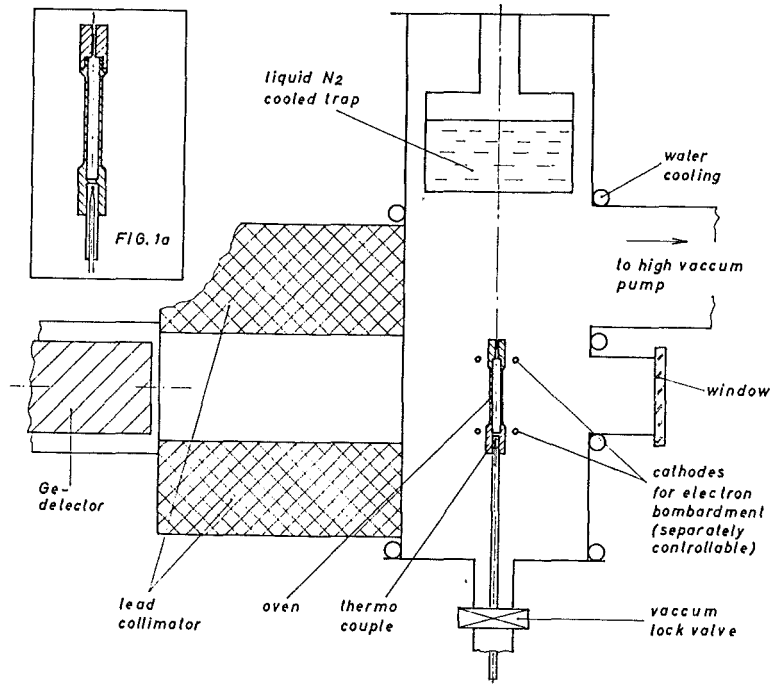
Fig. 1   Trial apparatus for studying the distillation separation of polonium from a lead target.
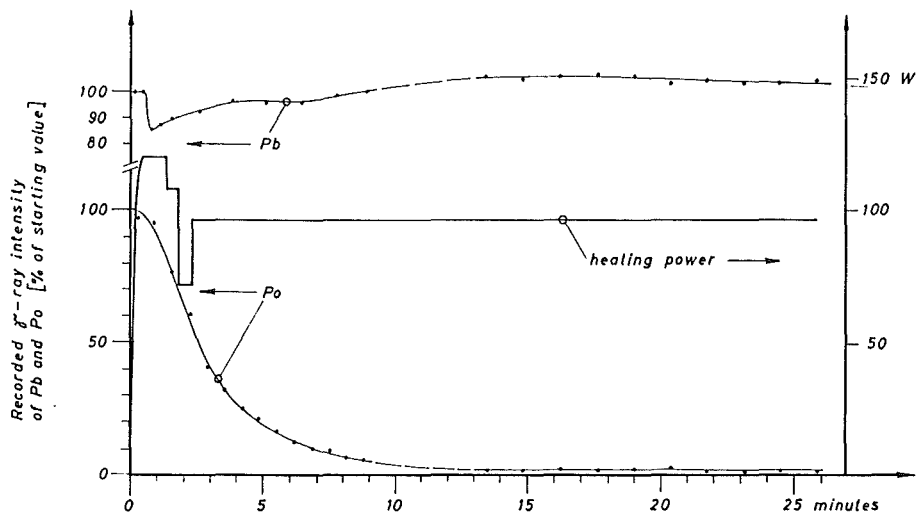
Fig. 2   Typical separation run, if a long oven is used which is heated only at the bottom. (Explanation of the lead curve: First, the lead foil melts forming a drop, which increases the self-absorption of the 279 keV lead γ-ray. Then the lead evaporates and recondenses at the inner wall of the oven.)

somewhat colder upper part with the exit channel; so the emission rate of lead is ruled by a lower temperature. Fig. 2 shows a separation run. One can hope that the emission rate of lead is low enough as not to perturb the beam of polonium atoms pre-collimated by the long exit channel of the oven. However, there is no knowledge to what extent the polonium atoms leaving the oven are combined with other atoms to molecules.

(1)   K.W. Bagnall, Chemistry of the Rare Elements, Polonium-Actinium, Butterworths Scientific Publications, London (1957)

3.5   LASER SPECTROSCOPY OF POLONIUM ISOTOPES

D.Kowalewska, G.Meisel

The measurements of hyperfine structure and isotope shift for a series of polonium isotopes will be performed using the method of laser induced fluorescence on an atomic beam (1). The preparation of the experimental setup, concerning mainly the atomic beam apparatus and the cw dye laser system for UV generation, is expected to be finished in the near future.

The new atomic beam apparatus has been improved, tested on europium at the wavelength $\lambda = 576.5$ nm and found to perform better than the old one (2). However, separate measurements of the background counts with polonium detection optics are required.

The ring dye laser (Coherent model CR 699-21) has been modified for intracavity frequency doubling of light at $\lambda = 511.6$ nm using a BBO crystal (3). The laser is operated with Coumarin 498 dye. The new dye was tried as an alternative to Coumarin 510 used before which required special conditions to perform efficiently and caused serious problems if they were not met: it has been found for Coumarin 510 that the reabsorption of the generated wavelength $\lambda = 511.6$ nm is strongly dependent on the purity of the used solvents. An improved purity (probably concerning water) causes a dramatic negative effect - namely an absorption increase in the wing of the absorption curve at the operating wavelength. This means a considerable increase of the fundamental losses of the laser resonator and thus the dye efficiency is greatly impaired. On the contrary, Coumarin 498 shows no such effect, and the absorption at $\lambda = 511.6$ nm in the dye solution is lower than for Coumarin 510. In the jet of thickness d = 0.2 mm the absorption values are 0.30 % for Coumarin 510 and 0.04 % for Coumarin 498 for fresh solutions. Moreover the Coumarin 498 performance at $\lambda = 511.6$ nm is even better than that one of Coumarin 510, since the peaks of the gain curves for these

two dyes are at different wavelengths ($\lambda \simeq 526$ nm for Coumarin 510 and $\lambda \simeq 508$ nm for Coumarin 498). Both dyes have approximately the same peak efficiency (24 - 25 %) but the power obtained at $\lambda = 511.6$ nm for Coumarin 498 is 95 % of the peak level, while for Coumarin 510 it is only 75 %; for an almost empty linear laser resonator, with a one-element Lyot filter for frequency selection and a high reflecting mirror instead of an output coupler, the internal power obtained at that wavelength with Coumarin 498 is approximately twice as high as in the case of Coumarin 510.

The ring dye laser with an almost empty resonator has been found to perform as efficiently as the linear dye laser under similar conditions. However, for the experiment a tunable single-mode UV light with $\lambda = 255.8$ nm is required. For UV output one of the high reflecting mirrors has to be replaced by a dichroic one as a UV output coupler. To abtain single-mode operation, additional frequency selective elements have to be inserted. This leads to an increase of the losses and a decrease of the internal power. Since only 1.8 W pump power at $\lambda = 457.9$ nm is available, the internal laser power is very sensitive to internal losses and the original rather lossy CR 699-21 frequency selection unit (called ICA - "intra cavity assembly") cannot be used. A relatively stable single-mode operation can be obtained nevertheless with a three-element Lyot filter and one uncoated etalon with a thickness of 2 mm (FSR = 50 GHz); in case of a mode hop the frequency can be easily returned to the original value. With this low loss frequency selection scheme the total additional loss (including the UV output coupler) amounts to 1 % which causes a power drop to 50 % of the initial value.

The first two BBO crystals obtained proved to be useless from the point of view of the intracavity frequency doubling - one was cut for $\lambda \simeq 575$ nm instead of $\lambda = 511.6$ nm and the other had very high insertion losses, so that the laser could be operated just slightly above the threshold. The third crystal, obtained recently, proved to be of a quality sufficient for the chosen frequency doubling scheme. The single pass total loss has been measured in the linear laser by comparison with the reflexion losses of a plane-parallel plate which was rotated off Brewster's angle such that the same power was obtained as with the crystal inserted. For this particular crystal the single pass total loss amounts to 1.3 % and this value does not vary too much over the crystal's cross-section. The frequency doubling efficiency is similar to the efficiency observed for the two other crystals as tested in an external beam with $\lambda = 514.5$ nm from an Ar^+ laser. When inserted into the ring laser resonator, the crystal causes a power drop to 50 %. In the CR 699-21 resonator the waist size amounts to $w_0 = 27$ μm, which is approximately twice as large as the optimum value ($w_0 = 13$ μm (4)) for our crystal of length l = 5 mm;

this means a decrease in efficiency by only 20 % compared to the optimum one. So far an external UV power of 800 μW has been measured. Under improved conditions, i.e. with a fresh dye solution, 2 - 3 mW of single-mode UV at $\lambda = 255.8$ nm should be available for the experiment.

Thanks are due to Dr. Güsten, Dr. Rinke and Dr. Faubel of the Institut für Radiochemie of the KfK for their help with the absorption measurements.

(1)   D. Kowalewska, K. Bekk, S. Göring, A. Hanser, G. Meisel, H. Rebel, Report KfK 4508, Kernforschungszentrum Karlsruhe (1989) p. 75
(2)   P. Pietruk, Diploma thesis, Universität Karlsruhe (1989)
(3)   A. Hanser, D. Kowalewska, G. Meisel, unpublished report, Kernforschungszentrum Karlsruhe (1989)
(4)   G. Boyd, D.A. Kleinman, J.Appl.Phys. 39 (1968) 3597

3.6   A FAST PREPROCESSOR FOR WAVEMETER INTERFEROGRAMS

R. Schruft, G. Meisel, K. Bekk

Experimental work with tunable dye lasers requires the determination of the actual laser wavelength to enable the user to tune the laser to the required frequency. For this purpose a wavemeter with three Fabry-Perot interferometers and a grating spectrograph has been built (1-3). The ring shaped interference pattern of each interferometer as well as the output of the spectrograph are picked up by linear photodiode arrays with 1024 diodes each. The four arrays are read repetitively every 50 msec. Fig. 1 is an oscilloscope display of the diode arrays' output. The diode signals are digitized for data processing, resulting in a 12 bit word every 12 μsec. If this data flow were fed to a state of the art digital processor via a CAMAC interface under RSX-11M control, the computer would almost be fully occupied by this side activity alone, not allowing all the other experimental data to be handled. We therefore designed and built a pre-processor to reduce the data rate 160 fold from 4096 words/50 msec to about 25 words/50 msec.

The essence of this pre-processing is a peak position detection for the interference rings and the position of the entrance slit image in the spectrometer. The algorithm applied is very simple: the intensities for neighboring photodiodes are compared with each other; if the intensity for a diode is above that one for the two neighbors, its address is taken as a peak position. It was found that this procedure is adequate for the peak determination since they are sharp enough and the noise level is low. The peak positions determinated in this way have a worst case uncertainty of ± 1 diode spacing or ± 25 μm; the resulting accuracy is fully sufficient for the present purpose.
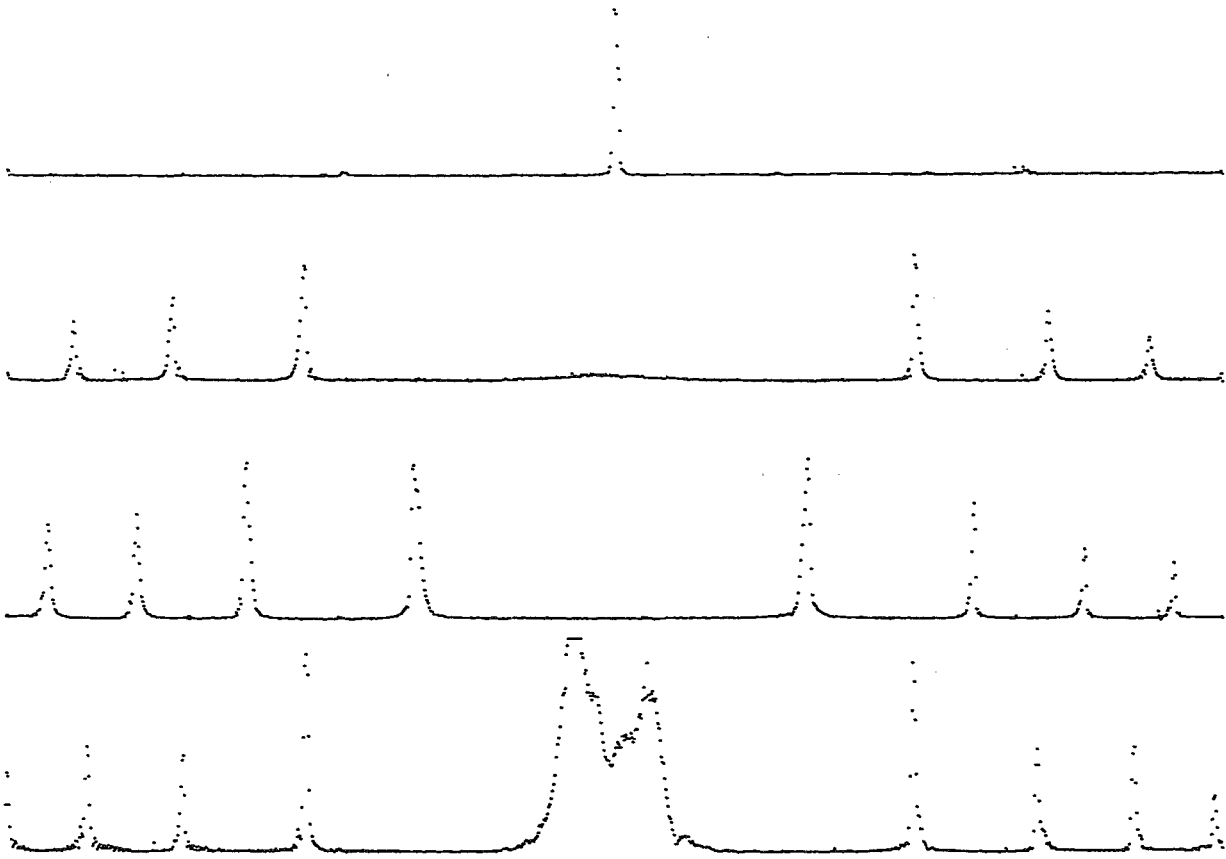
Fig. 1 Oscilloscope display of the light pattern picked up by the four linear photodiode arrays. The top trace belongs to the spectrograph, the other traces show the interference pattern of the Fabry-Perot etalons.

The hardware was realized with standard TTL logic elements. Its central part is a shift register with three positions, A, B, and C (Fig. 2). The digitized photodiode signals are first fed into position A and thereafter shifted to B and C. Thus three neighboring output words are simultaneously present in the shift register for comparison. A 12 bit counter is used to count the clock pulses in such a way that its content gives the diode number corresponding to the word momentarily contained in register B; it runs from 0 to 4095.

The peak condition $A \leq B > C$ is modified by further restrictions before a peak is accepted as such:

1.) All three values A, B, and C must exceed some manually set threshold value to avoid that baseline noise is inadvertently interpreted as peaks. The threshold can be set individually for each one of the four arrays.

2.) During two edge cycles, in the beginning and at the end of each 1k block, the shift register contains less than three meaningful data words. Therefore a peak detected during these cycles is ignored.

4k begin load overflow 4k end

clock peak address

shift-register from shift-register peak height position B

12 bit words A B C 1k blocks

delay

comparators:

A ≤ B 1k edge suppression center suppression reconstructed analog signal to oscilloscope

B > C

DAC

C>thr. & 'peak found' signal

B>thr. o→ '1'

A>thr. & mono-flop & blanking signal to oscilloscope

4 threshold values
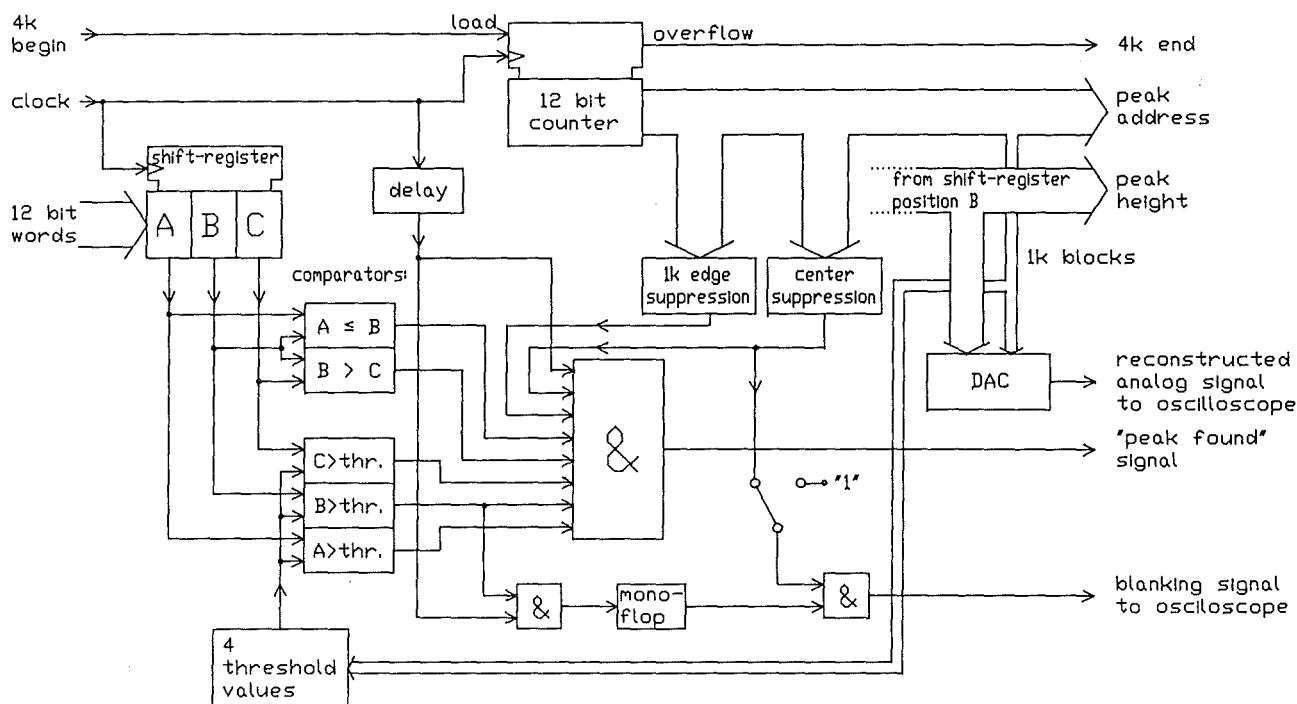
Fig. 2 Schematic diagram of the peak detection hardware for the wavemeter. The left hand input signals came from the wavemeter electronics. The right hand output signals are fed to an on-line computer and an oscilloscope.

3.) It can happen that the laser frequency is such that the so-called etalon excess is close to zero (1,2); under these circumstances the innermost interference ring degenerates to a central spot which has no simple signature suited for evaluation (bottom trace in Fig. 1). Therefore peaks detected among the 128 or 256 center diodes of the interferometers are suppressed.

If a peak is accepted, its address and intensity value are transmitted into a CAMAC FIFO register for temporary storage in order to derandomize the data flow to the computer. The end of a full 4k cycle is signalled to the computer which then may read the data from the FIFO and further process them if required.

For visual inspection and control the digitized intensity data from the photodiodes are reconstructed and displayed as four traces on an oscilloscope (Fig. 1). Blanking signals are derived from the center area and the threshold suppression signals to display the effect of the actual switch settings by dimming the points which are excluded.

(1) A. Steiger, Report KfK 3820, Kernforschungszentrum Karlsruhe (1984)
(2) A. Fischer, R. Kullmer, W. Demtröder, Opt. Comm. 39 (1981) 277
(3) R. L. Byer, J. Paul, M.D. Duncan, in: 'Laser Spectroscopy III' (Springer, Heidelberg 1977) p. 414

4.   NEUTRINOPHYSICS

T. Csabo, G. Drexlin, V. Eberhard, K. Eitel, H. Gemmeke, G. Giorginis,
W. Grandegger, R. Gumbsheimer, H. Hucker, L. Husson, J. Kleinfeller,
R. Maschuw, P. Plischke, J. Rapp, F.K. Schmidt, G. Spohrer, J. Wolf,
S. Wölfle, J. Wochele, B. Zeitnitz, B. Bodmann*, F. Burtak*, E. Finckh*,
A. Glombik*, W. Kretschmer*, F. Schilling*, J.A. Edgington**,
T. Gorringe**, A. Malik**, A. Dodd***, A.G.D. Payne***, N.E. Booth****

4.1   STATUS OF THE KARMEN EXPERIMENT

The KArlsruhe Rutherford interMediate Energy Neutrino experiment KARMEN makes use of pulsed 'beam dump' neutrinos v_μ, v_e and $\bar{v}_\mu$ from π^+ - decay at rest produced at the spallation facility ISIS of the Rutherford Appleton Laboratory, England. A 56 ton all active scintillation calorimeter (see fig. 1) is looking for various neutrino induced reactions. Major physics aims of the experiment are to search for appearence oscillations $v_\mu \rightarrow v_e$ and $\bar{v}_\mu \rightarrow \bar{v}_e$, to observe charged and neutral current excitations of ^{12}C by v_e and v_μ and to measure v_e - e elastic scattering. (The physics program has been described elsewhere (1,2).)
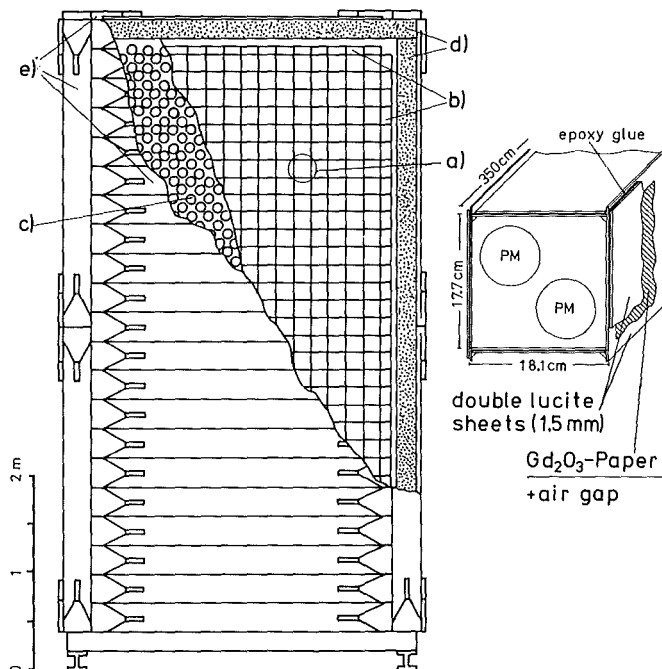

Fig. 1 Front view of the KARMEN neutrino detector. a) 512 central modules
17.7x18.1x350 cm b) inner active shield of 96 half width modules
c) 2240 PM (3 inch VALVO XP3462) d) passive inner shield 20 cm
steel e) outer active shield 3 cm NE110 plastic scintillator.

In autumn 1988 the KARMEN calorimeter with half its detector modules installed has for the first time been looking for neutrinos from ISIS. Preliminary results from this test run are described below.

After the end of the ISIS 1988 beam period the detector was removed from its data taking position for final completion outside the 6000 ton shielding bunker. The remaining five out of nine submodules of the optical segmentation have been assembled and installed. A submodule consists of 38 vertical and 152 horizontal 3 mm acrylic double sheets to form a square box structure of $3.5*3.2*0.7$ m^3 size. All 2240 phototubes have been mounted to the detector and connected to the front end electronics of the data acquisition system. The anticounter system of 3 cm plastic scintillator sheets tightly covering the main detector has been refined and completed. Experience from our test run led to some improvements of shielding, detector operation and the electronics system. A 7 cm wall of borated polyethylene is currently installed in front of the detector together with a B$_4$C lining of the upstream and downstream end of the passive inner shield for better suppression of slow neutrons entering the central detector. An additional 1.2 m steel wall in front of the shielding bunker should provide better overall shielding against beam correlated background radiation by increasing the shielding thickness towards the target station to 7.5 m equivalent steel. Circulating and cooling the coupling oil between phototubes and detector windows will remove the heat dissipation from the phototube bleeders. The trigger system has been improved to ensure that the history of each stopped muon is completely recorded, because secondary particles from unidentified stopped muons were found to be a major source of background to any neutrino induced event (see below). The detector is currently in its final stage of completion and is scheduled to start long term data taking in October 1989 which will extend over several years.

4.2   RESULTS FROM THE 1988 ISIS RUN

In the three month data taking period at ISIS from August to October 1988 a total of $7.6 * 10^7$ events were recorded consisting mainly of through-going muons, electrons from muon decay, and low energy background. Data reduction and evaluation has been done at Karlsruhe with emphasis on the study of cosmic ray background and the identification of the first neutrino signatures. Cosmic ray muons entered the 22 ton calorimeter at a rate of 640 Hz. About 7 % were stopped within the active volume. Identification of these stopped muons is of vital importance because otherwise their decay could mean a serious background to the

experiment as the energy spectrum of the decay electrons partly matches the spectrum of inverse beta decay reactions induced by beam dump neutrinos.

On the other hand 'Michel'-electrons from muon decay are an ideal tool to study detector and electronics performance. The 'Michel' spectrum of decay electrons (fig. 2) demonstrates the very good calorimetric properties of the detector: the electron energy is almost completely transformed into visible energy reflecting the 98 % active mass of the calorimeter. A GEANT3 Monte Carlo simulation is in good agreement with the experimental data. The measured muon
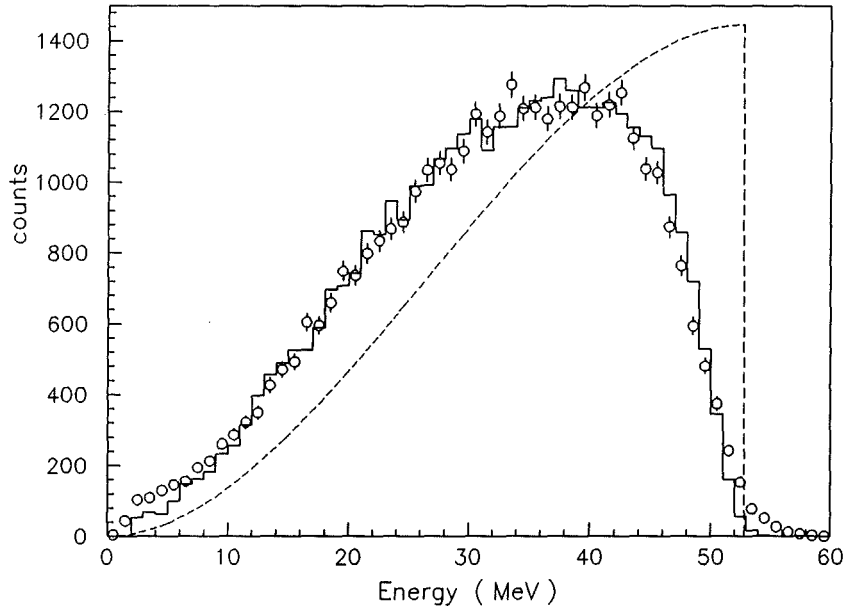
Fig. 2 Visible electron energy from muon decay (o); histogram: GEANT3 simulation; broken line: theoretical Michel shape.
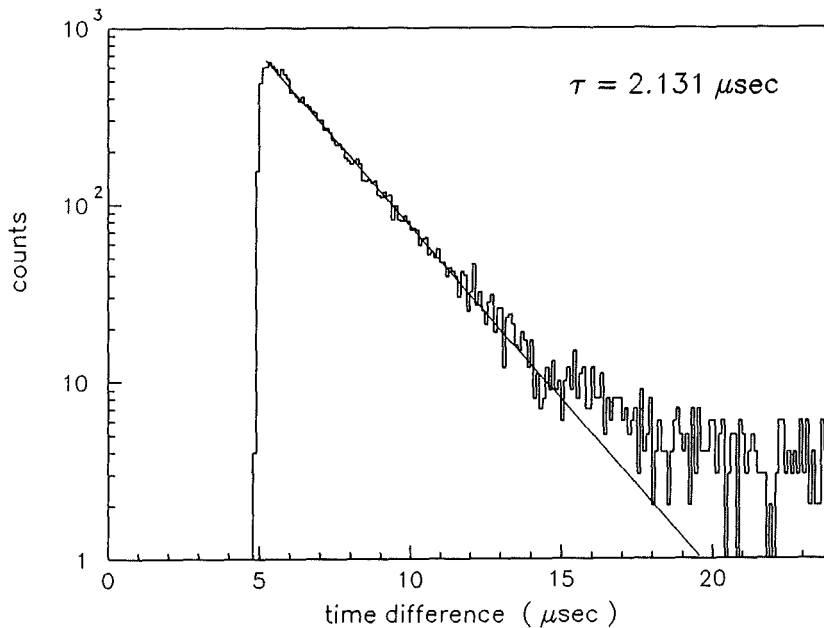
Fig. 3 Muon lifetime plot with exponential fit yielding a lifetime of 2.131 µs.

lifetime (fig. 3) of τ = 2.131 μs is within 1 % of the calculated one for the KARMEN scintillator compound taking into account μ^+ decay, μ^- decay and μ^--^{12}C capture.

A further background source would be the emission of neutrons following nuclear muon capture in the ^{12}C nuclei of the liquid scintillator (μ^- + ^{12}C → n + ^{11}B + v_μ). The single neutron from the μ^- capture process is thermalized and then captured by Gadolinium (Gd$_2$O$_3$) contained inside the optical segmentation, emitting on average three γ-quanta with a sum energy of 8 MeV. The time dependence of the delayed coincidence between the stopped muon and the detection of the neutron via the Gd(n,γ) reaction is shown in fig. 4. The specific time constant of τ = 106 μs for neutron detection in KARMEN is verified by a MORSE Monte Carlo simulation using an evaporation type neutron energy spectrum. The ^{12}C(μ^-, n v_μ)^{11}B reaction can thus be used to measure the neutron detection efficiency of KARMEN at any time. Assuming a capture probability of 4 % for a stopped muom, a neutron detection efficiency of 20 % was deduced.
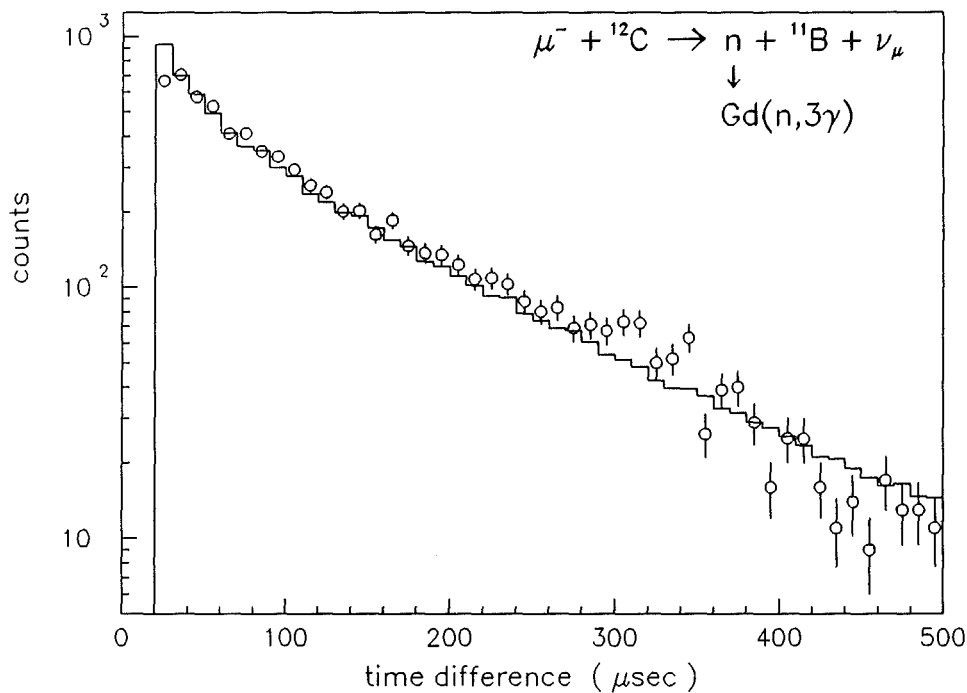
Fig. 4 Measured time distribution of Gd(n,γ) capture reactions for
neutrons from μ^- capture in ^{12}C; histogram: MORSE simulation.

Muon capture leading to bound states of ^{12}B(μ^- + ^{12}C → ^{12}B + v_μ) can be detected by the subsequent β-decay of ^{12}B back to ^{12}C. Fig. 5 shows the visible energy of the electrons from ^{12}B decay with a half life of 20.2 msec.

$$\mu^- + {}^{12}C \longrightarrow {}^{12}B + \nu_\mu$$
$$\longrightarrow {}^{12}C + e^- + \bar{\nu}_e$$
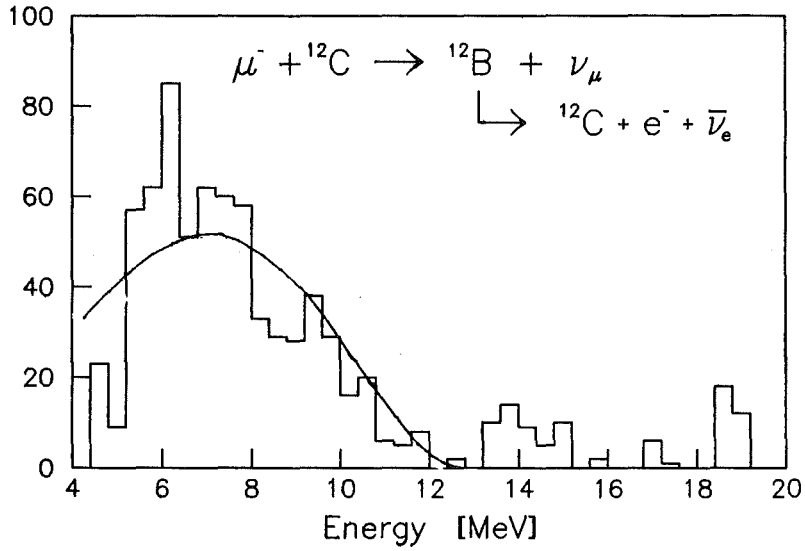
Fig. 5 Visible electron energy from ^{12}B decay; solid line: theoretical energy spectrum.

NEUTRINO CANDIDATE EVENT

PROMPT EVENT

TIME = 3.627 μs

Σ E = 14.8 MeV

DELAYED EVENT

TIME = 9.266 ms

Σ E = 5.3 MeV
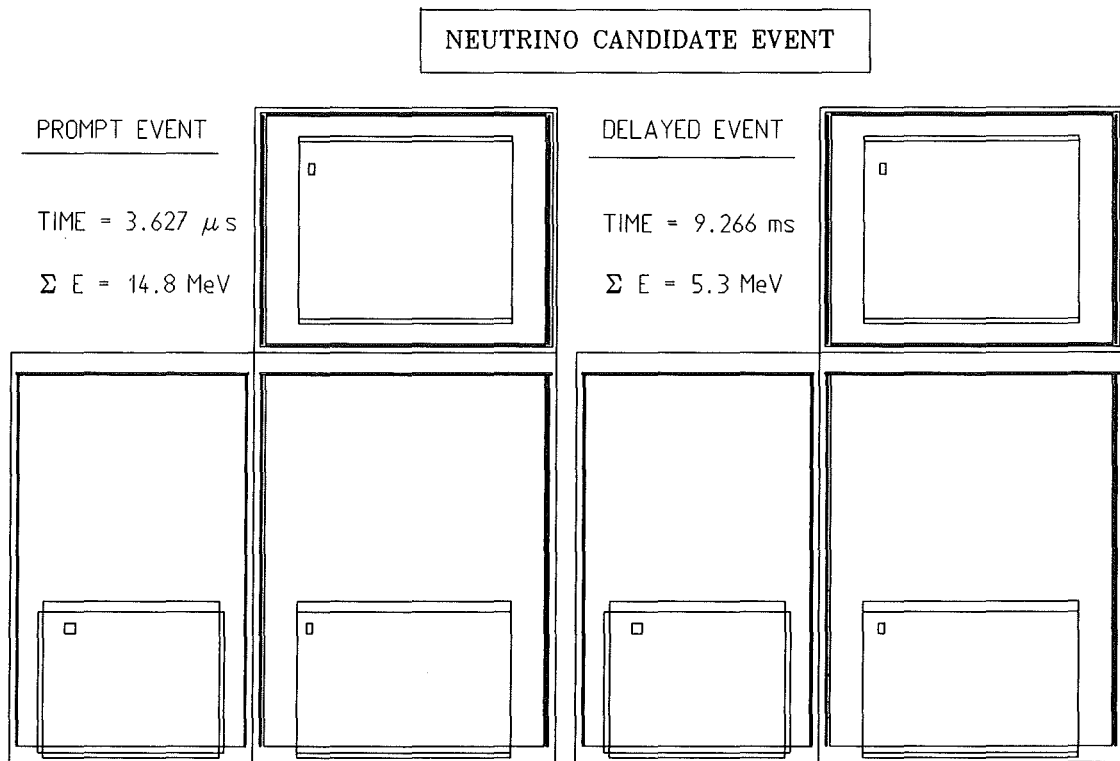
Fig. 6 Neutrino Candidate Event. Delayed coincidence of a 'prompt' electron from the inverse β-decay of ^{12}C with a positron from the subsequent ^{12}N decay.

The various muon induced delayed coincidences demonstrate the ability of KARMEN to detect complex sequential signatures similar to those of ν-

reactions, as for instance $v_e + {}^{12}C \rightarrow e^- + {}^{12}N \rightarrow {}^{12}C + e^+ + v_e$. This inverse β-decay reaction on ^{12}C was looked for to identify the first neutrinos from ISIS.

In the three month data taking period ISIS was running at a mean current of 60 μA and a proton energy of 750 MeV. A total of 210 C of protons were incident on the UD_2O beam stop during the life time of the experiment yielding $1.1 \cdot 10^{12}$ v's / cm^2 at the detector. In order to extract signatures of beam dump v_e various software filters were subjected to the raw data. The delayed coincidence signature of the detection reaction in combination with the low duty cycle of 10^{-4} for v_e allows very stringent cuts with respect to energy, time and spatial correlation. This resulted in a final sample of 3 neutrino candidate events (fig. 6) in good agreement with the expected 3.6 events. The most serious background source for v_e signatures was found to be random coincidences of Michel electrons from unidentified stopped muons. A modified trigger logic together with improvements in the active shield counters will reduce this background to a negligible level.

(1)   KARMEN collaboration, Proc. of Int. Workshop on Neutrino Physics, Springer Verlag, Heidelberg (1987), p. 147-152
(2)   B. Zeitnitz, Progr. in Part. and Nucl. Phys. 13 (1985) 445

*   Physikalisches Institut, Universität Erlangen-Nürnberg, Germany
**   Queen Mary College, London, United Kingdom
***   Rutherford Appleton Laboratory, Chilton, Didcot, United Kingdom
****   Oxford University, United Kingdom

5. DEVELOPMENT AND INSTRUMENTATION
5.1 DETECTORS

5.1.1 Al-Al$_2$O$_3$-Al SUPERCONDUCTING TUNNEL JUNCTIONS AS DETECTORS FOR PARTICLES AND X-RAYS

P. Jany, F. Finkbeiner, W. Heeringa, H.O. Klages, T. Strobelt

Superconducting aluminium tunnel junctions were examined with α-particles to clarify the observed pulse height distribution. Irradiation experiments were performed in which the α-particles were collimated only onto the tunneling region of the diode, only onto the substrate or onto the tunneling region and a part of the substrate. Both rise time and pulse height of the signals were recorded.

A rise time versus pulse height matrix for the last constellation with the assigned origins of the signals is shown in figure 1. This shows that the tunnel junctions are also sensitive for phonons coming from the substrate after energy deposition therein.
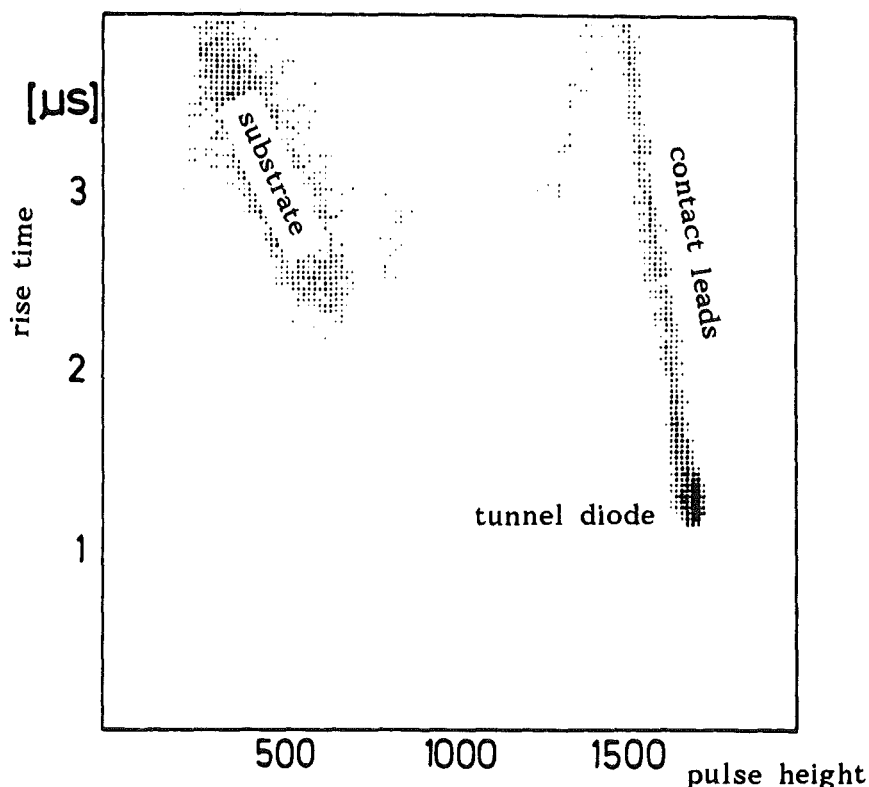
Fig.1 Rise time versus pulse height matrix for an Aluminium tunnel junction irradiated by α-particles through a collimator.

In the next experiment a ^{55}Fe X-ray source was used in order to measure the energy resolution of the tunnel junctions. The thickness of the aluminium layers was reduced to 30 nm to decrease the tunnelling time, and the top layer was covered by an Indium absorber layer of 350 nm thickness in which the X-rays are stopped. This kind of detector is a prototype for planned studies of the trapping mechanism proposed by N.Booth (1). Figure 2 shows a measured pulse height distribution with an energy resolution of 7% at 6 keV.

The so far produced tunnel junctions show still a too high subgap current arising from leakage currents through the insulating barrier. This is probably due to the use of a mechanical evaporation mask. To solve this problem first experiments were performed in collaboration with the Institut für Mikrostruktur-technik of the KfK in order to develop a suitable photolithographic lift-off process for the layer structuring.
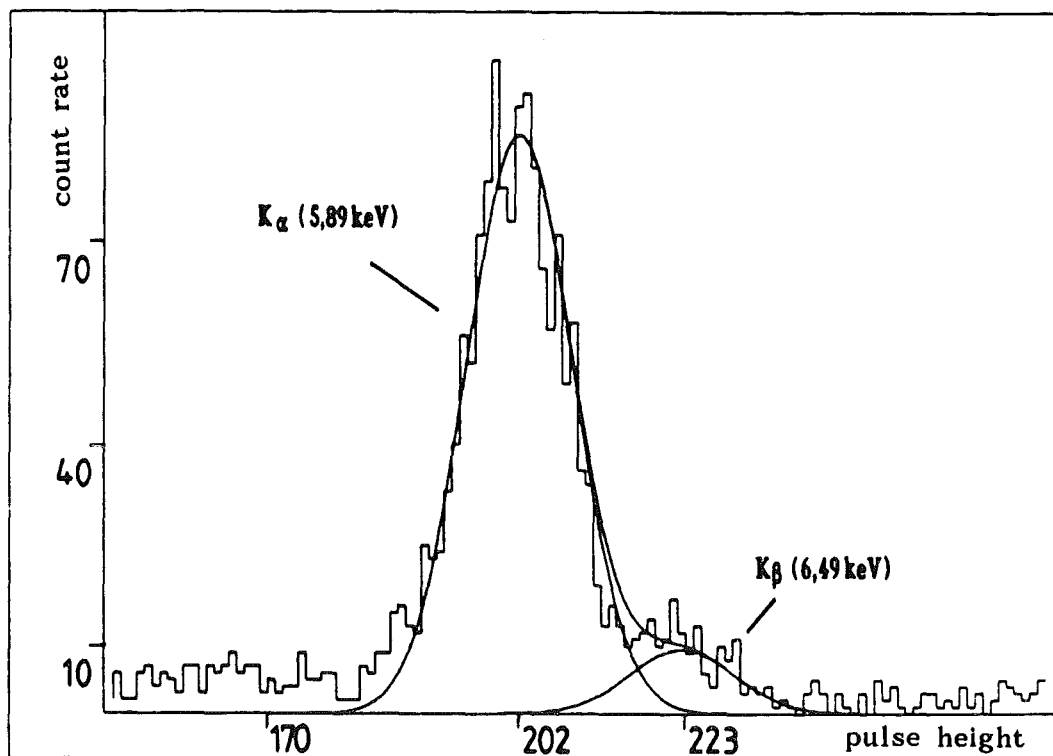
Fig.2   Pulse height distribution of an Aluminium tunnel junction with Indium absorber irradiated by X-rays. The lines are fits to the spectrum.

(1)   N.E. Booth, Appl. Phys. Lett. **50** (1987) 293

5.1.2   THERMISTORS FOR MICRO - CALORIMETERS

R. Bayer, G. Foltin, W. Heeringa, T. Schreiner*

Microcalorimeters are intended for the detection of particles or γ-rays with energies down to the keV-range. They are usually small (of the order of mm^3), are made of electrically insulating materials and are run at very low temperature (typically 100 mK or below) in order to have a sufficiently low heat capacity. A highly sensitive temperature sensor is needed to detect the small temperature change after absorption of radiation. Mostly thermistors are employed for this purpose. They can be obtained from heavily doped semi-conductors. This requires elaborate techniques, however. They also can be made from thin carbon layers, but those are sometimes unstable after thermal cycling.

We produce thermistors from a basic material for the production of SMD-resistors, a paste containing RuO_2 particles. Steep characteristics in the desired temperature region are especially obtained with the high resistance pastes. A characteristic from a thermistor made from the 1MΩ-paste is shown in fig. 1. After baking this thermistor had a thickness of about 30 μ with outer dimensions of 10 mm x 1.5 mm. The flattening of the curve towards the lowest temperatures is probably due to self-heating by the measurement.
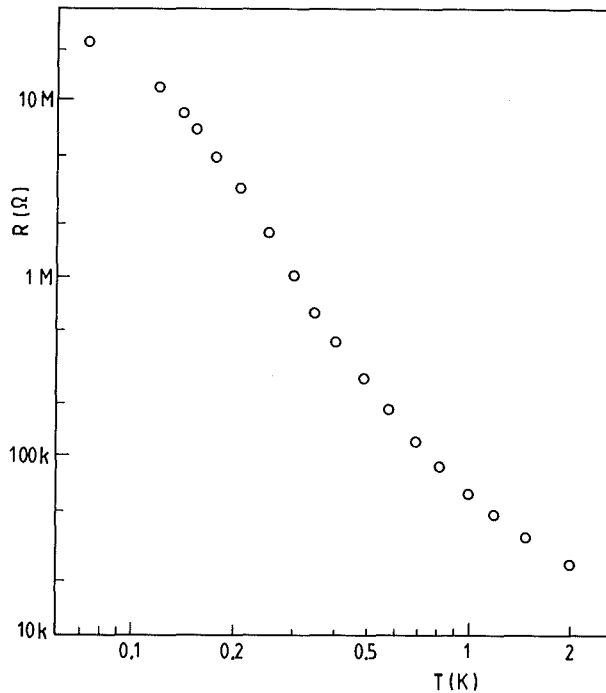
Fig. 1 Characteristic of a RuO_2-paste thermistor.

The high DC-resistance in the operating point requires very low capacitance in the read-out circuit in order to prevent too long pulse rise times. This can only be realized with a cold FET installed inside the cryostat near the microcalorimeter. Presently the distance is about 30 cm and the FET is run at about 70 K. It is properly shielded in order to reduce thermal radiation to the microcalorimeter. Fig. 2 shows the electronic set-up. The bias resistors each have a value of 20 MΩ. The thermistor (R_{th}) is shielded by LC-filters against disturbing signals from outside.
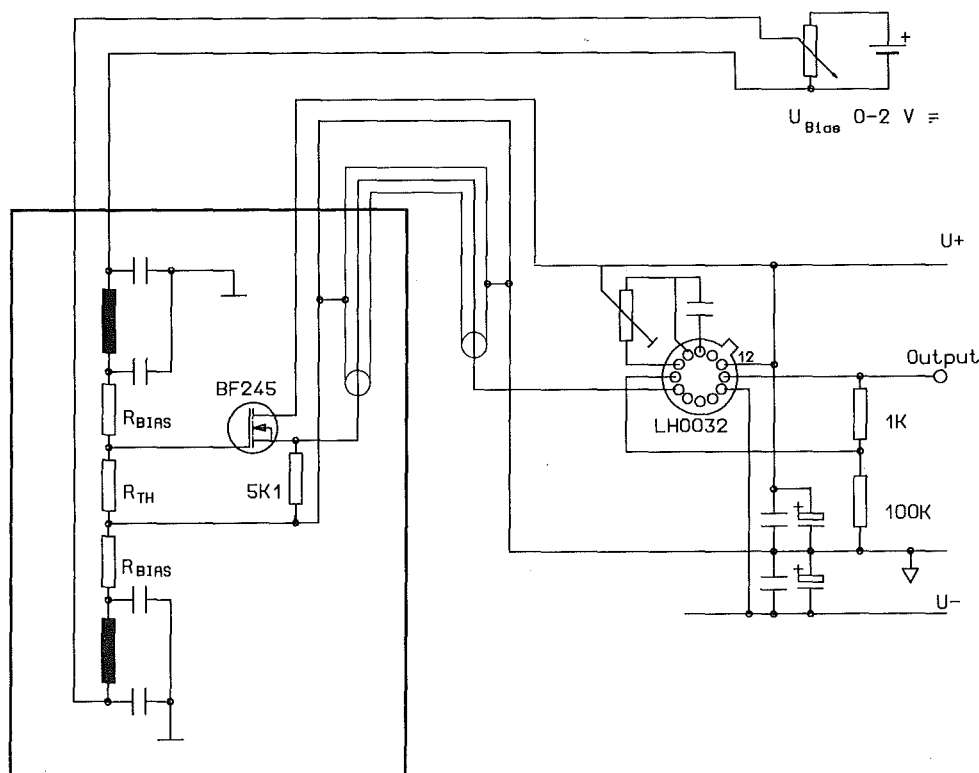
Fig. 2 Read-out electronics of the thermistor.

The properties of the micro-calorimeter (a 27 x 7 x 0.5 mm saphire substrate with the thermistor) are presently tested with heat pulses, generated in a heater resistor, and by 5 MeV α-particles.

*   Kernforschungszentrum Karlsruhe, Institut für Nukleare Festkörperphysik, Germany

5.1.3 A SCINTILLATING LIQUID-NEON TARGET FOR FAST NEUTRON CAPTURE EXPERIMENTS

G.Mondry*, F.Smend*, P.Doll, H.O.Klages, H.Skacel

The scintillating properties of the liquid noble gases He (1), Ar, Kr, and Xe (2) have been investigated thoroughly. However, up to the present liquid neon has not been tested or used as a scintillator. The scintillating neon target designed and tested by us is, to our knowledge, the first application of the scintillating properties of liquid neon.

From recent experiments carried out with gaseous Ne at low pressure (3), it is known that the main emission bands of excimer transitions lie between 70 and 100 nm. Therefore, use of a wavelength shifter is an essential prerequisite for observing the scintillation light.

Fig.1 is a schematic drawing of the target cryostat. The inner cell (8 cm diameter, 9 cm height) contains the liquid neon. It is cooled, via a finned copper block, by a two-stage helium refrigerator having a cooling capacity of about 3.5 W at 25 K. A copper cylinder cooled by liquid nitrogen shields the inner cell from the outer wall of the cryostat. The cooling-down time from starting the refrigerator at room temperature until beginning of condensation was about 10 h. The condensation rate was 1.2 mol/h for neon.
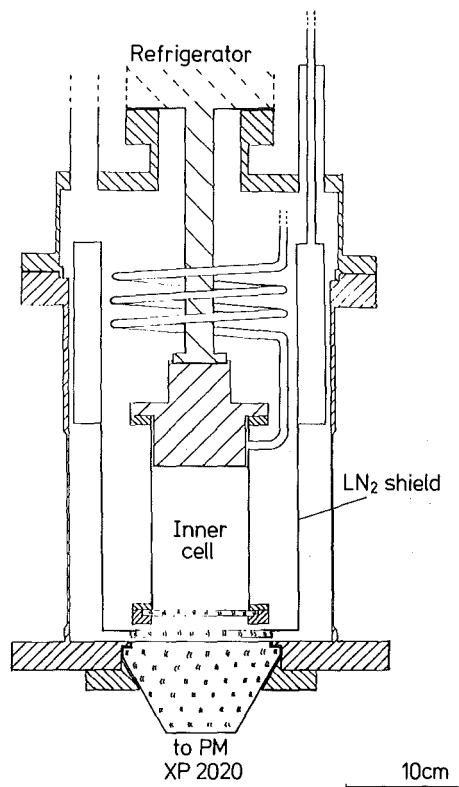
Fig.1 Liquid-neon target cryostat.

Since neon is only liquid over a very narrow temperature range (24.6 K to 27.1 K), the temperature has to be regulated precisely. This was done in the usual way by balancing the net cooling power of the refrigerator by a well regulated electrical heating of the copper block. For calibrating the temperature sensor, the saturation pressure of the liquid was measured using a precision capacitive pressure sensor. During the experiments, the temperature was kept at 25.5 K and the pressure at 900 Torr.

The inner cell was coated with reflecting paint (NE 560) and with vacuum-evaporated DPS. Care had to be taken in choosing the right thickness of the reflector as well as of the wave-length shifter. The reflecting layer had to be very thin at the edges of the cell in order to avoid its peeling off at low temperatures. The thickness of the DPS coating was, in accordance with ref. (1), chosen as 150 and 30 μg/cm² on the walls and on the window, respectively.

The volume of the cell is quite large, and the scintillation light has to pass two quartz windows before reaching the light guide of the photomultiplier (XP 2020). Therefore, both the light collection and the energy resolution of the scintillating target are not optimal. Nevertheless, using gamma sources, Compton edges could be clearly identified.

The design of the target did not allow the insertion of a calibration source, e.g. an alpha-emitting radioactive source, into the target volume. Therefore, an exact evaluation of the scintillation response of liquid neon to ionizing particles was not possible. However, the target was able to detect neon nuclei, recoiling after neutron capture, in coincidence with gamma rays observed in the NaI detectors. From this fact we conclude that the scintillating response of neon for heavily ionizing particles, compared to that for electrons, is as good as that of liquid He or Ar.

(1)   R. van Staa, J.Reher, B.Zeitnitz, Nucl. Instr. and Meth. **136** (1976) 241
(2)   T.Doke, Portgal. Phys. **12** (1981) 9
(3)   A.Ulrich, B.Busch, W.Krötz, G.Ribitzki, J.Wieser, Jahresbericht 1987, Beschleunigerlabor der LMU und der TU München, p.58

*   II. Physikalisches Institut, Universität Göttingen, Germany

5.1.4 MUON DETECTION WITH SCINTILLATOR AND WAVELENGTH SHIFTER READOUT

H.O. Klages, W. Kriegleder

For the EAS experiment KASCADE (1) a scintillator based muon detector is under study to measure the number and lateral distribution of muons outside the shower core. The separation of the muons from the electron / photon component is done with an absorber, an energy cut and a radius cut.

The absorber consists of lead (10 cm) upon iron (4 cm) and stops most of the low energy e/γ component. To separate 'faked muons' generated by the high energy e/γ component punching through the absorber, an energy cut must be used. This enforces a good uniformity of the detector response. To achieve that a partitioned structure was developed as shown in fig. 1.
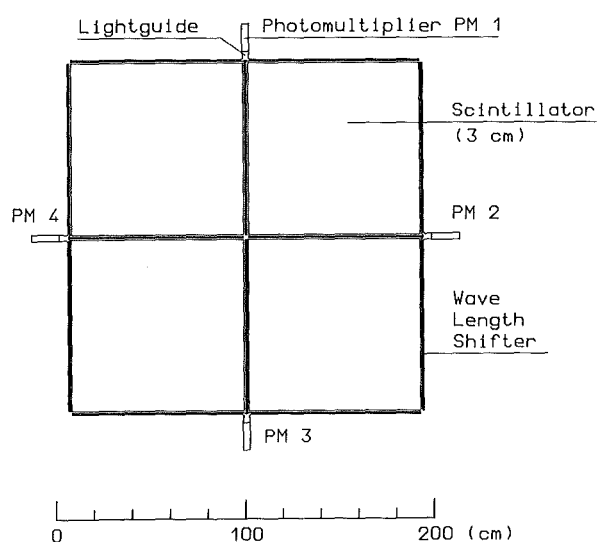
Fig. 1 Schematic view of the muon counter set-up.
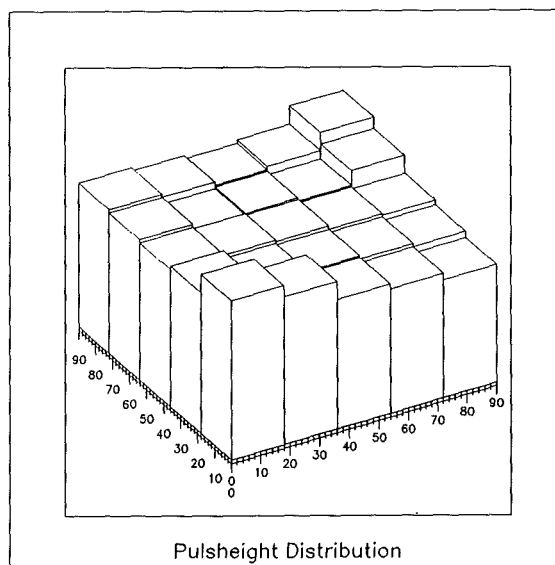
Fig. 2 Light output distribution of one square of the counter.

It consists of 4 squares of high quality scintillator (90 x 90 x 3 cm³), read out by WLS bars at all edges through air gaps of 1 mm to preserve total reflection in the WLS. Tests have shown that the attenuation length of the WLS can be improved by a factor 2 using a good reflector at the open end. Three bars are coupled to one 1.5" photomultiplier with branched lightguides, while every scintillator is looked at with 2 photomultipliers. The coincidence of 2 neighboured photomultipliers defines an event and the signals of these photomultipliers are summarized to compensate attenuation effects in the scintillator. The system is

wrapped in highly reflective aluminium foil to improve the light output and is housed in a box of black polyethylene.

Fig. 2 shows the light output distribution of a test sheet (90 x 90 x 2 cm^3) according to the lower right square in fig. 1. It was measured with cosmic muons selected by coincidence of 2 small scintillator paddles and without absorber. A good uniformity of the pulse height for penetrating muons was achieved with maximal deviations from the mean value of about 10 %.

To estimate the signal to background ratio simulations were performed using the CORSIKA and GEANT 3 program packages.

The detector response was simulated for electrons and photons with fixed energies ($3 \cdot 10^6$ eV - 10^9 eV) punching through the 20 r.l. absorber. An energy threshold of ~ 3 MeV was used to get a detection probability as a function of the particle energy. This function was folded with simulated lateral - and energy - distributions of electrons and photons in an EAS. Fig. 3 shows one result for an EAS, induced by a 10^{14} eV proton, integrated from r = 0 up to R for a sampling density of 2.5 %.
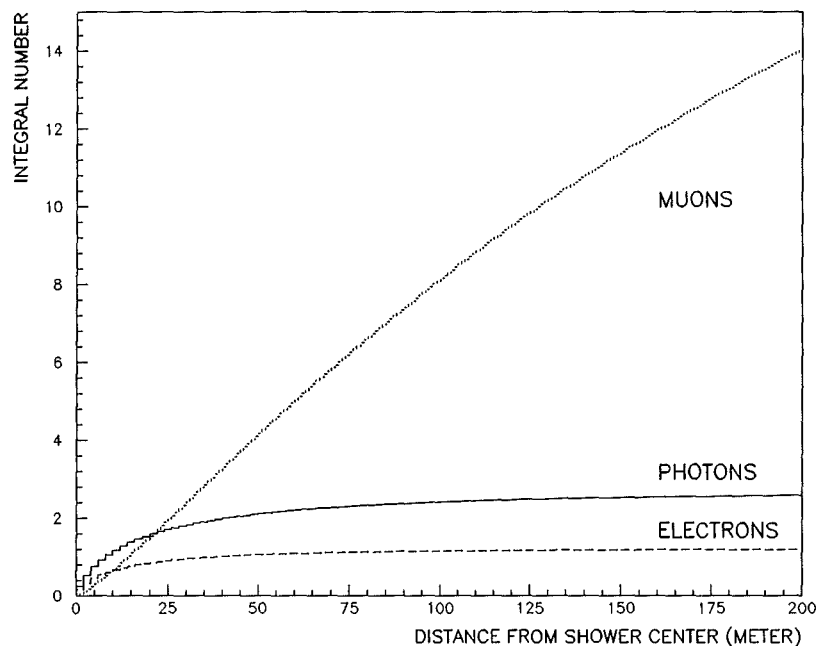
Fig. 3   Punchthrough and real muons of an EAS, induced by a 10^{14} eV proton.

It shows that most of the remaining background could be distinguished by neglecting detectors with core distances < 15 m without loosing more than 1 real muon through this radius cut.

(1)   P. Doll, J. Engler, H.J. Gils, D. Heck, N. Heide, H. Keim, H.O. Klages, J. Knapp, H.J. Mayer, H. Müller, J. Oehlschläger, H. Rebel, G. Schatz, G. Schmalz, T. Thouw, S. Zagromski and B. Zeitnitz, this report, contr.2.1

5.1.5   PLASTIC STREAMER TUBES FOR THE KASCADE EXPERIMENT

K. Daumiller, P. Doll, H.O. Klages, W. Kriegleder, H. Müller

For detecting the number of electrons or muons from air showers penetrating through a position sensitive detector of a typical area of several square meters, we started to investigate the operational features of plastic streamer tubes (1). The electron and / or muon identification would be based on tracking the particle trajectories by means of cathode pad structures. The encouraging features of streamer mode are large anode signals, low noise and a wide high voltage efficiency plateau, for a wide range of wire diameters (60 - 200 μm) and tube diameters (several centimeters down to few millimeters). Inspite of their extensive usage in high energy experiments covering areas of thousand square meters, only little literature is available describing the discharge mechanism in the streamer mode (2). Very recently detailed investigations appeared in the literature on the drift time (3) and spatial charge distribution (4) of self-quenching streamers. We started to investigate commercially available tubes (5) in an 8 cell (9 x 9 mm^2) and 8 cell (30 x 30 mm^2) geometry using several cells and cosmic particles which trigger the tubes by a plastic scintillator telescope.
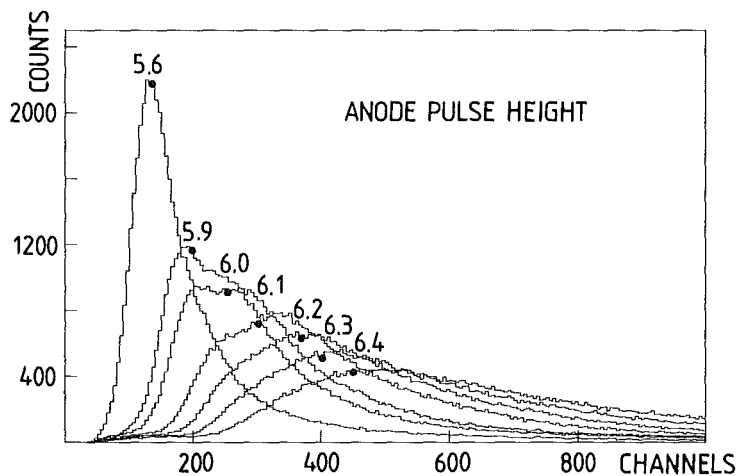
Fig. 1
Anode pulse height spectra of cosmic particles for various voltage settings.

Fig. 1 shows the variation of the anode pulse height spectra with high voltage for the 8 cell (30 x 30 mm^2) geometry and a 1 : 2 argon-isobutane gas mixture. Looking for the efficiency plateau of this geometry and gas setting it is found to extend from 5.9 to 6.6 kV. The free countrate of the quarter square meter area of 8 tubes amounts to about 100 Hz.

Fig. 2 shows the intrinsic information of an 30 x 30 mm^2 cell presenting the drift time distribution to the 100 μm anode wire versus the anode pulse shape (PS) distribution. The pulse shape parameter is obtained by integrating the anode

signal and after-shaping in a double-delay-line amplifier. The zero crossing time of the bipolar signal with respect to the constant - fraction discriminator time leads to the information whether a 2. or 3. streamer follows a primary streamer. The PS parameter exhibits the grouping of two streamers (S2, S3) following a primary streamer S1 at 6.7 kV anode operation voltage. Data like those presented in fig. 2 help to clarify the details of the streamer tube operation with respect to gas composition and geometry. In the future we plan to investigate the properties of conductive plastic tubes and an economic cathode read-out structure.
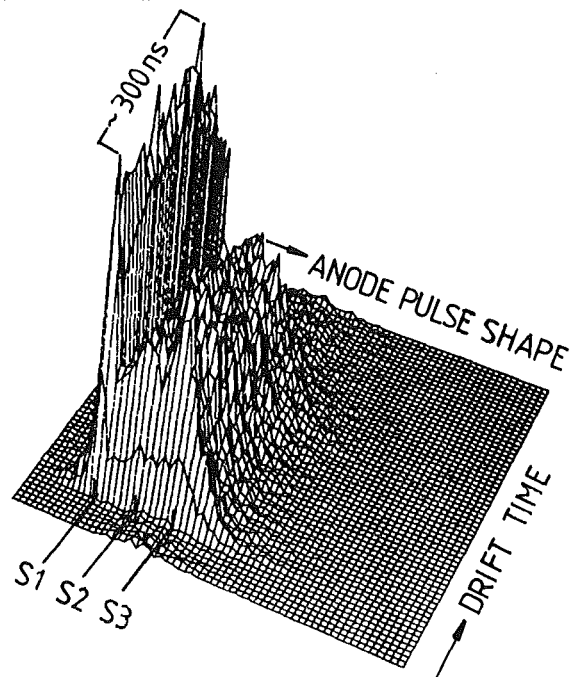
Fig. 2 Drift time versus anode pulse shape for a 30x30mm^2 streamer tube cell operated at 6.7 KV.

(1)   E. Iarocci, Nucl. Instr. and Meth. 217 (1983) 30
(2)   G. Charpak, G. Petersen, A. Policarpo, F. Sauli, IEEE, Trans. Nucl. Sci. NS25 (1978) 122
(3)   S.F. Biogi, P.S.L. Booth, Nucl. Instr. and Meth. A273 (1988) 530
(4)   E.P. Delime, J.L. Pinto de Cunha, R.F. Marques, A.J.P.L. Policarpo, Nucl. Instr. and Meth. A267 (1988) 93
(5)   Polyvar, Pomezia, Italy

5.1.6   A DETECTOR FOR THE e/γ-COMPONENT OF EXTENSIVE AIR SHOWERS

G.Völker, H.O.Klages

For the proposed KASCADE array a detector for the electron / photon component of extensive air showers has to compromise the requests of large effective area, good resolution in time and energy and low cost per detector unit.

After testing a number of scintillation materials (1), a detector prototype has been built to test scintillators, geometries, reflectormaterials, light collection processes and photomultipliers. In parallel Monte Carlo calculations for light transportation and light collection have been carried out. As a result, we chose a cylindrical scintillator shape with 100 cm of diameter viewed by a system of a 3"

photomultiplier coupled to a conical lucite lightcollector at a distance of 60 cm, as shown in fig. 1. We decided against square shape since our test shows, that light collection from the corners is problematic (2).
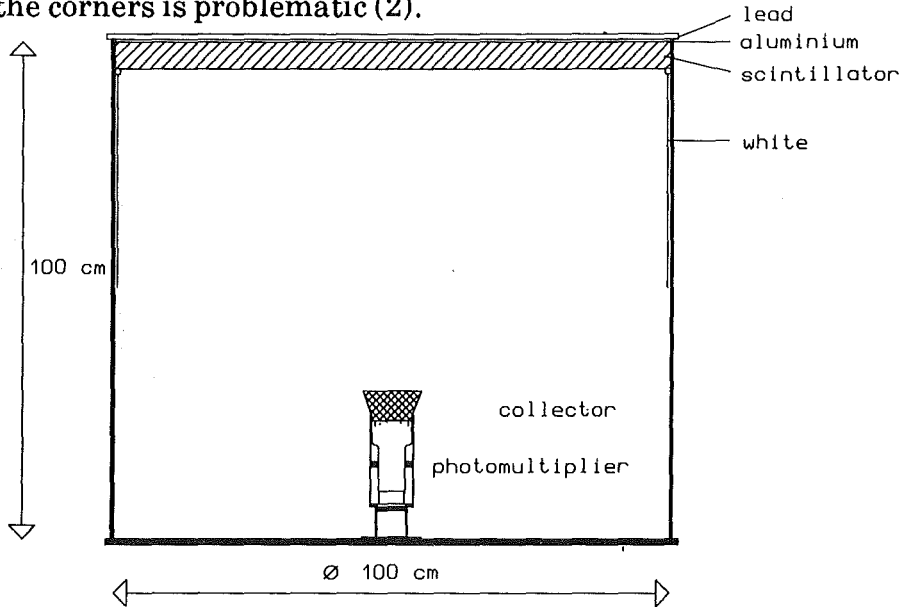
Fig.1   Schematic drawing of the e/γ-detectors for the KASCADE array.

To investigate the properties of this set up, we used cosmic muons triggered by a 18cm x 18cm plastic scintillator telescope located just above the scintillator. Fig.2 shows an experimental pulse height and time spectrum of this detector.

Pulse Height (Channels)   Counter Time (nsec)
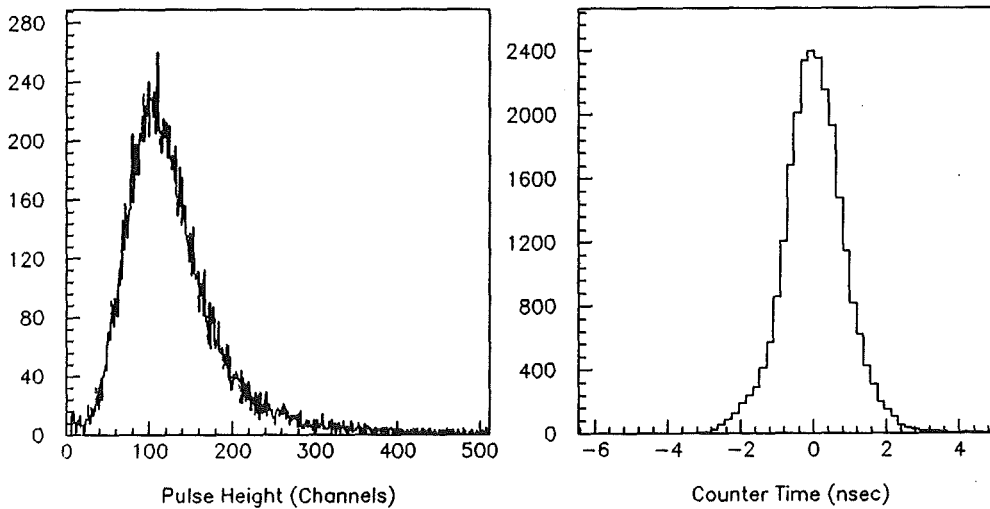
Fig.2   Experimental pulse height (a) and timing (b) distribution for single muons traversing the counter in the central position. (b) has not been corrected for time resolution effects in the muon telescope.

By coating the scintillator with highly reflecting aluminium foil, the "prompt" light is enhanced nearly by a factor of 2. The white reflector of fig.1 causes a 20-30% higher pulse height. Measurements with different set ups and the

results of Monte Carlo calculations are shown in fig.3. An "ideal" conical light collector has about the following dimensions: 14 cm upper diameter, 10 cm lower
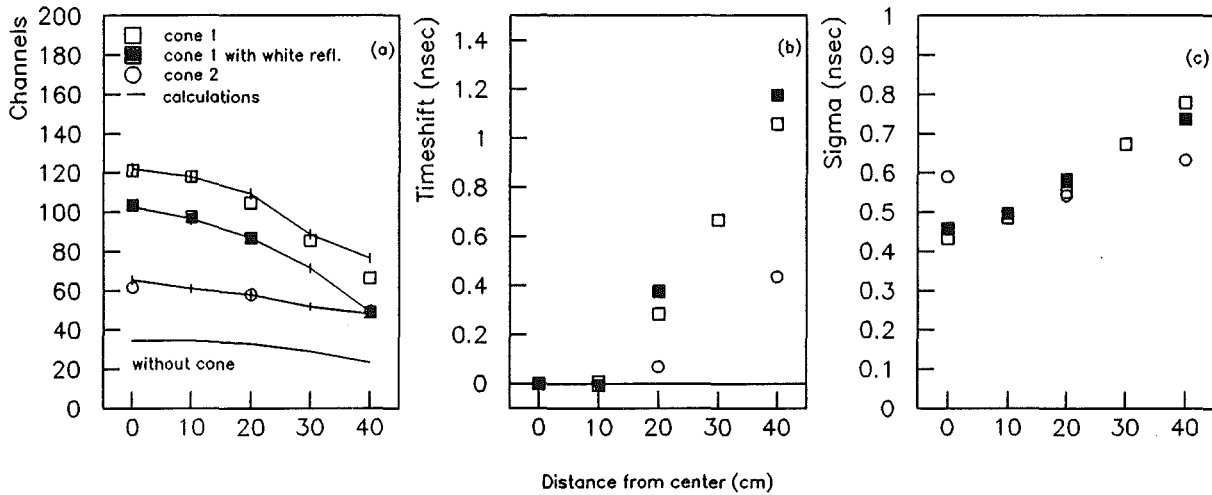
Fig.3 Measurements and calculations of different detector set ups :
(a) lightoutput, (b) time difference to central position, (c) time resolution.

diameter, 7.5 cm height. The advantages are good timing properties (time resolution $\sigma(t) = 0.7$ nsec and small maximal time shift caused only by the counter geometry) and a double light output over the whole detector area in comparison to a detector without lightcollector. The energy resolution is about 30% for penetrating vertical muons.

(1)   H.O.Klages, W.Kriegleder, G.Völker, Report KfK 4508, Kernforschungs-zentrum Karlsruhe (1989) p. 119

(2)   E.Böhm, U.J.Rose, R.Staubert, J.Trümper, Nucl. Instr. and Meth. 40 (1966) 73

5.1.7   FLUORESCENCE EFFICIENCIES OF A LARGE NaI CRYSTAL TO VARIOUS CHARGED PARTICLES

P. Doll, G. Fink, M. Haupenthal, R.W. Finlay*, S. Hauber, H.O. Klages, H. Schieler, F. Smend**, G.D. Wicke**

The light output response of inorganic scintillators such as NaI(Tl) to various particles, charged or neutral, and photons has been the subject of several experimental studies in the past. Besides NaI other inorganic crystals like LiI, KI and CsI were frequently investigated for their response to various charged particles. Measurements of the light yield of some common inorganic scintillators were reported recently (1). There, the crystals were coupled to a light sensitive silicon

diode. However, only a limited number of investigations (2) of pulse shape properties of inorganic scintillators have been reported so far.

It was the purpose of the present investigation to study the neutron induced reactions in a NaI crystal (16 x 16 x 24 cm³) over the neutron energy range from 18 to 36 MeV. In a fast neutron scattering experiment the heavily shielded crystal was viewed by 5 PMs from the backside. The pulse height for various interactions in the NaI was investigated. Similar studies are presently carried out at various laboratories, because little is known about neutron interactions in NaI at high energies. Very often, large NaI detector systems are operated in heavy ion collision experiments where, in addition to γ-multiplicities, large neutron multiplicities must be taken into account. Therefore, pulse shape discrimination provides besides time-of-flight an additional means, separating photons from hadrons originating from an irradiated target.
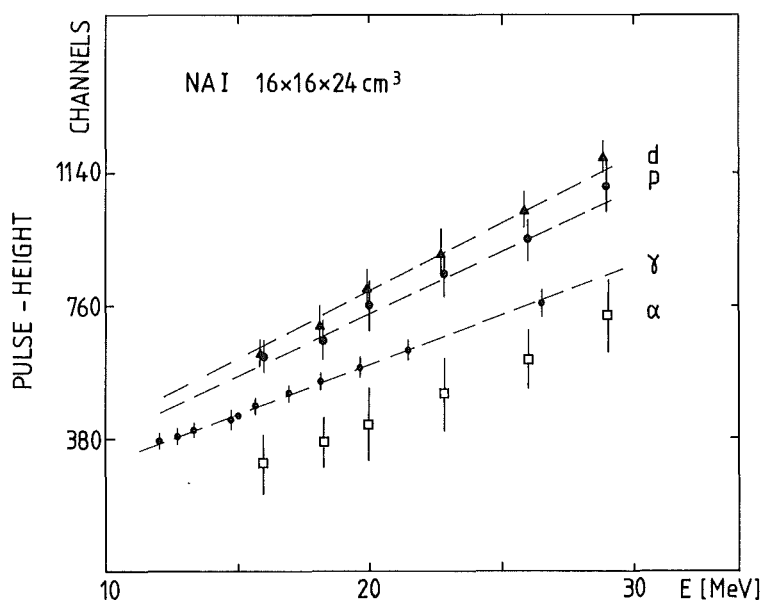
Fig. 1
Light yield for various charged particles in a NaI crystal.

Fig. 1 shows the variation of the proton, deuteron, α-particle and γ pulse height versus energy. The error bars account for the uncertainty in determining the pulse height defined by the Q-value of the corresponding (n, charged particle) reaction in NaI. The large pulse height from protons and deuterons is quite surprising but has also been reported for energies above 30 MeV in a recent paper (3). It remains to be clarified, why charged particles of different mass show a systematic variation of their light decay times used for pulse shape discrimination, however, their energy dependent fluorescence efficiency is grouped quite different from most organic scintillators.

(1)   I. Holl, E. Lorenz, G. Mageras, Report-MPI-PAE / Exp. E1.<u>185</u>, MPI für
        Physik und Astrophysik, München (1987)
(2)   D.M. Whittal, C.U. Bartle, Nucl. Instr. and Meth. **A247** (1986) 390
        P. Doll, G. Fink, M. Haupenthal, R.W. Finlay, S. Hauber, H.O. Klages,
        H. Schieler, F. Smend, G.D. Wicke, Nucl. Instr. and Meth., in print
(3)   G.A. Needham, J.L. Romero, F.P. Brady, C.M. Castaneda, T.D. Ford, to
        be published

*   Ohio University, Athens, USA
**   II. Physikalisches Institut, Universität Göttingen, Germany

5.2   INSTRUMENTATION

5.2.1   DESIGN OF A NEW DILUTION REFRIGERATOR FOR THE 50 mK RANGE

A. Hahn, W. Heeringa, H. Skacel

The development of cryogenic detectors for particles and γ-radiation requires a flexible cooling system with a short cool down time and a base temperature of the order of 50 - 100 mK. Our present cryostats are not able to fulfill both requirements simultaneously. Therefore we decided to build a new apparatus with these properties. In order to keep the total costs low and to achieve a short production time, we ordered a standard 75 μmol dilution insert (without dilution unit) from Oxford Instruments. It comprises a room temperature top plate, a 4K-plate and a 1K-pot with all the tubings and electrical connections necessary to run a ^{3}He-^{4}He dilution unit. The helium bath cryostat and the dilution unit were built in our institute.

The still of the dilution unit is shown in fig. 1. It contains some special features. The electrical heater and the ^{3}He return line both are wound on copper-bolts below the stainless steel bottom of the still. These are connected via copper rods through the bottom to copper plates in the liquid. This set-up guarantees good thermal contact from the heater and from the return line to the liquid without the necessity of feed throughs. A specially designed copper shield in the empty space above the liquid catches the ^{4}He, evaporating at the film burner, before it can escape through the pumping tube. Below the destiller the upper end of the continuous heat exchanger is shown. It consists of a 1.5 m long and 4.65 mm inner diameter CuNi tube, which contains a coiled CuNi tube of 1 mm outer diameter and a total length of about 10 m. The mixing chamber contains one copper plate with sintered silver powder to enlarge the effective contact area from the metal to the helium. This is well sufficient for the design temperature of the unit. All parts of the cryostat have been completed now. It is being assembled and tested presently.
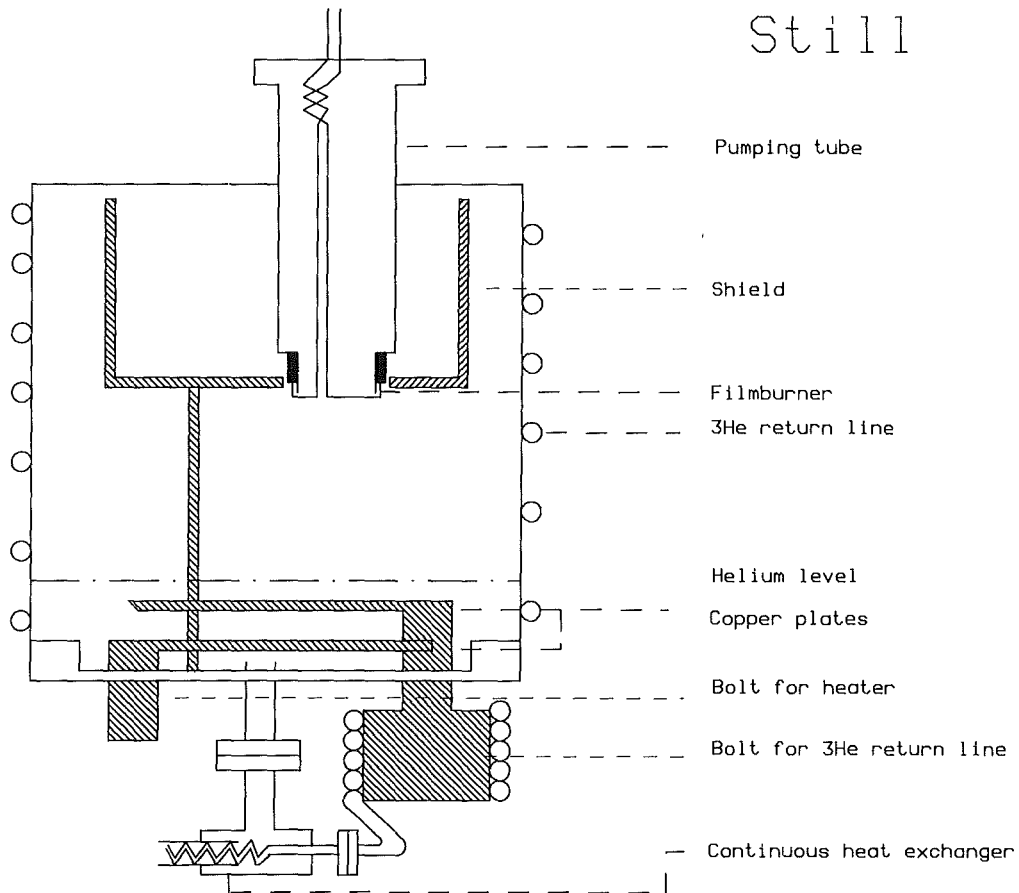
Fig. 1 Design of the still.

5.2.2 A COMPUTER CONTROLLED GAS SUPPLY SYSTEM FOR DETECTORS

C. Garcia-Orijuela, H. J. Gils, S. Zagromski

In nuclear and particle physics experiments using gas-filled detectors the pressure of the gas inside the detector volume is an important operation parameter. In particular in spectroscopic measurements the pressure is often required to be constant within less than one percent. In addition, in most applications fresh counting gas has to flow continuously through the detector in order to avoid signal quenching due to destroyed gas molecules.

The prototype of a computer control of such a gas system was developed for applications where a hardwired control circuit turns out to be impractical.

The system consists of a PDP 11/73 computer implemented into a CAMAC-bus, a standard CAMAC I/O register, and an interface, which performs

the necessary A/D and D/A conversions. The full assembly of the prototype control system including some components for test measurements is shown in Fig. 1.
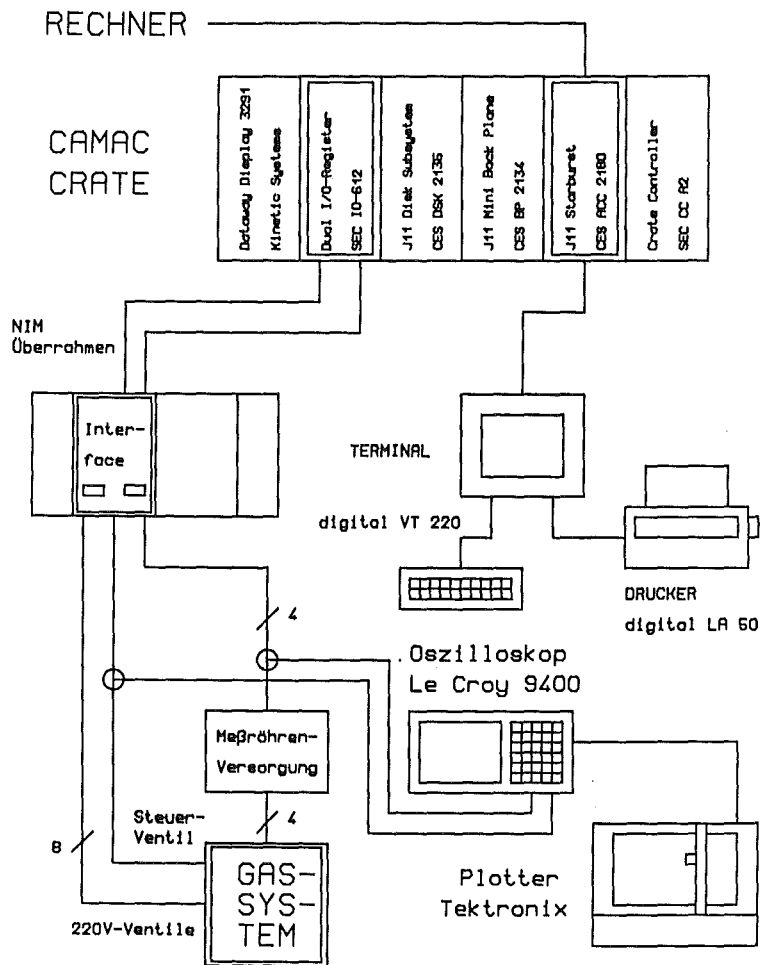
Fig. 1   Prototype of a computer controlled detector gas supply. The oscilloscope and plotter are needed for test purposes only.

The interface is a NIM module containing cards for A/D conversion and D/A conversion, respectively, and a relais card for switching the valves.

The interactive (menu) control program for the system written in FORTRAN 77 allows the following operation alternatives:

a) evacuation of the detector (cleaning)
b) gas filling and pressure control
c) flooding with air or nitrogen and standby position

During evacuation and flooding of the two-chamber detector to which the gas supply was connected a maximum difference pressure between the two chambers must not be exceeded. This was realized by bistable valves, which were opened or closed according to the measured pressure difference. For controlling the gas pressure in the operation mode of the detector a valve with adjustable gas
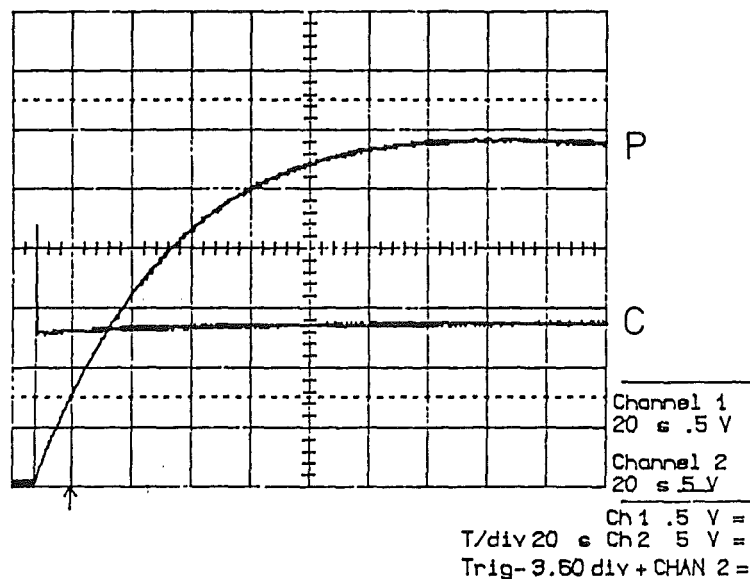
Fig. 2   Transmission functions of the control system P: gas pressure,
C : current of regulation valve.

flow (regulation valve) was implemented into the gas system, which was driven by the computer control.

Due to the very inert behaviour of the system a 1 Hz sampling of its state was sufficient. In Fig. 2 the gas pressure and the electric current driving the regulation valve is plotted versus time.Stable operation conditions for the detector are reached until 2 minutes after filling with gas.

Parameters of the control system can easily be changed due to the modular structure of the control program. This is important if different counting gases or different detector types (volume, flow rates etc.) are to be controlled by the system. The computer control can also be extended to operate a larger number of independent detectors of the same type.

5.2.3   A MULTI-TRANSPUTER SYSTEM FOR PARALLEL MONTE CARLO SIMULATIONS OF EXTENSIVE AIR SHOWERS

H.J. Gils, D. Heck, J. Oehlschläger, G. Schatz, T. Thouw and A. Merkel*

A multi-transputer system was built up, which is dedicated to Monte Carlo simulations of extensive air showers induced by ultra-high energy cosmic rays. The architecture shown in Fig. 1 consists of two independently working VMEbus systems each with a 68020 micro-processor as host computer and twelve T800 transputers for parallel processing. The two systems are linked via Ethernet for data exchange. The T800 transputers are equipped with 4 MByte RAM each,

Ethernet and TCP/IP   IBM

System 1   System 2

PROTEUS

| UNIX HOST | TP subsystem 1 .. 12 |

12 x CPUT1B
4MB RAM
1xT800

RAM-Board
Ethernet Controller
Tape Controller
CPU20D: 68020 CPU + 4MB RAM
System Controller + Ports
460MB Hard Disk

PROTEUS

| UNIX HOST | TP subsystem 1 .. 12 |

12 x CPUT1B
4MB RAM
1xT800

RAM-Board
Ethernet Controller
Tape Controller
CPU20D: 68020 CPU + 4MB RAM
System Controller + Ports
460MB Hard Disk

flexible
expansion
as required

Fig. 1   Hardware configuration of the Karlsruhe multi-transputer system.

Applications

Server Process 1	Shower Simulation	Transputer 1
Server Process 2	Shower Simulation	Transputer 2
Server Process 3	Shower Simulation	Transputer 3
Server Process n	Shower Simulation	Transputer n

Unix Operating System

PROTEUS Unix Host   Transputer
with 68020   Subsystem

Fig. 2   Handling of user software on the transputers by the operating system
of the host computer.

sufficient to run rather large codes. The host computers are operated under UNIX 5.3. On the transputers compilers for PARALLEL FORTRAN, C, and PASCAL are available.

The application software (Monte Carlo simulation of extensive air showers) is independently run on each of the transputers. Server processes on the host processors control the data input, start of program runs, and data output from the transputers as shown in Fig. 2.

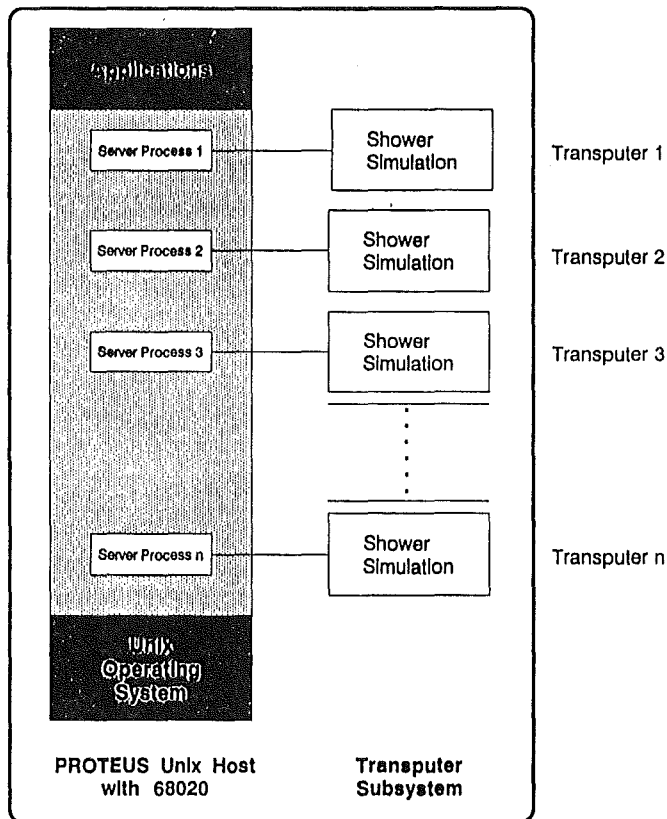The execution times of well known bench marks, which show the same time behaviour as the Monte Carlo simulation codes, are determined for a single transputer processor. They are longer by a factor 17 in comparison with the KfK universal large scale somputer (Siemens 7890 M). As the transputers act independently, the total performance of the system is directly proportional to the number of transputers and hence exceed the one of the Siemens 7890 M.

By the use of this system for air shower simulations a cost reduction by more than a factor of 20 is achieved as compared to a universal computer.

* Proteus GmbH, Karlsruhe, Germany

5.2.4 PHOTOMETER FOR SCINTILLATOR LIGHT TRANSMISSION

K. Eitel, H. Gemmeke, R. Maschuw, J. Rapp, F.K. Schmidt, J. Wolf

Optimization of large volume liquid scintillation counters not only requires knowledge of the light output but also precise information on the wavelength dependent transmission properties of the scintillator.

To measure attenuation lengths of liquid scintillators a two beam photometer schematically shown in fig. 1 was used to cancel any light source instabilities. The transmission coefficient deduced from the relative light intensity of the two beams after having passed scintillator cuvettes of different lengths normalized to the reference intensities without absorber in first approximation is given by the relation $I(x, \lambda) / I(0, \lambda) \approx e^{-x/l}$ where l denotes the attenuation length. However accurate determination of l has to take into account surface transmission effects from the quartz windows of the sample cuvettes as well as geometry effects due to light imperfections.

In a first approach a photometer using a halogen lamp with interference filters for monochromatisation and sample cuvettes of 1 cm and 11 cm length respectively were applied. With this device an accuracy of better than 2 % was achieved for the measurement of attenuation lengths up to about 1 m in the range of wavelengths from 380 nm to 560 nm. This corresponds to an accuracy of the

1: light source
2: monochromator
3: beam-splitter
4,5: sample cuvettes
6: photodiodes
7: ADC's and host computer
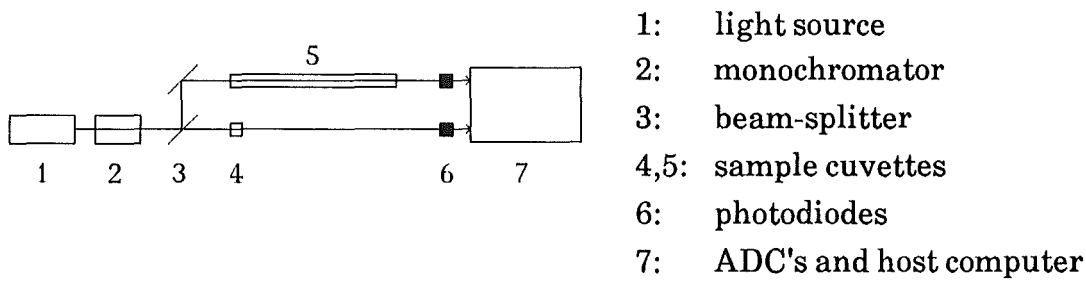
Fig. 1   Two-beam photometer.

order of 10^{-3} in the determination of the transmission coefficent predominantly due to dust contamination on the quartz windows of the cuvettes. It should be mentioned that the accuracy of a single measurement is of course much higher but that the uncertainties quoted, represent the reproducibility of completely independent measurements.

With longer sample cuvettes of about 1 m length a 2 % accuracy can be maintained even for attenuation lengths of 10 m and more. However light divergencies due to the halogen light source optics do not allow the application of samples of that length for this photometer.

Therefore a second photometer using a dye laser and cuvettes of 6 cm and 148 cm length was built. Depending on the dye applied a range of wavelengths from 390 nm to 800 nm can be covered.
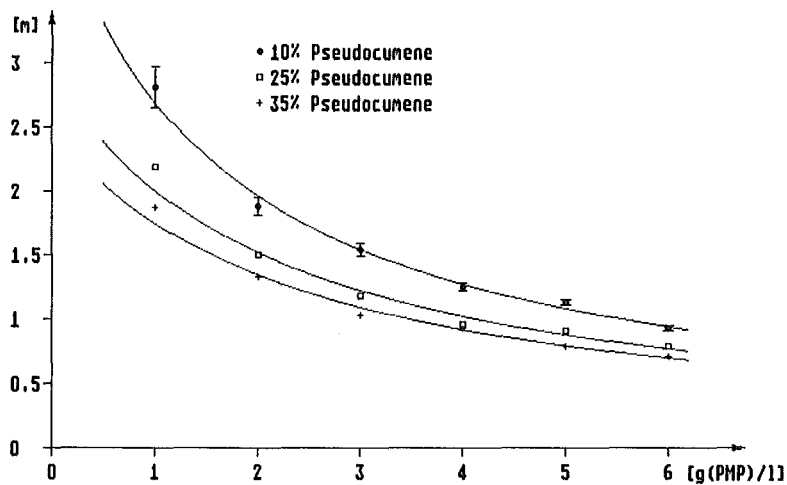
Fig. 2 Attenuation length for 410 nm incident light.

With the halogen lamp photometer the attenuation length for the KARMEN PPP scintillator has been measured for various concentrations of its components. PPP is a mixture of paraffin oil, 1,2,4 trimethylbenzene (Pseudo-cumene) and the one component fluor PMP (1-phenyl-3-mesityl-1-pyrazoline). Fig. 2 shows the attenuation length for various compositions of the scintillator

cocktail at a wavelength of 410 nm. Fig. 3 shows how the attenuation length varies with wavelength.

First measurements with the dye laser photometer showed similar results but precision measurements have only just started with this facility to provide accurate information on transmission properties of liquid scintillators.
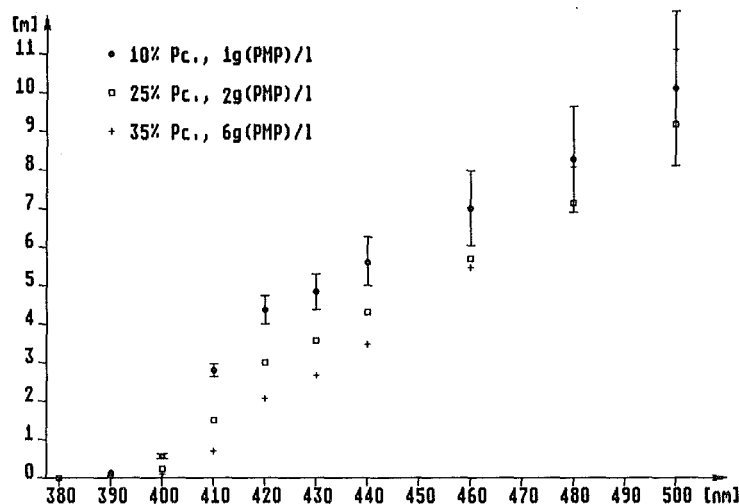
Fig. 3 Wavelength dependent attenuation length.

5.2.5 THE QQDS MAGNETIC SPECTROGRAPH "LITTLE JOHN" AT THE KARLSRUHE CYCLOTRON

I. Design and construction

H.J. Gils, J. Buschmann, S. Zagromski, J. Krisch* and H. Rebel (1)

A magnetic spectrograph for charged-particle spectroscopy, named "Little John", consisting of two quadrupoles, one diopole and one sextupole magnet was constructed and put into operation at the Karlsruhe isochronous cyclotron. The ion-optically rather simple system covers a particle rigidity of 2.5 Tm and was especially designed for small reaction angle experiments. A modest resolving power of $\rho / \Delta\rho = 5200$, a momentum acceptance of $(\rho_{max} - \rho_{min}) / \rho_{mean} = 20\%$ and an acceptance solid angle of $\Omega > 1$ msr were the design goals. The momentum dispersion and consequently the acceptance of the spectrograph can be varied by a factor of 2 without varying other imaging properties considerably. The design, construction and equipment of the spectrograph are described.

(1)   Nucl. Instr. and Meth. A276 (1989) 151

*   Kernforschungszentrum Karlsruhe, Hauptabteilung Ingenieurtechnik

5.2.6 THE QQDS MAGNETIC SPECTROGRAPH "LITTLE JOHN" AT THE KARLSRUHE CYCLOTRON

II. Experimental procedures and performance

H.J. Gils, H. Jelitto, H. Schlösser*, S. Zagromski, J. Buschmann, W. Eyrich*, A. Hofmann*, J. Kiener, A. Lehmann* and H. Rebel (1)

The measured ion-optical properties of the Karlsruhe magnetic spectrograph "Little John" and the properties of its detector system are described. Moreover, the procedures for an efficient use of the spectrograph, in particular concerning small angle and zero degree experiments, are presented in detail. Characteristic experimental results from ^{6}Li-induced nuclear reactions demonstrate the performance of the whole setup.

(1) Nucl. Instr. and Meth. **A276** (1989) 169

* Physikal. Institut der Universität Erlangen-Nürnberg, Germany

5.3 ACCELERATORS

5.3.1 OPERATION OF THE KARLSRUHE ISOCHRONOUS CYCLOTRON (KIZ)

F. Schulz, H. Schweickert

During the period of report the isochronous cyclotron KIZ was in full operation (Tables 1 and 2). The 5881 h of beam time for experiments in 1 year where a 6 week shut down period for the exchange of the correction coils was needed, is a very good value. However, even with the almost round-the-clock operation we could not fulfill all the beam time requirements. In 1988/1989 our machine was overbooked by more than 30 %. This situation is expected to change at the end of 1990 when the nuclear physics activities are planned to be drastically reduced.

The highlights concerning the performance of the machine were the extraction of up to 2.5 µA of $^6Li^{3+}$-ions at 156 MeV and the availability of 100 µA α-particles in the internal beam from an improved internal source.

Cyclotron Operational	With Internal Ion Source		With external Ion Sources*		Total	
For Experiments	2485 h	33.7 %	2845 h	38.6 %	5330 h	72.3 %
Beam Development, Testing new Components, Developments for Isotope Production	316 h	4.3 %	235 h	3.2 %	551 h	7.5 %
Total Time of Operation with the Beam on Targets	2801 h	38.0 %	3080 h	41.8 %	5881 h	79.8 %
Scheduled shut-down for Maintenance, Repair and Installation	579 h	7.9 %	59 h	0.8 %	638 h	8.7 %
Unscheduled Shut-down	684 h	9.3 %	165 h	2.2 %	849 h	11.5 %
Total Shift Time	4064 h	55.2 %	3304 h	44.8 %	7368 h	100.0 %

*Polarized Deuterons 1991 h; $^6Li^{3+}$-Ions (156 MeV) 1188 h

Table 1: Beam statistics of KIZ from July 1988 to June 1989

Pie chart:
- Operation Measurements 9 %
- Others 1 %
- Engineering 10 %
- Material Research 14 %
- Neutron Physics 14 %
- Solid State Physics 14 %
- Nuclear Reactions 38 %
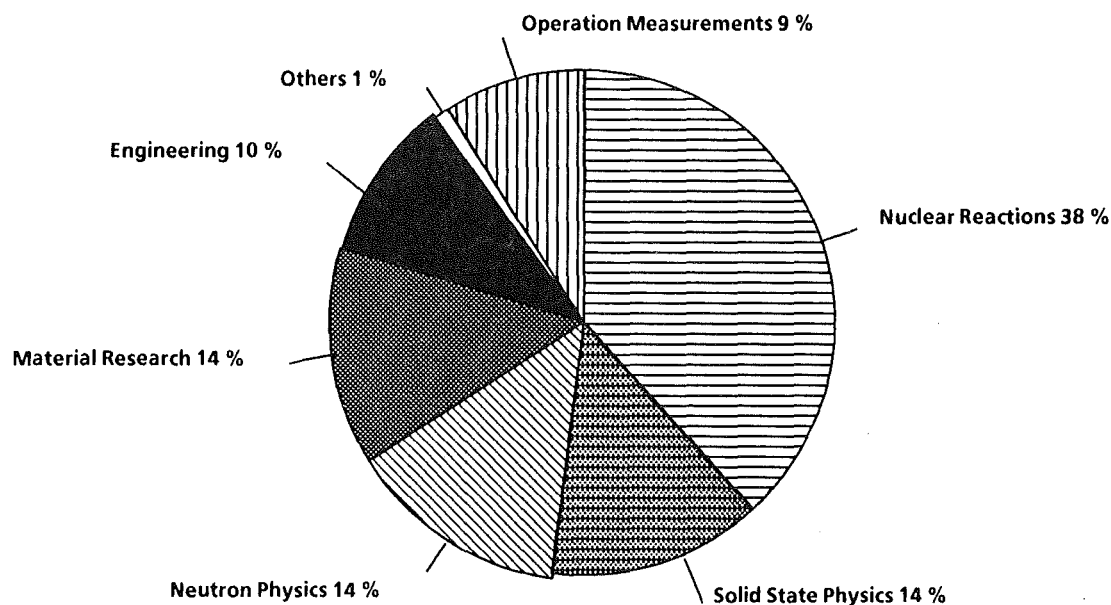
Internal Users

Institut für Kernphysik III	1189.25 h	22.32 %
Institut für Materialforsch. u. Festkörperphysik II	803.83 h	15.08 %
Institut für Kernphysik I	798.00 h	14.97 %
Institut für Neutronenphys. u. Reaktortechnik	31.58 h	0.59 %
Institut für Radiochemie	9.67 h	0.18 %
	2832.33 h	53.14 %

External Users

Universität Erlangen	596.75 h	11.20 %
Technische Universität München	594.83 h	11.16 %
Universität Tübingen	568.59 h	10.67 %
Max-Planck-Institut Heidelberg	475.75 h	8.93 %
Freie Universität Berlin	199.75 h	3.75 %
Universität Münster	38.50 h	0.72 %
Universität Mainz	14.33 h	0.27 %
Universität Frankfurt	5.25 h	0.10 %
Universität Heidelberg	3.92 h	0.07 %
	2497.58 h	46.86 %
Total	5329.91 h	100.00 %

Table 2: Use and users of KIZ from July 1988 to June 1989

The following important improvements have been performed:

- The replacement of the complete correction coil system after an operation period of 19 years (Fig. 1 and 2).

- A new diaphragm system was built in the extraction area to improve the transversal beam properties.

- Extensive maintenance and improvements were carried out on the primary cooling loops.
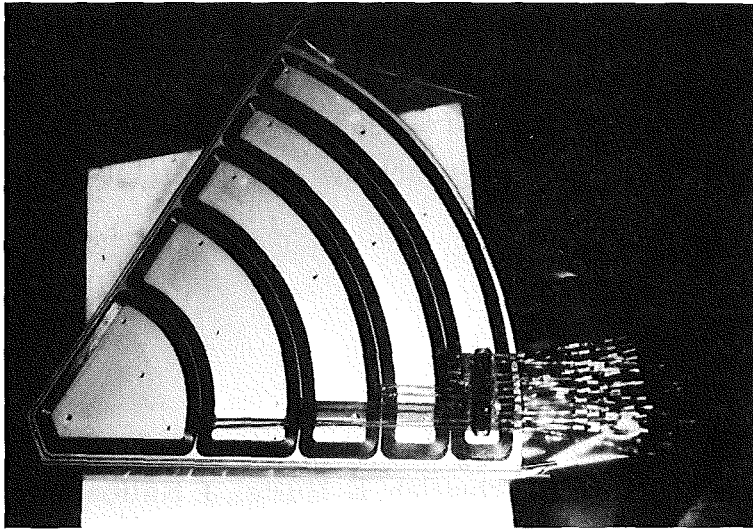

Fig. 1 One of the six new correction coil bases without the copper covers.

Fig. 2 Installation of the new correction coil base on the lower pole tip.

5.3.2 OPERATION OF THE COMPACT CYCLOTRON (KAZ)

J. Möllenbeck, H. Schweickert

During the period of report the cyclotron was operated successfully for isotope production and irradiation of machine parts, as well as for basic research. The 3930 h of beamtime were distributed equally among these activities. Nevertheless, the machine is only booked for about 50 % of the maximum available time. The reliability of the machine was again excellent and no major breakdowns occurred during operation.

A number of activation of machine parts must be carried out with deuterons with an energy between 10 and 15 MeV. This is not possible with the CP42H⁻ cyclotron at present, as it is designed for protons only.

Preliminary trials at the end of 1988 have shown that the oscillator and the Dee-system can be modified in order to achieve the conditions necessary for deuteron acceleration.

5.3.3 THE KARLSRUHE ECR ION SOURCES

H.P. Ehret, R. Ernst, L. Friedrich, E. Huttel, J. Kaltenbaek, F. Schulz,

L. Wiss, P. Ziegler and P.A. Schmelzbach* (1)

Two external ion sources are used for nuclear physics experiments at the Karlsruhe fixed frequency cyclotron, an ECRIS for Li^{+++} ions and a polarized atomic beam source. The output of the Li^{+++} ion source has been increased considerably since it is operated with two stages and the heating of the discharge tube has been improved. In the first stage the $2\omega_{CE}$ mode is used. In order to increase the intensity and to improve the beam quality of the polarized atomic beam source the electron beam (EB) ionizer of this source will be replaced by an ECR ionizer. First tests of such a new ionizer have been performed successfully in cooperation with the PSI.

(1)   Journal de Physique 50 (1989) C1 - 867

*   Paul Scherrer Institute, Villigen, Switzerland

5.3.4 IONIZATION OF A POLARIZED HYDROGEN ATOMIC BEAM IN AN ECR DISCHARGE

L. Friedrich, E. Huttel and P.A. Schmelzbach* (1)

The production of an intense beam of polarized hydrogen ions with an ECR ionizer has been investigated. A deuteron tensor polarization of up to 85 % of the theoretical value has been observed. The intensity is significantly improved compared to an electron beam ionizer.

(1)   Nucl. Instr. and Meth. A 272 (1988) 906

*   Paul Scherrer Institute, Villigen, Switzerland

5.3.5 THE EXTERNAL ION SOURCES OF THE KARLSRUHE CYCLOTRON

H.P. Ehret, R. Ernst, L. Friedrich, E. Huttel, J. Kaltenbaek, F. Schulz,
L Wiss, P. Ziegler

At the Karlsruhe fixed-frequency cyclotron two external ion sources were used for nuclear physics experiments. LISKA (Lithium Ion Source Karlsruhe), a two stage ECR source specially designed for Li^{3+} ions, delivers a current of 60 µA Li^{3+} after 90° deflection. PASKA (Polarised Atomic Beam Source Karlsruhe) delivers 30 µA of polarized d^{+} ions after 90° deflection. Accelerated to maximum energy (26 MeV/amu) up to 5 µA of Li^{3+} and 2 µA of polarized d^{+} can be obtained.
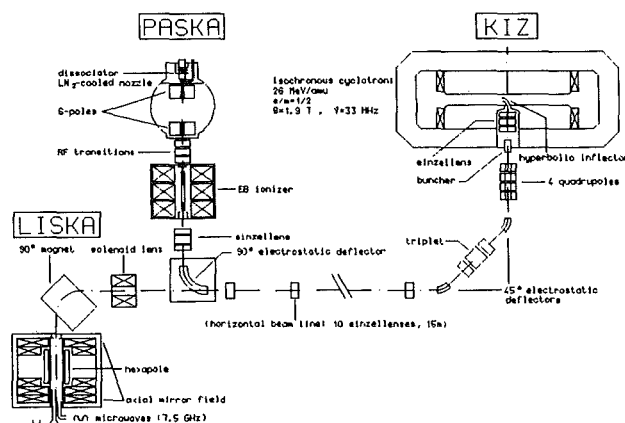

Fig. 1 The external ion source of the Karlsruhe cyclotron.

THE LITHIUM ION SOURCE LISKA

The ion source LISKA is a two stage ECR source specially designed for Li^{3+} ions. At 350° C a suitable vapour pressure to operate an ECR discharge is obtained. Otherwise at room temperature the lithium condenses immediately at the surface of the vacuum system. Thus, as a construction principle the Li plasma must not be allowed to see any cold surface. Fig. 2 shows the essential characteristics of the Li source. Lithium vapour from an oven is guided into a small cylindrical tube (diameter 28 mm, length 80 mm) where it is ionized by 7.5 GHz microwave in the $2\,\omega_{CE}$ mode (1).
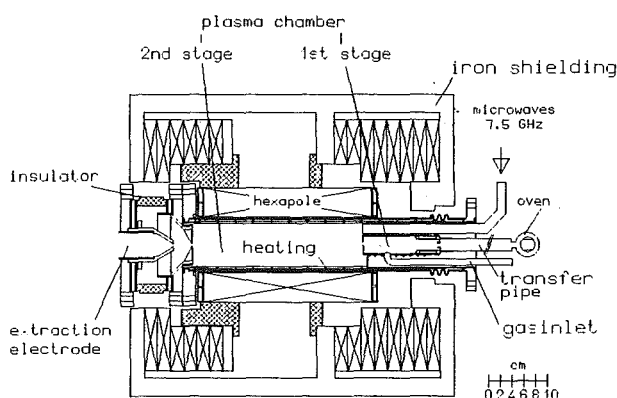
Fig. 2 Schematic view of the Lithium ion source.

Lithium ions and vapour then diffuse into the main plasma chamber (diameter 68 mm, length 300 mm), where further ionization takes place in the ω_{CE} mode. This plasma chamber is a double-wall construction with vacuum insulation. The inner wall is completely heated including the plasma electrode. In order to achieve the optimum Li vapour pressure five heating systems (Li oven, transfer pipe, first stage plasma chamber, second stage plasma chamber and plasma electrode) have to be adjusted.

The microwave power is fed into the second stage off-axis. There is no additional microwave line for the first stage, instead the 3 mm exit hole of the first stage is extended to a slit of approximately λ/2 length (24 mm, width 0.2 mm). Thus only one microwave power has to be adjusted to about 100 W.

The extraction system consists of two electrodes. The plasma electrode has a diameter of 6 mm and the gap between the electrodes is 30 mm. Without any focusing elements the Li source is connected directly to a 90° double focusing analyzing magnet. Fig. 3 shows the charge state distribution of lithium. The small admixture of ^7Li enables the calculation of the $^6Li^{3+}$ ion current if one assumes the relative charge

state distribution of both Li isotopes to be equal. So one can conclude that 60 μA of Li^{3+} are delivered by the source.
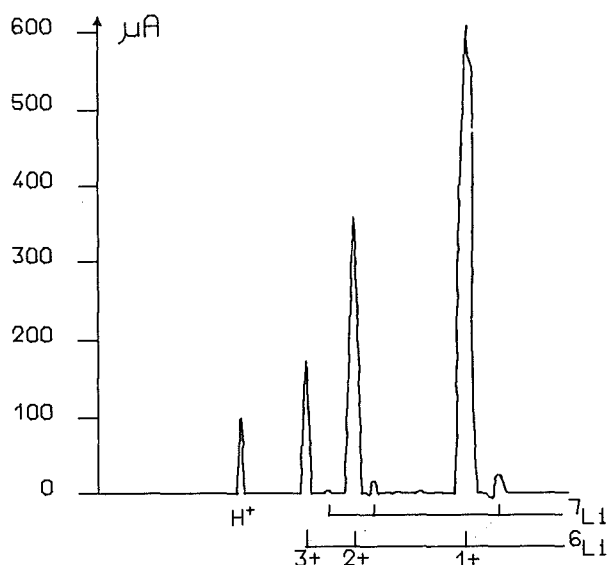
Fig. 3 Charge state distribution of the Li source.

POLARIZED D^+ SOURCE PASKA

The polarized atomic beam source PASKA was built by SENTEC (ANAC), Geneva. At the KfK the source output was increased considerably and its reliability improved. 30 μA of polarized d^+ are obtained routinely after 90° deflection. Fig. 4 gives a schematic view of this source.

ECR IONIZER FOR ATOMIC BEAM SOURCES?

For further improvement of efficiency, brightness and energy spread of an atomic beam source the replacement of the electron beam (EB) ionizer by an ECR ionizer was proposed (2). Within a cooperation between KfK and PSI an ECR ionizer was built at KfK and installed in a test stand equipped with a 25 K cold atomic beam at the PSI. After some modifications a polarized beam of 150 μA within an emmittance of 60 mm mrad √MeV was obtained (3).

Fig. 5 presents a schematic view of this ionizer. The plasma is confined axially by the field of two ironshielded solenoids and radially by the field of a permanent sextupole. The plasma chamber (length 300 mm, diameter 80 mm) is made of pyrex in order to prevent recombination of atoms by wall collisions. Microwaves (2.45 GHz, 30 W) are transmitted through the pyrex tube. The atomic beam enters the ionizer through a 20 mm pyrex tube. A three-electrode system with 40 mm apertures and 20 mm electrode separation is used as extraction system.
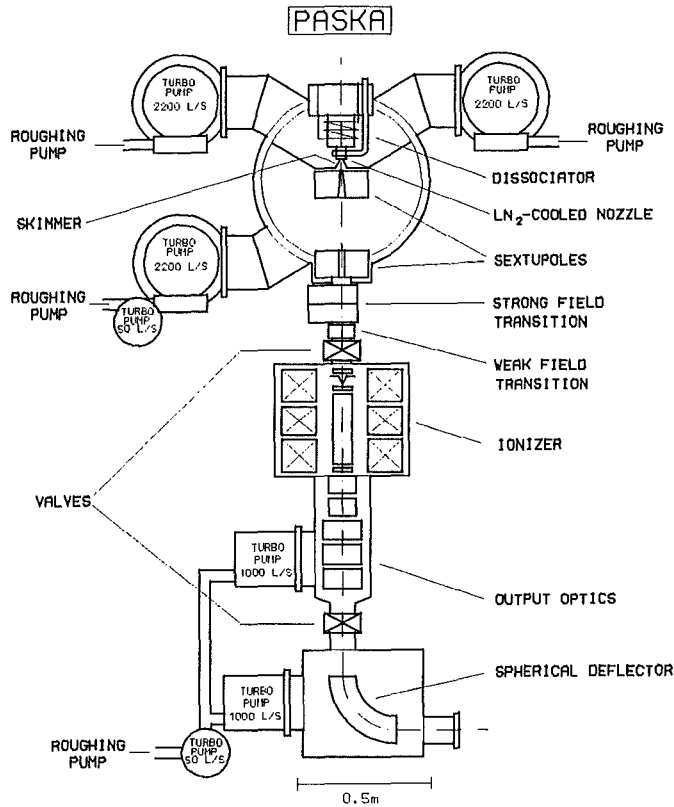
Fig. 4 Schematic view of the polarized ion source.
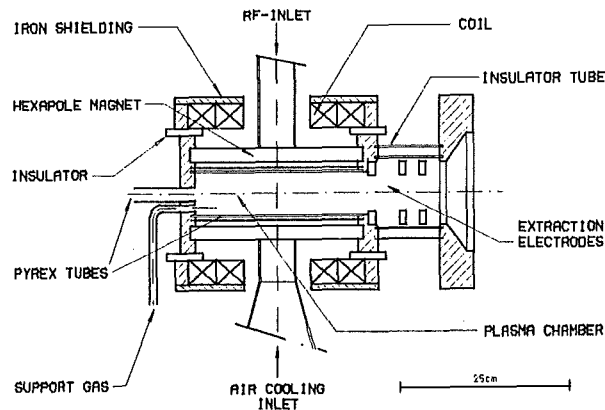
Fig. 5 Schematic view of the ECR ionizer.

A slightly modified version of this ionizer has been used to replace the EB ionizer of PASKA. After 90° deflection 60 μA of polarized d^+ were measured and 3 μA accelerated to full energy. This is about twice the value which was obtained by the EB ionizer. Using hydrogen as support gas led to a further increase of the intensity. But the polarization measured by elastic d-C scattering at 52 MeV was only 2/3 of that obtained by the EB ionizer.

Clearly these results request further studies of the ECR ionizer. To do this independently from the cyclotron and Paska a new 30 K polarized atomic beam has been built up and a T(d,α) n polarization monitor is under construction. The emittance of the ion sources was measured with the apparatus shown in Fig. 6. A part of the beam is cut out by a movable slit. The position and the width of the partial beam was measured with a beam scanner positioned 333 mm beyond the slit. A value of 90 mm mrad $\sqrt{MeV}$ was found for the lithium ion source and 100 mm mrad $\sqrt{MeV}$ for the polarized ion source.
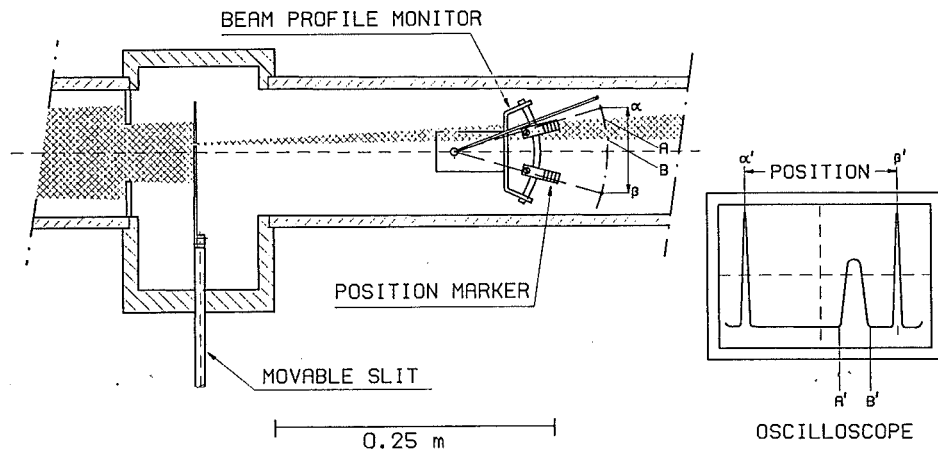
Fig. 6 Emittance measurement device.

(1)   B. Jacquot, P. Briand, F. Bourg, R. Geller, Nucl. Instr. and Meth. **A269** (1988) 1
(2)   S. Jaccard, Proc. of the Int. Workshop on Pol. Proton Sources, Ann Arbor, AIP Conf. Proc. **80** (1982) 95
(3)   L. Friedrich, E. Huttel, P.A. Schmelzbach, Nucl. Instr. and Meth. **A272** (1988) 908

5.3.6   THE BEAMLINE COMPUTER CONTROL OF THE KARLSRUHE ISOCHRONOUS CYCLOTRON

J. Bialy, H. Heinzmann, R. Kappel, J. Peters, K. Schlösser, M. Schmitt, S. Sheikh*

The necessity for a new beamline computer control for the Karlsruhe Isochronous Cyclotron (KIZ) was dictated by the fact that the existing Data General NOVA 3 computer is obsolete, is not extendable and incorporates numerous programming restrictions. Apart from that, the Dual Beam facility, which requires both KIZ and the Karlsruhe Compact Cyclotron (KAZ), also made it imperative that the beamlines of both cyclotrons have the same hardware and software standards for reasons of

compatibility. The KIZ beamline control is based on that of the KAZ control to simplify the operation of both systems by the operators.
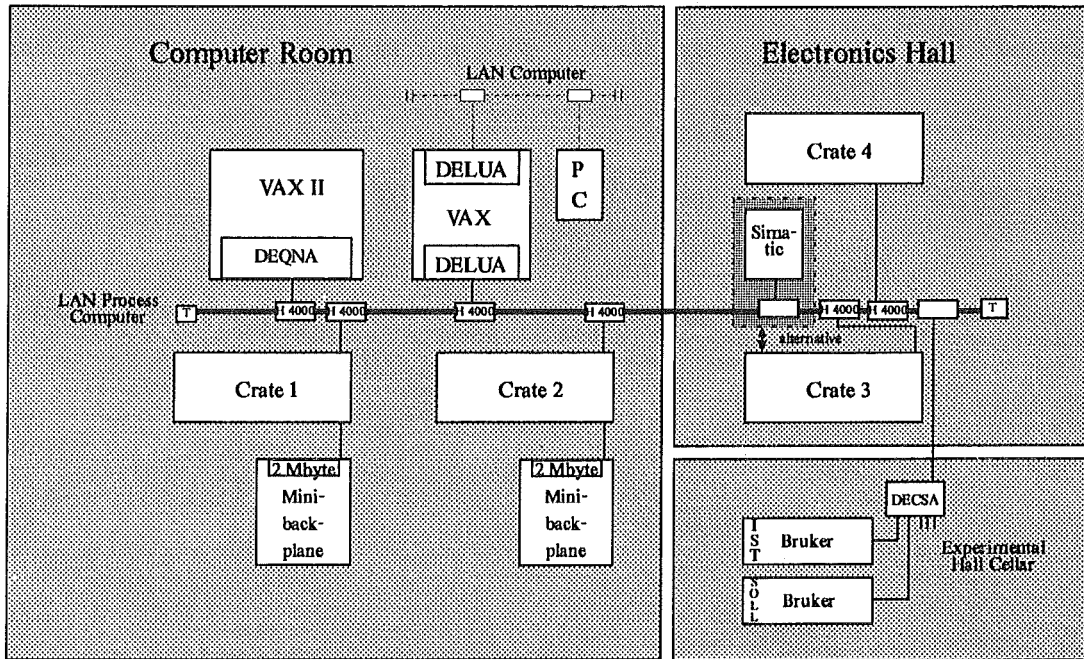
Fig. 1 The hardware of the beamline computer control.

The hardware of the control system consists of the following components:

- 4 CAMAC crates, each controlled by a CES Starburst computer
- a DEC μVAX II computer
- a Siemens PLC (Simatic)
- a Bruker microprocessor
- 3 touch panels
- 4 incremental knobs
- 3 colour TV monitors
- a video terminal

The starbursts, which are based on the DEC J11 μ-processor and operate under real-time conditions, are used for all the process control tasks. These consist of touch panel control via CAMAC, magnet power supply control via the Bruker μ-processor, control of the beamline components via the Simatic and the safety control system. The process software is written in FORTRAN 77 and runs under the RSX-11 multi-tasking operating system. The multi-tasking capability facilitates the creation of modular-structured software, which simplifies maintenance and future upgrades of the software.

One starburst also monitors the various components and displays all the processes on the TV screens. The displays consists of block diagrams of the beamline

components and the safety control, as well as the status information of the lenses and their current values. The μVAX is used for software development and management, and plays a very important role as a central data storage computer. It also offers the possibility of carrying out backups of the starburst Winchester disk. The Simatic is mainly used to operate the beamline components and to perform the interlocks for the personnel safety system.

The CAMAC vertical highway has been replaced by a so-called Control-LAN, which allows the linkup of all the existing computers, which communicate with one another by means of DECnet. Data transfer using DECnet is carried out by means of a single co-axial cable (ETHERnet), which is much more reliable than complex multi-wire cables. The Control-LAN is decoupled from the main KfK-LAN to prevent interferences, which might adversely affect the process control. The other advantages such a dedicated LAN offers are the possibility of using the VAX software development tools (VAXSET) and the vast storage capacity of the VAX for backup purposes.

*   Kraftanlagen AG, Heidelberg, Germany

5.3.7   PULSED RF ION SOURCE USING SEMICONDUCTOR DEVICES
Th.W. Gerstenhöfer

The investigation of the synthesis of heavy elements in stars requires a neutron beam with specific parameters (energy range up to 150 keV, Maxwellian averaged spectrum). Such a beam can be produced via the $^7Li(p,n)^7Be$ reaction. The pulsed proton beam obtained from the Karlsruhe 3.75 MV Van-de-Graaff (VdG) accelerator enables the use of the time-of-flight method to measure neutron capture rates versus neutron energy of the isotopes under investigations (1).

The proton pulse ratio and the pulse repetition rate are decisive beam characteristics concerning the exploration of radioactive isotopes (branching points in the nucleosynthesis path during s-process neutron capture). Higher proton yields and reduced pulse frequencies improve the signal to background ratio. In order to enable the accelerator to serve such experiments, the ion source equipment and the pulsing assembly of the accelerator installation have to be revised.

These two components are contained in the VdG high voltages terminal. A new electronic design, now using semiconductors instead of electronic valves, has been developed. Interchangeable units simplify maintenance (Fig. 1). The environmental conditions of the available volume of appr. 27 ℓ include an insulation gas atmosphere at
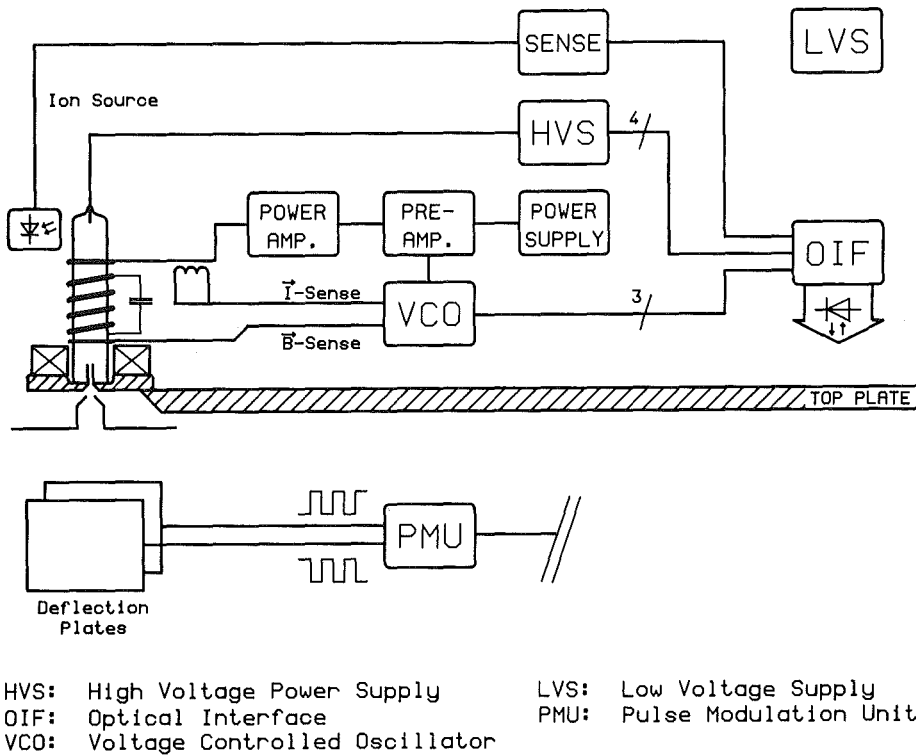
Fig. 1   Block diagram of the electronic equipment in the upper section of the high voltage terminal. The optical interface transmits control commands to the lower section, a subsequent optical link will connect the terminal to the operator console.

HVS: High Voltage Power Supply   LVS: Low Voltage Supply
OIF: Optical Interface   PMU: Pulse Modulation Unit
VCO: Voltage Controlled Oscillator
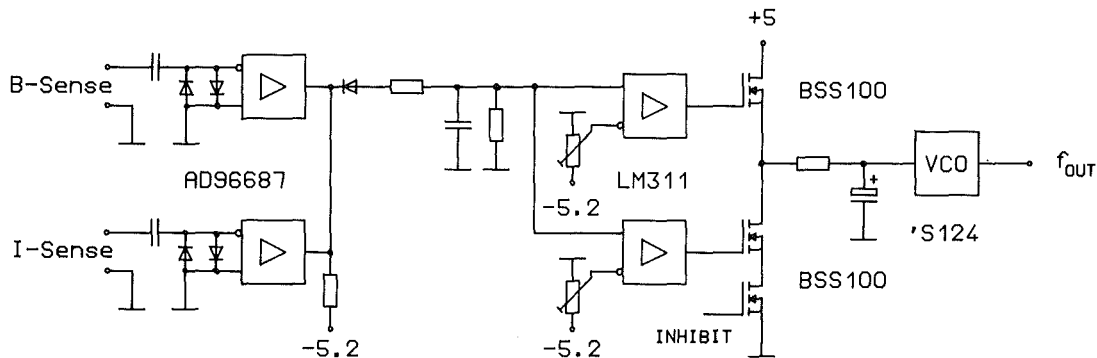
Fig. 2   Phase detection and frequency generating circuit of the VCO. Fast ECL-comparators level varying input amplitudes.

$20 \cdot 10^5$ Pa, voltage differences of 3.75 MV above ground and 20 kV inside the terminal section.

The rf ion source consists of a glass tube containing gaseous hydrogen (2,3,6). A wide band rf amplifier ($P \leq 200$ W) inductively feeds the energy necessary for ionization of the plasma. The voltage controlled oscillator (VCO, 26 . . 32 MHz) serving as a signal source for the amplifier monitors the phase shift between the sole-

noid current and the resultant alternating magnetic field to adjust frequency to the resonance value (Fig. 2). The phase shift results from the different (complex) impedance of the resonance circuit above and beyond resonance frequency, respectively.
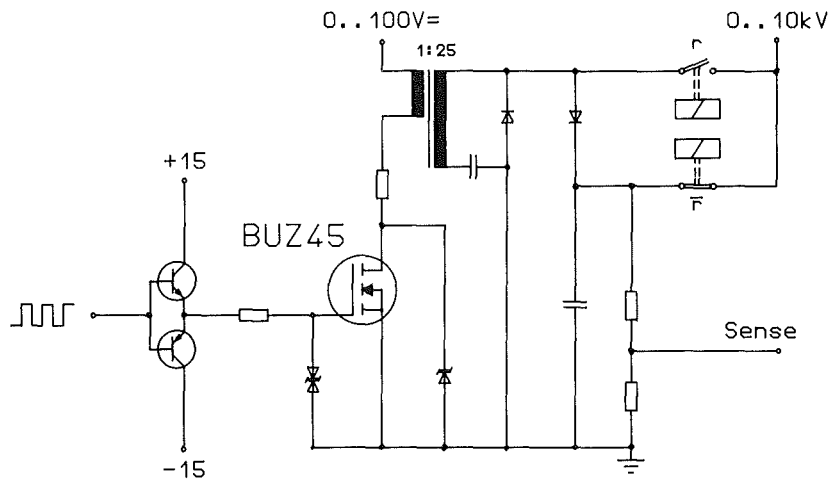
Fig. 3   High voltage generating circuit of the HVS-unit. The MOSFET switching frequency is tuned to the resonance of the secondary winding of the transformer (Tesla principle).

Proton pulses will be formed in two steps: a pulsed extraction voltage produces a proton beam with a duty cycle of appr. 40%. This reduces thermal stress of the ion source extraction channel. The pulse modulation unit (PMU) then will shape the required 10 ns pulse duration.

A high voltage supply (HVS) provides the pulsed extraction voltage. According to the Tesla principle the primary winding of the transformer is stimulated at the resonance frequency of the secondary winding. The switching MOSFET works as a ' quenched spark gap ' to prevent the reflow of the energy stored in the secondary resonance circuit. The latter one consists of the transformer winding and its intrinsic capacity (N. Tesla, 1892).

Transient voltage suppressor diodes protect the power MOSFET from overvoltage conditions (Fig. 3). Up to 10 kV, 80 W at a repetition rate of 100 kHz or in DC mode are available from the unit (5).

Electrostatic deflection plates perform the pulse shaping. Two plates are alternately connected to the deflection voltage (≤ 1 kV) and ground level by SIP-MOS transistors in a push-pull configuration (Fig. 4) (6).

First measurements of the current extracted from the ion source at various gas pressures using the new equipment showed a current increase by a factor of two (Fig. 5). Further improvements are required to optimize the ion optical system of the beam line following the ion source.
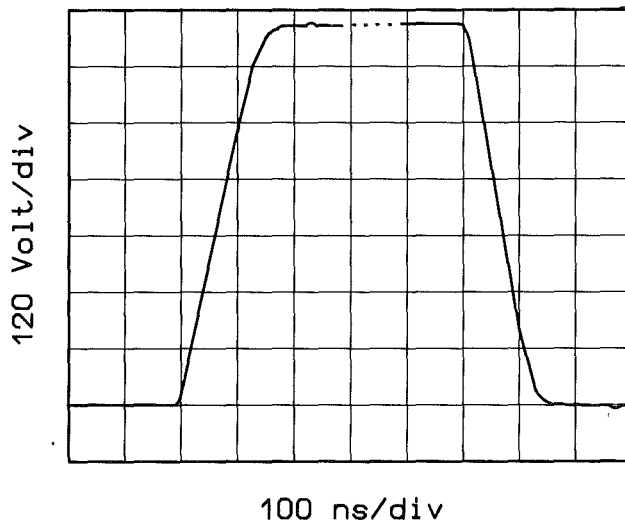
Fig. 4   Output signal of the pulse shaping unit (PMU). Transition rates reach
6 kV/µs with deflection plates connected as shown in the figure with
$R_Z = 1$ MΩ, 150 pF or up to 8 kV/µs without capacity.
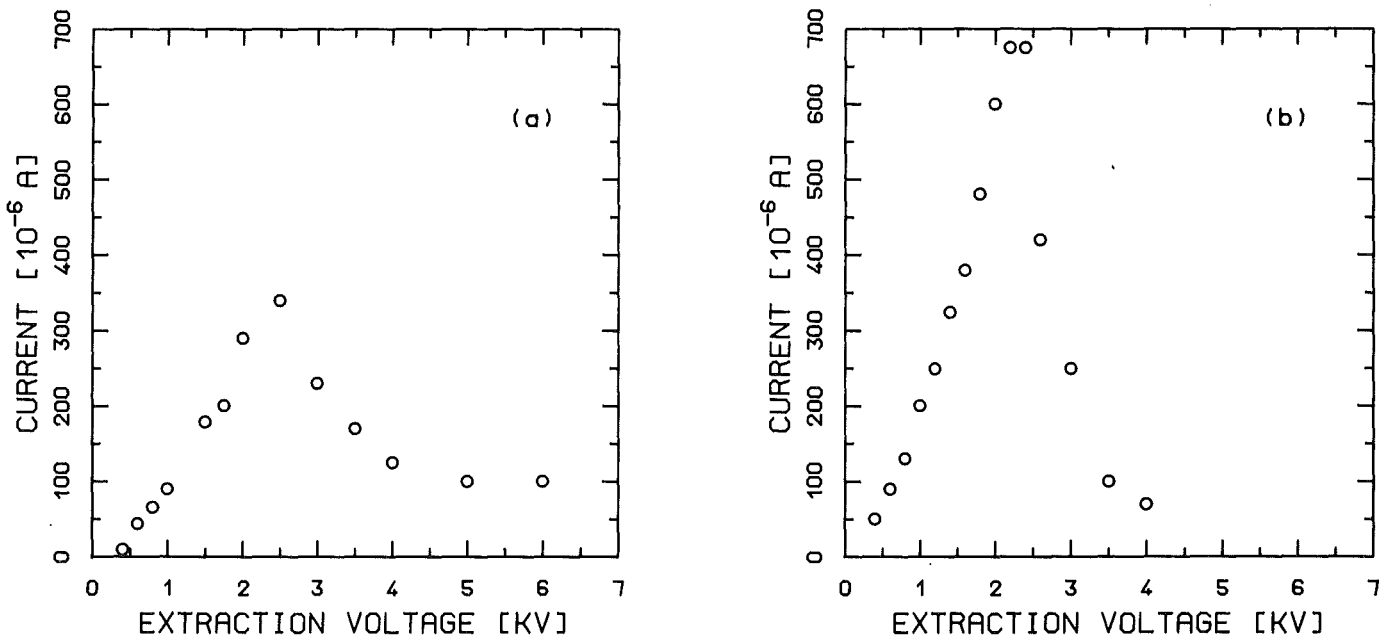
Fig. 5   Comparison of the extracted ion current (DC mode) versus extraction
voltage using the hitherto existing equipment (a) and the new
installation (b).

(1)   F. Käppeler, H. Beer, K. Wisshak, Rep. on Progr. in Phys. **52** (1988) 945

(2)   L. Valyi, 'Atom and Ion Sources', John Wiley & Sons, London (1977)

(3)   K. Körper, Z. f. Naturforschung **15a** (1960) 235

(4)   A. Schlüter, Z. f. Naturforschung **5a** (1950) 72

(5)   G. Chryssis, 'High frequency switching power supplies', Mc Graw-Hill, USA (1984)

(6)   W. Skavadore, in 'General Semiconductor Industries Product Data Book' (1977) p. 568

5.4   APPLICATIONS

5.4.1   NUCLEAR MEDICINE WITH SIMPLE DEVICES

J. Bialy, J.W. Peters, M. Schmitt

The development of the portable gamma-measuring device "ENGYPAN", described in the previous annual report, has been continued. The system hardware design and measuring software was developed further. The CsJ-scintillation counters were adapted to the system. But due to small differencies in the crystals, the photodiodes, and the hybrid preamplifiers, each set of detectors has to be tested and selected individually. Further development is necessary to overcome these problems for routine production.

In addition to these technical improvements, tests in different nuclear medical clinics have begun. Two major goals will be achieved by these studies.

The results obtained by the ENGYPAN system for commonly used diagnostic routines have first to be compared with the methods used currently in order to define simple application procedures with the Engypan system. The first such application currently being tested is the study of renal gland clearance. Research is also being carried out on diagnostic methods, which are not possible with common equipment. An example is given in fig. 1. showing the relative blood volume in different organs depending on physical stress. It can be clearly seen that the blood volume in both lungs increases under stress, resulting in a better oxygen supply, whereas the volume in the other organs is reduced.
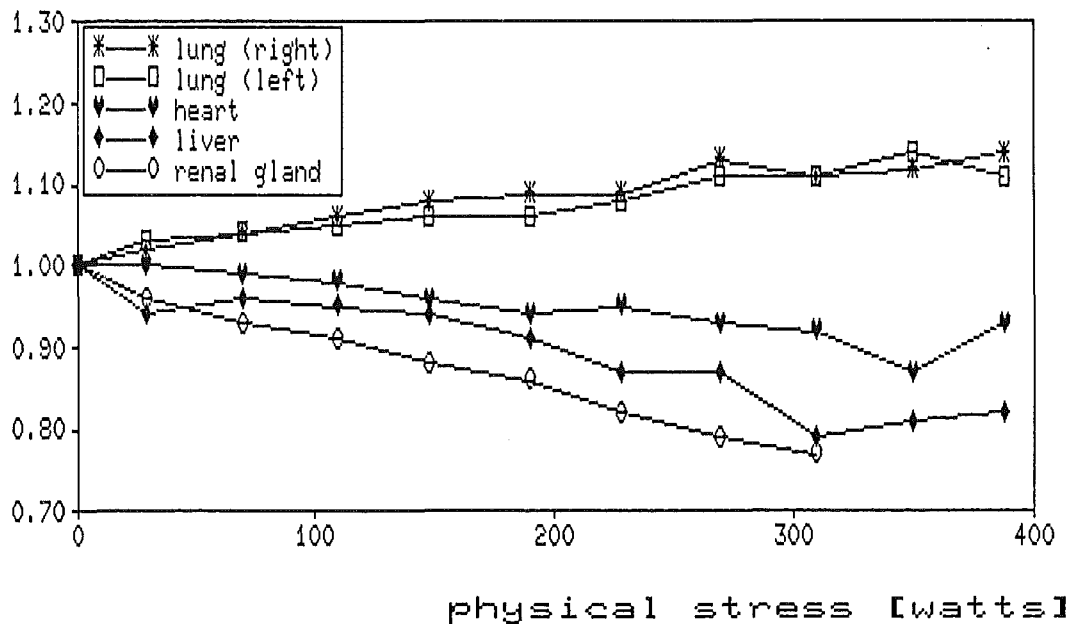
Fig. 1   Blood pool changes in different organs depending on physical stress.

5.4.2 PRODUCTION OF ISOTOPES FOR MEDICAL APPLICATIONS

K.H. Assmus, V. Bechtold, H.D. Dennerlein, H. Dohrmann,
S. Dosenbach, D. Erbe, E. Foßhag, A. Hanser, E. Heitz, R. Hüfner,
N. Kernert, J. Kraft, W. Maier, A. Martin, H. Ripp, U. Sahm,
S. Uhlemann

Several radioactive isotopes for medical diagnosis are routinely produced at the Karlsruhe compact cyclotron (CP42H$^-$)

In 1988 nearly all documents for the registration of these cyclotron products as radiopharmaceuticals were prepared and submitted in time to the "Bundesgesundheitsamt".

Ultra pure J-123

The amount of J-123 produced with the gas target system KIPROS was nearly constant since last year. During the routine maintenance at the end of 1988 the target body was replaced providently to maintain good reliability. The chemistry unit (Fig. 1) for the production of iodide as a radiochemical was modified to deliver on
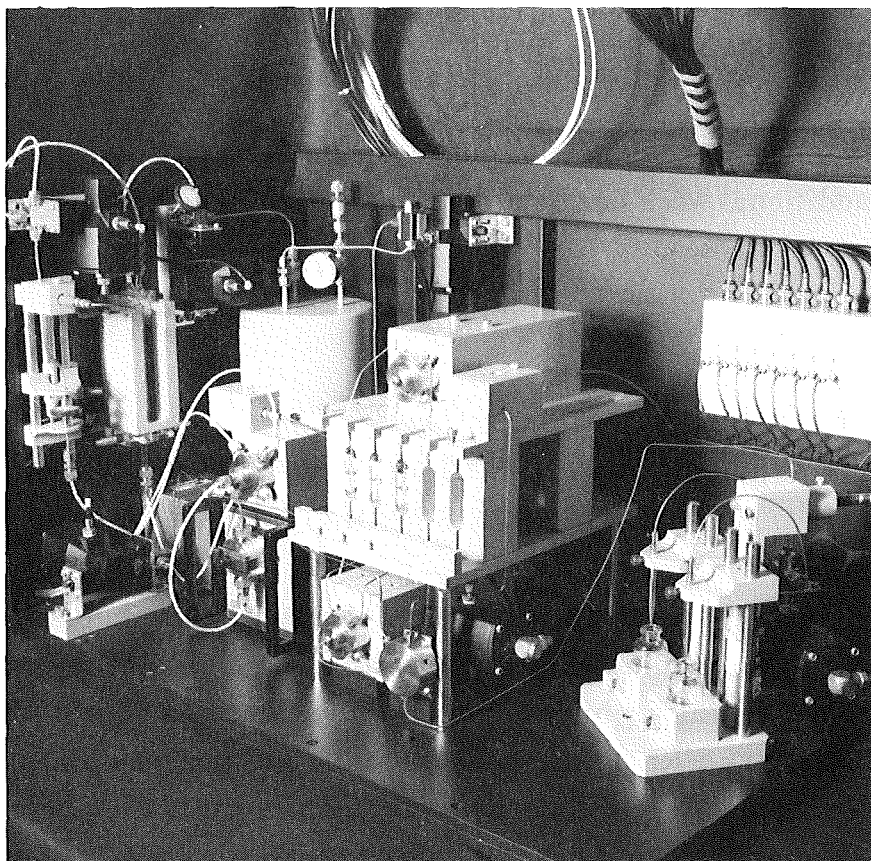
Fig. 1 Shows the chemistry unit which is located in a hot cell. The iodine dissolved in the washout of the target is purified and concentrated with highly specialized ion exchangers .

request also iodine as a radiopharmaceutical. First tests for the preparation of this iodine solution for injection were carried out in summer 89.

The KIPROS system for a pharmaceutical company in St. Louis, USA, was installed in time and is operating routinely since September 1988.

Rb-81/Kr-81m generator

No substantial changes have occured in the production. The number of generators is unchanged compared to last year. Systems for the determination of the activity of the loaded generators were optimized to meet licensing requirements.

A new gas target system for the irradiation of enriched Kr-gas was built up. First tests are scheduled for autumn 89.

Ultra pure Rb-81

Ultra pure Rb-81 is produced twice a week. The Rb-catcher in the mass-separation system was replaced by a modified one to get easy preparation of a rubidium containing sodium-chloride solution. The equipment for the distribution was installed. Since March 89 only Rb-chloride solution for injection is delivered.

Quality control

Since March 89 all analyses are carried out in the KAZ facility. Beside the routine analyses, some additional work has to be done to support licensing procedures and to validate production processes.

5.4.3 ROUTINE PRODUCTION OF HIGH PURITY ^{81}Rb BY MEANS OF ELECTROMAGNETIC ISOTOPE SEPARATION

A. Hanser (1)

The ^{81}Rb activity is generated by irradiation of natural krypton with 34 MeV protons. The strongly contaminated ^{81}Rb is purified by means of electromagnetic isotope separation resulting in highly pure ^{81}Rb with $\leq 7 \times 10^{-5}$ ^{82m}Rb, $\leq 4 \times 10^{-7}$ ^{83}Rb and $\leq 2 \times 10^{-7}$ ^{84}Rb. Further contaminating radioisotopes are not found. The important details of the specially-developed isotope separator are described. The isotope separation process efficiency is ≥ 85 % (corrected with respect to radioactive decay). The batch size of ≤ 4 GBq at present can be increased by a multiple factor. The facility has proved to be very reliable.

(1)   Appl. Radiat. Isot. 40 (1989) 309

5.4.4 RADIONUCLIDE TECHNIQUE FOR MECHANICAL ENGINEERING (RTM)

R. Blank, E. Bollmann, P. Fehsenfeld, B. Gegenheimer, P. Herrmann,
A. Kleinrahm, H. Roth, B. Schüssler

The interest in the high-precision technique RTM for wear and corrosion diagnosis in mechanical and process engineering, as has been developed systematically during the recent years, is increasing world-wide. A licence and cooperation agreement with an important Japanese industrial company for the utilization of the RTM know-how in Japan has been worked out.

An attractive demonstration of RTM technology, methods and instruments was exhibited at the KfK stand, within the AGF-pavilion, during the international Hannover Industry Fair, April 1989 (Fig. 1, Fig.2).
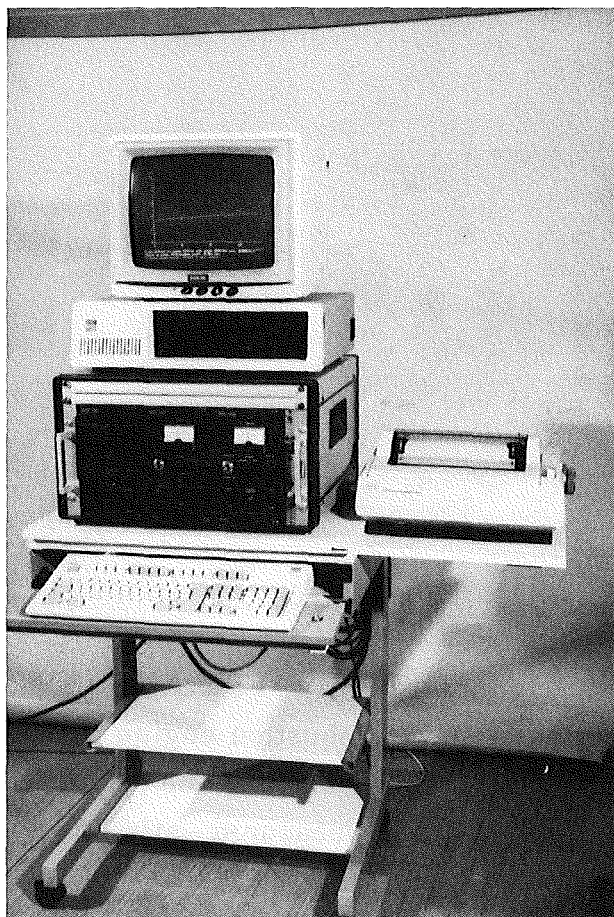
Fig. 1   RTM exhibit at the Hannover Industry Fair (April 1989).
The computer controlled wear monitoring instrument demonstrated the in-situ wear measurement of the valve seats (simulation) of the running engine (Fig. 2). The proceeding wear is continuously displayed on the screen (on the top of the figure).

The activation service supplying thin layer activated machine components for wear analysis in industry and research laboratories operated without major problems during the period of report. The modern, fully automated irradiation facility for machine parts functioned with the expected reliability.

Development work of RTM has been concentrated in two fields: Improvement of efficiency and reliability of the ceramics thin layer activation, and the construction and test of highly advanced components for the wear measurement equipment. Promising results have been achieved in both fields of development, for which the work has to be continued.
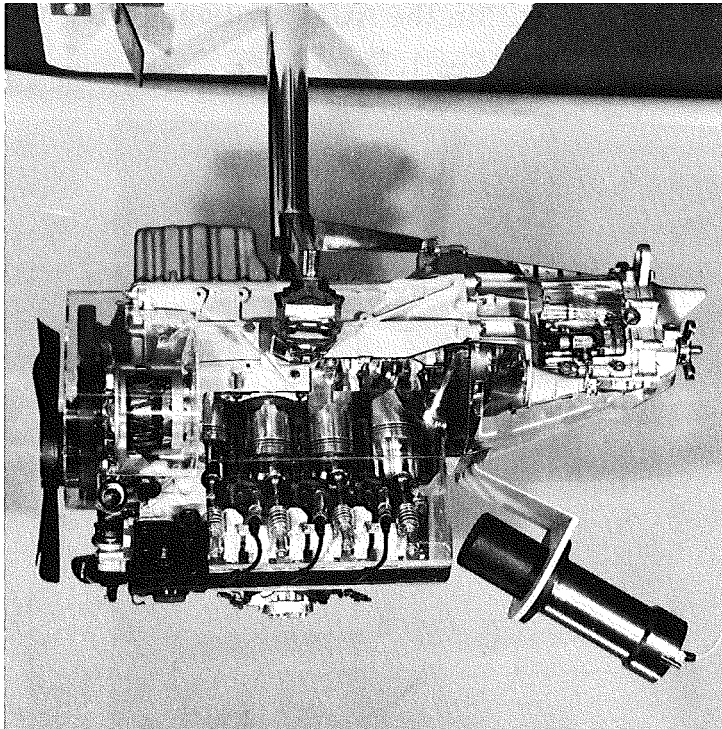
Fig. 2   RTM exhibit at the Hannover Industry Fair (April 1989).
The longitudinally sectioned combustion engine with plexi- glass housing, operated by a small electrical motor, and the cylindrical radiation detector near the valve seats to be measured, attractively demonstrated the measurement technique.
The sectioned engine was loaned from the Daimler-Benz AG, Stuttgart, Germany.

5.4.5 PERFORMANCE DATA OF AN XRF ANALYZER FOR THE ON-LINE MONITORING OF URANIUM

H. Ottmar, I. Michel-Piper

In the preceding annual report we have described the principal layout of an XRF analyzer for the on-line monitoring of uranium in process solutions within a reprocessing plant for nuclear fuels (1). Based upon the previously outlined design features we have built an optimized laboratory prototype as shown in Fig. 1.
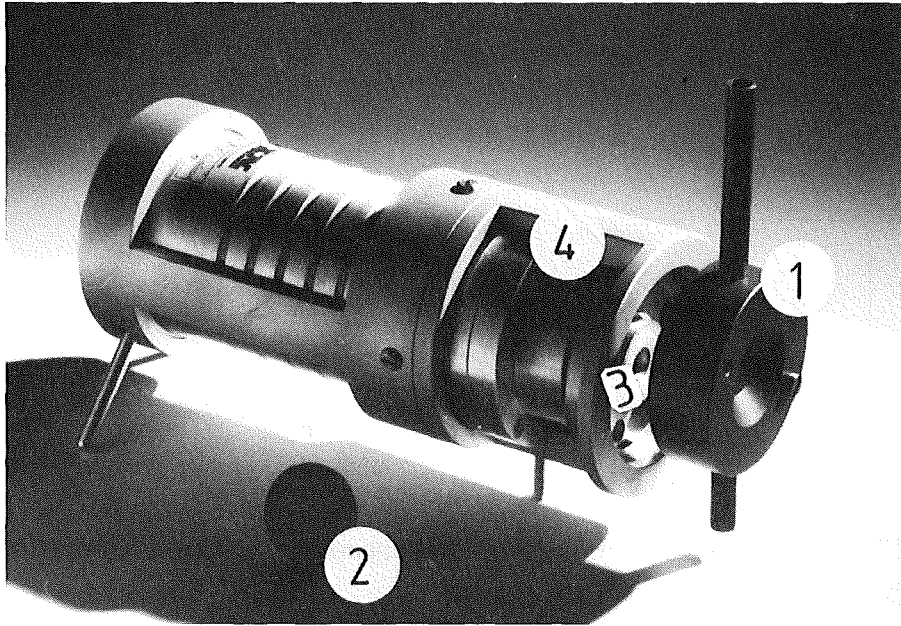
Fig. 1 Explosion view of the XRF analyzer showing titanium flowing-through cell (1), separate boron carbide window (2), ^{241}Am excitation source (3), and shielded Si-detector assembly (4).

In order to evaluate the performance data for the lower limit of detection and for measurement precision, we have carried out test measurements on static solutions filled into the sample cavity of the flowing-through cell. Both pure uranium solutions and real process solutions containing fission products at typical activity levels (10^8 - 10^9 Bq/ℓ) were used in this manner for the measurements.

Fig. 2 shows the calibration curve and the measurement precision obtained for pure uranium solutions. The calibration curve appeared linear up to a uranium concentration of about 1 g U/ℓ. At higher concentrations small corrections for self-attenuation in the 0.8 cm thick solution layer within the flowing-through cell are necessary in order to restore the linearity of the instrument response.
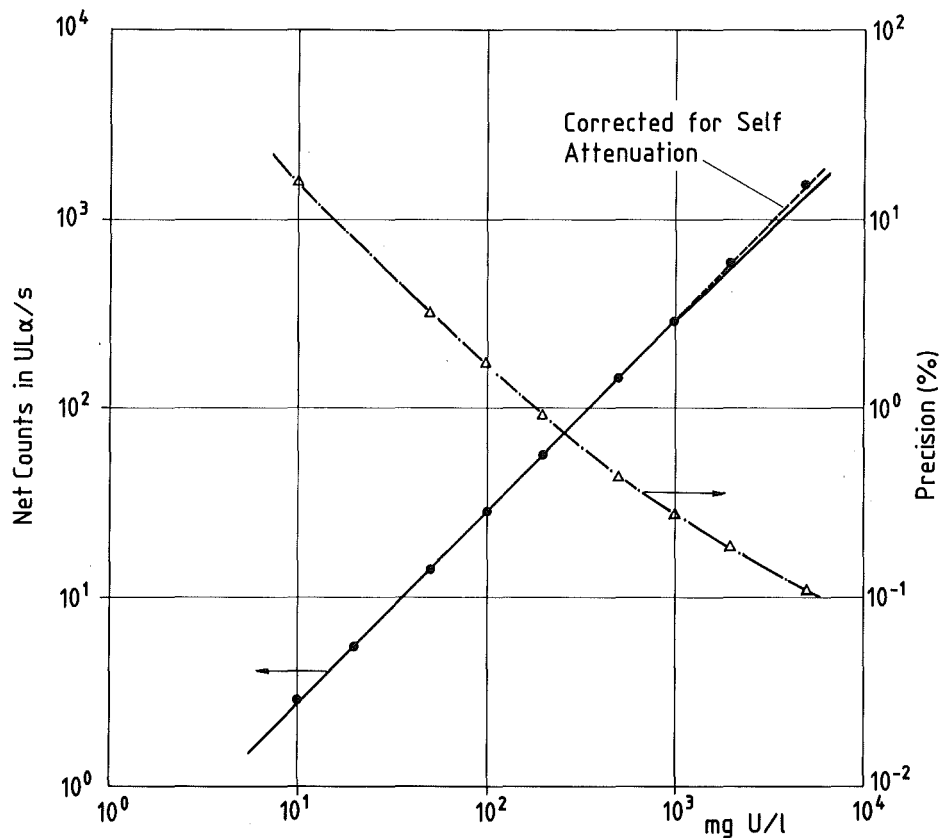
Fig. 2   Calibration curve and measurement precision for the XRF monitor.

The lower limit of detection for uranium (3 σ, 10 min. counting time) was determined to 3 mg U/ℓ in the absence of radioactive fission products, when using the fluorescence UL_β X-ray for analysis. For solutions containing fission products this value is only slightly deteriorated due to the optimized measurement conditions for the excitation and detection of fluorescence X-rays. With fission products (mainly [106]Ru, [134]Cs and ^{137}Cs) present at activity levels of 10^9 Bq/ℓ in the analyzed solutions a detection limit as low as 3.5 mg U/ℓ could be achieved.

(1)   I. Michel-Piper, H. Ottmar, Report KfK 4508, Kernforschungszentrum Karlsruhe (1989) p. 147

5.4.6   INSTRUMENTAL DESIGN OF AN X-RAY SPECTROMETER FOR SAFEGUARDS VERIFICATION MEASUREMENTS

H. Eberle, H. Ottmar

The mechanical setup as well as the major part of the software packages for the X-ray spectrometer, which we have developed for the International Atomic Energy Agency

(IAEA) as a part of the support of the Federal Republic of Germany to IAEA (1), has been completed by mid of 1989. By that time the instrument was shipped to the IAEA for installation in its Safeguards Analytical Laboratory (SAL) in Seibersdorf, Austria. There it will be used for the measurement of uranium and plutonium in safeguards verification samples taken at nuclear facilities throughout the world. So far the instrument has been primarily designed for the measurement of solutions.
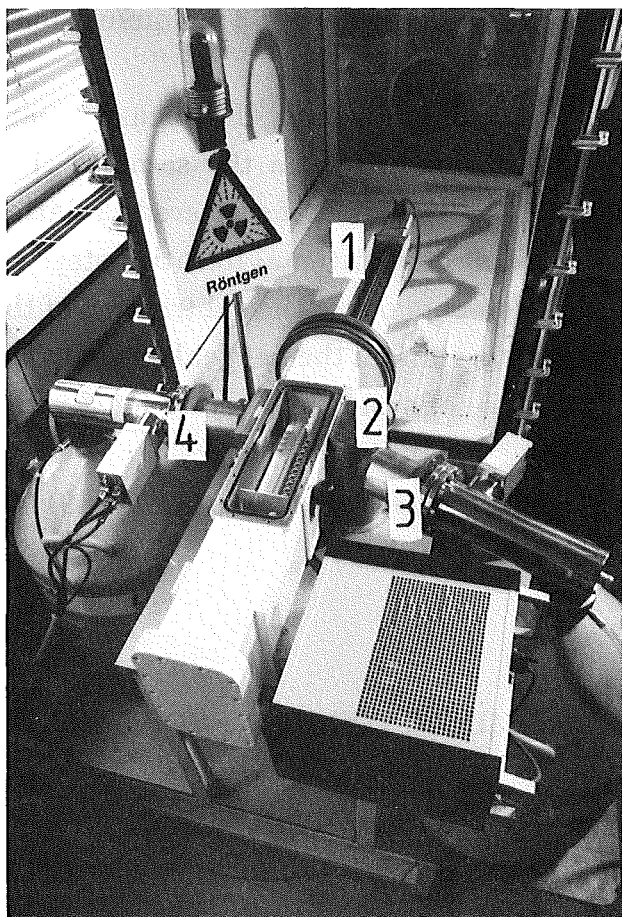
Fig. 1

Top view of the spectrometer. (1) Linear sample drive, (2) shielded X-ray tube, (3) HpGe detector for XRF, (4) HpGe detector for K-edge densitometry.

The photograph in Fig. 1 shows a top view of the spectrometer, which is coupled to a glovebox for safe sample handling. Inside the glovebox the samples are manually loaded onto the carrier of a linear drive with attached stepping motor.

The sample carrier can accommodate up to 28 samples. After loading, automated measurements are initiated from a VAX 2000 - based system for data acquisition, analysis and measurement control.

The instrument employs two planar HpGe detectors for simultaneous or separate K-absorption edge and K-XRF spectrometry.The straight-through X-ray beam for K-edge densitometry passes through spectroscopic cells with a path length of 4 cm. In the range of concentrations optimum for K-absorption edge spectrometry

($\geq$ 100 mg/ml) the attained precision is about 0.15% for a counting time of 1000 s. At 20 mg/ml the precision decreases to about 0.5%.

Lower concentrations are measured by K-XRF. The majority of the analyses will have to be done on plutonium samples containing about 3 mg of plutonium. The sample quantities are dissolved in aliquots of about 0.3 ml of nitric acid and measured in polyethylene vials with an inner diameter of 5 mm. In order to improve the accuracy of the X-ray fluorescence method an internal lead standard is added to the samples. The expected overall accuracy for the measurement of 3 mg quantities is 0.5%.

The major problem that had to be overcome with the K-XRF measurement was to assess correctly the background due to scattering from the samples. The procedure finally adopted consists of measuring the spectrum of scattered radiation from a blanc sample, and to modify this spectrum in computational iterative steps for the attenuation by the actually present heavy elements. After the subtraction of the appropriate background spectrum generated in this manner the net peak areas of the fluoresced K-X ray peaks could be determined free of systematic errors for a wider range of concentrations.

(1)   H. Ottmar, Report KfK 4508, Kernforschungszentrum Karlsruhe (1989) 145

5.4.7   U/Pu RATIO MEASUREMENTS ON MIXED OXIDE POWDER AND PELLET SAMPLES

H. Eberle, H. Ottmar

In a collaboration with the Siemens Brennelementwerk, Hanau, we have carried out a series of energy-dispersive X-ray fluorescence measurements on mixed U-Pu powders and pellets. The studies have been prompted by plans of the plant operator to replace current wet chemistry methods by a nondestructive assay technique for a rapid and accurate determination of the U/Pu ratio in those materials. Energy-dispersive X-ray fluorescence analysis, based on the measurement of the K X-rays, had been selected as the most promising alternative for this application.

The major purpose of the present studies was to examine to what extent sample properties like density, inhomogeneity and grain size distribution affect the accuracy and reliability of the X-ray measurements on the particular materials. It has been expected that some influences from these sample properties might exist in view of the fact that even the energetic K X-rays exhibit only a limited range in the dense materials. For example, the mean free path length of uranium and plutonium

K X-rays only amounts to about 1.5 mm in powders ($\rho \sim 3$ g $\cdot$ cm^{-3}), and about 0.5 mm in pellets ($\rho \sim 10$ g $\cdot$ cm^{-3}).

Different mixed U-Pu oxide samples were prepared for the measurements, starting from a common batch material of mechanically blended UO_2 and PuO_2 powders with a U/Pu ratio of about 30. To study possible segregation effects, the base material was filled into vials made of different materials (polyethylene, polyamide). Further, the base material was treated in different manners for a variation of the microscopic powder characteristics. The sample treatment prior to the measurement included grinding in a ball mill, pressing to pellets, and the transformation of pellets back into powders by thermal oxidation, resulting in powders of mixed U-Pu crystals with fairly small average particle sizes of less than 10 μm.

The XRF measurements on the different samples, all having nominally the same U/Pu ratio, were carried out with the XRF branch of the hybrid X-ray spectrometer described in contr. 5.4.6. In order to increase the measured sample volume, the set-up was modified to allow rotation of the samples in the X-ray beam. For the given experimental conditions the contribution of X-rays from self-radiation could be kept below 0.2% compared to the externally excited X-ray intensity.

The analysis of the experimental results showed that the measured U/Pu ratios varied by up to 3% for the differently treated mixed oxide samples. It was concluded that for direct XRF measurements, aiming at an accuracy of better than 1%, the different types of oxide materials typically occurring in the fuel fabrication process require some kind of pre-treatment in order to produce sufficiently homogeneous samples. One possibility currently investigated is to fuse the oxide powder into glass discs as is practiced in other applications of the XRF method.

5.4.8   DIMENSIONAL CHECK OF SAMPLE VIALS BY K-EDGE DENSITOMETRY

H. Eberle, H. Ottmar

Initial studies for the installation of a hybrid K-edge / K - XRF spectrometer in the reprocessing plant at La Hague, France, considered the option to measure the solutions directly in the sample vials used in the pneumatic rabbit system of the facility. The respective sample containers consist of a cylindrical polyethylene vial with a diameter of about 2 cm, surrounded by an outer plastic container (Fig. 1).

The direct use of these rabbit samples would have simplified the measurement procedure by avoiding the transfer of the sample into special spectroscopy cells prior to the measurement.
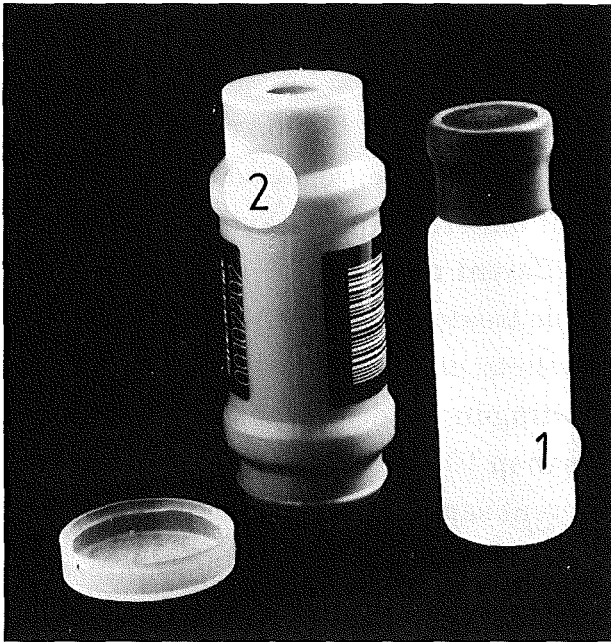
Fig. 1

Photograph of rabbit sample container. (1) Inner polyethylene bottle, (2) outer plastic container with bar code label.

When proceeding in this way, two conditions must be fulfilled in order to maintain the accuracy of the K-edge densitometry measurement:

(1)   Reproducible positioning of the sample vial relative to the highly collimated X-ray beam used for the transmission measurement;

(2)   Tight dimensional tolerances for the inner diameter of the sample vial.

It was logical first to check if the existing sample vials comply with the required tight tolerance and uniformity of their inner diameter. Since this measure could not be determined with a gauge, we used the K-edge densitometry measurement itself to determine, from vial to vial, the relative variations of the inner vial diameter. As shown in Fig. 2, a highly collimated X-ray beam was transmitted through the sample containers, which were placed into a tightly fitting sample adapter. The [241]Am source indicated in the figure was used for digitally stabilizing the analog electronics. In order to obtain a useful measurement signal for K-edge densitometry, the sample containers were filled with a solution of lead acetate. The concentration of lead (~ 190 g Pb/ℓ) was chosen such to provide optimum precision. With a counting time of 10 minutes the solution depth, and hence the inner vial diameter, could be determined with a precision of 0.14%.

Measurements on a set of 20 sample containers showed variations of up 1% of the inner vial diameter. The observed standard deviation of 0.40% for the mean value of the 20 measurements was significantly higher than the expected precision of 0.14%, which had been verified from repeated measurements on the same sample. It was concluded that this loss of measurement performance due to poorly defined sample containers could not be tolerated for the intended instrument application in
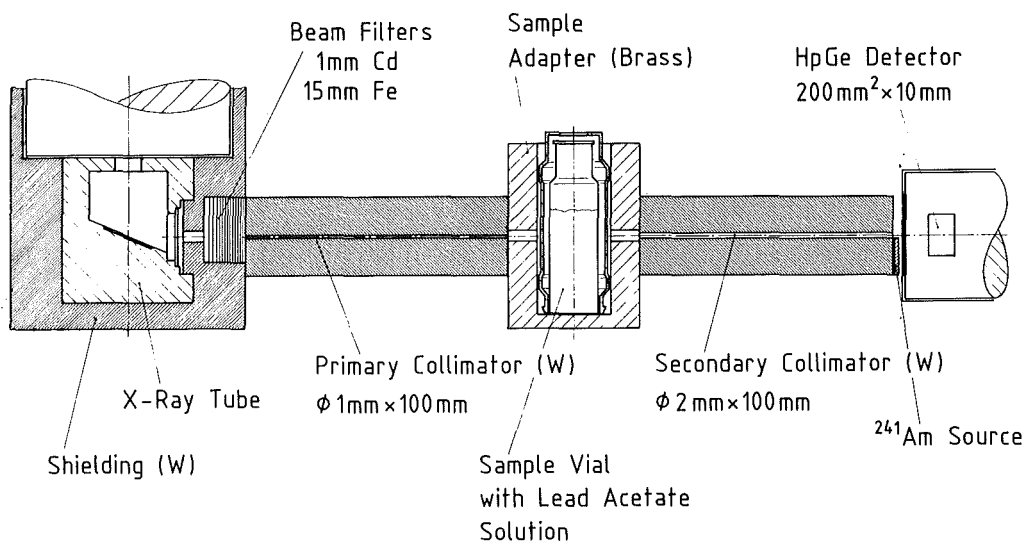
Fig. 2 Setup for the measurement of the inner vial diameter.

international safeguards. Therefore it was decided to continue with the traditional procedure of transfering the samples into well-defined spectroscopic cells for the measurement.

5.4.9 IMPROVEMENT OF THE LOWER LIMIT OF DETECTION IN ENERGY - DISPERSIVE XRF ANALYSIS BY WAVELENGTH - DISPERSIVE PREFILTERING

P. Matussek, I. Michel-Piper

In energy-dispersive X-ray fluorescence analysis (EDXRFA) the limiting factors for the detection of trace elements in the presence of large amounts of matrix material - such as small uranium or plutonium concentrations in aqueous and organic solutions - are mainly determined by the height of the background below the fluorescence peak of interest and by the total counting rate that can be handled by the detector system. For typical actinide concentrations of some mg per liter solvent the ratio of fluorescence to scattering is about 10^{-4} only; this limits the throughput of fluorescence events with present solid-state detector systems to ≈ 1 count per second maximum. Moreover, the strong scattering by the solvent unfavourably increases the Compton background below the fluorescence peak. In order to improve the detection limit at lower element concentrations one may therefore either prevent the scattered radiation from reaching the detector, or remove the main source of scattering through evaporation of the solvent. Both approaches have been investigated.

Our studies have been restricted to the excitation of L X-rays of the actinides because of the superior sensitivity as compared to the excitation of K X-rays. We used a 3 kW X-ray tube with Rhodium anode and with a 200 µm thick Rhodium beam filter as a strong source of excitation radiation. A new scattering chamber and new sample supports have been built that increase the available X-ray flux at the sample position and further reduce the scattering from structural materials. Fig. 1 shows a picture of the compact experimental set-up: The shielding cylinder of the X-ray tube is seen at the upper right hand side of the figure above the scattering chamber, the Si-Li detector head is located in the center of the photograph.

In order to reduce the scattered radiation we utilized in the first approach an energy-selective filter inserted into the beam path between sample and detector. This
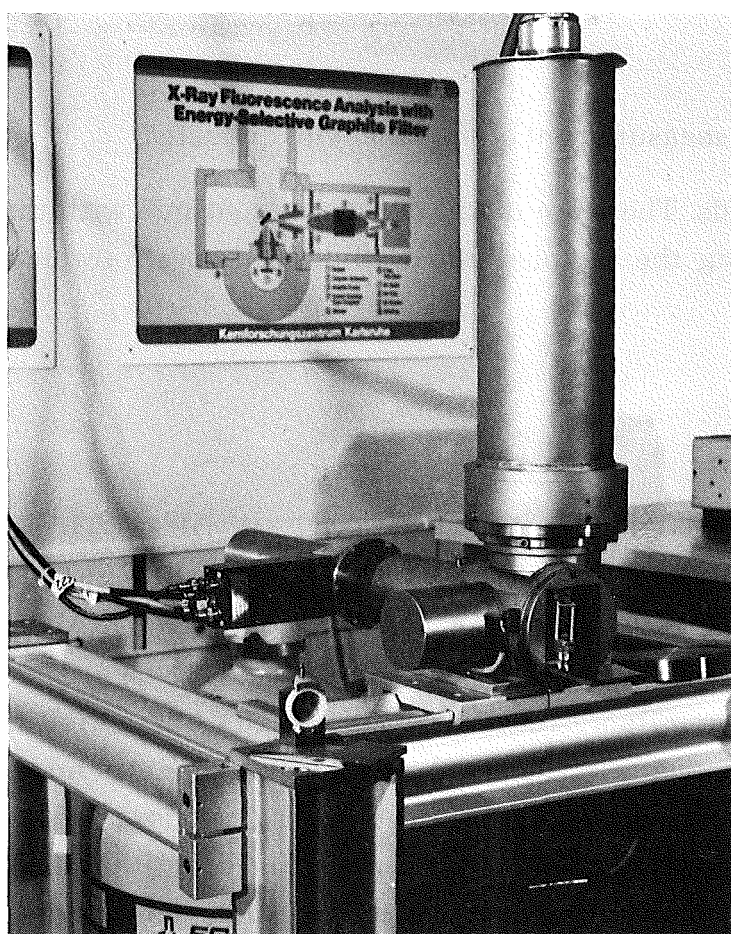
Fig. 1 View of the measurement system.

filter consists of a cylindrical arrangement of graphite monocrystals. It transmits only a relatively narrow energy band around the L_α X-rays from the actinides (13-15 keV) that satisfy the condition for Bragg reflection. The central shielding cone of the filter not only prevents the scattered radiation from reaching the detector, but also protects the detector against the self-radiation of highly radioactive samples. With this equipment actinide solutions of various concentrations have been measured. The

sample quantity used was about 1 ml, no sample preparation was required. The lower limit of detection (LLD) within 10 minutes counting time was found to be about 100 µg actinide per liter solvent. The high-resolution SiLi detector used (FWHM ≈ 210 eV at 13 keV) allowed simultaneous measurements even of neighbouring elements. Fig. 2 shows a typical example: 1 ml of process solution from the 2DW stream in a re-processing plant was measured with and without graphite filter. The sample contained about 300 mg U/l and 100 mg Np/l. The figure demonstrates the significant reduction of the scattered radiation (17 - 24 keV) by more than 99%, as well as the capability of analyzing neighbouring elements (here uranium and neptunium).
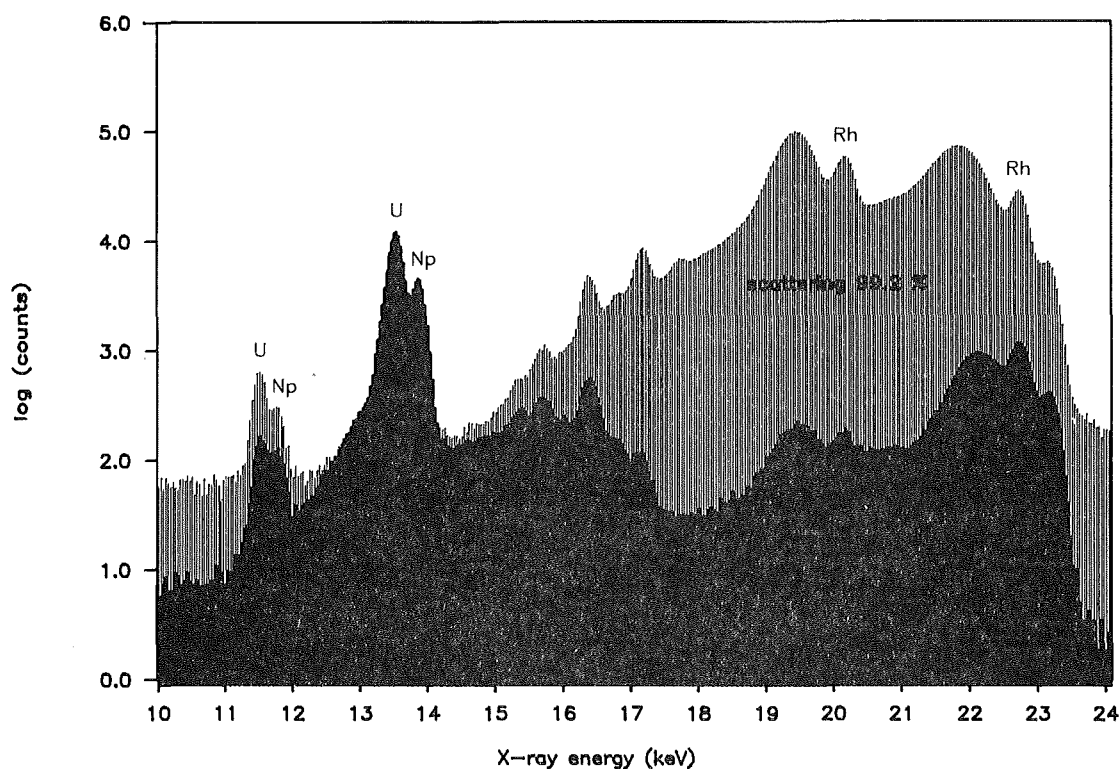
Fig. 2   Spectrum taken from 1 ml of a 2DW solution (containing 300 mg U/l and 100 mg Np/l), measured without (above) and with (below) graphite filter.

In the second approach the scattering matrix has been reduced by pipetting droplets of some 10 µl of the actinide solutions on 6 µm thick Trespaphan foils and evaporating the solvent by means of infrared radiation. Measurements performed in combination with the wavelength-dispersive prefilter yielded a LLD of 300 pg acti-nide in the dried microsample, corresponding to a LLD of 10 µg actinide per liter in the solution (for 10 minutes counting time).

It could be demonstrated that the use of a wavelength-dispersive prefilter can improve the sensitivity of EDXRFA by a factor of 10 and more as compared to

conventional EDXRFA systems. This holds in particular when the measurements of the minor constituents are performed directly on solutions or other bulk-matrix samples. Further studies are presently performed to evaluate the dependence of the assay result on the sample composition (matrix, actinide mixtures) by experiments and Monte Carlo calculations.

5.4.10 INVESTIGATION OF INORGANIC DEPOSITS IN SELECTED ORGANIC MATRICES

T. Cichocki*, D. Heck, L. Jarczyk**, E. Rokita**, A. Strzalkowski**, M. Sych*** (1)

Inorganic deposits in the wall of human and animal arteries and in experimental tumor (Morris hepatoma 7777) were examined using proton induced X-ray emission (PIXE) and PIXE in combination with proton microprobe (micro-PIXE) techniques. The sections adjacent to the irradiated ones partly were submitted to histological investigations and one part of the material was additionally investigated by infrared (IR) spectroscopy.

For identification of mineral deposits, the micro-PIXE method appeared the most sensitive. The mineral deposits were detected in the artery samples, even in those without visible morphological changes, as well as in tumor samples. The deposits showed different localization and composition, depending on age and type of vessel. There were also differences between human and animal arteries. IR spectroscopy revealed the presence of carbonate apatite within the artery samples from old individuals. Matching of histological observations with data obtained by micro-PIXE method allows a better correlation of morphological and analytical results.

6. LIST OF PUBLICATIONS

6.1 PUBLICATIONS AND REPORTS

BATTY, C.J.; FRIEDMAN, E.; GILS, H.J.; REBEL,
H.
Experimental methods for studying nuclear
density distributions.
Advances in Nuclear Physics, 19(1989) S.1-188

BECHTOLD, V.; SCHWEICKERT, H.
Moderne Produktionstechnologien zur
Herstellung von Radioisotopen fuer die
Medizin.
KfK-Nachrichten, 21(1989) S.13-16

BEER, H.; MACKLIN, R.L.
The ^{151}Sm branching, a probe for the
irradiation time scale of the s-process.
The Astrophysical Journal, 331(1988)
S.1047-57

BEER, H.; RUPP, G.; VOSS, F.; KAEPPELER, F.
Measurement of the ^{22}Ne(n,γ)cross section at
kT=25 keV.
5th Workshop on Nuclear Astrophysics,
Ringberg Castle, Bad Wiessee, January 30 -
February 4, 1989
In: Cierjacks, S. [Hrsg.]
Progress Report on Nuclear Data Research in
the Federal Republic of Germany for the
Period April 1, 1988 to March 31, 1989
NEANDC(E)-302 U Vol. 5(June 1989) S.1-2
INDC(Ger)-34/LN + Special

BEER, H.; WALTER, G.; KAEPPELER, F.
s-process studies on tin.
Astronomy and Astrophysics, 211(1989)
S.245-49

BEER, H.; MACKLIN, R.L.
Measurement of the ^{85}Rb and ^{87}Rb capture
cross sections for s-process studies.
The Astrophysical Journal, 339(1989) S.962-77

BIALY, J.; PETERS, J.W.; SCHMITT, M.
Blutflussanalysator auf der Basis des
81-Rb/81m-Kr-Generatorsystems.
KfK-Nachrichten, 21(1989) S. 17-21

BRANCUS, I.M.; OEHLSCHLAEGER, J.; WENTZ, J.
IMFREM - a computer program for analyses of
intermediate mass-fragment emission in heavy
ion reactions.
KfK-4454B (September 88)

BRANCUS, I.M.
Extended sum-rule model for intermediate
mass-fragment emission.
KfK-4453 (Oktober 88)

BREHM, K.; BECKER, H.W.; ROLFS, C.;
TRAUTVETTER, H.P.; KAEPPELER, F.; RATYNSKI,
W.
The cross section of ^{14}N(n,p)^{14}C at stellar
energies and its role as a neutron poison for
s-process nucleosynthesis.
Zeitschrift fuer Physik A, 330(1988) S.167-72

BUSSO, M.; PICCHIO, G.; GALLINO, R.;
KAEPPELER, F.; RAITERI, C.M.
Comparison of s-processing occuring in a low
mass AGB star of low metallicity and the
results of s-classical analyses.
Johnson, H.R. [Hrsg.]
Evolution of Peculiar Red Giant Stars :
Proc.of the 106th Colloquium of the
Internat.Astronomical Union, Bloomington,
Ind., July 27-29, 1988
Cambridge [u.a.] : Cambridge Univ.Press, 1989
S.237

CICHOCKI, T.; HECK, D.; JARCZYK, L.; ROKITA,
E.; STRZALKOWSKI, A.; SYCH, M.
Investigation of inorganic deposits in
selected organic matrices.
8th European Anatomical Congress, Antwerpen,
B, September 6-12, 1987
Folia Histochemica et Cytobiologica, 26(1988)
S.187-92

CICHOCKI, T.; HECK, D.; JARCZYK, L.; ROKITA,
E.; STRZALKOWSKI, A.; SYCH, M.
Microcalcification of malignant tumors.
Trace Elements in Medicine, 5(1988) S.158-60

COLE, A.J.; GROTOWSKI, K.; KOZIK, T.; REBEL,
H.
A multistep evaporation model for
intermediate mass fragment emission.
KfK-4484 (November 88)

DEMBCZYNSKI, J.; ELANTKOWSKA, M.; BEKK, K.;
REBEL, H.; WILSON, M.
Reanalysis of the Am I level spectrum and the
nuclear quadrupole moments of Am-isotopes.
Zeitschrift fuer Physik D, 13(1989) S.181-92

DIERCKX, R.; BONDAR, L.; BOSSER, R.; BREMNER,
W.B.; CRESTI, P.; FILSS, P.; LEAKE, J.W.;
OTTMAR, H.; WUERZ, H.
European interlaboratory test measurements on
waste containing alpha-emitting
contaminants.
Proc.of the 11th Annual Symp.on Safeguards
and Nuclear Material Management, Luxembourg,
May 30 - June 1, 1989
Luxembourg: Commission of the European
Communities, 1989. - S.195
ESARDA-22
EUR-12193-EN

FRIEDRICH, L.; HUTTEL, E.; SCHMELZBACH, P.A.
Ionization of a polarized hydrogen atomic
beam in an ECR discharge.
Nuclear Instruments and Methods A, 272(1988)
S.906-08

FROEHNER, F.H.; KAEPPELER, F.
Stand der Physik der Kernspaltung.
KfK-Nachrichten, 20(1988) S.211-16

GABRIEL, P.
Modellunabhaengige Analyse des dritten Jets
in der e$^+$e$^-$-Annihilation.
KfK-4490 (Dezember 88)

GALACHMATOVA, S.; ROMANOVSKY, E.; SHIROKOVA,
A.; SHITIKOVA, K.V.; GILS, H.J.; REBEL, H.
Nuclear structure effects in elastic ^{12}C +
^{12}C scattering.
KfK-4584 (Mai 89)

GEMMEKE, H.; HUSSON, L.; MASCHUW, R.;
PLISCHKE, P.; WOCHELE, J.; ZEITNITZ, B.;
DEIMLING, B.; FROMHEIN, O.; HEEP, W.;
HELLMANN, G.; KARBSTEIN, W.
Front end electronics and triggersystem for
the KARMEN neutrino experiment.
IEEE Nuclear Science Symp.1988, Orlando,
Fla., November 9-11, 1988
IEEE Transactions on Nuclear Science,
NS36(1989) S.718-22

GILS, H.J.; BUSCHMANN, J.; ZAGROMSKI, S.;
KRISCH, J.; REBEL, H.
The QQDS magnetic spectrograph 'Little John'
at the Karlsruhe cyclotron.
I. Design and construction.
Nuclear Instruments and Methods A, 276(1989)
S.151-68

GILS, H.J.; JELITTO, H.; SCHLOESSER, H.;
ZAGROMSKI, S.; BUSCHMANN, J.; EYRICH, W.;
HOFMANN, A.; KIENER, J.; LEHMANN, A.; REBEL,
H.
The QQDS magnetic spectrograph 'Little John'
at the Karlsruhe cyclotron.
II. Experimental procedures and performance.
Nuclear Instruments and Methods A, 276(1989)
S.169-82

GILS, H.J.; REBEL, H.
Evidenz fuer einen Neutronenhalo im Kern
Lithium-11.
Physikalische Blaetter, 45(1989) S.58-59

GILS, H.J.; MERKEL, A.
Monte-Carlo-Simulationen auf Transputer
verteilt.
VMEbus, (1989) Nr.1, S.35-39

GIORGINIS, G.; MANN, D.; OTTMANN, K.;
WOELFLE, S.; GEMMEKE, H.; MASCHUW, R.;
ZEITNITZ, B.
A liquid argon TPC.
Proc.of the London Conf.on Positron Sensitive
Detectors, London, GB, September 7-11, 1987
Nuclear Instruments and Methods A, 273(1988)
S.650-53

GROTOWSKI, K.; ILNICKI, J.; KOZIK, T.;
LUKASIK, J.; MICEK, S.; SOSIN, Z.; WIELOCH,
A.; HEIDE, N.; JELITTO, H.; KIENER, I.;
REBEL, H.; ZAGROMSKI, S.; COLE, A.J.
Compound nucleus emission of intermediate
mass fragments in the ^{6}Li+Ag reaction at
156 MeV.
Physics Letters B, 223(1989) S.287-90

HANSER, A.
Routine production of high purity ^{81}Rb by
means of electromagnetic isotope separation.
International Journal of Radiation
Applications and Instrumentation A, 40(1989)
S.309-14

HEIDE, N.; REBEL, H.; CORCALCIUC, V.; GILS,
H.J.; JELITTO, H.; KIENER, J.; WENTZ, J.;
ZAGROMSKI, S.; SRIVASTAVA, D.K.
Elastic break-up of 156 MeV ^{6}Li projectiles
with large asymptotic relative momenta of the
fragments.
KfK-4564 (Mai 89)
Nuclear Physics A, 504(1989) S.374-90

HEIDE, N.
Experimentelle Untersuchung des direkten
elastischen Aufbruchs von 156 MeV ^{6}Li bei
grossen asymptotischen Relativimpulsen der
Aufbruchfragmente.
KfK-4551 (Maerz 89)

JELITTO, H.; BUSCHMANN, J.; CORCALCIUC, V.;
GILS, H.J.; HEIDE, N.; KIENER, J.; REBEL, H.;
SAMANTA, C.; ZAGROMSKI, S.
Inclusive measurements of the break-up of 156
MeV ^{6}Li-ions at extreme forward angles and
the quasi free break-up model.
KfK-4480 (November 88)

JELITTO, H.; BUSCHMANN, J.; CORCALCIUC, V.;
GILS, H.J.; HEIDE, N.; KIENER, J.; REBEL, H.;
SAMANTA, C.; ZAGROMSKI, S.
Inclusive measurements of the break-up of 156
MeV ^{6}Li-ions at extreme forward angles.
Zeitschrift fuer Physik A, 332(1989) S.317-30

KAELBER, W.
Kernladungsradien und Kernmomente von
Thorium-Isotopen aus laserspektroskopischen
Untersuchungen an gespeicherten Thorium-Ionen
in einer Hochfrequenz-Ionenquelle.
KfK-4513 (Februar 89)
Dissertation, Universitaet Heidelberg 1989

KAEPPELER, F.; WISSHAK, K.
Neuer Gamma-Detektor untersucht die stellare
Elementsynthese.
Spektrum der Wissenschaft, (1988) Nr.9,
S.25-34

KAEPPELER, F.; BEER, H.; WISSHAK, K.
s-process nucleosynthesis - nuclear physics
and the classical model.
Reports on Progress in Physics, 52(1989)
S.945-1013

KARMEN-COLLABORATION; MASCHUW, R.
KARMEN: neutrino physics at ISIS.
Klapdor, H.V. [Hrsg.]
Neutrino Physics : Proc.of an
Internat.Workshop, Heidelberg, October 20-22,
1987
Berlin [u.a.] : Springer, 1988 S.147-52
Conf.on Nuclear and Particle Physics, London,
GB, April 5-7, 1989

KIENER, J.; GILS, H.J.; REBEL, H.; BAUR, G.
Observation of nonresonant Coulomb break-up
of 156 MeV ^{6}Li projectiles.
Zeitschrift fuer Physik A, 332(1989) S.359-60
(short note)

KLAY, N.; KAEPPELER, F.
ß-decay rate of supra(79m)Se and its
consequences for the s-process temperature.
Physical Review C, 38(1988) S.295-306

KLEINRAHM, A.; FEHSENFELD, P.
Neuere Entwicklungen der
Verschleissmesstechnik mit dem Verfahren der
Duennschichtaktivierung.
KfK-Nachrichten, 21(1989) S.22-26

OCHS, A.; HECK, D.; KRAFT, A.; STROBEL, S.;
HOY, F.; HERBST, E.W.; PAUSCH, J.; KROEPELIN,
T.; GEROK, W.
Thorotrast induziertes cholangiolaeres
Carcinom mit 45 Jahren Latenz - Fallbericht -
Diagnostik.
43.Tagung der Deutschen Gesellschaft fuer
Verdauungs- und Stoffwechsel-Krankheiten,
Heidelberg, 21.-24. September 1988
95.Tagung der Deutschen Gesellschaft fuer
Innere Medizin, Wiesbaden, 2.-6.April 1989
Klinische Wochenschrift, 67(1989) Suppl. XVI,
S.288

REBEL, H.
Laserspectroscopic studies of nuclear
structure.
Petrovici, M. [Hrsg.]
Recent Advances in Nuclear Physics : Lectures
of the 1988 Internat.Summer School of
Nuclear Physics,
Poiana Brasov, R, August 30 - September 9,
1988
Singapore [u.a.] : World Scientific, 1989
S.223

REBEL, H.; BRANCUS, I.M.; COLE, A.J.;
GROTOWSKI, K.; KOZIK, T.
Intermediate mass fragment emission in ^{6}Li
induced nuclear reactions at E/A = 26 MeV.
Proc.of the Symp.on Nuclear Physics, Bhabha
Research Centre, IND, December 27-31, 1988
Bombay : Board of Research in Nuclear
Sciences, 1988 S.209-30

REBEL, H.
Break-up of light projectiles - a source of
astrophysical information.
Wilhelmi, Z. [Hrsg.]
Theoretical and Experimental Methods of
Heavy-Ion Physics : Proc.of the 19th
Mikolajki Summer School of Nuclear Physics,
Mikolajki, PL, August 31 - September 12, 1987
Chur [u.a.] : Harwood Acad.Publ., ca. 1989
S.215
(Nuclear Science Research Conference Series ;
15)
Conf.on Nuclear Reaction Mechanism, Calcutta,
IND, January 3-9, 1989

SCHWEICKERT, H.
Isotopenproduktion und -messtechnik am
Karlsruher Kompaktzyklotron KAZ.
Technologietransfer durch Kooperation: 10
Jahre TT-Programm des Kernforschungszentrums
Karlsruhe : Tagungsbericht vom Symp.,
Karlsruhe, 9.-10.Mai 1989
Koeln : Verl. TUEV Rheinland, 1989 S.230-50
(Technologie-Transfer ; Bd. 15)

SRIVASTAVA, D.K.; BASU, D.N.; REBEL, H.
Investigations of direct and sequential
Coulomb break-up of light ions.
KfK-4446 (Juli 88)

SRIVASTAVA, D.K.; BASU, D.N.; REBEL, H.
The dynamic polarization potential from
Coulomb dissociation of deuterons and ^{3}He.
Nuclear Physics A, 485(1988) S.221-32

SRIVASTAVA, D.K.; BASU, D.N.; REBEL, H.
Features of direct and sequential Coulomb
breakup of ^{6}Li ions.
Physical Review C, 38(1988) S.2148-56

SRIVASTAVA, D.K.; REBEL, H.
Slowly converging integrals in the DWBA
theory of stripping to unbound states and
break-up.
Journal of Physics G, 15(1989) S.L35-L39

SRIVASTAVA, D.K.; REBEL, H.; HEIDE, N.
A prior-form distorted wave born
approximation analysis of the elastic
break-up of 156 MeV ^{6}Li projectiles.
KfK-4565 (Juni 89)

WISSHAK, K.; KAEPPELER, F.; VOSS, F.; GUBER,
K.
The Karlsruhe 4π BaF$_2$ detector.
Fruehjahrstagung DPG, Kern- und
Mittelenergiephysik, Physikausstellung,
Berlin, 21.-25.Maerz, 1988
Verhandlungen der Deutschen Physikalischen
Gesellschaft, R.6, Bd.23 (1988) H-8.7
Proc.of the IEEE Nuclear Science Symp.,
Orlando, Fla., November 9-11, 1988
IEEE Transactions on Nuclear Science,
36(1989) S.101-05

6.2   CONFERENCE CONTRIBUTIONS

3rd La Rabida Summer School,
LaRabida, E, June 19 - July 2, 1988

WISSHAK, K.; GUBER, K.; KAEPPELER, F.; VOSS,
F.
Present status of the Karlsruhe 4π barium
fluoride detector.

11th Internat.Conf.on Atomic Physics
(ELICAP), Paris, F, July 4-8, 1988

BEKK, K.; FAUBEL, W.; GOERING, S.; HANSER,
A.; KAELBER, W.; MEISEL, G.; REBEL, H.; RINK,
J.; SAMEH, A.ALI; SCHATZ, G.; THOMPSON, R.C.
Laserspectroscopic studies of Am and Th
isotopes.

5th Internat.Conf.on Clustering Aspects in
Nuclear and Subnuclear Systems (Cluster 88),
Kyoto, J, July 25-29, 1988

KIENER, J.; GILS, H.J.; REBEL, H.;
SRIVASTAVA, D.K.; BAUR, G.
When does Coulomb dissociation dominate the
break-up of Li-projectiles?

STRIEBEL, CH.; NEU, R.; ABELE, H.; STAUDT,
G.; GILS, H.J.
Measurement and folding-potential analysis of
the inelastic α-scattering on light nuclei.

Internat.Summer School 'Recent Advances in
Experimental Nuclear Physics',
Poiana Brasov, R, August 30 - September 9,
1988

BRANCUS, I.M.; REBEL, H.
Extended sum-rule model for light and
intermediate mass-fragment emission in heavy
ion reactions.

HEIDE, N.; CORCALCIUC, V.; GILS, H.J.;
KIENER, J.; REBEL, H.; ZAGROMSKI, S.;
SRIVASTAVA, D.K.
Evidence for diffractive dissociation of ^{6}Li
and obtainability of the half-on-shell
T-matrix from break-up experiments.

20th Summer School on Nuclear Structure
Studies by Means of Nuclear Reactions,
Mikolajki, PL, September 2-11, 1988

KIENER, J.; GILS, H.J.; REBEL, H.; BAUR, G.;
GANTENBEIN, G.; HEIDE, N.; JELITTO, H.;
WENTZ, J.; ZAGROMSKI, S.
Search for non-resonant Coulomb break-up of
^{6}Li.

2nd Workshop on Experimental Problems in Low
Countrate, Low Energy Particle Physics,
Neuchatel, CH, September 8-9, 1988

MASCHUW, R.
The KARMEN project.

13th Internat.Symp.on Nuclear Electronics,
Varna, BG, September 12-18, 1988

BIALY, J.; EULENFELD, J.; HEINZMANN, H.;
KAPPEL, W.R.; THOUW, T.J.
The computer control system at the Karlsruhe
cyclotron facility.

HEINZMANN, H.; PETERS, J.; THOUW, T.J.
Usage of the cyclotron facility LAN.

Workshop on ECR-Ion-Sources, Grenoble, F,
September 14-16, 1988

EHRET, H.P.; ERNST, R.; FRIEDRICH, L.;
HUTTEL, E.; KALTENBAEK, J.; SCHULZ, F.; WISS,
L.; ZIEGLER, P.; SCHMELZBACH, P.A.
The Karlsruhe ECR ion sources.

Internat.Workshop on Liquid State
Electronics, Berlin, November 7-11, 1988

ENGLER, J.; GETTERT, M.; KEIM, H.
Liquid ionization chamber using
tetramethylsilane (TMS).

GIORGINIS, G.
Particle tracking using a self purifying LAr
time projection chamber.

Workshop on Transputers in Computational
Science, Bad Honnef, November 30 - December
2, 1988

GILS, H.J.; HECK, D.; OEHLSCHLAEGER, J.;
SCHATZ, G.; THOUW, T.J.; MERKEL, A.
A multi transputer system for parallel
Monte-Carlo simulations of extensive air
showers.

5.Tagung der German Association for the Study
of the Liver, Duesseldorf, 20.-21.Januar
1989

OCHS, A.; HECK, D.; THOM, H.; BUSCHER, H.P.;
SCHAEFER, H.E.; GEROK, W.
Die Langzeitligatur des Ductus Choledochus
der Ratte fuehrt zur Kupferueberladung und
zur sekundaeren biliaeren Zirrhose.

5th Workshop on Nuclear Astrophysics,
Ringberg Castle, Bad Wiessee, January 30 -
February 4, 1989

KAEPPELER, F.
Very small (n,γ) cross sections: two
measurements for primordial and stellar
nucleosynthesis.

KLAY, N.
The level scheme of ^{176}Lu: a key for thermal
effects during s-process nucleosynthesis.

Cosmic Ray Cascade Simulation Workshop, Salt
Lake City, Utah, March 2-3, 1989

SCHATZ, G.
Air shower simulations for the KASCADE
project.

53.Physikertagung gemeinsam mit der
Fruehjahrstagung DPG, Kern- und Hochenergie-
physik, Energietechnik - Physikalische
Grundlagen, Fachdidaktik der Physik,
Gravitation und Relativitaetstheorie,
Strahlenwirkung und -schutz, Physiker in der
Automatisierungstechnik, Fortbildungsveran-
staltung, Bonn, 13.-17.Maerz 1989
Verhandlungen der Deutschen Physikalischen
Gesellschaft, R.6, Bd.24 (1989) PC-4

ASCHENAUER, E.; EYRICH, W.; HOFMANN, A.;
LEHMANN, A.; MOOSBURGER, M.; RUDELOFF, R.;
SCHLOESSER, H.; WIRTH, H.; GILS, H.J.; REBEL,
H.; ZAGROMSKI, S.
Systematische Untersuchung von
Spin-Isospin-Staerke mit Hilfe der
(^{6}Li,^{6}He)-Reaktion.

BELLM, D.; GEMMEKE, H.; GENTNER, R.; KELLER,
K.; LASSEN, L.; LUECKING, W.; SEIBERT, U.
Vorgleichgewichtsemission von Neutronen bei
zentralen Stoessen im System 14.6 MeV/A ^{16}O +
^{64}Ni.

BOLZ, J.; ENGLER, J.; KEIM, H.; KNAPP, J.
Entwicklung von grossflaechigen
Plattenionisationskammern mit
Tetramethylsilan.

BRANCUS, I.M.; REBEL, H.
Extended sum-rule model for light and
intermediate mass fragment emission in heavy
ion reactions.

DAUMILLER, K.; DESCHNER, K.; DOLL, P.;
HEERINGA, W.; KLAGES, H.O.; KRIEGLEDER, W.;
MAYER, H.J.; MUELLER, H.; SCHMALZ, G.;
VOELKER, G.
Detector development for EXTASE.

DOLL, P.; FINK, G.; KLAGES, H.O.; SCHEIB, S.
Analyzing power of the ^{12}C(n,p)^{12}B reaction.

DOLL, P.; FINK, G.; HAUBER, S.; KLAGES, H.O.;
KNOEPFLE, K.T.
Efficiency and line shapes of a large NaI
detector.

DOLL, P.; FINK, G.; HAUBER, S.; HAUPENTHAL,
M.; KLAGES, H.O.; SCHIELER, H.; SMEND, F.;
WICKE, G.
Studies of γ-ray emission in the ^{1}H(n,γ)^{2}H
reaction.

DOLL, P.; FINK, G.; HAUBER, S.; HAUPENTHAL,
M.; HEERINGA, W.; KLAGES, H.O.; SCHIELER, H.;
SMEND, F.; WICKE, G.
Investigation of the ^{3}He(n,γ)^{4}He capture
reaction.

DREXLIN, G.; EBERHARD, V.; GEMMEKE, H.;
GIORGINIS, G.; GRANDEGGER, W.; KLEINFELLER,
J.; MASCHUW, R.; PLISCHKE, P.; SCHMIDT, F.K.;
WOELFLE, S.; WOCHELE, J.; ZEITNITZ, B.;
BODMANN, B.; BURTAK, F.; FINKCKH, E.;
KRETSCHMER, W.; SCHILLING, F.; VOETISCH, D.;
STEGEN, R.; ZELL, E.; BOOTH, N.E.; EDGINGTON,
J.A.; GORRINGE, T.; MALIK, A.; DODD, A.
KARMEN: Neutrinophysik bei ISIS.

ENGLER, J.; GILS, H.J.; HECK, D.; HEERINGA,
W.; KLAGES, H.O.; KNAPP, J.; KRIEGLEDER, W.;
MAYER, H.J.; OEHLSCHLAEGER, J.; REBEL, H.;
SCHATZ, G.; THOUW, T.; ZEITNITZ, B.
Das Karlsruher Luftschauerexperiment.

ENGLER, J.; GETTERT, M.; KEIM, H.
Strahlenbelastbarkeit von
Fluessigionisationskammern mit
Tetramethylsilan.

GERSTENHOEFER, TH.W.; ERNST, A.; KNAETSCH,
E.P.; ROLLER, D.
Halbleitertechnologie an einer gepulsten
RF-Ionenquelle.

GILS, H.J.; HECK, D.; OEHLSCHLAEGER, J.;
SCHATZ, G.; THOUW, T.; MERKEL, A.
Ein Multi-Transputer System fuer
Monte-Carlo-Simulationen von ausgedehnten
Luftschauern.

GIORGINIS, G.; ENGLER, J.; KEIM, H.
Purification of liquid detector media by
electron injection.

HEIDE, N.; CORCALCIUC, V.; GILS, H.J.;
KIENER, J.; REBEL, H.; WENTZ, J.; ZAGROMSKI,
S.; SRIVASTAVA, D.K.
Break-up of 156 MeV ^{6}Li at large asymptotic
relative momenta of the fragments and the
prior-DWBA.

JANY, P.; FINKBEINER, F.; HEERINGA, W.;
KLAGES, H.O.; SKACEL, H.; STROBELT, T.
Detection of laser pulses and α-particles
with superconducting tunnel junctions.

KARMEN-KOLLABORATION; KLEINFELLER, J.
Das KARMEN Szintillationskalorimeter.

KARMEN-KOLLABORATION; GEMMEKE, H.
Trigger und Elektronik des KARMEN Neutrino
Kalorimeters.

KARMEN-KOLLABORATION; DREXLIN, G.
Neutrinoidentifikation mit KARMEN.

LEHMANN, A.; EYRICH, W.; HOFMANN, A.;
MOOSBURGER, M.; RUDELOFF, R.; SCHLOESSER, H.;
WIRTH, H.; GILS, H.J.; REBEL, H.; ZAGROMSKI,
S.
Untersuchung des Neutronenzerfalls aus der
Riesenresonanzregion in Sn-Isotopen nach
Anregung durch ^{6}Li-Streuung.

NEUMANN-COSEL, P.VON; OBERSTEDT, A.; RICHTER,
A.; SCHRIEDER, G.; ROESCH, W.; BELLM, D.;
GENTNER, R.; KELLER, K.; LASSEN, L.; SEIBERT,
U.; HILSCHER, D.; LEHMANN, H.; CASSING, W.;
GEMMEKE, H.
Praeaequilibriums-Teilchenemission in
zentralen Schwerionenstoessen.

REBEL, H.; BAUR, G.; GILS, H.J.; KIENER, J.;
SRIVASTAVA, D.K.; HEIDE, N.; JELITTO, H.;
ZAGROMSKI, S.
Coulomb-Aufbruch nuklearer Projektile als
Informationsquelle von astrophysikalischem
Interesse.

RUDELOFF, R.; DENNERT, H.; EYRICH, W.;
LEHMANN, A.; SCHLOESSER, H.; GILS, H.J.;
KIENER, J.; ZAGROMSKI, S.
Testmessungen mit einem winkelaufloesenden
Detektorsystem am Karlsruher
Magnetspektrosgrafen 'Little John'.

WENTZ, J.; REBEL, H.; CORCALCIUC, V.; GILS,
H.J.; HEIDE, N.; JELITTO, H.; KIENER, J.;
BRANCUS, I.M.
Teilchenemission beim Zusammenstoss von 156
MeV ^{6}Li-Ionen mit supra(nat)Ag.

WISSHAK, K.; VOSS, F.; KAEPPELER, F.
Erste Messungen mit dem Karlsruher
$4\pi BaF_2$-Detektor: Neutroneneinfang an Nb, Ta
und Rh im Energiebereich von 5 bis 200 keV.

3rd European Conf.on Atomic and Molecular
Physics (ECAMP), Bordeaux, F, April 3-7, 1989

KAELBER, W.; MEISEL, G.; RINK, J.; BEKK, K.
Sub-doppler laser spectroscopy of ions in an
rf trap.

Internat.Nuclear Physics Conf., Sao Paulo,
BR, August 20-26, 1989
IOP-Conf.on Nuclear and Particle Physics,
Harwell, GB, April 5-7, 1989

KIENER, J.; GILS, H.J.; JELITTO, H.;
ZAGROMSKI, S.; REBEL, H.; BAUER, G.;
CORCALCIUC, V.; SRIVASTAVA, D.K.
Observation of resonant and nonresonant
Coulomb break-up of ^{6}Li.

12th Internat.Conf.on Cyclotrons and their
Applications, Berlin, May 8-12, 1989

BECHTOLD, V.; SCHWEICKERT, H.
Modern gas-target technology for the
production of high quality
radiopharmaceuticals.

EHRET, H.P.; ERNST, R.; FRIEDRICH, L.;
HUTTEL, E.; KALTENBAEK, J.; SCHULZ, F.; WISS,
L.; ZIEGLER, P.
The ion sources at the Karlsruhe cyclotron.

FEHSENFELD, P.; KLEINRAHM, A.
The application of cyclotron in mechanical
engineering.

Vortr.: American Gastroenterological
Association, Washington, D.C., May 14-17,
1989

OCHS, A.; HECK, D.; SCHAEFER, H.E.; GEROK, W.
Value of proton induced X-ray emission (PIXE)
in the diagnosis of iron overload.

Workshop on Neutrino Astrophysics,
Little Rock, Ark., May 15, 1989

DOLL, P.; ENGLER, J.; GABRIEL, P.; GILS,
H.J.; HECK, D.; HEERINGA, W.; HEIDE, N.;
KLAGES, H.O.; KNAPP, J.; MAYER, H.J.; REBEL,
H.; SCHATZ, G.; THOUW, T.; ZEITNITZ, B.
The KASCADE project.

Internat.Symp.on Weak and Electromagnetic
Interactions in Nuclei (WEIN 89), Montreal,
CDN, May 15-19, 1989

KARMEN-COLLABORATION; MASCHUW, R.
KARMEN: neutrino physics at ISIS.

4th Pisa Meeting on Advanced Detectors,
LaBiodola, I, May 21-25, 1989

GEMMEKE, H.
The high resolution neutrino calorimeter
KARMEN.

Workshop on Coulomb Break-up, Strasbourg, F,
May 22, 1989

KIENER, J.; GILS, H.J.; REBEL, H.
Status of the Coulomb break-up experiment of
^{6}Li.

REBEL, H.
Coupled channel analysis of elastic
scattering and sequential break-up of 156 MeV
^{6}Li projectiles at very forward scattering
angles.

Conf.on Special Applications of Radionuclide
Techniques in Mechanical Engineering,
Karlsruhe, May 30, 1989

KLEINRAHM, A..
Wear measurements with the concentration
method including filter measurements.

2nd Karlsruhe Internat.Conf.on Analytical
Chemistry in Nuclear Technology, Karlsruhe,
June 5-9, 1989

MATUSSEK, P.; MICHEL-PIPER, I.
Improvement of the lower limit of detection
in energy-dispersive XRF analysis by
wavelength dispersive prefiltering.

OTTMAR, H.; MICHEL-PIPER, I.
An XRF analyzer for the on-line monitoring of
uranium.

ISOLDE-Seminar on Nuclear Astrophysics, CERN,
Geneve, CH, 19.-20.Juni 1989

REBEL, H.
Coulomb dissociation as an alternative to
radiative capture.

5th IAP Astrophysics Meeting on Astrophysical
Ages and Datations, Paris, F, June 26-30,
1989

BEER, H.
The radiogenic ^{207}Pb component and the ^{235}U
clock.

ZHAO, W.; KAEPPELER, F.
An improved ^{175}Lu(n,γ)supra(176m)Lu cross
section: the cosmic clock supra(176g)Lu in
trouble.

6.3 SEMINARS

BASU, S.K.
Helium-jet transport system in the study of short-lived nuclei.
Vortr.: HMI Berlin, 14.November 1988
Vortr.: KFA Juelich, 21.November 1988
Vortr.: KVI Groningen, NL, 23.November 1988

BECHTOLD, V.
Modern gas technology for the production of high quality radiopharmaceutical.
Vortr.: Inst.of Nuclear Energy Research, Lung-Tan, Taiwan, 8.NOvember 1988
.Vortr.: Nuclear Technology Assessment Centre, Bata, Jakarta, RI, 15.November 1988

BECHTOLD, V.; FEHSENFELD, P.; SCHWEICKERT, H.
Das Karlsruher Kompaktzyklotron - ein Beschleuniger im Dienste der Medizin und Technik.
Vortr.: Technische Universitaet Muenchen, 16.Dezember 1988

FEHSENFELD, P.; SCHWEICKERT, H.
Thin layer activation of machine parts for in-situ and on-line detection of wear.
Vortr.: Michigan State University, East Lansing, Mich., 27.Maerz 1989

KAEPPELER, F.
Laborexperimente zur Synthese der schweren Elemente in Sternen.
Vortr.: Hahn-Meitner-Institut, Berlin, 10.November 1988

KAEPPELER, F.
Empirical constraints on the physical conditions during s-process nucleosynthesis.
Vortr.: Observatorium Torino, I, 17.Februar 1989

KLAGES, H.O.
EXTASE - a proposed cosmic ray experiment.
Vortr.: University of Chicago, Chicago, Ill., 13.Dezember 1988

KLAGES, H.O.
NN experiments and phase shift analyses.
Vortr.: University of Wisconsin, Madison, Wis., 16.Dezember 1988

MASCHUW, R.
KARMEN, Neutrinophysik zwischen 5 und 50 MeV.
Vortr.: Institut fuer Hochenergiephysik, Akademie der Wissenschaften der DDR, Berlin, 12.Oktober 1988

REBEL, H.
KASCADE-Karlsruher Vorschlag fuer ein Detektorfeld zum Studium der kosmischen Strahlung bei hohen Energien.
Vortr.: Inst.f.Kernphysik, KFA Juelich, 6.Juni 1989

SCHATZ, G.
Ausgedehnte Luftschauer und die Zusammensetzung der primaeren Hoehenstrahlung.
Vortr.: Max-Planck-Institut fuer Kernphysik, Heidelberg, 26.Januar 1989

SCHWEICKERT, H.
Modern compact cyclotrons for the large scale production of radioisotopes for medical and technical applications.
Vortr.: Institute of Nuclear Energy Research, Lung-Tan, Taiwan, 8.November 1988

SCHWEICKERT, H.
Medical and technical applications at the Karlsruhe Compact Cyclotron.
Vortr.: Korea Cancer Center Hospital, Seoul, Korea, 14.November 1988
Vortr.: Office of Atomic Energy for Peace, Bangkok, T, 21.November 1988

7. PERSONNEL

Head of the Institute, section IK I:

Prof. Dr. B. Zeitnitz

Scientific and Technical staff:

Apel, W.-D., Dr.	Haunschild, D.[1]
Argast, J.	Heeringa, W., Dr.
Bauer, F.[1]	Heneka, B., Mrs.
Bayer, R.[1]	Hucker, H.
Bolz, J.	Hüther, H., Dipl.-Ing.
Csabo, Th.	Husson, L., Ing.
Daumiller, K.[1]	Jany, P., Dipl.-Phys.
Deutsch, G.	Keim, H., Ing.
Dittmann, R.	Klages, H.O., Dr.
Doll, P., Dr.	Kleinfeller, J. Dr.
Drexlin, G., Dipl.-Phys.[2]	Knapp, J., Dr.
Eberhard, V., Dipl.-Phys.[2]	Kriegleder, W., Dipl.-Phys.[2]
Eitel, K.[1]	Kröner, F.
Engler, J., Dr.	Maschuw, R., Dr.
Foltin, G.[1]	Mayer, H.-J., Dr.
Fries, D.C., Prof. Dr.	Mielke, H.H., Dipl.-Phys.[2]
Gabriel, P., Dipl.-Phys.[2]	Plischke, P., Dr.
Gemmeke, H., Dr.	Plitt, K., Mrs.
Gettert, M.[1]	Rapp, J.[1]
Giorginis, G., Dr.	Schieler, H., Dipl.-Phys.[2]
Grandegger, W., Dipl.-Phys.[2]	Schmalz, G., Dipl.-Ing.
Grundel, G., Mrs.	Schmidt, F.K., Dr.
Gumbsheimer, R., Dipl.-Ing. (FH)	Skacel, H.
Hahn, A.[1]	Spohrer, G.

[1] Student
[2] Graduate student

Treceziak, R.[1]

Vater, G., Mrs.[1]

Völker, G., Dipl.-Phys.[2]

Wetzel, Y., Mrs.[1]

Wochele, J., Dr.

Wölfle, S., Mrs., Dipl.-Phys.[2]

Wolf, J.[1]

Ziegler, P.

[1] Student
[2] Graduate student

Head of the Institute, section IK III :

Prof. Dr. Gerd Schatz

Scientific and technical staff:

Antoni, I., Mrs.

Beer, H., Dr.

Bekk, K., Dr.

Burkhardt, S., Mrs.

Dorn, A.[1]

Eberle, H., Ing.

Feurer, B.

Friederich, H.-M., Mrs.

Garcia-Orijuela, C.[1]

Gerstenhöfer, Th., Dipl.-Phys.[2]

Gils, H.J., Priv.-Doz., Dr.

Gsottschneider, G.[1]

Guber, K., Dipl.-Phys.[2]

Göring, S., Dipl.-Phys.

Hanser, A., Dr.

Heck, D., Dr.

Heide, N., Dr.

Jelitto, H., Dr.

Jaag, S.[1]

Kälber, W., Dr.

Käppeler, F., Dr.

Kiener, J., Dipl.-Phys.

Klay, N., Dipl-Phys.

Köhler, A., Mrs.

Kowalewska, D., Mrs., Dipl.-Phys.[2]

Matussek, P., Dipl.-Phys.

Meisel, G., Priv.-Doz., Dr.

Michel-Piper, I. Mrs., Dipl.-Ing. (FH)

Müller, H.

Oehlschläger, J., Dipl.-Math.

Ottmar, H., Dr

Pietruk, P.[1]

Ratzel, U.[2]

Rebel, H., Prof. Dr.

Rink, J. Dipl-Phys.[2]

Rupp, G.

Schmidt, K.A., Dipl.-Phys.

Schruft, R.[1]

Steininger, R.[2]

Voß, F., Dr.

1 Student
2 Graduate student

Wentz, J.[1]

Wisshak, K., Dr.

Zagromski, S., Dipl-Ing. (FH)

[1] Student
[2] Graduate student

Guest Scientists :

Basu, S.K., Dr.

Brâncuş, I.M., Mrs., Dr.

Brzychczyk, J., Dr.

Capdevielle, J.N., Prof. Dr.

Corcalciuc, V., Dr.

Grotowski, K., Prof. Dr.

Khristiansen, G.B., Prof. Dr.

Panasiewicz, A., Ing.

Pârlog, M., Dr.

Popescu, D., Dr.

Sosin, S., Dr.

Wdowczyk, J., Prof. Dr.

Zhao, W., Mrs., Dipl.-Phys.

Head of the Cyclotron Laboratory :

Dr. H. Schweickert

Scientific and technical staff :

Acharya, H., Mrs.	Heger, V.
Assmus, K.H.	Heidenreich, K.
Bauer, G.*	Heinzmann, H., Dipl.-Inf.
Bechtold, V., Dr.*	Heitz, E.,
Bialy, J., Dipl.-Phys.	Herrmann, P.
Biber, J.	Höllmüller, S., Mrs.*
Blank, R.*	Hüfner, R., Dr.*
Bollmann, E.; Dipl. Phys.*	Huttel, E., Dr.*
Dennerlein, H.D.*	Immler, H., Dipl.-Ing.*
Dohrmann, H., Ing.	Kaltenbaek, J.
Dosenbach, S.,Mrs.*	Kappel, W.-R., Ing.
Dressen, R.	Kauther, P.
Ehret, H.-P.	Kernert, N., Dipl.-Phys.
Erbe, D.	Kessel, M.
Erdel, E.	Kirste, E., Fr.
Ernst, R.	Klar, T.[1]
Fehsenfeld, P., Dr.	Kleinrahm, J., Dr.*
Feuerstein, P., Mrs.	Klinger, G.
Fischböck, T.*	Konrad, J.
Foßhag, E., Dr.*	Kraft, J.*
Franz, J.	Kraus, H.*
Friedrich, L., Dr.*	Krieg, U.
Gegenheimer, B.	Kubat, R., Dipl.-Ing.*
Günther, O.	Lang, D.

* Specially financed
[1] Student
[2] Graduate student

Lang, R.	Schönstein, E.
Maier, W.	Schüssler, B.
Mangold, D.	Schütz, R.
Martin, A.*	Schulz, F., Ing.
Mayl, R.*	Seidel, H.
Möck, W.	Seitz, F.
Möllenbeck, J., Ing.*	Seitz, J.
Peters, J.W., Dipl.-Phys.	Seufert, H.
Rämer, Ch., Mrs., Ing.	Stöbener, E., Ing.
Ripp, H.*	Süpfle, M.
Roth, H., Ing.	Uchatius, R., Mrs.
Schimpf, P.	Uhlemann, S., Mrs.
Schlösser, K., Dr.*	Wiss, L.
Schmitt, M.*	Ziegler, P.

* Specially financed
1 Student
2 Graduate student